Establishing systems to characterise MH pathogenic RyR1 variants

A thesis presented to Massey University in partial fulfilment of the requirements for the degree of Doctor of Philosophy in Biochemistry

Jeremy Stephens

2020

Acknowledgments

Firstly, and most formally I would like to thank my supervisor Professor Kathryn Stowell. Thank you for providing me the opportunity to work in your lab and thank you for guiding me through this journey.

Thank you Anja for all of your continual help guidance, and for always having time to answer my questions.

Thank you Andrew for your help and guidance during protein purification and for providing a number of columns and reagents that were not available directly to me.

Thank you to my lab mates, Remai, Rowane, Shannon, Sophie and Liam for always answering my questions and making the lab such a fun and entertaining environment to work in.

Thank you Trevor Loo for always making time to answer my questions and providing some enzymes that were not directly available to me.

Thank you to Massey University and the School of Fundamental Sciences for providing the scholarship that made my study possible.

I would like to thank my parents for all of their support and encouragement throughout my time at Massey.

Finally, I would like to thank Jacob Farmer, Martin O'Kennedy, Jason Kelly, Andrew Neverman, Corrin Hulls, Chris Hill, Danny Donaghy and the rest of the family at Art of Combat along with my former coach Jeremy Fraser. Thank you for keeping me honest and motivated.

Abstract

Malignant hyperthermia (MH) is a potentially fatal, autosomal dominant, metabolic disorder triggered in susceptible individuals upon exposure to volatile anaesthetics. Following the onset of an MH episode, a patient will enter a hypermetabolic state, displaying the symptoms of intense muscle contraction, metabolic acidosis, increased oxygen consumption. Prolonged episodes can result in rhabdomyolysis. If left untreated, MH can manifest as an increase in body temperature and death by cardiac arrest. MH is diagnosed by the invasive *in vitro* contracture test, which requires a muscle tissue biopsy. DNA screening has been implemented and is commonly used to diagnose a genetic predisposition to MH; however, the test is currently limited to fifty variants confirmed to be pathogenic out of approximately 350 variants linked to the disorder. DNA-based tests are limited because of the technical difficulties associated with functional analysis. Thus, additional variants must be functionally characterised. The structural implications of MH-linked variants potentially leading to the onset of MH are not yet well defined. Potential structural changes induced by pathogenic variants have been modelled *in silico*, where variants were mapped to the rabbit RyR1 structure characterised by cryo electron microscopy. However, this does not confirm the role the variants play in the structural and functional alteration of the channel. To address, this a functionally significant region of RyR1 was cloned for recombinant expression in *E. coli*. The RyR1 region was shown to be soluble and efforts were made to purify the protein. However, the protein could not be purified to an extent acceptable for either biochemical analysis or crystallisation trials or for subsequent X-ray crystallography. A number of pathogenic variants were instead modelled *in silico* to provide some insights into their potential pathogenic functional role.

The viability of a new cell-based system for the functional characterisation of variants was also tested. Patient derived myoblasts were immortalised using lentivirus transduction with the cDNA for human telomerase and cyclin dependent protein kinase 4. The genome editing tool CRISPR Cas 9 was then used to successfully introduce the pathogenic variant c.14497C>T p.his 4833 tyr into the genome of MH negative myoblasts. Functional characterisation of the introduced variant has yet to be performed.

Abbreviations

ADP	Adenosine di-phosphate
APS	Ammonium peroxodisulfate
ATP	Adenosine tri-phosphate
Bp	Base pair
CCD	Central core disease
Cp	Crossing point
DAPI	4',6-diamidino-2-phenylindole
EDTA	Ethylenediaminetetraacetic acid
DHPR	Dihydropyridine receptor
DMEM	Dulbecco's Modified Eagle Medium
DMSO	Dimethyl sulphoxide
DP4	Domain peptide 4
DTT	Dithiothreitol
EC-coupling	Excitation-contraction coupling
EM	Electron microscopy
FBS	Foetal calf serum
FITC	Fluorescein isothiocyanate
FKBP12	12 KDa FK506-binding protein
HEK239	Human embryonic kidney cells
HEPES	4-(2-hydroxyethyl)-1-piperazineethanesulfonic acid
IPTG	Isopropyl β-D-thiogalactopyranoside
IVCT	*In vitro* contracture test
KDa	Kilo Dalton
MH	Malignant hyperthermia
MHN	Malignant hyperthermia negative
MHS	Malignant hyperthermia susceptible
N/A	Not applicable
PAGE	Polyacrylamide gel electrophoresis
PCR	Polymerase chain reaction
RyR	Ryanodine receptor

SDS	Sodiumdodecylsulfate
SR	Sarcoplasmic reticulum
TAE	Tris acetate EDTA buffer
TBST	Tris buffered saline Tween 20
TEMED	Tetramethylethylenediamine
TRITC	Tetramethyl rhodamine isothiocyanate
Tris	Trisaminomethane
T-tubule	Transverse tubule
UV	Ultraviolet light

Table of Contents

List of figures

List of tables

1. Introduction

Malignant hyperthermia (MH) is a potentially fatal, autosomal dominant, pharmacogenetic disorder of skeletal muscle. An MH episode is triggered following exposure to potent volatile anaesthetics or depolarising muscle agents. Susceptible patients exhibit symptoms characteristic of entering a hypercatabolic state including muscle rigidity, rapid breathing leading to increased oxygen consumption, metabolic acidosis, an increase in body temperature and rhabdomyolysis, ultimately resulting in death by tachycardia if left untreated (1). With prior diagnosis, alternative safe anaesthetics can be administered that would avoid such an episode. During day to day life susceptible patients do not display any visible symptoms. MH is particularly common within the Manawatu region of New Zealand where annually 1:200 people undergoing anaesthesia at the Palmerston North hospital must be treated as MH susceptible (2). This is compared to the world-wide estimation of between 1:10,000 and 1:250,000 (3).

1.1 Diagnosis

The current gold standard for the diagnosis of MH-susceptibility is the *in vitro* contracture test (IVCT) (1). The procedure is invasive and first requires the extraction of a muscle tissue biopsy from a patient's *quadriceps femoris* muscle. The biopsied muscle is then dissected into fibre bundles, tethered between two force meters and suspended in physiological buffer. From here, the muscle should then begin to gently contract without any external stimulation. The agonists, caffeine (a stimulant) and halothane (an anaesthetic), are added to the buffer individually in incremental amounts and the resulting muscle contraction is then measured. A MH negative patient (MHN) will display no significant alteration in contracture strength below the threshold limits, while the biopsied muscle of an MH-susceptible patient (MHS_{hc}) will undergo a strong and intense muscle contraction significantly above the threshold limit for both agonists which is based on a standardised protocol and local laboratory procedures (1). However, the IVCT does not always return a definitive result. In some cases, a patient will only display an increased contracture strength in the presence of either caffeine or halothane;

in this case, the patient is still classed as clinically MH-susceptible being noted as MHS_C or MHS_H respectively.

DNA-based diagnostic tests have been established and provide an alternative to the IVCT for certain members of the population. However, DNA testing is currently limited to the fifty variants confirmed by functional analysis to predispose a person to MH (4). Moreover, under current guidelines, the test can only be used to diagnose a patient as being susceptible to the disease; it cannot be used to diagnose a person as being MHN. While hundreds of variants have been linked to the disease, the role most of these variants play in the onset of MH has yet to be determined. The functional characterisation of these variants is both a bottleneck and currently a major objective in MH research worldwide. Achieving functional characterisation of such variants would increase the viability of DNA screening for more members of the population and hence limit the need for the IVCT. The following sections represent a brief summary of skeletal muscle and the ryanodine receptor in the context of excitation contraction coupling and their relevance to MH.

1.2 Skeletal muscle

The contraction of skeletal muscle is a voluntary process under the control of the somatic nervous system. Neural stimulation of the muscle tissue will cause the cells to depolarise, creating an action potential which travels along the cell membrane and down transverse tubules (T-tubules) which are invaginations of the cell plasma membrane. The T-tubules bring the cell membrane in close proximity to the terminal cisternae of the sarcoplasmic reticulum (SR) (figure 1.1). The interface between the T-tubule and SR is referred to as the terminal cisternae and is characterised by an enlargement of the SR in the local region surrounding the T-tubule. The increased surface area of the SR at the terminal cisternae allows for increased storage of Ca^{2+} ions in the local region and following cell depolarisation leads to mass release of Ca^{2+} from the organelle. Once in the cytosol, Ca^{2+} will interact with the protein troponin C forcing it to undergo a conformational change, which in turn leads to a conformational change in the protein tropomyosin. This ultimately allows myosin to interact with actin; the hydrolysis

of ATP then leads to the generation of tension as the two proteins move relative to each other, resulting in the contraction of the muscle cell. At the molecular level, this process is regulated by a number of protein channels spanning both sarcolemma and SR.

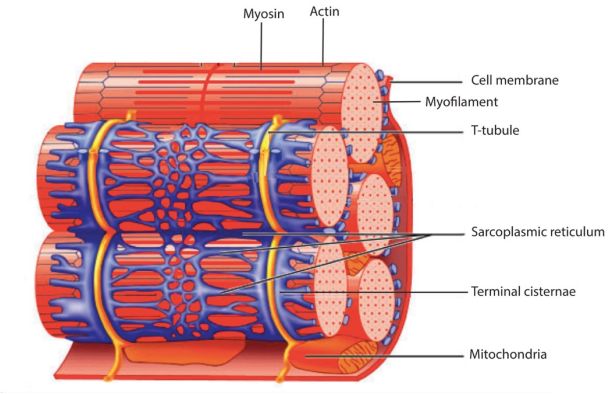

Figure 1.1. Architecture of skeletal muscle. The proteins actin and myosin, within a myofilament, have been highlighted in black and red respectively. The T-tubule is coloured in yellow and the SR in blue. Figure was adapted from (5). No permission was required to use the figure.

The dihydropyridine receptor (DHPR) is an L-type voltage dependent Ca^{2+} release channel located at the base of the T-tubule (6). Upon receiving electrical stimulation, the DHPR will undergo a conformational change releasing small amounts of Ca^{2+} into the cytosol from the extra cellular space. The DHPR forms a physical interaction with the SR membrane-spanning Ca^{2+} channel, the ryanodine receptor type 1 (RyR1) (figure 1.2). The conformational change in the DHPR forces a concomitant conformational change in RyR1 which allows mass Ca^{2+} to flow into the cytosol from the SR. The physical interaction between the two proteins couples the excitation of skeletal muscle with the release of Ca^{2+} from the SR and hence muscle contraction. This process is referred to as excitation-contraction coupling (EC-coupling). Following the opening of RyR1, the cytosolic Ca^{2+} concentration increases rapidly. Because cytosolic Ca^{2+} has such a drastic effect on cell physiology, where it plays a role in both muscle contraction as well as activation of metabolic pathways, its concentration must be tightly controlled. The protein sarcoplasmic/endoplasmic reticulum ATPase (SERCA) rapidly returns Ca^{2+} to the SR, where the hydrolysis of ATP provides the energy to move the ion across the membrane against a concentration gradient (figure 1.2). After being returned to the SR, Ca^{2+} is once again available to be released into the cytosol via RyR1, allowing for repeated rounds of muscle contraction.

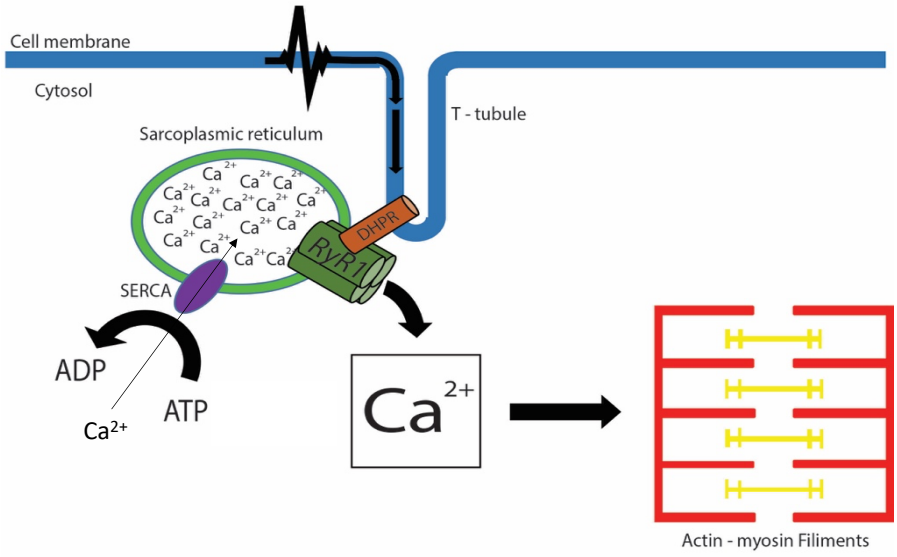

Figure 1.2. Schematic representation of Ca^{2+} release from the sarcoplasmic reticulum in skeletal muscle. The DHPR (orange) is stimulated following depolarisation of the cell membrane (blue). The DHPR stimulates RyR1 (green) to release Ca^{2+} from the sarcoplasmic reticulum into the cytosol. Cytosolic Ca^{2+} initiates muscle contraction and is then transported back into the SR via the SERCA (purple) powered by ATP hydrolysis.

Abnormal Ca^{2+} homeostasis is considered to be the cause of MH. Alterations in RyR1 function are commonly associated with the disease, with 50-70 % of MHS patients having a variant within the *RYR1* gene (7). Fifty nucleotide variants have been classed as being pathogenic for MH, forty-eight of these are within *RYR1*, while the other two are located in *CACNA1s* the α1 subunit of the DHPR (4). Approximately 350 other variants within *RYR1* have been linked to the disease, however the exact role they play in its onset have yet to be determined (7).

1.3 The Ryanodine Receptor

There are three RyR isoforms, each of which is a homotetramer. Each isoform is expressed in different tissues (8): type 1 is expressed mainly in skeletal muscle, type 2 is expressed in cardiac muscle and type 3 is expressed across a range of tissues (8). Type 1 is the only isoform associated with MH and is the only isoform to form a physical interaction with DHPR and as a

result is the only isoform in which the release of Ca^{2+} from the SR is physically coupled to the depolarisation of a muscle cell. All isoforms have an overall mushroom-like structure, where the transmembrane region of the channel forms the stalk, while the large and bulky cytosolic region forms the cap (figure 1.3) (9). Each subunit is approximately 5000 amino acids in length and is thought to be comprised of putative domains, each which plays a significant role in the function of the protein.

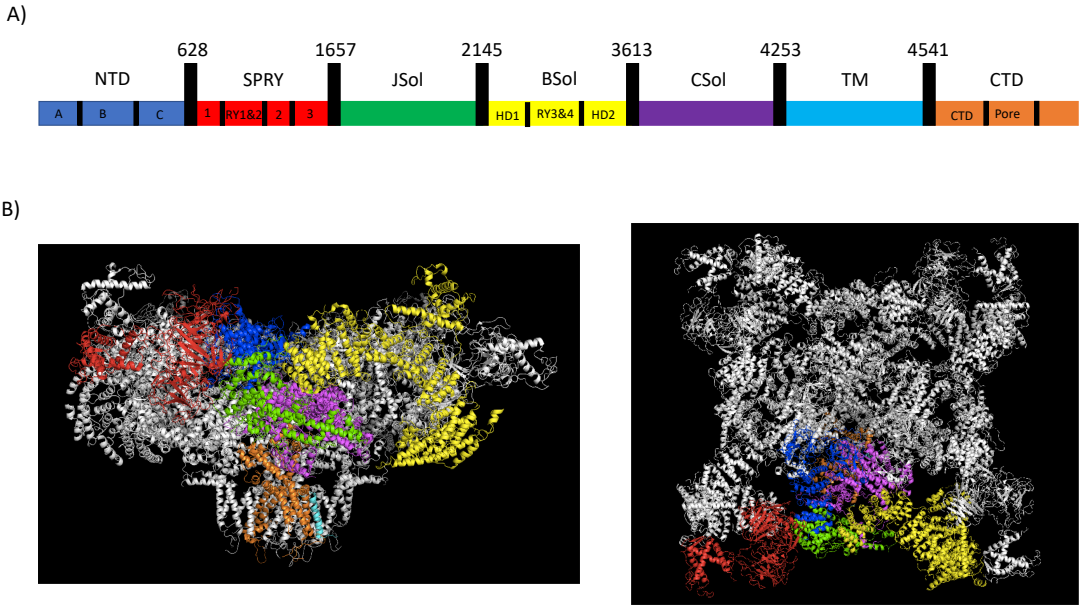

Figure 1.3. Representation of the domain distribution of RyR1. A) Proposed RyR1 domains have been represented by colour and the domain boundaries have been indicated by amino acid number. Amino acid numbers refer to the accession number NM_000540.2. B) Proposed location of each domain in the RyR1 tertiary structure. The left panel is a side on view of the channel, the right panel is a top down view of the channel. Proposed domains of a single subunit have been coloured as in section A. The figure was made using PyMOL version 2.4.0a0 using the PDB ID 5TB1.

Amino acid variants, both confirmed pathogenic and MH-associated, have been identified throughout the amino acid sequence of RyR1 (4)(appendix 1). These variants have been suggested to disrupt RyR1's function directly, by interfering with interdomain interactions or indirectly, by inhibiting cellular control mechanisms that regulate RyR1. MH-pathogenic variants are considered to result in a gain of function, where functionally these variants cause RyR1 to favour the open state under MH-inducing conditions leading to the excessive release of Ca^{2+} from the SR and the resulting onset of MH symptoms (10, 11).

MH is an autosomal dominant disorder in which patients are heterozygous for a pathogenic variant. Any RyR1 channel, within these individuals, can exist as one of six different combinations of tetramers, each with a different combination of WT and variant containing subunits. It is unknown how many variant containing subunits need to be present in the tetramer before the particular channel will lose normal function. This exact number may be different for each variant as some may have a more severe effect on the function of their particular subunit and potentially an adjacent subunit compared to others. The presence of one variant containing subunit might be enough to cause the onset of MH. While other variants may require all four subunits to contain the variant before the channel can lead to the onset of MH.

Other pathologies have also been linked to genetic variants within *RYR1*. The first of which, central core disease (CCD), is characterised by reduced muscle tension and muscle weakness consistent with a loss of function. Pathogenic variants resulting in CCD are predominantly located within the transmembrane region of the channel (12). Two mechanisms for the onset of CCD have been proposed. Firstly, pathogenic variants ultimately encourage the channel to favour the open state at rest and as a result a Ca^{2+} concentration gradient cannot be maintained across the SR membrane. Continually elevated cytosolic Ca^{2+} has been implicated in sarcoplasmic disorganisation and mitochondrial damage, leading to a decreased mitochondrial presence (13). These variants cause RyR1 to favour the open state and unlike MH, do so under normal physiological conditions. As a result, it could be argued the severity of these variants is increased over those that are MH pathogenic. The second mechanism results from amino acid variants which cause a non-responsive channel; in this case RyR1 and DHPR do not form a physical interaction (uncoupled). While a Ca^{2+} concentration gradient can be maintained across the SR, it is unlikely to be released rapidly following neural stimulation. For both mechanisms the number of variant-containing subunits that need to be present in a tetramer to alter function is unknown. Some variants are linked to both CCD and MH, but a molecular explanation for this remains elusive. Clinically, all patients diagnosed with CCD are treated as MH-susceptible for the purposes of general anaesthesia.

Multi mini core disease (MMD) is a non-progressive myopathy also linked to variants within RyR1. The disease is characterised by muscle weakness, distal joint laxity and respiratory

problems. Like CCD, MMD is also implicated in mitochondrial damage leading to reduced oxidative activity (14). Patient muscle has also been shown to contain internal nuclei and variable degrees of disruption to the sarcolemma. *RYR1* variants linked to MMD are distributed throughout the gene and all are recessive. It is believed that compound heterozygosity or allele silencing is the probable cause of the disease (15). Tissue-specific allele silencing has also been linked to MMD (16).

1.4 Regulation of RyR1

Because Ca^{2+} has such an important role in the cytosol, RyR1, which has a strong influence on Ca^{2+} homeostasis must be tightly controlled. RyR1 activity is regulated by several different mechanisms, which are summarised below.

1.4.1 The DHPR

A cytoplasmic region of the DHPR subunit α_{1s} (Uniprot accession number Q13698), loop II-III, interacts with RyR1 (17) (figure 1.4). This interaction is vital for the EC coupling process and upon receiving the electrical signal, this loop undergoes a conformational change forcing a concomitant conformational change in RyR1. The interaction between these two proteins is essential for the rapid release of Ca^{2+} from the SR following neural stimulation. Two amino acid variants within the α_{1s} subunit have been shown to be pathogenic for MH. The first, arg 1086 his is located on the III-IV loop and is not in direct contact with RyR1. The III-IV loop has been proposed to be involved in the negative regulation of RyR1 (18). Should this be the case, RyR1 will not be encouraged to close, ultimately resulting in prolonged Ca^{2+} release and the onset of MH. The second variant, arg 174 trp is located in a highly conserved region known to be important in sensing changes in membrane potential (19).

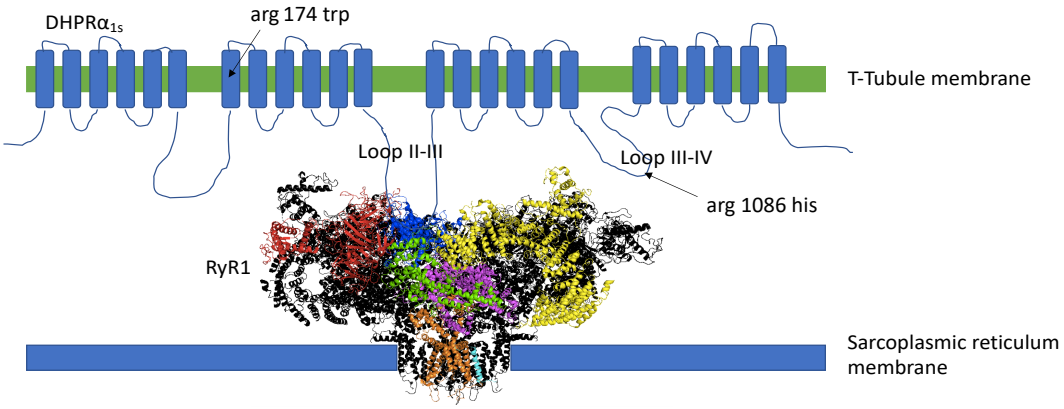

Figure 1.4. Representation of the interaction between RyR1 and the DHPRα_{1s} subunit. This figure was produced in part using PyMOL version 2.4.0a0 using the PDB ID 5TB1.

The localisation of DHPR to the base of the transverse tubule is thought to rely on the cytosolic protein Stac3 (20). Stac3 is also an essential component of the EC-coupling process, with its importance in the regulation of Ca^{2+} being highlighted in patients with an autosomal recessive variant that has been confirmed as being pathogenic for a debilitating myopathy, Native American Myopathy. The myopathy is characterised by a variety of symptoms including muscle weakness, difficulty with breathing and feeding, slower development, muscle cramps, stiffness and spasm, and in some cases has been linked to susceptibility to MH (21). There are, however, no reports to date of an individual with a variant in the *STAC3* gene having undergone an IVCT so as yet this gene has not been confirmed as having a role in MH-susceptibility. When the original pathogenic variant was functionally characterised in zebra fish, organisms containing the variant were shown to have a reduced presence of DHPR compared to WT, where there was no effect on the expression of RyR1 (22). Overall, *STAC3* variants appear to result in loss-of-function. This is not consistent with the pathogenicity of MH.

1.4.2 Molecule regulators

1.4.2.1 Calcium ions

The conformational change in DHPR upon voltage sensing leads to the dilation of its channel, allowing Ca^{2+} to flow from the extra cellular space into the cytosol. In this case, only a small amount of Ca^{2+} will enter the sarcoplasm. The increased concentration of Ca^{2+} in the local region surrounding the SR is unlikely to induce muscle contraction. However, these ions surrounding the SR are likely to be involved in the activation of RyR1 (9). RyR1 has two Ca^{2+} binding sites on its cytosolic face: one with a high affinity for Ca^{2+} and one with a low affinity. When bound to the high affinity site, Ca^{2+} will cause the cytosolic region of RyR1 to undergo a conformational change. RyR1 in this state is referred to as being in the primed conformation where the pore remains closed. However, the new conformation of the cytosolic region will allow the channel to easily open upon receiving a secondary stimulus. When Ca^{2+} concentrations rise to millimolar levels, the ion will bind to the low affinity site on RyR1 acting as an inhibitory signal. In this case, the ion encourages the protein to favour the closed state preventing further Ca^{2+} release. Therefore, Ca^{2+} in different concentrations can act as a positive or negative regulator.

RyR1 is also under the control of Ca^{2+} within the SR lumen. In a process called store overload-induced Ca^{2+} release, an increase in the luminal [Ca^{2+}] will lead to the opening of RyR1 (23). Release of Ca^{2+} from the SR via this mechanism is a spontaneous process and can result without DHPR stimulation. Pathogenic variants for both MH and CCD have been proposed to lower the threshold for Ca^{2+} release, and as a result can lead to the onset of MH under inducing conditions.

1.4.2.2 Inhibition by Mg^{2+}

Mg^{2+} competes with Ca^{2+} for binding to the high affinity site. Mg^{2+} has an opposing effect on RyR1 function, in that its binding will cause RyR1 to favour the closed state (24). There are two modes of Mg^{2+} inhibition (25). Type 1 inhibition is where Mg^{2+} and Ca^{2+} will compete for the same binding site. As Ca^{2+} concentrations rise, following the activation of DHPR and subsequent RyR1 opening, Ca^{2+} will bind RyR1 at the expense of Mg^{2+}. In the second mode of inhibition, type 2, Mg^{2+} binds to a second site on RyR1, independent of Ca^{2+}, and again encourages RyR1 to favour the closed state.

1.4.2.3 Adenine nucleotides

At millimolar concentrations ATP is also able to bind the cytosolic face of RyR1 (figure 1.5). Similar to the binding of Ca^{2+}, the binding of ATP will cause RyR1 to adopt the primed conformation (9). The binding of both ligands at once will cause RyR1 to open without the need for stimulation by the DHPR. In rabbit RyR1, amino acids met 4954, phe 4959, tyr 4979 and leu 4985 (Uni prot accession number P11716) were shown to interact with the adenine base of ATP when the full-length rabbit RyR1 channel was characterised by cryo electron microscopy (cryo-EM) (9). There is a high amino acid identity shared between rabbit and human RyR1 with the corresponding amino acids met 4955, phe 4960, tyr 4980 and leu 4986 in human RyR1 (accession number NM_000540.2) likely to be involved in the interaction. ATP seems to bind RyR1 only transiently, playing a role in the regulation of the channel, with no evidence to suggest RyR1 is able to hydrolyse ATP (26). ADP will compete with ATP for the same binding site on RyR1. ADP is a strong metabolic signal which in high concentrations indicates the cell is in an energy deficient state (26). Like ATP, the binding of ADP will cause RyR1 to adopt the primed conformation. Interestingly, the binding of this nucleotide will cause RyR2 to adopt the closed conformation, preventing further release of Ca^{2+} from the channel and the associated energy utilisation which highlights a difference in regulation of the isoforms by the nucleotides.

1.4.2.4 Reactive oxygen species

Metabolism, particularly in working muscle, has the potential to create reactive oxygen species, which alter the redox state of the cell. The SR membrane protein NADPH oxidase 4, in the presence of cytosolic oxygen, will oxidise NADPH to $NADP^+$ within the SR. The released electron is passed onto cytosolic oxygen, producing a superoxide ion (27). The increased concentration of superoxide ions surrounding the SR has the potential to oxidise RyR1, in doing so altering its function. Cysteine residues on the cytoplasmic surface of RyR1 will donate an electron from their thiol side chain to the superoxide ion, becoming oxidised themselves.

Cysteine in the oxidised state has the potential to form covalent interactions with other oxidised molecules within the cell (27, 28). Four cysteine residues on the cytoplasmic face of human RyR1, 35, 2326, 2363 and 3635 (accession number NN_000540.2) in the oxidised state can form disulphide bonds with each other, locking the channel in the open state and leading to further Ca^{2+} release (29). The same cysteine residues can also be oxidised by nitric oxide, a product of amino acid metabolism (30). Oxidised residues have also been shown to bind to the antioxidant S-glutathione (29) and once bound RyR1 will favour the open state prolonging Ca^{2+} release (29-31). In this case, the cysteine residues 35, 315, 811, 906, 1591, 2326, 2363, 3193 and 3635 were shown to be subjected to modification. The binding of S-glutathione limits the inhibitory effect of Mg^{2+} and as a result leads to further Ca^{2+} release from the SR (29). The modification of cysteine 3635 prevents the binding of the regulatory protein calmodulin which ultimately aids in the stabilisation of the open conformation (32, 33). Overall, the oxidation of RyR1 plays a role in creating a hypersensitive channel, which is likely to have functional effects in response to both normal neural stimulation and in the presence of MH-triggering agents.

1.4.3 Protein regulators

A large number of proteins are known to bind to and regulate RyR1. All of these proteins cannot be efficiently summarised in this thesis. However, a select few well characterised proteins have been summarised in the following section.

1.4.3.1 FKBP12

FK506 binding protein FKBP12 is a 12 kDa cytosolic protein which binds RyR1, an interaction thought to be mediated by the RyR1 amino acids Leu 674, pro 1780, phe 1782, val 1783, ala 1785 (accession number NM_000540.2) (9, 34). One FKBP12 can bind each RyR1 subunit and in doing so is thought to stabilise the closed state of the channel. The phosphorylation of RyR1 at serine 2843 by protein kinase A or calmodulin-dependent protein kinase will inhibit the

binding of FKBP12 causing the channel to favour the open state (35). Protein kinase A is activated upon an increase in cAMP which is produced by adenylate cyclase following receiving an extracellular signal which indicates the muscle needs to contract. The signal transduction ultimately results in the RyR1 favouring the open state. Calmodulin dependent protein kinase is activated following the binding of calmodulin, a process that only occurs following calmodulin's binding of Ca^{2+} (36). The elevated cytosolic Ca^{2+} levels are an indication the muscle is in a working state and the activation of the protein kinase and subsequent activity encourage the further release of Ca^{2+} from the SR. In this case Ca^{2+} once again perpetuates its own release from the SR.

1.4.3.2 Calmodulin

Calmodulin has also been shown to form an interaction with the RyR isoforms. Calmodulin will bind to different sites on the cytoplasmic face of RyR1 when in different Ca^{2+}-bound states. In the Ca^{2+}-free state, apo-calmodulin will bind within an elongated cleft; the exact RyR1 amino acids involved in this interaction have yet to be determined (37). Rabbit RyR2 has been structurally characterised in the calmodulin-bound state where the amino acids tyr 2203, tyr 2157, tyr 2558 and pro 3604 (accession number Q29621) were shown to mediate the interaction between the two proteins (37). Due to the high amino acid identity shared between the two isoforms (appendix 1), the equivalent amino acids in RyR1 (tyr 2238, tyr 2197, tyr 2587 and pro 3640 accession number NM_000540.2) may be involved in the binding of calmodulin. After binding Ca^{2+}, calmodulin undergoes a conformational change and as a result can interact with a different binding site on the RyR isoforms. The RyR2 amino acids pro 3604, trp 3588 and arg 2209 have been shown to be important in this interaction. The equivalent RyR1 amino acids, pro 3640, trp 3620 and arg 2244, may also play a role in this interaction. Interestingly, calmodulin in Ca^{2+}-free state has opposing effects on RyR1 and RyR2 (38). Calmodulin in the Ca^{2+}-free state will encourage RyR1 to favour the open state while its binding will cause RyR2 to favour the closed state. This highlights the differential regulation of each RyR isoform and the way in which they are important for Ca^{2+} release in their respective tissue.

1.4.3.3 Calsequestrin

Calsequestrin (CASQ) is a SR lumenal protein and binds free Ca^{2+} ions, effectively reducing the concentration gradient across the SR membrane. CASQ is able to bind Ca^{2+} with both high and low affinity binding sites making it an effective buffer for the ion, where roughly 75 % of luminal Ca^{2+} is bound to the protein (39). The reduced concentration gradient allows SERCA to easily transport Ca^{2+} from the cytosol back into the SR. Keeping the SR Ca^{2+} concentration low is also important in preventing store overload-induced Ca^{2+} release. CASQ is also subject to phosphorylation by casein kinase II, where in the phosphorylated state the protein is able to bind more Ca^{2+} (40). Two amino acid variants within CASQ have been linked to MH, met 87 thr and asp 244 gly (GenBank accession number AB277764.1) (41). Both variants have been shown to have an effect on the structure of the protein with reduced Ca^{2+} binding capacity. Interestingly, the met 87 thr variant has been predominantly identified in patients who also have known variants in RyR1, suggesting that the two variants may work in conjunction with each other to lead to the onset of symptoms. The asp 244 gly variant seems to be a stand-alone variant, however its functional consequence in MH-susceptibility has yet to be determined. CASQ knock out mice have been generated and have been used for functional characterisation where the mice exhibited spontaneous death which was thought to result from emotional stress, something which was more common in male mice. When the mice were exposed to anaesthetics they entered an MH-like episode which was lethal (42). CASQ and RyR1 do not have a direct interaction with each other. Rather, their interaction is mediated by CASQ binding Ca^{2+} and then forming an interaction with the anchoring proteins junctin and triadin in the lumen of the SR (43).

1.4.3.4 Triadin

Triadin mediates the interaction between RyR1 and CASQ, an interaction that only occurs when SR [Ca^{2+}] is low. CASQ will form an interaction with triadin only when it is not phosphorylated; this interaction will ultimately encourage RyR1 to favour the open state and

lead to the release of Ca^{2+} ions from the SR. As the Ca^{2+} concentration in the SR increases, CASQ and triadin will dissociate, encouraging RyR1 to favour the closed state. Knock out studies performed in mice have suggested that triadin is important in the formation of the terminal cisternae and SR volume. The triadin binding site on RyR1 is a region rich in CCD pathogenic variants (44). These variants, particularly the ile 4898 thr variant, have been proposed to interfere with the interaction between the two proteins which as a result have an effect on RyR1 regulation. This may be involved in the loss of function consistent with the CCD phenotype. The ile 4898 thr variant leads to a loss of function in RyR1, which may be due to the loss of triadin binding (10, 45).

1.4.3.5 Junctin

Like triadin, junctin is also an SR membrane spanning protein which interacts with CASQ and RyR1. CASQ in the phosphorylated state in combination with a low luminal [Ca^{2+}] has been reported to interact with junctin (40, 46). This interaction causes RyR1 to favour the closed state preventing Ca^{2+} release from the SR. Knock out studies suggested that junctin has a lesser effect on the organisation of the sarcoplasmic reticulum and cisternae compared to triadin but it does seem to play a role in maintaining Ca^{2+} store size in the SR (47).

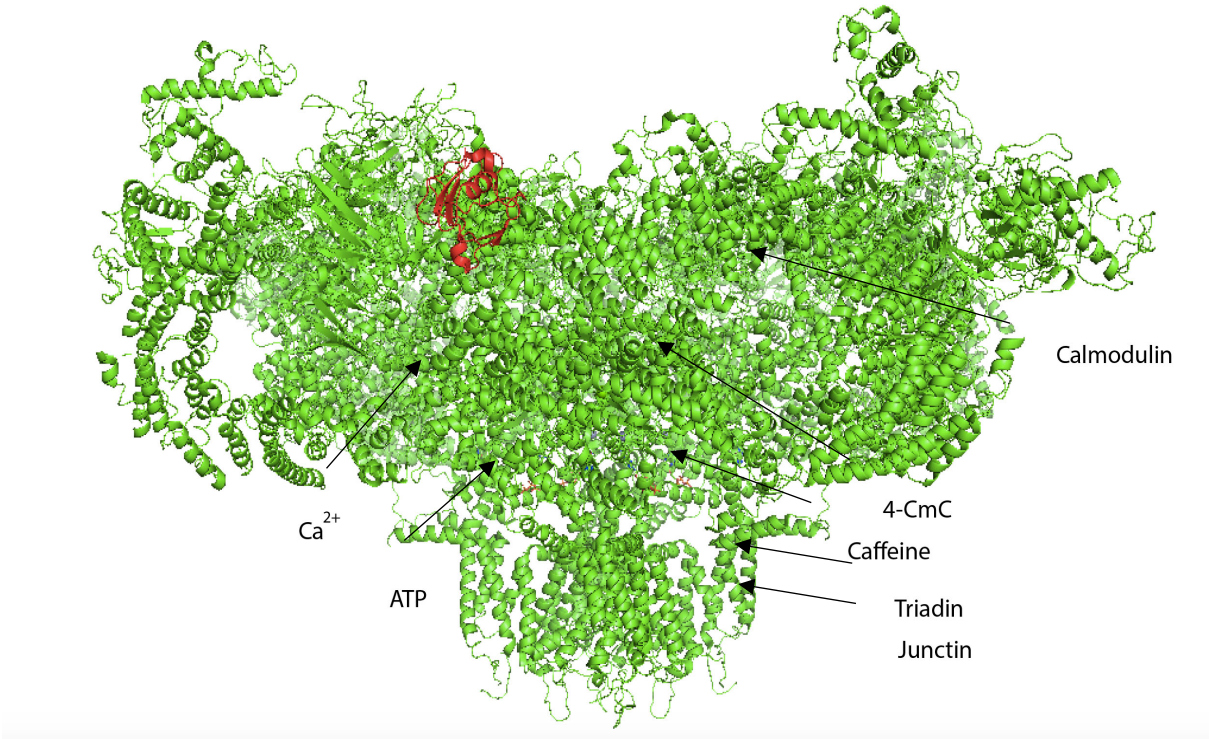

Figure 1.5. Schematic representation of selected ligand and protein interaction sites on the surface of RyR1. The RyR1 tetramer has been represented in green. A single FKBP12 has been coloured in red. The binding sites of Ca^{2+}, ATP, 4-CmC (4-chloro-m-cresol) and caffeine have been identified by arrows. The figure was produced using PyMOL version 2.4.0a0 using the PDB ID 5TAM.

1.4.4 Chemical modulators

The function of RyR1 is also modulated by a number of pharmaceuticals. Halothane, an anaesthetic commonly used in surgery between the 1950's and the 1980's, has been shown to have an effect on RyR1 function *in vitro*. Halothane is no longer commonly used as an anaesthetic, but it is used during the IVCT to diagnose MH-susceptibility (1). The mechanism of action leading to Ca^{2+} release from RyR1 following exposure to halothane has yet to determined. Caffeine is also used in the IVCT and has been previously shown to interact with RyR1 amino acids glu 4238, trp 4717 and ile 4997 (accession number NM_000540.2)(9). It has been suggested that binding of caffeine will cause RyR1 to adopt a primed conformation, whereupon receiving a secondary stimulus the channel will open. As discussed previously in this chapter, the binding of caffeine, ATP and Ca^{2+} have been shown to cause RyR1 to adopt

the open conformation. Four-chloro-m-cresol (4-CmC) is a significant activator of Ca^{2+} release from the SR *in vitro*. Four-CmC can induce Ca^{2+} release from the SR in both MHS and MHN representative cell lines, although it has a significantly higher sensitivity in MHS cells. Four-CmC is commonly used during functional characterisation of RyR1 variants where the RyR1 amino acids gln 4019 and lys 4020 (accession number NM_000540.2) are required for the activation of the channel by the ligand (48). Ryanodine, a metabolite found in the South American plant *Ryania speciosa*, has a high affinity for the open ryanodine receptor. Following the binding of ryanodine, RyR1 will remain locked in the open state. The binding of ryanodine has been utilised for *in vitro* binding assays in which the open probability of RyR1 can be characterised under different conditions (49, 50).

1.5 RyR2

The cardiac isoform of the ryanodine receptor, RyR2, shares significant amino acid identity with RyR1 (appendix 1). However, it doesn't form a physical interaction with DHPR. The protein must rely on cytosolic and SR luminal signals to open and close. The main signal for the opening of RyR2 is increased cytosolic Ca^{2+}, which occurs following the opening of DHPR (51). Similar to RyR1, Ca^{2+} will bind to the cytosolic face of RyR2, leading to its opening in a process referred to as Ca^{2+}-induced Ca^{2+}-release. RyR2 is also regulated by proteins, similar to RyR1, where calmodulin, FKBP12.6, the cardiac isoform of FKBP12, and calsequestrin, among others, are able to both up or down regulate the channel (37, 52). Like RyR1, amino acid variants in RyR2 have the potential to lead to a dysregulation in Ca^{2+} homeostasis within the cell which can be fatal (53). One such disorder is catecholaminergic polymorphic ventricular tachycardia (CPVT) which can be triggered following intense exercise or emotional stress, ultimately resulting in an irregular heartbeat. Many variants shown to be pathogenic for this disorder have a negative effect on the binding of regulatory proteins. For example, the variant arg 2474 ser has been shown to prevent binding of calmodulin to RyR2 (accession number Q29621) (54). The consequence of this variant means that at rest the closed state of RyR2 will not be stabilised. Other variants have been shown to inhibit the binding of the protein FKBP12.6, preventing the negative regulation of RyR2. Other variants have been shown to reduce the threshold for store overload-induced Ca^{2+} release (55). Pathogenic variants cluster

within three regions of RyR2: The N-terminal domain, the central region, and the C-terminal region of the channel. Seven of these variants correspond to RyR1 variants pathogenic for MH (55) (appendix 1). This highlights the importance of these regions of RyR1 and RyR2 and in particular the importance of these amino acids in the proper function of both isoforms to maintain Ca^{2+} homeostasis in their respective tissue. The identification of pathogenic variants within these three defined regions of the channel may be historical in nature. Initially DNA sequencing was expensive and time consuming and as a result, efforts were made to screen regions of the *RYR2* gene where other variants had been previously identified. This resulted in identifying new variants in these three regions, and therefore pathogenic variants in other regions of the gene may have been missed. However, with advancements in sequencing efficiency further additional pathogenic variants could be identified elsewhere in the *RYR2* gene.

Pathogenic variants have also been identified in the cardiac isoform of calsequestrin, which again have a reduced binding capacity for Ca^{2+}, similar to the skeletal muscle isoform (56). This leads to increased luminal [Ca^{2+}] and as in the case of RyR1, is predicted to result in the premature release of Ca^{2+} from the SR resulting from store overload-induced Ca^{2+} release, leading to the CPVT phenotype (57).

1.6 Functional characterisation of MH associated variants

1.6.1 *In vitro* contracture test

The *in vitro* contracture test is currently used as the gold standard for the diagnosis of MH in the U.K, Europe, Australia, South Africa and New Zealand. However, there are variations in the testing protocols used throughout the world (1). In North America the test is called the caffeine halothane contracture test (CHCT) and uses different concentrations of caffeine resulting in different contracture thresholds being utilised to diagnose a patient as being MHS (58). With respect to the CHCT, a contracture strength greater than 0.3 g in the presence of caffeine concentrations up to 2 mM is considered to be positive as well as a contracture strength of 0.7 g in the presence of 3 % halothane. This is compared to the IVCT where a

contracture strength of 0.2 g is considered positive in the presence of caffeine concentrations up to 2 mM, and a contraction strength of 0.2 g in halothane concentrations up to and including 3 % halothane (1). Both tests will broadly describe a patient as being MHS or MHN, however the test doesn't describe the role of a specific variant in MH-susceptibility. Both tests are invasive, requiring the extraction of a large sample of muscle removed by biopsy under anaesthesia. This procedure is also expensive, can be traumatic and also painful for the patient involved. Typically, it is not recommended that children undergo this procedure which can also make diagnosing younger patients difficult.

There is a shift towards establishing a DNA screening test which can act as an alternative to the contracture tests for families with a known pathogenic variant. Before a variant can be considered as being pathogenic however, it must first be shown to segregate with MH in two independent families (1). As a number of MH-linked variants have only been identified in one family the acceptance of the variant's pathogenicity by the governing body, the European Malignant Hyperthermia Group, can be problematic. The variant must also be shown to alter Ca^{2+} homeostasis consistent with MH, within an accepted controlled system. A range of *in vivo* and *ex vivo* systems are currently being used to characterise these variants. Using cell-based assays, cells can be labelled with a Ca^{2+} sensitive dye, with unique fluorescent properties in both the presence and absence of Ca^{2+}. Following the release of Ca^{2+} from the SR, changes in fluorescence intensity can be measured and attributed to changes in cytosolic Ca^{2+} concentrations.

1.6.2 Human embryonic kidney cells

Human embryonic kidney cells (HEK293T) are easily cultured and commonly used as a heterologous system to characterise *RYR1* variants (59). These cells do not express endogenous functional RyR1 and must be transfected with the *RYR1* cDNA before any functional analysis can be performed. HEK293T cells are non-contractile and do not express a number of other proteins required for muscle contraction including the DHPR. As a result, the expressed RyR1 is present in a system isolated from a number of other proteins that it would normally interact with and may not be under the same control as it would in a muscle cell.

Four-CmC and caffeine are commonly used to induce Ca^{2+} release through the recombinantly expressed RyR1 channel localised to the endoplasmic reticulum. Concentration-dependent Ca^{2+} release in wild type RyR1 and variant containing channels are compared, assessing the variant's ability to alter Ca^{2+} homeostasis. Due to the sheer size of the *RYR1* cDNA, producing constructs containing a specific variant can be very difficult and at times be very time consuming. Following transfection, the cells will be essentially homozygous for the variant. HEK293T cells can be functionally characterised following transient expression, a process which requires transfection with the *RYR1* cDNA prior to each functional assay (60). The HEK293 FLP-in cell line is also commonly used (59) where stably expressing cell lines are created with RyR1 containing the variant of interest under the control of an inducible promoter. This can save time and reagents compared to transient expression systems. In addition, cDNAs encoding regulatory proteins can be introduced using transient expression and assessment of their effects on Ca^{2+} release.

1.6.3 Lymphocytes

Lymphocytes are patient-derived cells which can be purified from a blood sample and subsequently immortalised (61). These cells express RyR1, with a proposed involvement in signal transduction, where it is thought RyR1 acts in combination with the main Ca^{2+} release channel the inositol triphosphate receptor, also located on the SR membrane, ultimately changing the cytosolic Ca^{2+} concentration leading to changes in gene expression. Once again, like HEK293T cells, lymphocytes will release Ca^{2+} from the ER in a concentration-dependent manner (62). Lymphocytes, being non-contractile, do not express a number of other proteins involved in EC-coupling. Lymphocytes also have a smaller endoplasmic reticulum compared to the sarcoplasmic reticulum of a skeletal muscle cell and as such have a smaller Ca^{2+} store to be released following RyR1 opening. Alternative splicing of the *RYR1* mRNA also occurs in lymphocytes; exon 70 is not present, resulting in the amino acids 3480-3485 (NM_000540.2) being absent from the protein (63). The loss of these amino acids can result in a change in structure of the central domain and may lead to cell specific regulation of RyR1 in lymphocytes. While RyR1 is still functional, variants within this region cannot be characterised in this system. In addition, genetic background is patient specific so any changes in Ca^{2+}

handling cannot be directly attributed to the RyR1 variant and could be due to variants in other proteins. This is a major disadvantage of using *ex vivo* lymphocyte-based assays for functional characterisation.

1.6.4 Myotubes

Myoblasts are primary muscle cells that can be extracted from a muscle tissue sample and then differentiated into myotubes (64). Myotubes express both RyR1 and DHPR which co-localise within the cell and as a result are a more physiologically relevant system for the characterisation of Ca^{2+} homeostasis (65). Like HEK293T cells and lymphocytes, myotubes release Ca^{2+} in response to agonists in a well-defined concentration-dependent manner in response to RyR1 agonists. However, they do not truly represent intact muscle as they do not contain optimally formed terminal cisternae, a critical feature in the mass release of Ca^{2+} in intact muscle cells (66). While the cells express a number of the proteins involved in the formation of this cellular structure, its establishment is not complete until the cells further differentiate into muscle fibres. Myoblasts also have the same genetic background as the patient they have been derived from, which limits their use in functional studies of single amino acid variants in RyR1.

1.6.5 Knock in mice

Knock in mice have also been used to characterise RyR1 variants. Following the generation of knock in mice, contracture strength can be measured directly in the mice or myoblasts can be extracted from the animal and characterised as described above (67-69). The generation of an animal model allows for the characterisation of the variant in a truly physiologically relevant system. In this case, the variant is expressed in fully differentiated muscle cells in the presence of all possible protein and ligand modifiers. The variant can also be assessed for functional effects in both heterozygous and homozygous mice. The use of animal models, while being a potentially relevant system, has several key limitations. These include obtaining

animal ethical approval, appropriate housing and ensuring the mice are not placed under excess stress as stress is known to cause premature death in some animal models of MH (70). The generation of mouse lines is also time consuming, technically difficult, expensive and moreover may not be an accurate model of the human situation.

Myoblasts prepared from the dyspedic (RyR1 knock out) mouse model are also commonly used in the characterisation of RyR1 variants (45, 71, 72). The *RYR1* cDNA must be introduced into the cells; a process commonly performed by either virial transduction or micro injection due to the difficulties associated with transfecting myoblasts. Following expression, RyR1 is expressed in a system closely resembling its native conditions within a muscle cell. The use of microinjection in this cell line also allows for the introduction of two separate vectors, each containing a different variant. In this case RyR1 variants can be characterised in a heterozygous system.

1.6.5 Electrophysiology

Electrophysiology has also been used to characterise Ca^{2+} release through RyR1. Single channel experiments have been performed where an RyR1 channel was extracted from an SR vesicle preparation and incorporated into a planar lipid bilayer (73). These techniques provide an insight into the flow of Ca^{2+} ions through RyR1 following stimulation and characterise how ligands effect RyR1 function. Patch clamp electrophysiology has also been used to characterise RyR1 function (45, 74). In this case, Ca^{2+} movement into the cytoplasm was measured in the context of the whole cell, the voltage across the cell membrane was controlled prior to the activation of RyR1. Following the activation of RyR1 the ion gradient across the cell membrane was measured. These experiments can provide an insight into the greater regulation of RyR1 as all protein and ligand modulators are present at the time of stimulation. In this case, the cells do not need to be stained with a dye as in other cell-based assays. Instead, changes in electrical current across the membrane are measured using electrodes. Open and closed probabilities can also be calculated as a read out of functional effects of variants. While all of these systems have been used with some success to characterise variants, a bottle neck of uncharacterised variants remains.

1.7 Structural characterisation of RyR1

The functional characterisation of variants may confirm if a variant is able to alter Ca^{2+} homeostasis, thus providing an insight into the potential role of a variant in the onset of MH. These methods however provide limited insight into the mechanism by which the variant alters RyR1 function. The structural characterisation of specific amino acid variants would provide an insight into changes within the tertiary structure of RyR1, potentially explaining why a variant is pathogenic for MH. The full length (2.3 MDa) RyR1 tetramer has been structurally characterised by cryo electron microscopy (EM) with an overall resolution of 3.8 Å (9). Cryo EM involves the purification of protein from skeletal muscle, an electron dense light is shone on the protein and the absorption of the electrons is measured and interpreted into a protein structure. The central regions of the channel surrounding the pore were resolved with high resolution where specific amino acid side chains could be visualised. The periphery of the channel was less well resolved, with a resolution of approximately 7 Å. While most amino acids could be identified at this resolution, in some cases only the secondary structure and domain boundaries could be visualised, which indicates that the channel has more freedom of movement compared to the central channel regions which are likely to be locked in place. The channel was structurally characterised in the closed, primed and open states where it was noted that the channel undergoes a substantial conformational change during opening. The transition from one conformation to another is a concerted effort, where proposed domains within RyR1 move relative to each other. As the channel transitions from the closed state to the primed conformation, following the binding of ATP or Ca^{2+}, the domains within the cytoplasmic region of the channel move relative to each other, while the channel pore remains closed. In this state, the channel has adopted a structure where upon receiving a secondary stimulus it can open easily. While making the transition to the open state, the pore dilates and isoleucine 4937 (UniProt accession number p11716.B, the equivalent residue in human RyR1 is ile 4938 accession number NM_000540.2), which blocks Ca^{2+} from passing through the channel, rotates out of the pore allowing the passage of the ion through the channel. The overall structure of RyR1 in all three states consists of a number of compact domains interspersed in a network of alpha helices (figure 1.3).

Some of the domains within RyR1 have been structurally characterised by X-ray crystallography. The first being the greater N-terminal domain of rabbit RyR1, amino acids 1-559 (GenBank accession number NP_001095188.1), represented in blue in figure 1.3 (75). This region of RyR1 was shown to consist of three smaller defined domains which are now referred to as A, B and C. Following the structural characterisation of MH pathogenic variants within this region, the variants were, in most cases, located at the boundaries of the domains and had little or no effect on the structure of the domain. It is believed these variants may interfere with inter domain interactions disrupting the movement of two domains relative to each other. The amino acids 121-179 (the equivalent amino acids in human RyR1 are 120-178, accession number NM_000.540.2) were shown to form interactions with the central regions of the channel (figure 1.6) (9), which have been proposed to be essential in the stabilisation of the channel in both the open and closed states.

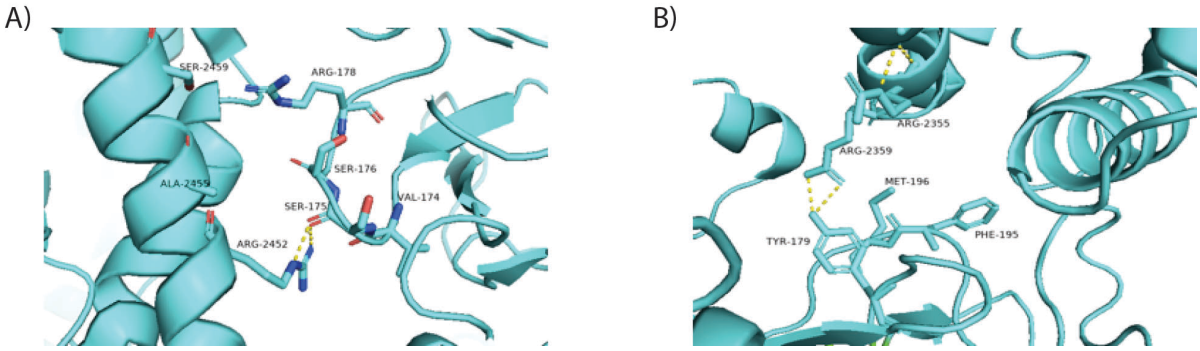

Figure 1.6. An example of the interface between the N-terminal domain and the central region of RyR1. A) Representation of the interaction between arg 2452 and ser 176. B) Representation of the interaction between arg 2359 and tyr 179. The figure was produced using the PyMOL software version 2.4.0a0 using the PDB ID 5TB1. Yellow lines indicate hydrogen bonds between atoms. The general protein and amino acid structure are coloured in pale blue. Dark blue represents regions of amino acids with a positive charge. Red represents regions of amino acids with a negative charge. Numbering refers to the rabbit RyR1 and the structure was produced using PyMOL version 2.4.0a0. The PDB ID 5TB1 was used to model the closed state, while the PDB ID 5TAM was used to model the open state.

Domains A and B of the recombinantly expressed protein were shown to adopt the same structure as the full-length channel (9). The C-terminal alpha helices of domain C adopted a slightly different structure compared to the domain in the context of the full-length channel. The difference in structure may result from the expression of the domain in isolation from

the rest of the protein. Alternatively, several other factors may influence the folding of the protein including: the use of an *E. coli* host, the presence of the maltose binding protein and $His_{(6)}$ purification tags as well as the likely presence of inclusion bodies (75).

The SPRY (SP1/RyR1 homology) domains 1 and 2, named for their high amino acid identity shared with the protein SP1, have also been structurally characterised (76-78). The domains were shown to be rich in beta sheets and, like the N-terminal domain, pathogenic variants were shown to be located at the boundaries of the domains, where they have once again been proposed to have an effect on inter domain interactions. The SPRY 1 domain has been implicated in the binding of FKBP12 where the amino acids phe 674 and leu 675 (accession number NP_001095188.1) have been shown to be essential in the interaction between the two proteins. Pathogenic variants within this domain have been proposed to interfere with the interaction between these two proteins, and as a result the closed state of the channel is less well stabilised and may lead to the onset of MH. The SPRY2 domain (RyR1 amino acids 1070-1246, GenBank accession number NP_001095188.1) had a similar distribution of MH-linked variants which were again shown to localise to the extremities of the domain.

The RyR1 domain Ry 3&4 is the final domain to have been structurally characterised by X-ray crystallography (79). This domain consists of amino acids 2734-2940 and includes the amino acid ser 2843 which is susceptible to phosphorylation by protein kinase A and calmodulin dependent protein kinase (35). The phosphorylation of this serine residue has been shown to inhibit binding of FKBP12. As FKPB12 binds elsewhere in RyR1, it is likely that long-range structural changes following the modification result in loss of binding. As for other regions of RyR1 characterised by X-ray crystallography, pathogenic variants were located at the extremities of the domain and are likely to have an effect on interdomain interactions.

A proposed domain within RyR1, the helical domain 1 (HD1), has yet to be structurally characterised in its entirety. A small region within the proposed domain has been characterised by nuclear magnetic resonance spectroscopy. This region has been entitled the domain peptide 4 (DP4) domain and corresponds to the RyR1 amino acids leu 2442 - pro 2477 (accession number NM_000540.2) (80). DP4 is of particular importance to the overall function of RyR1 as it has been shown to interact with the N-terminal domain with the amino acid arg 2452 forming a hydrogen bond with ser 175 (9) (figure 1.7 A). The N-terminal domain and

HD1 move relative to each other during the opening of the channel, the amino acids at the interface of the two domains likely play an important role in tethering the domains together and allowing them to move relative to each other. Interestingly, the mutation of arg 2452 to trp has been confirmed as being pathogenic for MH; highlighting the importance of the interaction between the two domains (60).

The greater HD1 domain (amino acids 2145-2735) contains 18 of the variants confirmed to be pathogenic for MH (4). The domain is proposed to be particularly important in the function of RyR1. Amino acids within this region are known to be subject to posttranslational modification; where the amino acids cys 2326 and cys 2363 within this region have been shown to be subjected to oxidation following the production of reactive oxygen species in working muscle (30). Once oxidised, the cysteine residues can form disulphide bonds with other oxidised cysteine residues in RyR1 locking the channel in the open state. They can also form covalent bonds with oxidised molecules within the cell. In this case, the residues have been shown to bind S-glutathione, encouraging the channel to favour the open state. The corresponding region of RyR2 has also been implicated in the binding of calmodulin (37) and the high amino acid identity shared between the two regions (appendix 1) may suggest that this region of RyR1 is also important in the interaction between the two proteins. The domains structurally characterised by X-ray crystallography represent 22.5 % of the total protein, suggesting this approach is feasible in the structural characterisation of the remaining RyR1 domains.

1.7 Motivation for the research described in this thesis

Changes in the tertiary structure resulting from pathogenic RyR1 variants within the helical domain 1 have not yet been fully characterised. The pathogenic variants can be modelled in the previously determined structure of rabbit RyR1 *in silico* and a resulting structural change can be predicted. However, the change in structure is simply a prediction; to truly characterise a variant in the context of the full-length RyR1, the variant containing channel would need to be extracted from a tissue sample. Ethical approval to perform this work can be difficult to obtain as pathogenic variants predominantly identified in humans are not commonly found

in other organisms. Thus, the tissue sample would have to come from human skeletal muscle tissue. A large amount of skeletal muscle tissue is required for the purification of enough RyR1 for the structural characterisation by cryo-EM (9). During the recent characterisation of rabbit RyR1, 100 g of muscle tissue was used for protein purification. Even more than this may be needed to initially optimise the purification protocol. The recombinant expression of RyR1 would provide a less invasive source for the purification of the protein. Due to the size of RyR1, the protein cannot be expressed in its entirety in an *E. coli* host. However, previous studies have used expression of defined domains which can adopt the correct conformation for structural characterisation (76, 79, 81). Bacterial cells are easy to grow and once a cDNA fragment has been cloned into an expression vector, variants can be introduced by site-directed mutagenesis, with subsequent expression and purification for structural and biochemical studies. Cloning, expression and purification of HD1 would facilitate structural and biochemical studies and subsequent characterisation of MH-associated variants within this region of RyR1.

One of the major current objectives in MH based research is to establish a comprehensive library of variants known to be pathogenic for MH, providing an alternative to the IVCT for more members of the population. The currently used methods for the characterisation of proposed variants can be costly in terms of time and reagents. In addition, several systems do not reflect muscle physiology and others require the use of animal models. The use of more modern and inexpensive protocols could be implemented to streamline the process making the characterisation more efficient. The utilisation of the CRISPR Cas 9 genome editing tool is becoming more commonly used worldwide for the targeted editing of genomes. Initially the process was reported to be inefficient, however, with its widespread use there has been an increased drive towards increasing efficiency. Patient extracted myoblasts could be subjected to genome modification utilising CRISPR Cas 9 to determine if the process can be utilised efficiently to characterise *RYR1* variants as an alternative method to those currently used. This would provide a more physiologically relevant system without using animal models or a large muscle biopsy as myoblasts could be isolated from patient needle biopsy samples.

1.8 Hypothesis of the study

1.8.1 Structural and biochemical characterisation of RyR1 variants can be achieved following cloning, expression and purification of the RyR1 HD1 domain

1.8.1.1 Objectives

1. Clone the RyR1 helical domain 1 for recombinant expression in an *E. coli* host.
2. Purify the recombinant protein following expression.
3. Crystallise the purified HD1.
4. Structurally characterise the HD1 using X-ray crystallography.
5. Determine structural changes induced by pathogenic variants, either experimentally or *in silico*.

1.8.2 CRISPR Cas 9 genome editing can be used in patient derived myoblast cell lines to introduce *RYR1* variants for functional characterisation RyR1 variants (proof of principle study)

1.8.2.1 Objectives

1. Isolate primary myoblasts from muscle tissue biopsies.
2. Immortalise primary myoblasts using a lentiviral system.
3. Characterise Ca^{2+} homeostasis in response to RyR1 agonists in both primary and immortal myoblasts.
4. Introduce the MH pathogenic variant c.14497C>T into the genome of an immortal myoblast cell line.
5. Functionally characterise the edited cell line in comparison to the non-edited cell line.

2. Materials Methods

2.1 Materials

Listed below are all products and kits utilised. All general laboratory chemicals were research grade or equivalent.

Item	Supplier	Catalogue number
Ampicillin	Sigma	A9518
Chloramphenicol	Sigma	C-0378
Charge switch^{R} Pro plasmid mini prep kit	Invitrogen	cs30050
Kapa Biosysystems 2x HiFi hotstart ready mix	Kapa Biosystems	KM2605
ZymoResearch one stepTM PCR inhibitor removal kit	Zymo	D6030
Restriction endonucleases	New England Biolabs	
Zymoclean gel DNA recovery kit	Zymo	D4008
T4 DNA ligase	Invitrogen	15224-017
cOmplete EDTA free protease inhibitor	Roche	11836170001
Amylose magnetic beads	New England Biolabs	E8035s
40 % acrylamide/bis solution 29:1	Bio-Rad	1610146
Tev protease	Sigma	T4455-1KU
Factor Xa protease	New England Biolabs	P8010s
Protein LoBind tube 0.5 mL	Eppendorf	0030108.094
MBPTrap^{TM} HP	GE life sciences	28-9187-80
Superdex 200	GE life science	28990944
HisTrap^{TM} FF	GE life science	17525501

Hi trap Phenyl FF (HS)	GE life science	17135301
Q Hi Trap™ FF	GE life science	17505301
FugeneR HD transfection reagent	Promega	28-9322-47
CD82-Biotin	Miltenyi biotech	130-101-300
Anti-biotin	Miltenyi biotech	130-090-485
34c monoclonal RyR1 antibody	ThermoFisher	MA3-925
Viva spin, 10 KDa MWCO	GE health care	28-9322-47
Anti-tubulin	Abcam	ab18207
Anti-desmin	Invitrogen	PA5-16705
Anti-myosin heavy chain	Santa Cruz	F1652
Anti-GST	Santa Cruz	sc-459
BM chemoluminescence blotting substrate (POD)	Sigma	11500694001
Prolong gold	Invitrogen	P36931
Tissue culture flasks	Thermo scientific	
entactincollagen IV-laminin	Millipore	08-110
Foetal bovine serum	Sigma	F8067-500 ml
Penicillin / streptomycin	Gibco	15140-122
0.25 % trypsin – EDTA	Gibco	25200-072
Collogenase B	Roche	11088815001
Dispase	Roche	04942078001
Easy strainer™,70 µm,	Greiner Bio-one	YSA0000215
Fibroblast growth factor	Sigma	F029125
MS columns	Miltenyi biotech	130-042-201
ReliaPrep™ syringe filter single use 0.45 µm	Ahlstrom	760506
Viral titration kit	ABM	LV900
Ssofast Evagreen mix	Bio-Rad	64248934
480 master mix	Roche	04909631001

Hygromycin B	Invitrogen	10687010
Geneticin	Gibco	15710-064
Pluronic acid	Sigma	P2443
Fura 2 AM	Invitrogen	F1221
P5 Primary cell solution nucleofection kit	Lonza	PBP5-00675
AmexaTM P5 primary cell 4D nucleofectorTM x kits 32 RCT	Lonza	v4xp-5037
Dexamethasone	Sigma	D4902-25mg

2.2 Methods

2.2.1 Preparation of *E. coli* cells for vector propagation and recombinant protein expression

2.2.1.1 Preparation of chemically competent *E. coli* cultures

Single *E. coli* colonies for DH5α, BL21 DE3 or Rosetta 2 ™ were picked from a Luria Bertani (LB) agar plate and grown in an LB broth overnight at 37 °C with constant shaking at 220 rpm. For Rosetta 2 ™ the LB contained 33 µg/mL chloramphenicol. One mL of this culture was used to inoculate a 100 mL LB broth which was then incubated at 37 °C until the culture reached an $O.D_{600}$ of 0.8. The cells were harvested by centrifugation at 7000 rcf for 15 minutes and resuspended in 10 mL ice cold 0.1 M $CaCl_2$ and incubated at 4 °C for twenty minutes. The cells were then harvested by centrifugation at 7000 rcf for 15 minutes and suspended in 3.4 mL ice cold 0.1 M $CaCl_2$ followed by incubation at 4 °C overnight with constant shaking. Fifty % (v/v) glycerol was added to the cell mixture to a final volume of 4 mL and the cells were dispensed into 50 µL aliquots and stored at -80 °C.

2.2.1.2 Transformation of competent *E. coli*

Chemically competent *E. coli* glycerol stocks stored at -80 °C were defrosted on ice. Fifty ng of vector DNA or a ligation solution as described in section 2.2.4.6 were added to the *E. coli* solution and incubated on ice for twenty minutes. The cells were heat shocked at 42 °C for 90 seconds and placed on ice for ten minutes. For DH5α and BL21 (DE3) the cells were then plated on LB agar containing 1 µg/mL ampicillin, while Rosetta 2^{TM} cells were plated on LB containing 1 µg/mL ampicillin and 33 µg/mL chloramphenicol. Plates were incubated upside down in a 37 °C incubator overnight.

2.2.1.3 Purification of plasmid DNA from *E. coli*

Single colonies of *E. coli* (DH5α) cultures containing a plasmid were picked and grown in 5 mL LB overnight at 37 °C with constant shaking. The cells were harvested by centrifugation at 7000 rcf for 15 minutes. The Invitrogen HiPure plasmid isolation kit, based on the alkaline lysis plasmid purification method, was used to purify the plasmid DNA according to the manufacturer's instructions. DNA was eluted in a final volume of 50 µL TE (10 mM Tris, 1 mM EDTA pH 8.0).

2.2.3 Gel electrophoresis

2.2.3.1 Agarose gel electrophoresis for DNA

Agarose was dissolved in 1 x TAE (4.84 g Tris, 1.14 mL glacial acetic acid, 2 mL 0.5 M EDTA, pH 8 final volume 1 L in purified water) to a concentration of 0.8 % (w/v) with heating. The agarose solution was cooled to approximately 55 °C and was then poured into a gel casting apparatus. DNA was separated by electrophoresis in 1 x TAE buffer at 100 mV for one hour. Gels were stained in 0.5 µg/mL ethidium bromide and DNA visualised under UV light using the Uvitec Cambridge Uvidoc HD6.

2.2.3.2 Polyacrylamide gel electrophoresis of separation of proteins

Polyacrylamide gels were prepared using the Bio-Rad mini protean® gel casting system using the components listed in tables 2.1 and 2.2

The resolving gel was used to separate proteins based on molecular mass. Ten % gels were cast to separate proteins with a molecular mass ranging between 40 and 150 KDa. Seven % gels were cast to separate any protein with a larger molecular mass.

	7 % acrylamide	10 % acrylamide
Water	5.5 mL	4.9 mL
40 % Acrylamide/Bis solution 29:1	1.9 mL	2.5 mL
1.5 M Tris-HCl (pH 8)	2.5 mL	2.5 mL
10 % SDS	100 µL	100 µL
10 % APS	100 µL	100 µL
TEMED	20 µL	20 µL

Table 2.1. List of components used to prepare the resolving gel for polyacrylamide gel electrophoresis.

The stacking gel was the same in all SDS polyacrylamide gels, the components of which are summarised in table 2.2.

	4 % acrylamide
Water	3.15 mL
40 % Acrylamide/Bis solution 29:1	500 µL
0.5 M Tris-HCl (pH 6.8)	1.25 mL
10 % SDS	50 µL
10 % APS	50 µL
TEMED	10 µL

Table 2.2. List of components used to prepare the stacking gel for polyacrylamide gel electrophoresis

Proteins were separated at 120 mV and stained in Coomassie blue (0.1 % w/v Coomassie blue-R250, 45 % methanol, 10 % glacial acetic acid) for 10 minutes. Excess dye was washed away

using several washes in fresh destain (10 % methanol, 10 % glacial acetic acid) and protein bands were visualised under UV light using the Uvitec Cambridge Uvidoc HD6.

2.2.3.3 Polyacrylamide gel electrophoresis for separation of DNA

A 10 % polyacrylamide gel was used to separate DNA smaller than 600 bp, gels were prepared using the Bio-Rad mini protein gel casting system the components of which have been summarised in table 2.3.

	10 % acrylamide
Water	5.5 mL
40 % Acrylamide/Bis solution 29:1	2.5 mL
50 x TAE	200 µL
10 % APS	100 µL
TEMED	20 µL

Table 2.3. List of components used to prepare polyacrylamide gels for the separation of DNA

DNA was separated in 1 x TAE buffer at 100 mV for ninety minutes. DNA was stained in 0.5 µg/mL ethidium bromide and visualised under UV light using the Uvitec Cambridge Uvidoc HD6.

2.2.4 Construction of expression vectors

2.2.4.1 Quantification of DNA and protein concentration

The Denovix DS-11FX spectrofluorometer was used to determine the concentration of DNA, RNA and protein samples. The instrument was set to zero using the buffer the sample was dissolved in. For DNA and RNA, the absorbance ratio of 260/280 nm was monitored to ensure purity, where a value of 1.8 and 2 is considered a pure sample for DNA and RNA respectively. Concentration of DNA and RNA was determined using the absorbance at 260 nm. Protein concentrations were determined using the absorbance at 280 nm.

2.2.4.2 PCR amplification of DNA

The Kapa biosystems 2x HiFi hot start ready mix was used to amplify DNA by PCR in combination with specific primers (summarised in appendix 2.2 and 3.1). The polymerase ready mix was diluted according to the manufacturer's instructions. Temperature cycling conditions were optimised for each primer pair. A general cycling protocol has been summarised as follows: Initial denaturation at 95 °C for five minutes; amplification for thirty cycles at 95 °C for 30 seconds, 57-65 °C for 15 seconds, 72 °C for one minute per 1000 base pairs. The final amplification was at 72 °C for seven minutes. The purity of the PCR product was assessed by agarose gel electrophoresis. The annealing temperatures for each primer used are listed in appendix 2.2

2.2.4.3 PCR product purification

The ZymoResearch, OneStep™ PCR inhibitor removal kit was used to purify PCR products following the manufacturer's instructions. A specially designed column was used to separate the PCR product from the excess primers and polymerase following a centrifugation protocol. The purified PCR product was eluted in a final volume of 50 µL TE and stored at -20 ° C. The progression of the purification was analysed by agarose gel electrophoresis.

2.2.4.4 Restriction endonuclease digestion

Restriction endonuclease digestion was performed to either confirm the identity of vectors or to digest vectors and DNA fragments for subsequent cloning. Restriction endonuclease digests were prepared in 1.5 mL microfuge tubes following the instructions of the manufacturer and buffers provided in a final volume of 20 µL. Digests were performed at the

recommended temperature for one hour. The efficiency of the digestion was assessed by agarose gel electrophoresis.

2.2.4.5 Purification of DNA from an agarose gel

The ZymoResearch DNA gel extraction kit, based on the crush gel method, was used to purify DNA fragments (prepared by restriction endonuclease digestion) from agarose gels in preparation for subsequent cloning. The manufacturer's instructions were followed, and DNA was eluted in 8 µL of water, the yield was assessed by agarose gel electrophoresis.

2.2.4.6 Construction of expression vectors

A desired DNA fragment was ligated into a target vector using T4 DNA ligase and the supplied buffers from Invitrogen. The insert:vector molar ratio of 3:1 and 100 ng vector DNA was used in all cases. The amount of insert DNA varied to maintain the desired molar ratio. The ligation mixture was incubated at 16 ° C overnight before being used to transform *E. coli*.

2.2.4.7 Sanger DNA sequencing

Sanger sequencing was performed using the capillary ABI3730 Genetic Analyser with BigDye^{TM} Terminator Version 3.1. The sequencing analysis was carried out by the Massey Genome Service to confirm the identity of plasmid DNA and PCR products.

2.2.5 Recombinant expression and purification of RyR1$_{(2091-2708)}$

2.2.5.1 Recombinant protein expression

E. coli cells (BL21 DE3 and Rosetta 2^{TM}) transformed with expression vectors were grown in 50 mL LB containing appropriate antibiotics (described in section 2.2.1.2) to an O.D$_{600}$ of 0.6. To encourage the expression of host chaperone proteins, *E. coli* cultures were placed on ice for twenty minutes, ethanol was added to a concentration of 2 % (v/v) and the cells were incubated at 18 °C with constant shaking at 220 rpm for 30 minutes. To induce expression IPTG was added to the cells to a final concentration of 0.1 mM followed by incubation at 18 °C for 16 hours with constant shaking at 220 rpm. Cells were harvested by centrifugation at 7000 rcf for fifteen minutes at 4 °C. The cells were resuspended in 1 mL lysis buffer (10 mM HEPES pH 7.4, 140 mM NaCl, 2.8 mM KCl, 1 mM $MgCl_2$, 10 mM glucose, 1 mM DTT, 1 mM EDTA, 1 x cOmplete mini EDTA free protease inhibitor) and sonicated for three bursts of 10 KHz for ten seconds using a 2 mm probe during which time the cells were kept on ice. The cell lysate was centrifuged at 17,000 rcf for ten minutes at 4 °C. Soluble protein was collected in the supernatant, with insoluble protein and cell debris remaining in the pellet.

2.2.5.2 Purification of recombinant protein using an amylose conjugated agarose

The pMALp2g or pMALp5x vectors containing *RYR1* cDNA fragments were expressed in either BL21(DE3) or Rosetta 2^{TM} cells in 200 mL LB. The cells were harvested and lysed by sonication at 10 KHz as above for ten seconds. The soluble fraction was incubated with 50 µL of an amylose-conjugated agarose resin for one hour at room temperature with constant end over end rotation. The resin was collected by centrifugation at 2000 rcf for 4 minutes and then washed by resuspension in 1 mL lysis buffer and again centrifuged at 2000 rcf. The resin was then washed by resuspension in 1 mL high ionic strength buffer (20 mM Tris HCl pH 7.4, 500 mM NaCl, 1 mM DTT, 1 mM EDTA) and centrifuged at 2000 rcf between washes. In preparation for protease digestion the resin was washed in 2 mL protease digestion buffer (20 mM Tris HCl pH 7.4, 140 mM NaCl, 0.5 mM EDTA).

2.2.5.3 Protease digestion of a MBP-tagged RyR1 HD1 while bound to the amylose conjugated agarose

The amylose resin (as prepared in section 2.2.5.2), following batch purification of the MBP-tagged RyR1 region, was resuspended in 50 µL of protease digestion buffer (20 mM Tris HCl, 100 mM NaCl, 0.5 mM EDTA); 1 unit of either tobacco etch virus (TEV) or Factor Xa protease was added to the solution and then incubated at 30 °C for 3 hours with constant end over end rotation. The resin was pelleted by centrifugation at 2000 rcf for five minutes and the supernatant collected. After washing the resin in 2 mL protease digestion buffer it was pelleted by centrifugation at 2000 rcf for five minutes. The supernatant containing the cleaved protein was collected and stored at - 20 °C.

2.2.5.4 Protease digestion of a MBP tagged RyR1 region following elution from the amylose conjugated resin

Following batch purification, as described in section 2.2.5.2, the amylose resin was resuspended in 50 µL protease digestion buffer containing 100 mM maltose and incubated at room temperature for five minutes. The resin was pelleted by centrifugation at 2000 rcf for five minutes and the protein containing supernatant was collected, this was repeated eight times with the supernatant being collected following each wash. One unit of either TEV or factor Xa protease was added to each of the eluted protein fractions and then incubated at 30 °C for 3 hours. The progress of the digestion was analysed by SDS polyacrylamide gel electrophoresis.

2.2.5.5 Mass spectrometry

Protein samples were separated by SDS-PAGE, the gel was fixed in 10 % (v/v) acetic acid 40 % (v/v) methanol for one hour at room temperature and then washed three times in distilled water. The gel was stained overnight in colloidal Coomassie blue (75.6 mM ammonium

sulphate, 2 mL 5 % Coomassie G250, 1.2 mL phosphoric acid and water to a final volume of 100 mL), then destained in three washes of distilled water at 60 °C. Protein bands were excised from the gel and all stain was removed using three 30-minute washes in 200 µL 50 mM ammonium bicarbonate, 50 % methanol v/v at 37 °C with a final wash in 200 µL 80 % acetonitrile. The supernatant was removed and the gel pieces in Eppendorf LoBind tubes were dried in a centrifugal evaporator at room temperature until all liquid was removed. The gel pieces were rehydrated in 50 µL 10 mM DTT in 50 mM ammonium bicarbonate and incubated at 37 °C for one hour. The gel pieces were then washed three times in 200 µL 50 mM ammonium bicarbonate and once in 200 µL 80 % acetonitrile followed by drying in a centrifugal evaporator as above. The gel pieces were rehydrated in 50 µL 0.5 mM iodoacetamide in 50 mM ammonium bicarbonate for one hour in the dark. The gel pieces were washed three times in 200 µL 50 mM ammonium bicarbonate, once in 200 µL 80 % acetonitrile and then dried in a centrifugal evaporator as above. Finally, the gel pieces were rehydrated in enough 15 ng/µL trypsin in 50 mM ammonium bicarbonate to submerge the gel pieces and incubated overnight at 37 °C. The supernatant was collected and protein was eluted following an incubation at room temperature for fifteen minutes from the gel in 60 µL 50 % acetonitrile, 5 % formic acid. Any remaining protein in the gel pieces was eluted following a fifteen minute incubation in 60 µL 80 % acetonitrile, 0.1 % formic acid. The eluted fractions were pooled and reduced in volume to 20 µL in a centrifugal evaporator and stored at -80 °C until analysis was performed.

The mass spectrometry and analysis was performed by Trevor Loo, SFS, Massey University. Digested samples were separated by on-line reversed-phase chromatography using a Dionex nanoLC system (ThermoFisher Scientific) with a reversed-phase peptide trap and a reversed-phase capillary analytical column. The liquid chromatography system was coupled on-line to a QExactive Plus mass spectrometer equipped with a higher-energy collision-induced dissociation (HCD) collision cell, an Orbitrap mass analyser and a Nano Flex ion source (ThermoFisher Scientific). A data-dependent tandem MS acquisition method was used and all runs were performed at least in duplicate. In all experiments, full MS1 scans were acquired over a mass range of 375-1,600 *m/z* with detection in the Orbitrap mass analyser at a resolution setting of 70,000. Fragment ion spectra produced via HCD were acquired with a resolution setting of 17,500. For data-dependent acquisition of HCD spectra, the top ten most

intense ions were selected for fragmentation in each scan cycle and full MS as well as fragment ion spectra were detected in the Orbitrap mass analyser. Exclusion conditions were optimised according to observed chromatographic peak width (typically 10-30 s). To perform the database search, raw data files were searched using Mascot™ v. 2.4.1 search engine (Matrix Sciences Ltd., London, UK). The search parameters applied in the database searches are listed in Table 3. The reverse database search option was enabled in Mascot, and all data were filtered to satisfy a false discovery rate (FDR) of 1% or better.

2.2.6 Purification of $RyR1_{(2091-2708)}$ expressed from the pMALp2g expression vector using the ÄKTA prime

2.2.6.1 Dextrin conjugated agarose.

$RyR1_{(2091-2708)}$ was expressed in *E. coli* BL21 (DE3) from the pMALp2g vector in 1 L LB overnight. The cells were harvested at 7000 rcf at 4 °C and resuspended in lysis buffer containing 10 % glycerol and 0.01 % triton x 100. The cells were passed twice through a French press at 5000 psi. The *E. coli* cell lysate was centrifuged for twenty minutes at 17,000 rcf at 4 °C to pellet cell debris. A MBPTrap™ HP attached to an ÄKTA prime was used to partially purify the soluble protein in the supernatant under the following conditions: The column was washed with 40 mL water then 25 mL of lysis buffer containing 10 % glycerol; the protein solution was loaded onto the column at the rate of 1 mL per minute; the resin was washed with 60 mL lysis buffer containing 10 % glycerol; the tagged protein was eluted from the resin in a total volume of 40 mL (collected in 5 mL fractions) of lysis buffer containing 100 mM maltose and 10 % glycerol. The column was washed in 10 mL 0.1 % SDS, 20 mL water to remove residual protein and stored in 20 % ethanol at 4 °C until the next use.

2.2.6.2 Ni Sepharose affinity chromatography

A HisTrap™ FF column was used to purify $His_{(6)}$ tagged proteins. The column was washed in 20 mL water, and pre-equilibrated with 40 mL lysis buffer or TEV digestion buffer depending on the buffer the protein sample was suspended in. The protein containing fraction was loaded onto the column at a rate of 1 mL per minute. The column was washed in 20 mL lysis buffer. Proteins immobilised on the column were eluted in 20 mL lysis buffer containing 500 mM imidazole, and 2 mL fractions were collected. The column was washed in water and stored in 20 % ethanol before use.

2.2.6.3 Anion exchange chromatography.

In preparation for anion exchange chromatography, $RyR1_{(2091-2708)}$ was partially purified from the dextrin conjugated agarose column as described in section 2.2.6.1 however, in this case the protein was eluted in anion exchange chromatography buffer (10 mM HEPES pH 8, 50 mM NaCl, 2.8 mM KCl, 1 mM $MgCl_2$, 100 mM maltose, 1 mM DTT, 1 mM EDTA, 10 % glycerol) and all fractions containing the RyR1 region were pooled. The HiTrap™ Q FF anion exchange column was washed in 20 mL water and pre equilibrated in 20 mL anion exchange chromatography buffer. The protein fraction was then loaded onto the column at a rate of 1 mL/min and the column was washed with 20 mL anion exchange column buffer. A gradient was established between anion exchange column buffer and anion exchange elution buffer (10 mM HEPES pH 7.4, 500 mM NaCl, 2.8 mM KCl, 1 mM $MgCl_2$, 1 mM DTT, 1 mM EDTA, 10 % glycerol) with the gradient being increased at 1 % per mL and two mL fractions were collected. The column was washed in 20 mL ion exchange elution buffer, 20 mL water and stored in 20 % ethanol until next use.

2.2.6.4 Hydrophobic interaction chromatography

Protein fractions containing the RyR1 region were pooled and dialysed against hydrophobic interaction chromatography buffer (10 mM HEPES pH 7.4, 1 M NaCl, 2.8 mM KCl, 1 mM $MgCl_2$, 1 mM DTT, 1 mM EDTA, 10 % glycerol) for one hour at room temperature. The protein fraction

was transferred to fresh dialysis buffer and was dialysed overnight at 4 °C. The protein fraction was centrifuged at 17,000 rcf for 20 minutes at 4 °C and the soluble fraction collected. Prior to loading, the HiTrap™ Phenyl FF (HS) column was washed in 20 mL water and pre equilibrated in 20 mL hydrophobic interaction chromatography buffer. The protein fraction was loaded onto the column at a rate of 1 mL/min and followed by a wash with 20 mL hydrophobic interaction chromatography buffer. Protein was eluted from the column following a decrease in the NaCl concentration, with the establishment of a gradient between hydrophobic interaction chromatography and anion exchange buffers. The concentration of anion exchange buffer increased at a rate of 1 % (v/v) per minute and 2 mL fractions were collected. Following elution of protein, the column was washed in 20 mL water and stored in 20 % ethanol before next use.

2.2.6.5 Size exclusion chromatography

A Superdex 200 column was washed in 40 mL water, and 40 mL of the buffer the protein sample was suspended in. Protein fractions were diluted to a concentration of 1 mg/mL and 200 µL of the sample was loaded onto the column at a rate of 0.5 mL per minute and 1 mL fractions were collected. The column was washed in 40 mL of the buffer the protein was suspended in, then washed in 40 mL water and 20 mL 20 % ethanol. The column was stored in 20 % ethanol until next use.

2.2.7 Pull down of the RyR1 N-terminal domain

The MBP-tagged $RyR1_{(2091-2708)}$ was partially purified from solution using an amylose-conjugated resin, as described in section 2.2.5.2. Following the small-scale expression of the recombinant RyR1 N-terminal domain from the pGEX6p3 vector, *E. coli* cells were lysed as in section 2.2.5.1 and the 500 µL soluble fraction was immobilised on 50 µL Glutathione Sepharose® resin at 4 °C for 5 hours. The resin was washed in 3 mL cell lysis buffer. Proteins were eluted from the column in three bed volumes of glutathione elution buffer (20 mM Tris

HCl pH 7.4, 150 mM NaCl, 1 mM DTT, 1 mM EDTA, 10 mM reduced glutathione). One hundred µg of the eluted GST-tagged RyR1 N-terminal domain was incubated with the immobilised MBP-tagged $RyR1_{(2091-2708)}$ at room temperature with constant end over end rotation for two hours. The supernatant was collected following centrifugation at 2000 rcf. The resin was washed in wash buffer and proteins collected in the soluble fraction as well as those still associated with the resin were analysed by SDS PAGE. The presence of the GST-tagged N-terminal was detected by western blot analysis as described in section 2.2.8.

2.2.8 Western blot analysis.

Thirty µg of protein was separated by SDS PAGE as described in section 2.2.3.2. Protein was transferred onto an immobilon P membrane at 30 mV for 16 hours at 4 °C using a wet transfer system. The membrane was blocked in 5 % (w/v) skim milk in TBST (100 mM Tris HCl pH 7.4, 150 mM NaCl, Tween 20 0.05 % v/v) buffer for three hours at room temperature. Proteins were labelled using the following primary antibodies, anti-GST, anti-tubulin, 34 C (RyR specific antibody) and myosin heavy chain each diluted 1:1000 in 2.5 % (w/v) skim milk in TBST. The membrane was then washed three times in TBST and proteins were detected with horse radish peroxidase conjugated secondary antibodies each diluted 1:1000 in 2.5 % (w/v) skim milk in TBST. The membrane was washed in TBST. The BM chemiluminescence blotting substrate (Roche) was prepared following the manufacturers' instructions added to the membrane and protein was visualised using the Azure biosystems c600 imaging system, 10 images were taken at 30 second intervals.

2.2.9 Structural predictions of RyR1 variants using Pymol

RyR1 sequence IDs were imported into PyMOL version 2.4.0a0 from the Protein Data Bank (PDB) (82). The PDB I.D 5tb1 was used to model RyR1 variants in the closed state while the ID 5tam was used to model variants in the open state. MH pathogenic variants were introduced into the structure and the orientation of the side chain with the lowest structural hinderance

was selected for further characterisation. Amino acids which clash with the introduced variants were identified.

2.2.10 General tissue culture techniques

2.2.10.1 Volumes of medium used to grow cells in a range of flasks and dishes has been summarised in table 2.4.

T25	8 mL
T75	15 mL
10 cm dish	15 mL
6 well plate	2 mL
12 well plate	1 mL
96 well plate	100 µL

Table 2.4. Summary of the volumes used to grow cells in a range of flasks and dishes.

Nutrient mixture F-10 Hams was used to grow myoblasts. The medium was supplemented with 20 % (v/v) foetal bovine serum (FBS) and 4 % (v/v) penicillin/streptomycin (pen/strep). Myoblasts were differentiated in Dulbeccos Modified Eagles Medium (DMEM) containing 2 % (v/v) horse serum and 4 % pen/strep. HEK293T cells were grown in DMEM containing 10 % FBS (v/v) and 4 % pen/strep.

2.2.10.2 Coating of tissue culture plasticware

Entactin-collagen IV-laminin (ECL) diluted in Hams F10 to a concentration of 20 µg/mL was added to 10 cm tissue culture dishes and wells of a 96 well plate. The ECL solution was added to tissue culture plastics to a concentration of 2.5 µg/cm^2 and incubated at 37 °C in 10 % CO_2 in a humidified atmosphere for one hour. The ECL was removed from the plate and the plate was washed in phosphate buffered saline (PBS) containing 2 % (v/v) pen/strep. Cells were

either seeded directly onto the plate, or the plates were sealed with parafilm wrap and stored at 4 °C until needed.

2.2.10.3 Trypsin treatment of myoblasts

Trypsin - EDTA (0.25 %) was used to remove myoblasts from plasticware for cell passage in the preparation of cells for nucleofection or the seeding of cells for immunofluorescence or functional assays. Myoblast growth medium was removed from the cell culture plate/flask and the cells were washed in an equal volume of PBS. Enough trypsin was added to the flask to cover the cells and the flask was incubated at 37 °C for one minute. Cells were released from the plastic surface by gently tapping the side of the flask. Trypsin was inactivated by adding an equal volume of FBS. Cells were aliquoted to the approximate densities for further growth: 40 % for the maintenance of cells, 60 % in the preparation of cells for immunofluorescence and Ca^{2+} release assays.

2.2.10.4 Passage of HEK293T cells

HEK293T cells were removed from plasticware surface by gentle pipetting for cell passage. One fifth of the cells were aliquoted into a new flask and fresh medium was added to the desired volume.

2.2.10.4 Freezing of cells

Cells were detached from the plate/flask surfaces as described in sections 2.2.10.3 and 2.2.10.4, the cells were pelleted by centrifugation at 1800 rcf for 6 minutes. The supernatant was discarded, and the cells were resuspended in 900 µL FBS. One hundred µL DMSO was added to the cell mixture and the cells were frozen slowly at -80 °C. Then stored in liquid nitrogen vapour.

2.2.10.6 Extraction of primary myoblasts.

Muscle biopsies were obtained from patients undergoing a normal diagnostic procedure for susceptibility to MH. Use of surplus tissue for research purposes was obtained by informed consent with approval from the Health and Disabilities Ethics Committees 19/NTB/18. Muscle tissue surplus to diagnostic biopsies was washed in PBS containing 2 % pen/strep. The muscle tissue was diced with a scalpel into a fine homogenate and suspended in 10 mL PBS containing 2 % pen/strep. The mechanically disrupted tissue was pelleted by centrifugation at 1800 rcf for 5 minutes and the supernatant was removed. The muscle homogenate was suspended in a pre-prepared collagenase (1 mg/mL) and dispase (2.4 U/mL) mix in PBS and was incubated in a 37 °C water bath for one hour with gentle tituration (pipetted up and down) every ten minutes. The cell mixture was further diluted in 25 mL PBS containing 2 % pen/strep and debris was removed from solution by passing through a 70 µm cell strainer. The cells were pelleted from the filtrate following centrifugation at 1800 rcf for 5 minutes and resuspended in 15 mL Hams F-10 containing 20 % FBS and 4 % pen/strep and were transferred to a 10 cm tissue culture dish, labelled as PP1 and incubated at 37 °C in 10 % CO_2, 5 % O_2 in a humidified atmosphere. After one hour the medium was transferred to a second tissue culture dish labelled as PP2, and fresh media was added to the PP1 plate. After one hour the medium in the PP2 was transferred to a third ECL-coated plate and fresh media was added to the PP2 plate. Basic human fibroblast growth factor suspended in Hams F10 to a concentration of 1 mg/mL was added to each plate to a final concentration of 0.01 µM (1.5 µL in 15 mL). Primary myoblasts were grown to a confluence of 80 % before freezing. Medium was changed every 3 days.

2.2.10.7 Extraction of primary myoblasts from muscle tissue using magnetic activated cell sorting.

Muscle tissue was disrupted and cells were extracted as per section 2.2.10.6. After being passed through the cell 70 µm strainer and centrifuged at 1800 rcf for 5 minutes, the cells

were resuspended in 200 µL PBS containing 2 % (v/v) pen/strep, 0.5 % (v/v) FBS. Ten µL of anti CD82-biotin antibody (Miltenyi Biotech reference number 130-101-300) was added to the cell mixture and incubated at 4 °C for ten minutes. Cells were pelleted by centrifugation at 1600 rcf for five minutes, excess antibody was removed by three wash steps, where cells were resuspended in PBS containing 2 % (v/v) pen/strep, 0.5 % (v/v) FBS and pelleted by centrifugation at 1600 rcf for five minutes. The cells were then resuspended in 200 µL PBS containing 2 % (v/v) pen/strep, 0.5 % (v/v) FBS and ten µL of the anti-biotin antibody conjugated to a magnetic particle (Miltenyi Biotech reference number 130-090-485) was added to the cell mixture and incubated at 4 °C for ten minutes. Cells were pelleted by centrifugation at 1600 rcf for five minutes and excess antibody was removed by three wash steps, where cells were resuspended in PBS containing 2 % (v/v) pen/strep, 0.5 % (v/v) FBS and pelleted by centrifugation at 1600 rcf for five minutes. Labelled myoblasts were resuspended in 500 µL PBS containing 2 % (v/v) pen/strep, 0.5 % (v/v) FBS. The cell suspension was added to and passed through an MS column within a magnetic separator (Miltenyi Biotec), and the flow through collected. The column was washed in 3 mL PBS containing 2 % (v/v) pen/strep, 0.5 % (v/v) FBS and removed from the magnetic separator. The cells were eluted from the column in 3 mL PBS containing 2 % (v/v) pen/strep. Cells collected from both purification points, the flow through and elution, were added to separate tissue culture dishes containing fifteen mL Hams F-10 supplemented with 2 % (v/v) pen/strep, 20 % (v/v) FBS and incubated at 37 °C, 10 % CO_2, 5 % O_2 in a humidified atmosphere.

2.2.10.8 Differentiation of myoblast into myotubes

Myoblasts were grown in wells of a 96 well plate to a confluence of 80 % in Hams F-10 containing 20 %, FBS 4 % pen/strep at 37 °C, 10 % O_2, 5% CO_2 in a humidified atmosphere. Medium was changed to DMEM containing 2 % horse serum, 4 % pen/strep and the cells were incubated at 37 °C, 10 % O_2, 5% CO_2 in a humified atmosphere until myotubes had formed. This was approximately one week for primary myoblasts and two weeks for immortalised cells. Medium was replaced with fresh differentiation medium every three days.

2.2.11 Immortalisation of primary myoblasts

2.2.11.1 Production of Lentivirus particles

HEK293T cells were grown in DMEM containing 10 % (v/v) FBS and 2 % (v/v) pen/strep in T25 flasks to a confluence of 50 %. Prior to transfection the medium was changed and the cells were incubated at 37 °C, 5 % CO_2 in a humidified atmosphere for one hour. The cells were transfected for transient expression with the following mix: 1.3 pmol transfer plasmid (pLenti), 0.72 pmol of the packaging plasmid (psPAX2) and 1.64 pmol of the envelope plasmid (VSVG). Four hundred µL of DMEM was added to the DNA and Fugene HD was added to a final ratio of 1:1 with the plasmid DNA. The transfection mix was incubated at room temperature for one hour then added to the HEK293T cells which were incubated at 37 °C, 5 % CO_2 in a humidified atmosphere for 24 hours. The medium was changed again and the cells were incubated at 37 °C, 5 % CO_2 for a further 24 hours. The medium was collected and centrifuged at 2000 rcf at room temperature for five minutes and the supernatant containing virus particles was passed through a 0.45 µm filter. Media were collected and passed through a filter every 24 hours until the cells reached a confluence of 100 %. The virus particles were concentrated as described in section 2.2.11.2 or used to infect cells immediately.

2.2.11.2 Concentration of viral particles

Medium containing viral particles was collected and filter sterilised using a 0.45 µM filter as in section 2.2.11.1. Polyethylene glycol 8000 was added to the virus mixture to a final concentration of 8.5 % and NaCl was added to a final concentration of 0.4 M. The medium was mixed by gentle pipetting and incubated at 4 ° C for ninety minutes with gentle mixing every thirty minutes. Viral particles were pelleted at 7000 rcf for 15 minutes at 4 ° C and then resuspended in 500 µL 50 mM Tris HCl pH 7.4. One hundred micro litre aliquots were snap frozen and stored at -80 ° C until use or used immediately to transduce primary myoblasts.

2.2.11.3 Quantifying the number of viral particles.

The quantitative PCR lentivirus titration kit supplied by Applied Biological Materials Incorporated was used to determine viral titre. The procedure was followed according to the manufacturer's instructions. Amplification of DNA was detected using SsoFast Evagreen (Bio-Rad) reaction mix. Conditions used for the reverse transcription and amplification of cDNA were as follows: Reverse transcription at 42 °C 20 minutes, enzyme activation at 95 °C 10 minutes, amplification of cDNA for 30 cycles, denaturation at 95 °C 15 seconds followed by annealing/extension at 60 °C 1 minute. The concentration of viral particles produced was quantified in comparison to two positive controls of known concentration supplied with the kit. The genomic concentration of viral particles was converted to viral titre.

2.2.11.4 Immortalisation of primary myoblasts using lentivirus.

Medium containing viral particles was added to a 10 cm tissue culture dish containing myoblasts grown to 50 % confluence attached to the plate surface. The cells were incubated at 37 °C, 5 % CO_2, 10 % O_2 in a humidified atmosphere for 24 hours. The medium was replaced with fresh Hams F-10 containing 20 % FBS and 4 % pen/strep. The cells were grown for two days until reaching a confluence of approximately 70 % at which time antibiotic for selection was added to the medium depending on the virus used, 25 µg/mL hygromycin or 100 µg/mL geneticin.

2.2.11.5 Nucleofection of primary myoblasts

Primary myoblasts were grown to a confluence of 70 % in a T75 flask in Hams F-10 containing 20 % FBS and 4 % pen/strep. The cells were trypsin treated and washed in PBS as described in section 2.2.10.3. The cells were counted using a haemocytometer (described in section 2.2.11.6) and two hundred thousand myoblasts, were collected following centrifugation at 200 rcf for 6 minutes and the supernatant was discarded. The nucleofection mix consisting of

16.5 µL P5 nucleofector solution, 3.5 µL supplement solution (both proprietary solutions) and 400 µg of plasmid DNA was used to resuspend the cells. The cell mixture was added to a well of the Nucleofector strip, the program CM-189 was used to electroporate the cells within the Lonza 4D Nucleofector core unit. Eighty µL Hams F-10 containing 20 % FBS, 4 % pen/strep was added to the cells which were then incubated at 37 °C, 5 % CO_2, 10 % O_2 in a humidified atmosphere for 10 minutes before being transferred to a T25 flask containing fresh growth medium. The cells were incubated for 2 days before selection with antibiotic depending on the vector used, either 25 µg/mL hygromycin or 100 µg/mL geneticin. Cells were allowed to establish colonies by incubation at 37 °C, 5 % CO_2, 10 % O_2. Medium containing fresh antibiotic was changed every three days.

2.2.11.6 Counting cells using a haemocytometer

One hundred µL of a cell suspension was diluted 2 fold in 0.4 % trypan blue. One hundred µL of the cell suspension was then applied to the haemocytometer. Live cells which were unstained by the dye were counted in each of the four corners of the haemocytometer grid. The average number of cells per grid was determined and multiplied by 10^4, then multiplied by 2, to correct for the initial dilution of the cells.

2.2.11.7 Magnetic activated cell sorting of myoblasts

Myoblasts shown to be resistant to both hygromycin and geneticin by lentiviral transduction were grown to a confluence of approximately 70 %. The cells were trypsin treated and washed in PBS. The purification of the cells was then performed as described in section 2.2.10.7 to remove non myoblast cell lines from the culture.

2.2.11.8 Relative telomer length determination by PCR

Thirty-five ng of genomic DNA extracted from myoblasts was PCR-amplified with primers specific for the telomer repeat region or the IFNB1 gene. The Ssofast Evagreen (Bio-Rad) master mix was used to amplify the telomer repeat amplicon, while the Roche 480 HRM mix was used to amplify the IFNB1 amplicon. Different master mixes were used for each primer pair as efficiencies for both primers could not be optimised for a single mastermix. The amplification of each amplicon is a relative measurement so different mixes could be used. The cycling conditions used were as follows: initial denaturation at 95 °C for 10 minutes, amplification for 35 cycles at 95 °C 30 seconds, 55 °C for 15 seconds, 72 °C for one minute. The LightCycler ® 480 SW 1.5.1 software was used to analyse the amplification of genomic DNA. Three biological replicates were used for each time point and three technical replicates were produced from each of these. The Cp values for each technical replicate were averaged to generate each biological replicate for each time point. The following equations were used to calculate the relative telomer length.

1. $\Delta Cp = Cp_{Tel} - Cp_{INFB1}$
2. relative telomer length = $2^{-\Delta Cp}$

2.2.11.9 Immunofluorescence

Primary and immortal myoblasts were grown to a confluence of approximately 70 % on a microscope slide and differentiated into myotubes as described in section 2.2.10.8 if required. The cells were fixed in 2 % paraformaldehyde for fifteen minutes and washed three times with 1 mL PBS. Cells were permeabilised using 500 µL 0.1 % triton X-100 for five minutes and washed three times with 1 mL of PBS. The slide was blocked with 5 % BSA + 0.5 % Tween 20 for 30 minutes with shaking. Cells were labelled with a primary antibody against desmin, RyR1 or protein disulphide isomerase each diluted 1:500 in PBS and incubated at 4 °C overnight. The cells were then washed three times in 1 mL PBS and labelled with a secondary antibody conjugated with FITC for RyR1 and desmin or TRITC for protein disulphide isomerase diluted 1:1000 in PBS and incubated for one hour in the dark. A drop of Prolong® gold mounting

solution was added to each well and a cover slip was added to the microscope slide. The presence of DAPI was detected at 488 nm (excitation at 340 nm), FITC was detected at 525 nm (excitation at 490 nm) and TRITC was detected at 576 nm (excitation at 557 nm). Proteins were detected within 2 days of labelling by visualisation using the Leica SP5 DM6000B Scanning Confocal Microscope located at the Manawatu Microscopy and Imaging Centre Palmerston North New Zealand.

2.2.12 Functional characterisation of myotubes

2.2.12.1 Labelling of myotubes for Ca^{2+} with fura 2-AM

Myotubes were washed in balanced salt solution (BSS: 10 mM HEPES, 140 mM NaCl, 2.8 mM KCl, 1 mM $MgCl_2$, 10 mM glucose, pH 7.4) containing 2 mM $CaCl_2$. The cells were labelled with 0.5 µM fura 2-AM containing 0.0005 % pluronic acid in BSS including 2 mM Ca^{2+} with incubation at 37 °C for an hour in the dark. The cells were washed twice in BSS containing 2 mM $CaCl_2$ and 100 µL BSS containing 2 mM Ca^{2+} was added to each well. Cells were imaged directly after labelling.

2.2.12.2 Characterising Ca^{2+} homeostasis in myotubes

Labelled myotubes (as per section 2.2.12.1) were imaged using an Olympus IX81 fluorescence microscope at 40 x magnification measuring the emission at 510 nm with excitation at 340 and 380 nm using a wavelength switcher. A baseline fluorescent measurement was established before the addition of agonist at predetermined concentrations. One hundred µL of agonist of known concentration was added to each well and the change in fluorescence was monitored. Final concentrations of the agonist 4-CmC were 1200 µM, 1000 µM, 800 µM, 600 µM, 400 µM and 300 µM. For K^+, the concentration of positive ions was kept consistent ($[Na^+] + [K^+] = 140$ mM). K^+ concentrations included 60 mM, 50 mM, 40 mM, 30 mM, 20 mM and 10 mM. Concentrations of caffeine used to induce Ca^{2+} release included 10 mM, 8 mM, 6

mM, 5 mM, 4 mM and 2 mM. The change in fluorescence was recorded within the Metafluor® software, where the base line measurement was subtracted from the peak recorded measurement to calculate the change in fluorescence (Δ F) after the addition of agonist. Ten replicates were performed for each cell line and the average relative change in Ca^{2+} release was determined for each concentration. The results were represented as mean +/- standard error of the mean for each concentration of agonist used. Sigmoidal curves were plotted using the OriginLab version 8 software.

2.2.13 Characterisation of gene expression in myotubes

2.2.13.1 RNA extraction from myotubes.

Myotubes were lysed using 1 mL Trizol followed by the addition of 200 µL chloroform and mixing using a vortex for 1 minute and then incubation at room temperature for one hour. The RNA containing mixture was centrifuged for 10 minutes at 17,000 rcf at 4 °C and the colourless top layer was collected and added to 500 µL isopropanol. After gentle mixing by pipetting and incubation at room temperature for 10 minutes, the RNA was pelleted by centrifugation at 17,000 rcf for 10 minutes at 4 °C, washed in 70 % ethanol and air dried. RNA was suspended in 20 µL diethyl pyrocarbonate (DEPC) treated water, the concentration of RNA was determined using the Denovix DS-11FX spectrofluorometer as described in section 2.2.4.1. Either first strand cDNA was produced (described in section 2.2.13.2) or the RNA was stored at -80 °C until later use.

2.2.13.2 First strand cDNA synthesis

The iScript gDNA clear cDNA synthesis kit (Bio-Rad) was used to produce cDNA from 0.5 µg RNA according to the manufacturer's instructions. A no reverse transcriptase control was also included for each preparation of RNA.

2.2.13.3 Relative Quantitative PCR

The Roche 480 HRM mastermix was used to amplify the cDNA along with specific primers (summarised in appendix 3.1) according to the manufacturer's instructions. Three biological replicates were used for each assay as well as three technical replicates for each biological replicate. The following cycling conditions were used to amplify cDNA: initial denaturation at 95 °C for 5 minutes, followed by thirty-five cycles of 95 °C for one minute, 58 °C for 15 seconds, 72 °C for one minute. The LightCycler ® 480 SW 1.5.1 software was used to monitor the amplification cDNA. To compare the relative expression of each gene, the technical replicates were averaged, then the average for the biological replicates was determined as shown in the equation below, acidic ribosomal phosphoprotein P0 was used as a reference gene.

$$\text{Relative expression} = \frac{(\text{Efficiency}_{\text{target}})^{\Delta CP \text{ target (mean control – mean sample)}}}{(\text{Efficiency}_{\text{reference}})^{\Delta CP \text{ reference (mean control – mean sample)}}}$$

2.2.14 CRISPR Cas9 modification of myoblasts

2.2.14.1 Nucleofection of immortalised myoblasts for CRISPR Cas 9 modification

Two hundred thousand immortalised myoblasts prepared from an MHN patient were pelleted at 200 rcf and all medium was removed from the cell pellet. The cells were gently resuspended in the following: 400 ng of the Cas 9 vector and 300 pg of the repair template mixed with 16.4 µL P5 primary cell Nucleofector solution and 3.6 µL supplement solution. The cell mixture was transferred to a well of the Nucleofector strip which was then placed in a Lonza 4D Nucleofector core unit. The program CM-189 was used to electroporate the cells. Eighty micro litres of myoblast growth medium was added to the well which was then incubated at 37 °C for fifteen minutes. The cells were transferred to a T25 flask containing Hams F-10 supplemented with 20 % FBS, 2 % pen/strep and allowed to attach to the plate

surface. Cells were grown at 37 °C, 10 % O_2, 5 % CO_2 in a humidified atmosphere for seven days, then trypsinised and suspended in Hams F-10 supplemented with 20 % FBS, 2 % pen/strep. The cells were dispensed into wells of a 96 well plate at a rate of 1 cell per three wells followed by incubation at 37 °C, 10 % O_2, 5 % CO_2 in a humidified atmosphere until colonies had formed.

2.2.14.2 DNA extraction from myoblasts

Wells in which a single colony were identified were washed in PBS followed by the addition of 20 µL 0.25 % trypsin – EDTA, releasing the cells from the surface. The trypsin was inactivated by adding an equal volume of FBS. Ten µL of the cell suspension was added to a new well of a 96 well plate and fresh medium was added to these cells to allow continual cell growth. The remaining cells were washed in PBS and pelleted by centrifugation at 1800 rcf for 5 minutes. The cells were suspended in 60 µL of Promega nuclei lysis solution (reference number A7941) and incubated at room temperature for 10 minutes. Proteins were precipitated by adding 20 µL Promega protein precipitation solution (reference number A795A) to the mix followed by centrifugation at 17,000 rcf for ten minutes. The DNA containing supernatant was collected and added to 60 µL isopropanol and mixed by pipetting up and down. DNA was precipitated during a 10 minute incubation at room temperature and collected by centrifugation at 17,000 rcf for 10 minutes. The supernatant was discarded, and the DNA pellet was washed with 1 mL 70 % ethanol, air dried and DNA suspended in 6 µL TE.

2.2.14.3 T7 endonuclease assay

The region surrounding the Cas 9 modification site was PCR amplified. Two hundred and fifty ng of the purified PCR product was diluted to a final volume of 19 µL in 1 x New England biolabs buffer 2. The DNA was denatured using the following protocol; initial denaturation 95 °C 5 minutes, annealing was performed in two stages; 95–85 °C, -2 °C / second; 85-25 °C, -0.1 °C / second. One µL of the T7 endonuclease was added to the DNA and incubated at 37 °C for 15 minutes. The result of the digest was analysed by polyacrylamide gel electrophoresis.

2.2.14.4 High resolution amplicon melting

High resolution amplicon melting was used to screen for the presence of the c.14497C>T variant. In this case the Roche 480 HRM mastermix and specific primers (summarised in appendix 3.1) were used to PCR amplify the region surrounding the variant. The cycling conditions used to amplify the DNA were as follows: denaturation at 95 °C for 10 minutes followed by amplification for 70 cycles 95 °C for 10 seconds, 65 °C for 10 seconds, 72 °C for 30 seconds. For allele discrimination PCR products were melted at 95 °C for one minute, the temperature was dropped to 40 °C and was then increased to 76 °C at a rate of 1.50 °C per second and further increased from 76 °C to 96 °C at a rate of 4.40 °C per second. The LightCycler ® 480 SW 1.5.1 software was used to analyse the results.

3. Recombinant expression and partial purification of the RyR1 HD1

3.1 Introduction

The full-length rabbit RyR1 channel has been structurally characterised by cryo-EM in both the open and closed states (9). During this characterisation it was shown the channel was comprised of large rigid regions, connected by flexible linker regions, which move relative to each other during the opening and closing of the channel. One region in particular, the bridging solenoid (BSol), comprised of the amino acids 2145-3613 (figure 3.1) was shown to move relative to the junctional solenoid (JSol), amino acids 1657-2144, and the N-terminal domain (NTD) amino acids 1-628 (rabbit RyR1 accession number p11716.B).

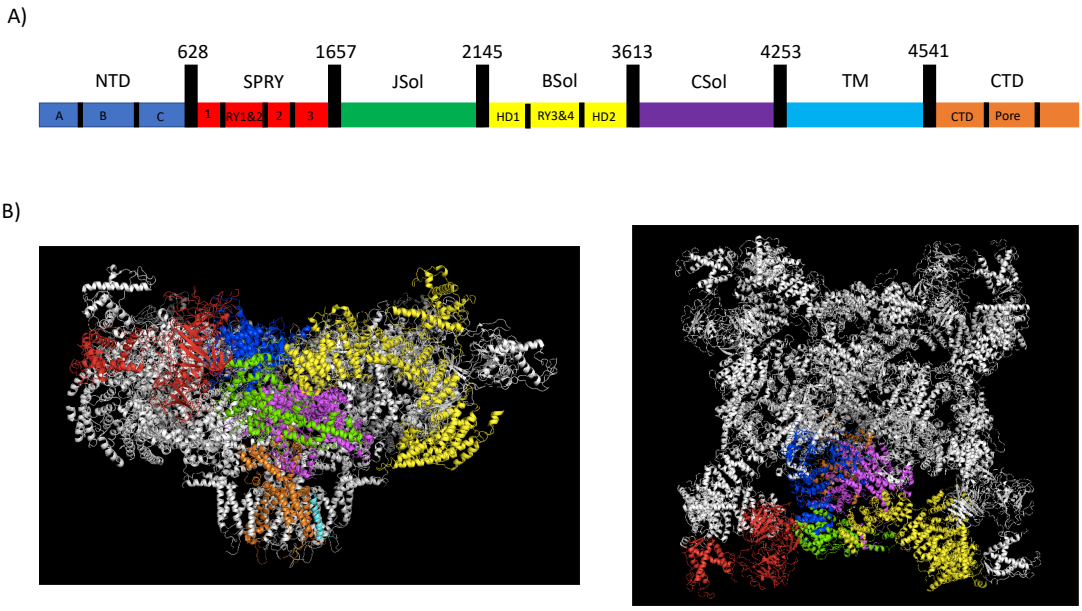

Figure 3.1. Representation of the domain distribution of RyR1. A) Proposed RyR1 domains have been represented by colour where the domain boundaries have been indicated by amino acid number. Amino acid numbers refer to the human RyR1 accession number NM_000540.2. B) Proposed location of each domain in the RyR1 tertiary structure. The left panel is a side on view of the channel, the right panel is a top down view of the channel. Proposed domains of a single subunit have been coloured as in section A. The figure was made using PyMOL version 2.4.0a0 using the PDB ID 5TB1 (rabbit RyR1).

Many of the rigid regions of RyR1 can be further broken down into smaller more definable proposed domains. For example, the BSol can be further defined as the Helical domains 1 and 2 and the Ry 3&4 domain. Each of these proposed domains has been suggested to play a specific role in the overall regulation of the channel leading to it either favouring the open or closed state under specific conditions. This region (amino acids 2145-3613) has been shown to be a target for posttranslational modification in the form of S-glutathionylation and nitrosylation (83-85). Reactive cysteine residues within this region have also been shown to form disulphide bonds with other regions of the channel, which encourages the channel to remain in the open state (30). Ry3&4 in particular has been shown to be a target for phosphorylation by protein kinase A (79), which leads to the dissociation of FKBP12 and in doing so encourages RyR1 to favour the open state.

Eighteen of the variants confirmed to be pathogenic for MH have been identified in the region referred to as the helical domain 1, HD1 (2145-2735) (4). Five of these variants have been identified within a more definable region of this proposed domain referred to as the DP4 domain, RyR1 amino acids 2442-2477, a region which has been characterised by nuclear magnetic resonance (80). The DP4 domain has been shown to form an interaction with the adjacent N-terminal domain, an interaction which is important for stabilising both the closed and open states of the channel. The amino acid arginine 2452 (human RyR1 NM_000540.2) has been proposed to play a significant role in this interaction (figure 3.2), and mutation of this amino acid to tryptophan has been previously confirmed to be pathogenic for MH (60). The amino acid arginine 2355 (human RyR1 NM_000540.2) has also been proposed to be important in the interaction between the HD1 and the N-terminal domain. Mutation of this amino acid to tryptophan has also been confirmed as pathogenic for MH (86).

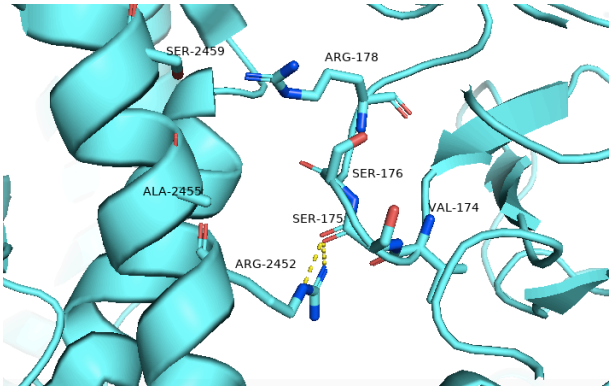

Figure 3.2. The interaction between arginine 2452 and serine 175. The figure was produced using the PyMOL software version 2.4.0a0 using the PDB ID 5TB1 using the protein data bank ID 5tam. Yellow lines indicate hydrogen bonds between atoms.

A region within porcine RyR2 which shares a high amino acid identity with the RyR1 HD1 has been recombinantly expressed and was shown to form an interaction with ATP *in vitro* (87). The proposed ATP binding site, a Walker A motif complemented with Walker B and lid motifs, is maintained in RyR1. These observations suggest the RyR1 HD1 may also be able to form an interaction with ATP, a process which may lead to the overall regulation of the channel. The human RyR1 amino acids 2370-2377, 2433-2437 and 2460-2464 have all been proposed to play a significant role in binding of ATP. Interestingly the amino acids lys and thr/ser of the Walker A motif which are required for the hydrolysis of ATP in other enzymes are not present in either RyR1 or RyR2 (figure 3.3). In both isoforms, these amino acids have been substituted for two leu residues which suggests if the proposed motif exists *in vivo*, the RyR isoforms will not be able to hydrolyse ATP.

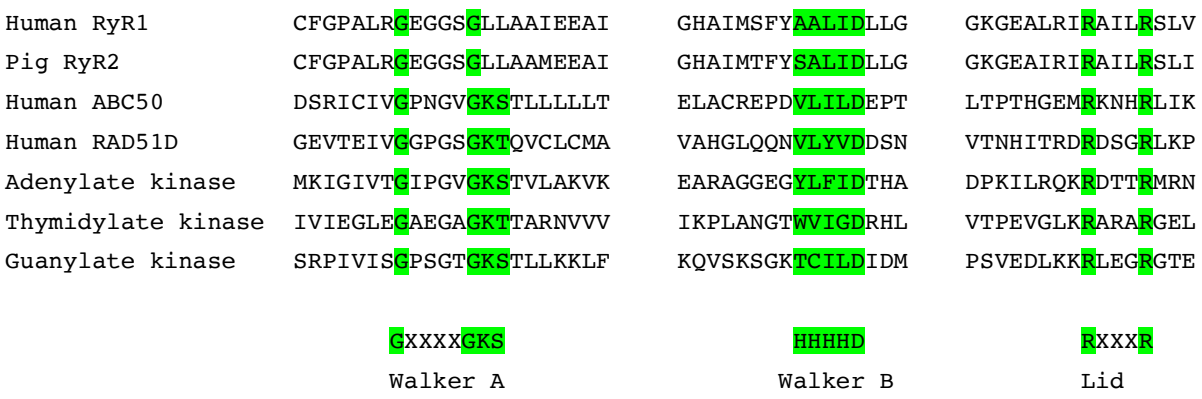

Figure 3.3. Sequence alignment of the proposed ATP binding motif of RyR1, RyR2 and three examples of P-loop kinases. The Walker A, Walker B and lid motifs have been highlighted. Human RyR1 was compared to the previously characterised pig RyR2 (87), along with previously characterised kinases; ABC 50, human, NP_001081.1, (88); RAD51D, human, AAC39719, (89); adenylate kinase, *Solfolobus acidocaldarius*, PDB ID 4AKE, (90); thymidylate kinase, *E. coli*, PDB ID 4TKM, (91); guanylate kinase, *Saccharomyces cerevisiae*, PDB ID 1GKY; (92).

In the recent structural characterisation of RyR1 in the ATP bound state no ATP was shown to bind to this region whereas an ATP binding site appeared to be in the C-terminal region of the channel. The amino acids met 4960, phe 4959, tyr 4980 and leu 4986 of human RyR1 were shown to be important in the interaction (9). While the HD1 was not able to bind ATP in this study, under specific conditions the proposed RyR1 domain may be able to form an interaction with the ligand. ATP was bound to RyR1 *in vitro* prior to the structural characterisation of RyR1. The lack of ATP bound to the HD1 does not rule out an ATP binding site existing in this region of the channel. The HD1 may only bind ATP following the binding of another ligand, alternatively the HD1 may have a low affinity for ATP and the concentration of ATP in the buffer was not high enough to induce binding. The situation *in vivo* may also be different.

With increased efforts to structurally characterise the full length RyR1 channel by cryo-EM, the resolution of the channel has increased dramatically. Early cryo-EM studies provided insights into the overall organisation of the channel, where regions surrounding the pore could be visualised, however the resolution of the channel extremities was very low and only

the overall structure of the channel could be analysed (93, 94). In recent years, the overall resolution of the channel has increased to the extent that amino acid side chains can be visualised from all regions of the channel, in particular the channel extremities which were once poorly resolved (9). There are still regions of the channel in which amino acid side chains could not be identified; the HD1 is one such region where the amino acids 2479 - 2734 (p11716.B) could not be positively identified, with only the amino acid back bone and secondary structure observed. A structure of a protein determined by cryo EM is an average of a number of RyR1 tetramers. The more flexible a particular region of the structure is the less consistency there will be between individual monomers and as a result the average structure will be less well defined in these specific regions.

Rabbit RyR2 has also been structurally characterised by cryo-EM. RyR2 was structurally characterised in the calmodulin bound state. In the Ca^{2+} free state calmodulin was shown to bind within a cleft formed between the HD1 and the central regions of the channel where the amino acids tyr 2157, tyr 2203, tyr 2558 (Q29621) were shown to be pivotal in the interaction between the two proteins. Calmodulin will bind Ca^{2+} as cytosolic levels rise and in doing so will undergo a conformational change and in this new state the protein will bind a different region of RyR2. The amino acid arg 2209 is important in the interaction between the two proteins, however amino acids located in other regions of RyR2 are also pivotal in this interaction including trp 3588 and pro 3604. Due to the high sequence identity shared between RyR1 and RyR2, it is likely the corresponding amino acids in RyR1 are also important in the interaction. In the Ca^{2+} free state the corresponding RyR1 amino acids are tyr 2197, tyr 2238, tyr 2587, while in the Ca^{2+} bound state the corresponding RyR1 amino acids are arg 2244, trp 3620, pro 3640. Apo-calmodulin has opposing effects on both RyR1 and RyR2. Binding of apo-calmodulin causes RyR1 to favour the open state, while its binding causes RyR2 to favour the closed state (38).

Currently it is unknown how specific variants within HD1 lead to the onset of MH from a structural standpoint. While the region, as part of the full tetramer, has been structurally characterised following its purification from rabbit muscle, specific variants must be present within the protein at the point of purification for direct structural characterisation of each variant. Many of the characterised MH-associated variants in humans are not present in the

rabbit genome and as such are difficult to structurally characterise by this method. Currently, MH pathogenic variants are often structurally characterised following the recombinant expression of a specific domain in an *E. coli* host (76, 77, 79, 81). Previous studies have shown that there is little or no difference in the structural organisation of RyR1 domains following recombinant expression. As these variants are expressed from a bacterial expression vector, there is a template for the simple introduction of specific variants into the RyR1 cDNA, allowing for the expression of the variant containing protein. An *E. coli* cell lysate provides a non-invasive source for protein purification, where several purification steps can be trialled. For cryo-EM studies, 100 g of rabbit muscle tissue was used in the experimental purification of RyR1. However, the optimisation and replication of the characterisation would have required more tissue which may have required several animals to be euthanised. From an ethical standpoint few or no mistakes could be made during purification or characterisation.

The helical domain 1 was selected for structural characterisation by X-ray crystallography in the current research, as this region has been proposed to be functionally significant where it has been shown to be subjected to post translational modification and has been proposed to be involved in the binding of calmodulin. Of the 48 pathogenic variants identified in RyR1, 18 reside within HD1 which is a strong indication the domain and these particular amino acids are essential in the proper function of the channel. Being located at the extremity of the channel, the domain was not well resolved during structural characterisation by cryo-EM and as a result it can be difficult to map certain variants to the full-length structure *in silico* and understand their role in the onset of MH. The human HD1 shares an almost 100 % sequence identity with the rabbit HD1 (appendix 2.1), suggesting the proposed domain will also be present in the human protein.

3.2 Results

3.2.1 Cloning of the *RYR1* cDNA corresponding to the HD1

PCR primers were designed for the amplification of the cDNA corresponding to HD1 and subsequent cloning into a range of bacterial expression vectors (appendix 2.2). In addition, primers were designed for the amplification of slightly different regions of the RyR1 HD1, to increase the chance of expressing a soluble fusion protein. A number of bacterial expression vectors were chosen for the expression of the RyR1 regions as each contains a different solubility or purification tag potentially aiding in the expression or purification of a soluble fusion protein (table 3.1 and appendix 2.3 and 2.4).

3.2.2 Recombinant expression of the RyR1 HD1.

Initial expression of each RyR1 region was induced individually by IPTG in transformed *E. coli* BL21(DE3). The cells were harvested, lysed and insoluble and soluble fractions were analysed by SDS-PAGE to determine the expression and solubility of each protein as described in section 2.2.5.1 and summarised in table 3.1.

		Expressed	Soluble
pMALp2g	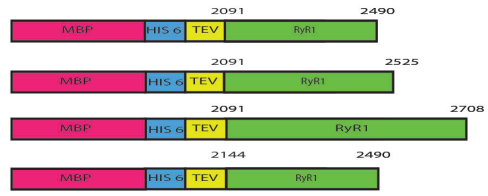	+ - + -	+ N/A + N/A
pMALp5x	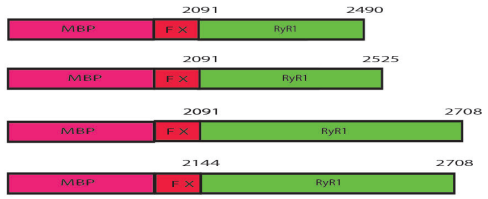	+ - - -	+ N/A N/A N/A
Modified pMALp5x	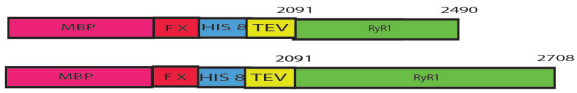	+ -	- N/A
pPROEXhtB	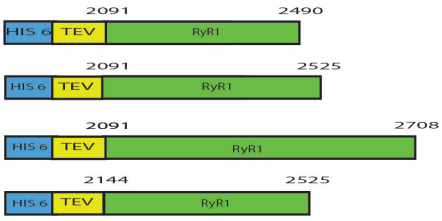	- + + -	N/A - - N/A
pET32a	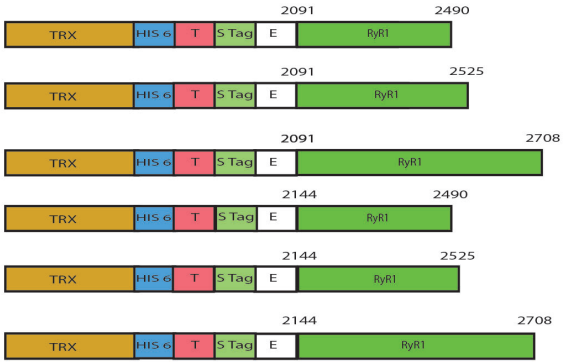	+ - - + - -	- N/A N/A - N/A N/A
pGEX6p3	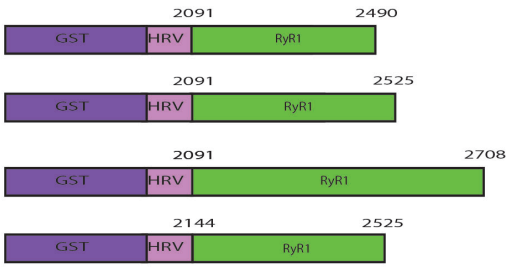	+ + - +	+ + N/A -
pHUE	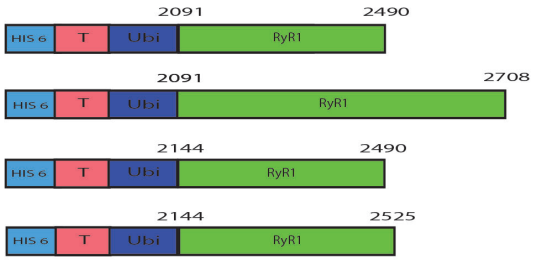	- - - -	N/A N/A N/A N/A

Table 3.1. Summary of the expression and solubility of various RyR1 regions from a range of expression vectors. The name of the vector and a schematic representation of the fusion protein expressed from each vector is represented. MBP indicates the solubility tag maltose binding protein, His represents the $His_{(6)}$ purification tag, TEV represents the recognition site for the Tobacco Etch Virus protease and RyR1 represents the region of RyR1 expressed. The boundaries of each region are denoted by amino acid number. FX represents the recognition site for the protease Factor Xa, TRX represents the solubility tag thioredoxin reductase, T represents the recognition site for the protease thrombin, S-tag represents the solubility tag, S-tag , E represents the recognition site for the protease enterokinase, GST represents the solubility tag glutathione S transferase, HRV represents the recognition site for the protease Human Rhino Virus 3C and Ubi represents the solubility tag ubiquitin. Amino acid numbering is according to human RyR1 (NM_000540.2). A plus in the "Expressed" column indicates the protein was expressed following the addition of IPTG, a negative symbol indicates the protein was not expressed when transformed cells were exposed to IPTG. A plus in the "soluble" column indicates the protein was soluble following expression, a – indicates the protein was insoluble and N/A indicates the protein was not expressed to a visible extent.

A recombinant protein was expressed from only 11 vectors, with only five proteins being soluble. It is interesting to note that following the addition of IPTG, cells that expressed a protein regardless of solubility continued to grow, while the cells that did not express a protein did not increase in density. This may suggest that certain proteins are toxic to the host cell possibly resulting from the production of detrimental inclusion bodies within the cell, which may have been expressed to a level so low they were not visible by SDS-PAGE.

A second cell line, Rosetta ^{TM} 2, was transformed with each vector to aid in expression or solubility. Rosetta ^{TM} 2 cells contain a second expression vector which leads to the expression of tRNAs corresponding to codons heavily used in eukaryotic genomes (95). These codons rarely occur within prokaryotic genomes and as a result the corresponding tRNAs are less prevalent within the cell. Increasing the concentration of these tRNAs has been shown in previous studies to increase the solubility of recombinantly expressed proteins. The increased pool of tRNAs supposedly increases the translation efficiency aiding in protein folding and solubility. The use of Rosetta ^{TM} 2 cells did not lead to the expression of a construct that previously did not express in BL21(DE3) cells. Additionally, the use of Rosetta ^{TM} 2 cells did not increase the solubility of those proteins that were expressed.

3.2.3 Purification of the RyR1 helical domain 1.

A soluble RyR1 region was expressed from five different expression vectors. Each of these proteins was subjected to initial batch purification using either an amylose conjugated agarose resin for the three MBP-tagged proteins or a glutathione conjugated Sepharose resin for the two GST-tagged proteins (summarised in appendix 2.5). Each of these proteins was then subjected to protease digestion, to separate the RyR1 region from its purification tag. The solubility of each region was then confirmed by centrifugation. The initial purification steps performed on each recombinant protein have been summarised in table 3.2. Mass spectrometry was performed prior to and following the protease digestion confirming the identity of each protein and the solubility of the RyR1 region.

Vector name	Can the protein be Batch purified?	Can the tag be removed while bound to the resin?	Can the tag be removed following elution from the resin?	Was the identity of the RyR1 region confirmed following protease action?
pMALp2g (2091-2490)	yes	no	Yes	yes
pMALp2g (2091-2708)	yes	no	yes	yes
pMALp5x (2091-2490)	yes	no	yes	yes
pGEX6p3 (2091-2490)	yes	yes	yes	yes
pGEX6p3 (2091-2525)	yes	yes	yes	yes

Table 3.2. Summary of the batch purification of RyR1 regions expressed from different vectors. The vector and RyR1 region indicated by amino acid number have been indicated. The proteins ability to be batch purified has been summarised in the second panel. The proteins ability to be digested by its designated protease has been summarised in columns 3 and 4, either bound to the resin or following elution. Column 5 indicates that the identity of the RyR1 was confirmed following protease digestion.

The proteins expressed from the three pMAL vectors were soluble. The two separate proteins expressed from the pMALp2g vectors could be enriched and partially purified from solution using an amylose conjugated resin and could be subjected to digestion by the protease TEV, however this was successful only after the protein had been eluted from the resin. The resin

may shield the protease recognition site preventing TEV from accessing the protein. The MBP tagged protein expressed from the pMALp5x protein was shown to be marginally soluble and very small amounts of protein were enriched using the amylose conjugated resin, however the expression of a soluble protein from this vector was not consistent, where a soluble protein was expressed in only 25 % of the cultures transformed with this vector. In the other 75 % of the expression attempts an insoluble protein was expressed. Efforts were made to keep conditions consistent during expression and cell lysis, however not all bacterial cultures lead to the expression of a soluble protein. When a soluble protein was expressed from this vector it was unable to be digested while bound to the amylose resin, while it could be digested following elution from the resin. The two soluble proteins expressed from the pGEX6p3 vectors also had very limited levels of solubility. Despite efforts to increase the solubility of the protein only a very limited amount could be obtained. Both proteins could be digested while bound to the Glutathione Sepharose® resin as well as following elution from the resin.

The RyR1 region corresponding to the amino acids 2091-2708 (accession number NM_000540.2) expressed from the pMALp2g vector was chosen for further purification steps. This recombinant protein contains two purification tags, maltose binding protein (MBP) and $His_{(6)}$, as well as the recognition site for the tobacco etch virus (TEV) protease (figure 3.4). The region could consistently be enriched from an *E. coli* cell lysate using an amylose resin exploiting the MBP tag, however a pure sample could not be obtained. The region could be digested by the protease TEV, however a complete digestion could not be achieved. Large scale purification of $RyR1_{(2091-2708)}$ was attempted where more in depth purification steps could be utilised compared to batch purification.

Figure 3.4. Schematic representation of $RyR1_{(2091-2708)}$ expressed from the pMALp2g vector. Different regions of the recombinant protein have been represented by colour. MBP refers to the maltose binding protein tag. HIS 6 refers to the $His_{(6)}$ purification tag. TEV refers to the tobacco etch virus protease recognition site. The amino acid boundaries of the RyR1 domain are indicated and have been numbered according to NM_000540.2.

Steps taken in an attempt to purify the RyR1 region have been summarised in figure 3.5 and presented in more depth in the following sections. The purification tags MBP and $His_{(6)}$ were initially utilised, using dextrin affinity and Ni-NTA purification steps, respectively. Ion exchange, hydrophobic interaction and size exclusion chromatography were utilised in attempts to further purify the protein.

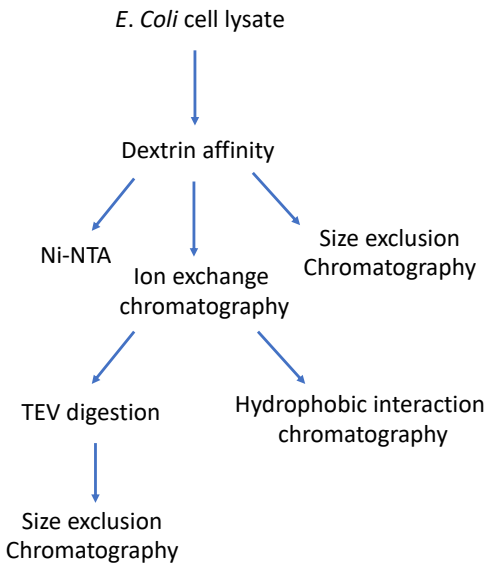

Figure 3.5. Summary of the purification steps that were taken in an attempt to purify $RyR1_{(2091-2708)}$ expressed from the pMALp2g vector.

3.2.4 Affinity purification of the of $RyR1_{(2091-2708)}$

A dextrin-conjugated agarose column attached to an ÄKTA prime system was used to partially purify the RyR1 region (figure 3.6). The conditions used to partially purify the protein have been summarised in methods section 2.2.6.1.

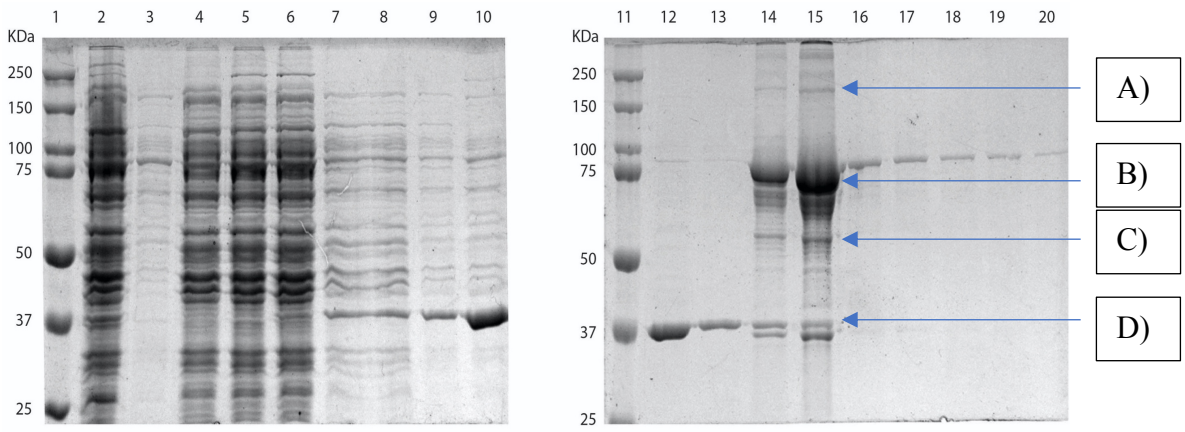

Figure 3.6. Purification of the MBP tagged RyR1 2091-2708 using a dextrin-conjugated agarose column. 1&11, Precision plus protein standard. 2, *E. coli* cell lysate following expression of MBP tagged RyR1 2091-2708. 3-5 flow through following loading of the column. 6-10,12-13 column washes. 14-20, protein fractions eluted from the column. The proteins whose identity was confirmed by mass spectrometry have been indicated by blue arrows. Band B) was confirmed to correspond to $RyR1_{(2091-2708)}$ the identity of bands A), C) and D) have been described in appendix 2.6

The RyR1 region migrated through the gel at a rate faster than its theoretical mass of 120 kDa, suggesting a protein with a mass of approximately 90 KDa had been produced and partially purified from the cell lysate. Mass spectrometry was used to confirm the identity of the expressed protein as the RyR1 amino acids 2091-2452 along with the MBP tag (appendix 2.5.2.1). The theoretical mass of this RyR1 region along with the purification tag is 90 kDa. This may suggest the RyR1 region is being subjected to protease digestion by host proteases. A protein with a mass of approximately 40 KDa, the theoretical mass of the RyR1 region also appears to be expressed following the cells exposure to IPTG (appendix 2.5.2.1).

The MBP-tagged RyR1 region was partially purified from the *E. coli* cell lysate, however a number of other proteins were also eluted from the column. The identity of three of these proteins were confirmed to correspond to outer membrane protein F, 39 kDa, and the 60 kDa chaperone protein (appendix 2.6). Interestingly the protein with an apparent mass of approximately 200 kDa was confirmed to correspond to the RyR1 region along with the maltose binding protein tag, which may suggest the tagged RyR1 region is forming an interaction with itself that is strong enough to withstand the denaturing conditions used to prepare proteins for SDS PAGE. There are also proteins visible on the gel with a higher

molecular mass than this protein, with the mass of each increasing by the approximate mass of the expressed RyR1 region. This may suggest the expressed RyR1 region is forming multimers and possibly a soluble aggregate. The maltose binding protein tag is still functional as the protein can be enriched using both the amylose conjugated agarose and dextrin Sepharose purification resins. The identity of these proteins has not been confirmed.

A protein with a mass of approximately 40 KDa was visible in the flow through during dextrin column purification. This protein had a very long elution window and may correspond to the cleaved C-terminal region of the protein. There are a number of hydrophobic amino acids within the region which may be involved in self-association. Transient separation may explain why this protein has such a broad wash window as it is likely forming an interaction with immobilised protein and migrating very slowly through the column. This protein was not analysed by mass spectrometry.

The tagged RyR1 region also has a very broad elution window following column washes in 20 mM maltose, with a large amount of the protein remaining bound to the column after being washed in 8 bed volumes of elution buffer, the concentration of maltose in the elution buffer was increased to 100 mM in an attempt to increase the elution efficiency however there was little or no change (figure 3.7). The protein remaining immobilised on the column could only be eluted from the column under denaturing conditions in 0.1 % SDS (labelled SDS in figure 3.7).

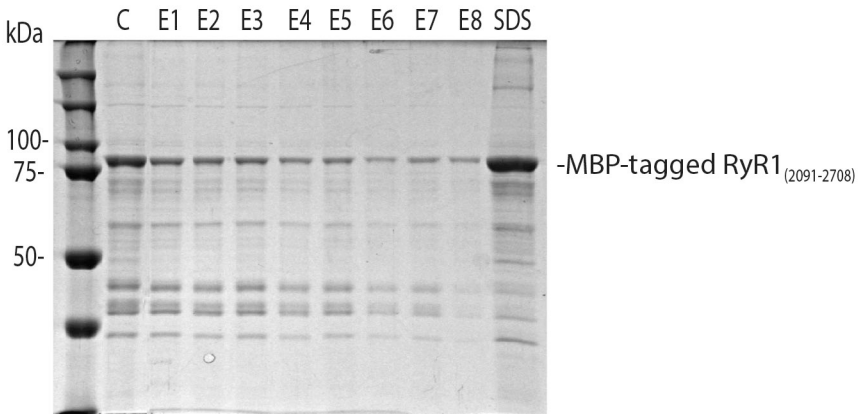

Figure 3.7. Example of the elution of MBP tagged $RyR1_{(2091-2708)}$ from an amylose conjugated resin. C, the resin prior to elution. E1-8 individual protein fractions collected following elution in 100 mM maltose. SDS, Proteins eluted from the resin under denaturing conditions in 0.1 % SDS. The Precision plus protein standard was used to estimate the approximate mass of proteins. Proteins were separated by SDS-PAGE for ninety minutes at 120 mV and visualised by Coomassie blue staining.

When the MBP tag, expressed from the empty pMALp2g was subjected to the same elution steps process, the protein was completely eluted when washed in 6 column volumes of 10 mM maltose (appendix 2.7). No MBP was eluted from the column when the column was washed in SDS suggesting all protein had been eluted in the prior wash steps. The prolonged elution characteristics of the tagged RyR1 region may result from the RyR1 region inhibiting maltose's access to the binding site of MBP. This may also result from another protein immobilised on the column inhibiting the interaction between maltose and MBP. Should an aggregated protein have formed it may also have inhibited MBP from undergoing the conformational change required to bind maltose allowing release from the resin. Should this be the case it is interesting to note that MBP is still functional and can bind both amylose and maltose, which may suggest any aggregation occurs solely due to the RyR1 region.

The expressed RyR1 region also contained a $His_{(6)}$ purification tag located between the MBP tag and the TEV recognition site. A Ni-NTA column was used to determine if this purification tag could be utilised to further purify the recombinant protein as described in methods section 2.2.6.2. In this case the majority of the tagged RyR1 region was located in the flow through during the purification indicating most of the protein did not form an interaction with

the column. A small amount was immobilised on the resin and could be later eluted in 500 mM imidazole (figure 3.8).

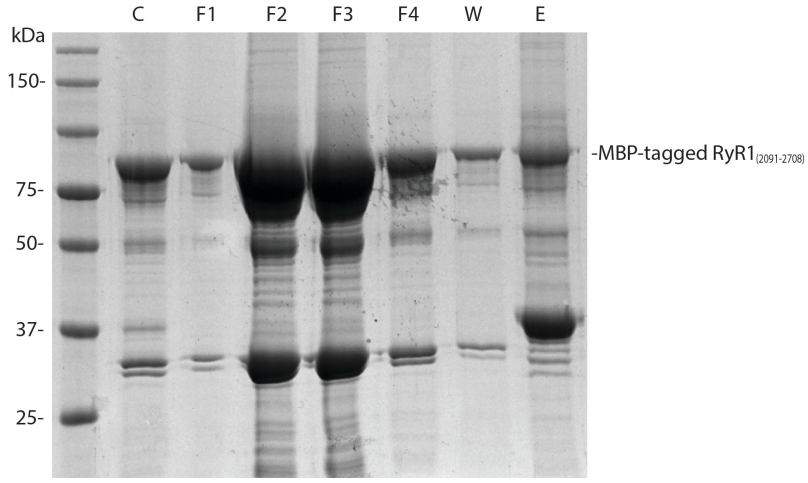

Figure 3.8. Ni^{+} affinity purification of the MBP-tagged $RyR1_{(2091-2708)}$. C, the protein sample prior to purification. Lanes F1-4 represent the flow through fractions collected during purification. W represents the wash fraction. E represents the protein fraction eluted from the column. The Precision plus protein standard was used to estimate the approximate mass of proteins. Proteins were separated by SDS-PAGE at 120 mV for ninety minutes and visualised by Coomassie blue staining.

Interestingly a protein with a molecular mass of approximately of 37 KDa was enriched and eluted from the column. This suggests that this protein is able to form a stronger interaction with the column compared to the RyR1 region, the identity of this protein was not determined by mass spectrometry. As the MBP-tagged $RyR1_{(2091-2708)}$ could not form a strong interaction with the column it suggests the $His_{(6)}$ tag may be not be accessible to the environment under conditions of the column and as a result a Ni-NTA resin cannot be utilised to purify RyR1.

3.2.5 Anion exchange chromatography

Protein fractions eluted from the dextrin resin were pooled and ion exchange chromatography was used to further purify the tagged RyR1 region from solution. A HiTrap Q FF ion exchange column was used to purify the RyR1 region based on the overall surface charge of the protein. The column has a positively charged immobile phase, to which proteins with an overall negative charge can form an interaction. Increasing the concentration of NaCl

ions in the buffer can lead to elution of immobilised proteins, where Cl^- ions will compete with binding sites on the immobile phase and Na^+ ions will form an interaction with the negative amino acid side chains. The protocol used to partially purify the RyR1 region by anion exchange was described in methods section 2.2.6.3. The RyR1 region has a theoretical isoelectric point of pH 6.23. Therefore, the protein was eluted from the dextrin column in a buffer with a pH of 8, which should cause the protein to have a net negative charge. The buffer also contained a NaCl concentration of 50 mM, which should allow the protein to immobilise on the column and prevent premature elution.

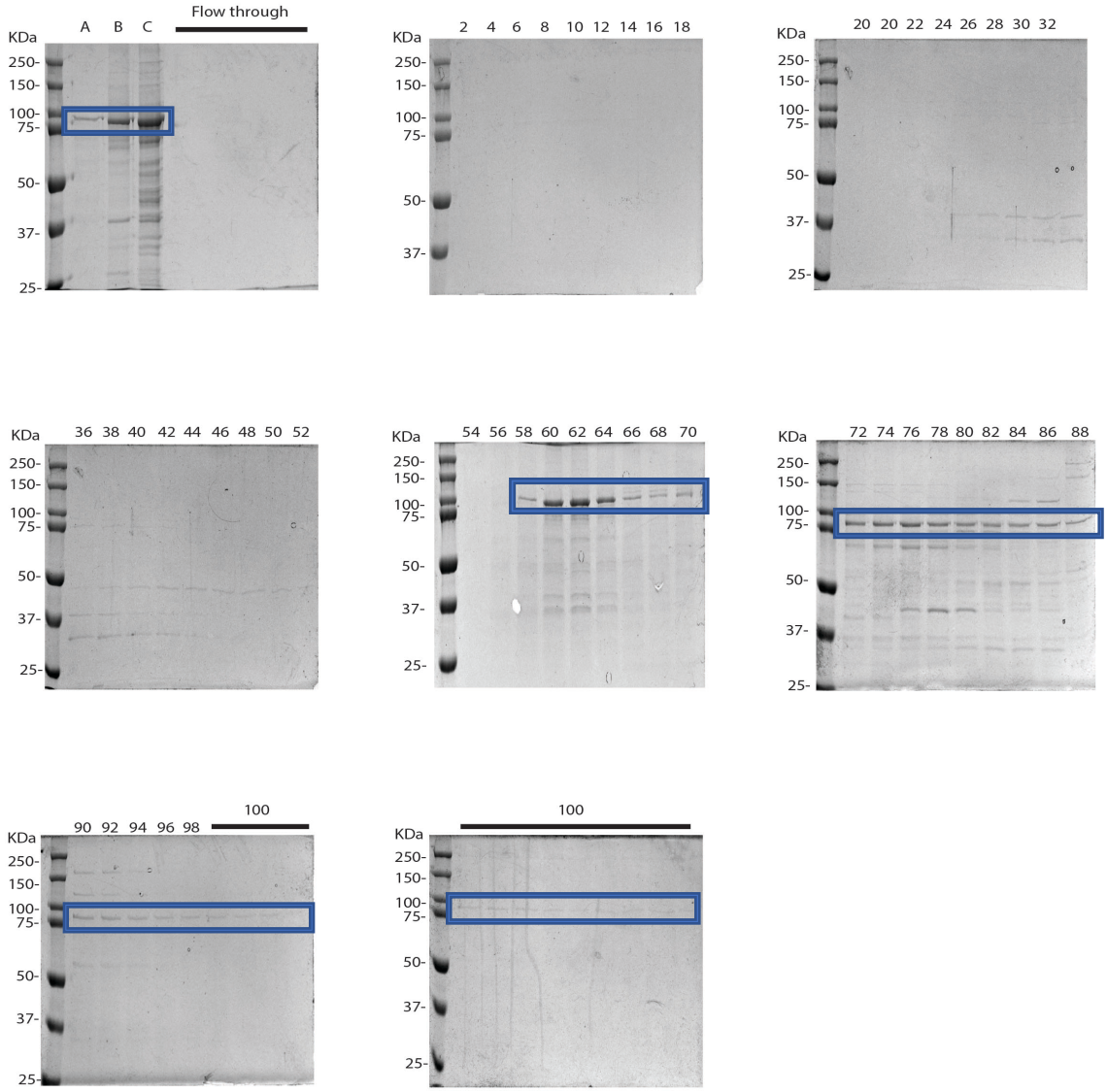

Figure 3.9. Ion exchange chromatography partially purifying the MBP-tagged RyR1 amino acids 2091-2708. Lane 1 of each gel contains the precision plus size marker. A, the protein fraction collected following partial purification using a dextrin conjugated agarose resin. B, the protein fraction following dialysis, with ion exchange buffer. C, the protein fraction following concentration prior to performing ion exchange chromatography. The lanes titled flow through refer to fractions eluted from the column following the loading and washing of the column. Lanes titled 2-100 refer to the percentage increase of elution buffer. $RyR1_{(2091-2708)}$ has been boxed in blue. The Precision plus protein standard was used to estimate the approximate mass of proteins. Proteins were separated on a 10 % acrylamide gel at 120 mV for 90 minutes and visualised by Coomassie blue staining.

The RyR1 region had a very broad elution window, where it was visible in fractions 58-100 (figure 3.9) with biphasic distribution. The RyR1 region may exist in solution in a number of

different populations, each with their own individual physical properties leading to different elution characteristics. The RyR1 region appears to be in a higher proportion in the fractions 60-64 and 74-78, which correspond to the NaCl concentrations 270 mM – 288 mM NaCl and 324 – 342 mM NaCl respectively. This may indicate that a population of RyR1 is more prevalent in these fractions compared to other fractions. No fraction exists that contains a pure RyR1 region. Other proteins are present in all fractions, all of which were eluted from the column within small defined windows. Individual fractions were collected and subjected to digestion by the protease TEV. Regardless of the NaCl concentration used for elution of the MBP-tagged RyR1 region the protein was able to be digested by TEV, however in all concentrations only a partial digestion could be achieved (figure 3.10). Following digestion, both $RyR1_{(2091-2708)}$ and MBP have the same molecular mass of 42 KDa. Should the different fractions each contain a unique population of the RyR1 region it seems that they all contain a TEV recognition site with potentially limited access.

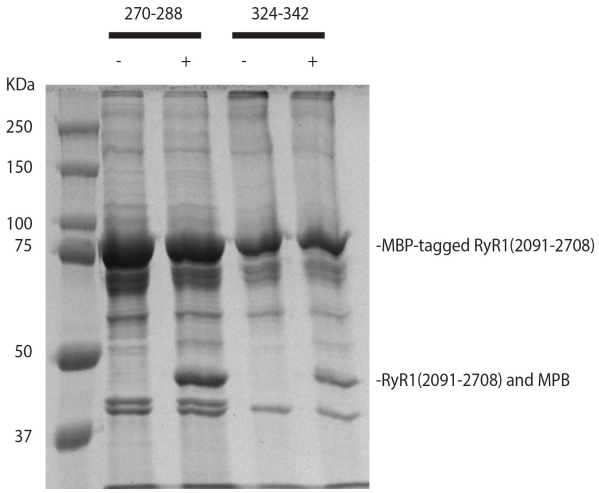

Figure 3.10. An example of TEV digestion of the MBP tagged RyR1 2091-2708 following elution from the Q ion exchange column. Pooled fractions following ion exchange chromatography have been indicated by concentrations of NaCl in mM. A – symbol indicates fractions prior to TEV protease digestion. A + symbol indicates protein fractions following TEV digestion. The Precision plus protein standard was used to estimate the approximate mass of proteins. Proteins were separated on a 10 % acrylamide gel at 120 mV for 90 minutes and visualised by Coomassie blue staining.

3.2.6 Size exclusion chromatography

To further understand if the MBP-tagged RyR1 region exists in solution as a number of different physical states, including monomers and multimers or monomers with different physical size, the protein fraction following elution from the dextrin column was subjected to size exclusion chromatography, a purification method which separates proteins based on size. A Superdex 200 column was used consisting of dextrin covalently linked to porous agarose beads. These pores are large enough to allow smaller proteins to enter, yet small enough to block the entry of larger proteins. As a result, large proteins travel very quickly through the column, while smaller proteins which can enter the pores and have more distance to travel will elute from the column more slowly. The protocol used to partially purify the RyR1 region by size exclusion chromatography is described in methods section 2.2.6.5.

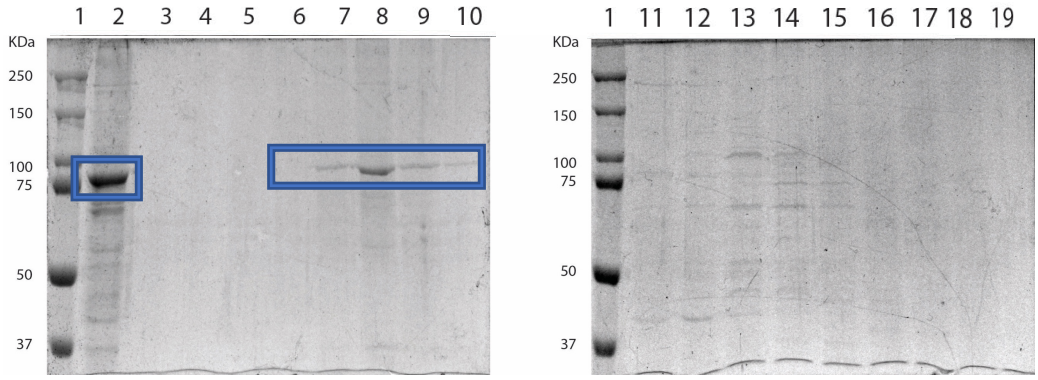

Figure 3.11. Size exclusion chromatography purification of the MBP-tagged RyR1 2091-2708. Lane 1 precision plus protein standard. Lane 2, the protein fraction prior to purification. Lanes 3-19 fractions eluted from the column during purification, the MBP-tagged $RyR1_{(2091-2708)}$ has been boxed in blue. The Precision plus protein standard was used to estimate the approximate mass of proteins. Proteins were separated on a 10 % acrylamide gel at 120 mV for 90 minutes and visualised by Coomassie blue staining.

The tagged RyR1 region eluted very quickly from the column (figure 3.11). Other proteins were also visible in the fractions that contained the tagged RyR1 region including a protein of approximately 37 KDa and a number of proteins between the mass of 50 KDa and 70 KDa. As all of these proteins vary in mass and elute in the same fraction it may suggest the proteins have formed an interaction with each other. Unlike ion exchange chromatography, the RyR1 region eluted from the column in a very defined window, suggesting that all of the MBP-tagged RyR1 proteins have a similar surface area. The RyR1 region eluted more quickly than other proteins with a higher molecular mass, when analysed by SDS PAGE, suggesting that

the RyR1 region possibly in combination with the other proteins in solution has a larger native mass than expected.

Size exclusion chromatography was also performed on the RyR1 region following ion exchange chromatography and TEV digestion. A similar elution pattern with respect to the non-digested RyR1 region was noticed as before (visible in fractions 12-14 along with other smaller proteins in figure 3.12). The digested RyR1 region was not visible on the gel following SDS PAGE. The protein would have been diluted during this purification step and as a result was not visible.

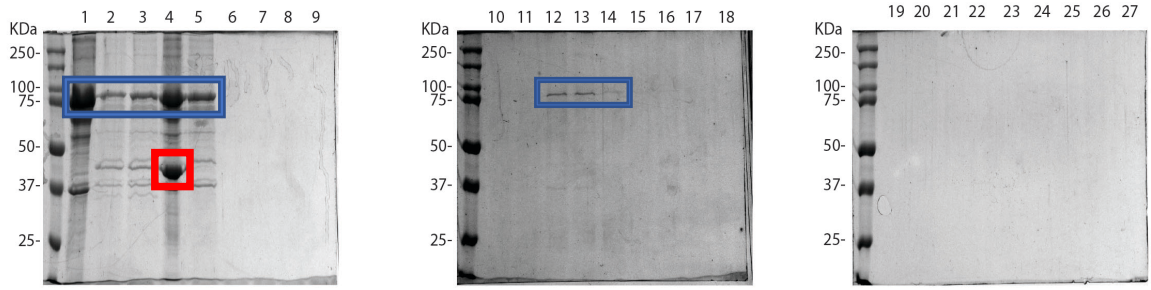

Figure 3.12. Size exclusion chromatography of $RyR1_{(2091-2708)}$ following TEV digestion. 1, partial purification of $RyR1_{(2091-2708)}$ using dextrin conjugated agarose. 2, fraction eluted from during the Q ion exchange column in 270 mM NaCl. 3, fraction eluted from the Q ion exchange column in 288 mM NaCl. 4, Pooled protein fraction following digestion with TEV, this also serves as the protein fraction loaded onto the S200 column. 5, Pooled fractions eluted from the Q ion exchange column before digestion with TEV. Fractions 6-27 were individual fractions collected following size exclusion chromatography. The MBP-$RyR1_{(2091-2708)}$ is boxed in blue, MBP and $RyR1_{(2091-2708)}$ following TEV digestion is boxed in red. The Precision plus protein standard was used to estimate the approximate mass of proteins. Proteins were separated by 12.5 % acrylamide SDS PAGE at 120 mV for ninety minutes and visualised by Coomassie blue staining.

The chromatogram observed following this purification step suggested a local peak in protein concentration was observed in fractions A12-B1 (figure 3.13 A) corresponding to lanes 17 and 18 in figure 3.11. As no protein was visible in these fractions following SDS-PAGE analysis, the fractions were pooled and concentrated to determine if the fractions contained the cleaved RyR1 region (figure 3.13 B). Following concentration, no protein was visible following SDS PAGE which may suggest the protein was not present in the fraction to begin with. The cleaved $RyR1_{(2091-2708)}$ was present in the protein fraction prior to the purification being

performed, however it was not visible following size exclusion which may suggest the protein was diluted during the process such that the final concentration was insufficient to be visualised.

A)

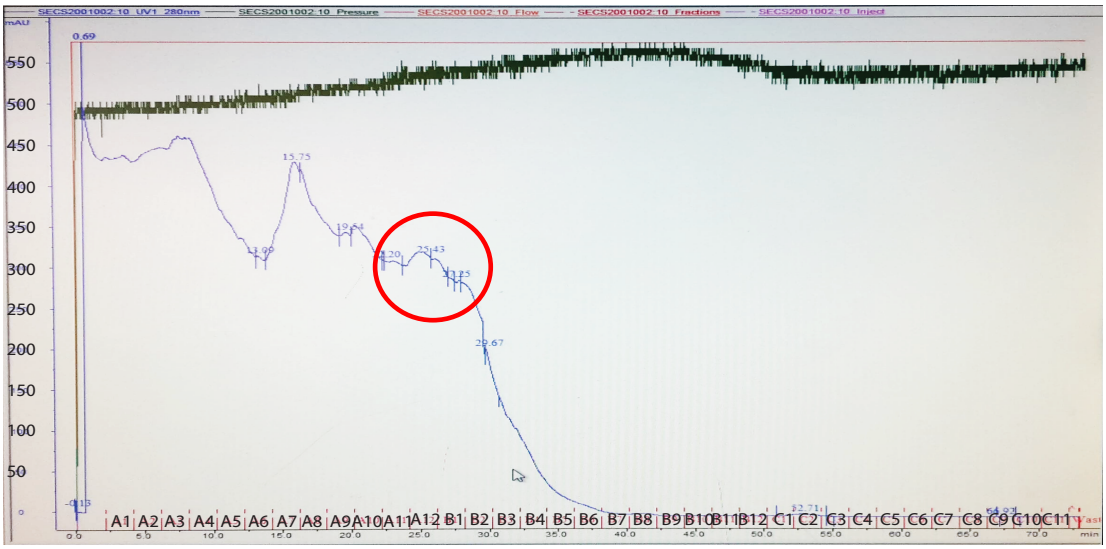

B)

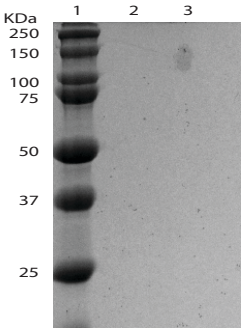

Figure 3.13. Chromatogram observed following size exclusion chromatography and concentration of fractions thought to contain the cleaved RyR1$_{(2091-2708)}$. A) chromatogram following size exclusion of the cleaved RyR1$_{(2091-2708)}$. The green line represents the pressure within the column. The blue line represents the protein concentration of the eluted fractions. Individual fractions have been represented at the bottom of the figure. The fractions pooled and concentrated have been highlighted with a red circle. B) concentration of the fractions A12-B1. 1, Precision plus size marker. 2, pooled protein fractions prior to concentration. 3, Protein fractions following concentration.

3.2.7 Hydrophobic interaction chromatography

Hydrophobic interaction chromatography was attempted to further purify the tagged RyR1 region following ion exchange chromatography as described in methods section 2.2.6.4. A HiTrap™ Phenyl FF (HS) column was used which consists of a hydrophobic, phenyl, immobile phase. Suspending the protein in a high ionic strength buffer encourages exposed hydrophobic amino acids to form an interaction with the column. Reducing the ionic strength of the buffer eventually leads to the elution of the protein. Pooled protein fractions following ion exchange chromatography were dialysed against a buffer containing 1 M NaCl and loaded onto the column. As the ionic strength of the buffer decreased, the pressure within the system increased, eventually increasing to the maximum column pressure recommended by the manufacturer. The flow rate was decreased in order to lower the pressure in the system to drop allowing the fractionation to continue, however the pressure within the system slowly increased as the salt concentration decreased. The flow rate within the system was further decreased and eventually a flow rate of 0.1 mL per min was used to finish the fractionation. No protein appeared to be eluted from the column when collected fractions were analysed by SDS PAGE (figure 3.14). The protein may have precipitated within the column and may be the reason why the pressure within the system increased, as the precipitate may have prevented flow through the system. Further attempts at purifying the HD1 region of RyR1$_{(2091-2708)}$ were discontinued.

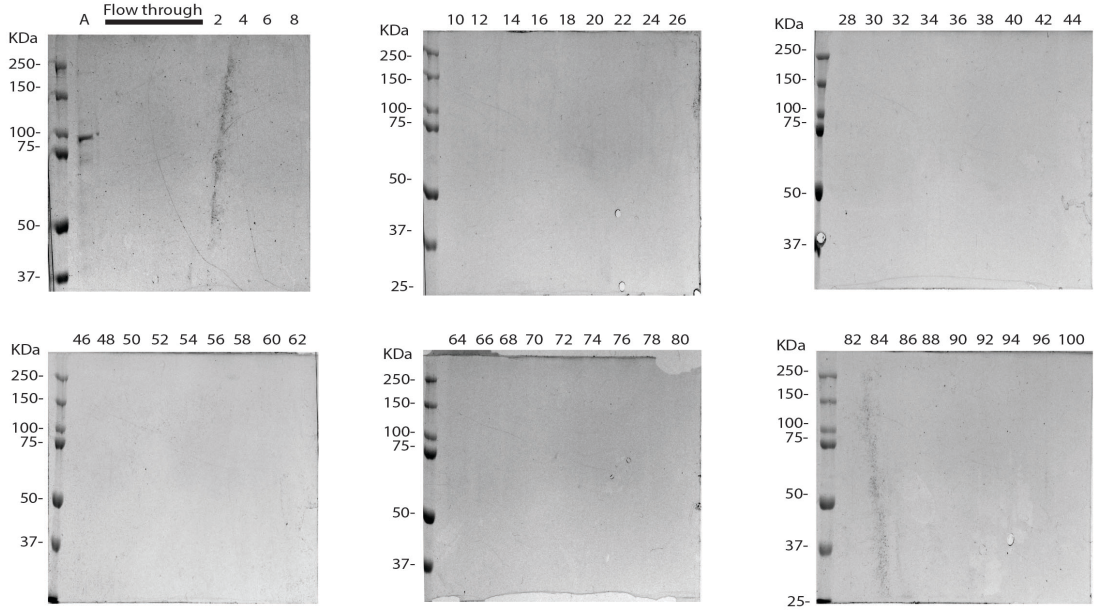

Figure 3.14. Hydrophobic interaction chromatography of the MBP-tagged RyR1$_{(2091-2708)}$. A) protein fraction prior to performing hydrophobic interaction chromatography. The lanes titled flow through refer to fractions eluted from the column following the loading and washing of the column. Lanes titled 2-100 refer to the percentage increase of elution buffer. The Precision plus protein standard was used to estimate the approximate mass of proteins. Proteins were separated on a 10 % acrylamide gel at 120 mV for 90 minutes and were visualised by Coomassie blue staining.

3.2.8 Characterising a potential interaction between the RyR1 NTD and HD1.

The helical domain 1 has been shown to form an interaction with the adjacent N-terminal domain of RyR1 in the context of the full-length channel purified from rabbit skeletal muscle (9). The arginine residues 2360 and 2452 have been shown to be pivotal in the interaction between the two domains both of which form hydrogen bonds across the domains. The N-terminal domain of human RyR1 had been previously cloned into the pGEX6p3 vector and shown to be soluble following recombinant expression (96). The expressed region corresponds to the RyR1 amino acids 1-558 (accession number NM_000540.2) and corresponds to the region of rabbit RyR1 previously structurally characterised (75). The N-terminal domain contains an N-terminal GST tag for partial purification from solution using Glutathione Sepharose®.

To initially characterise a potential interaction between the HD1 and the N-terminal domain pull-down assays were attempted. The MBP-tagged RyR1$_{(2091-2708)}$ was partially purified from an *E. coli* cell lysate using an amylose conjugated resin. The resin was incubated with an *E. coli* cell lysate containing the expressed GST-tagged N-terminal domain as described in methods section 2.2.7. As both the tagged N-terminal domain and the MBP-tagged HD1 have approximately the same molecular mass, it is difficult to analyse the interaction using SDS-PAGE. Therefore, western blot analysis, using an antibody against the GST tag, was used to characterise the potential interaction (figure 3.15).

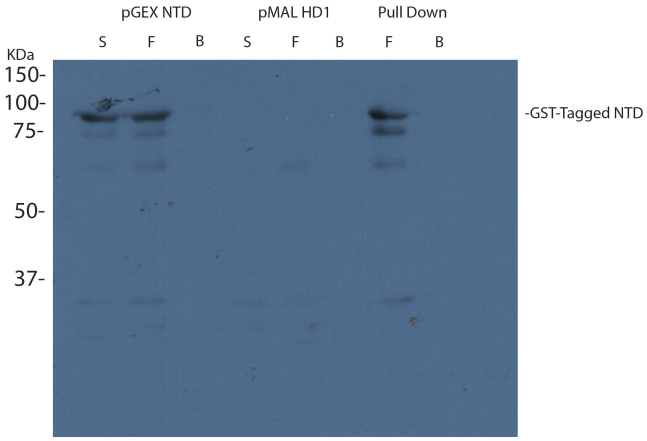

Figure 3.15. Western blot to analyse the potential interaction between the RyR1 N-terminal domain and the HD1. S, supernatant prior to pull down. F, Flow through collected following incubation with the beads. B, beads collected following incubation. Proteins were separated by SDS-PAGE at 120 mV for ninety minutes and transferred to an immobilin membrane at 70 mV for one hour. Proteins were labelled with a GST specific antibody and visualised using a horse radish peroxidase conjugated secondary antibody.

The N-terminal domain of RyR1 did not appear to form a measurable interaction with the HD1 under the conditions used. As the HD1 is likely being subjected to digestion by an *E. coli* host protease (an event thought to occur surrounding the amino acid arginine 2452, an amino acid previously shown to be essential in the interaction between the two regions (9)) the N-terminal binding site within the HD1 may not be present in its entirety or correct conformation. Other amino acids known to be located at the interface between the two regions including arginine 2355 and arginine 2359 were present. However, the truncation of the RyR1 region may lead to an alteration in the tertiary structure in the local region which

may have had an effect on the interaction of the two proteins. The region of the N-terminal domain which forms an interaction with the HD1 is proposed to consist largely of loop regions (9). The variability in the structure of these regions may also account for the lack of interaction between the two regions following recombinant expression. As neither protein was able to be purified to an extent acceptable for circular dichroism it is impossible to say if either recombinantly expressed protein adopted the correct secondary structure which may suggest the correct tertiary structure is present. The possibility still remains neither protein had adopted the correct overall tertiary structure. Contaminating *E. coli* host proteins which potentially form an interaction with the RyR1 HD1 may also block the interaction between the two recombinantly expressed proteins.

3.3 Discussion

Different regions of the HD1 were expressed from a range of expression vectors, this was performed to increase the possibility of expressing a soluble protein. Of the 28 vectors that were constructed, a protein was expressed from only 11. Interestingly, following the addition of IPTG to the cells that did not express a protein the cells stalled in growth and their $O.D_{600}$ did not increase. This could suggest that the tagged RyR1 was being expressed, however this may have had a negative effect on cell growth possibly resulting from the expression of inclusion bodies. The solubilisation of inclusion bodies in denaturing conditions followed by in vitro refolding was not trialled in this study. It has been trialled previously for the HD1 and was shown to be unsuccessful (96). The process can be difficult to optimise as each protein requires a specific set to conditions to firstly solubilise the aggregated protein and secondly to refold the protein following the removal of the denaturant (96, 97). When conditions are optimal the protein will typically adopt the aggregated structure with minimal amounts of the protein being soluble. In most cases inadequate amounts of soluble protein were produced to perform crystallisation trials because of this the use of this technique could not be justified.

Personal discussion with another researcher who has previously attempted to purify recombinant proteins provided insight into the difficulties of expression and purification of domains in isolation from the rest of RyR1 (M. Cassarotto, personal communication, 18 April

2018). It was discussed how a number of vectors are commonly expressed before one is identified as being able to express a soluble recombinant protein, which was the case for this thesis. The purification of recombinant proteins also presented problems in which multiple steps needed to be optimised before sufficient amounts could be obtained. Once purification was successful the crystallisation of the purified protein presented further challenges where a number of different conditions needed to be trialled before the optimal conditions for crystal formation were determined. These discussion point highlight the difficulties in protein purification and the consistency between observations presented in this thesis.

The HD1 was recombinantly expressed in an *E. coli* host and was shown to be soluble in limited amounts. The HD1 in the context of the full length RyR1 interacts with other domains of the channel, including the N-terminal domain and the junctional solenoid. At the interface of these domains are a number of hydrophobic amino acids, which in the context of the full length RyR1 are hidden from the hydrophilic cytosol. However, when the HD1 is expressed in isolation, these residues may be exposed the cytosol or may be folded in a non-native manner. The exposed hydrophobicity is likely a driving force with the predominant amount of the expressed protein adopting an insoluble structure. It would be more energetically favourable for the expressed protein to adopt this alternative structure compared to having the hydrophobic amino acids exposed. In a discussion with Oliver Clark (Columbia University, USA) the researcher who performed a structural characterisation of RyR1 by cryo EM, the high number of hydrophobic amino acids at the extremities of the HD1 was highlighted and it was indicated the recombinant expression of this particular domain as well as other RyR1 domains can be a difficult task. As some of the expressed protein was soluble it is an indication that the protein was able to adopt what could be its native structure. It is still currently unknown if the soluble HD1 expressed in this current research was able to adopt its correct conformation.

Of the 11 proteins that could be expressed only 5 were soluble. While these proteins were soluble each presented their own difficulties during partial purification. The two proteins expressed from the GST tagged proteins RyR1$_{(2091\text{-}2490)}$ and $_{(2091\text{-}2525)}$ were soluble to a very small extent, in which the expression of enough protein for subsequent purification could not be justified. The RyR1 regions (2091-2490) and (2091-2708), expressed from the pMALp2g

vector and (2091-2490) expressed from the pMALp5x vector were more soluble and could be enriched using an amylose conjugated resin. The MBP tagged proteins could be eluted from the amylose resin, however only a relatively small percentage of the protein could be eluted. This could result from the tagged HD1 adopting a structure which shields the MBP from maltose in the elution buffer. The presence of the RyR1 domain may also prevent the MBP from undergoing a conformational change as it releases the amylose or dextrin bound to the resin as it binds maltose which even in the case of drastically increasing the maltose concentration did not aid in the protein being released. It was confirmed that an *E. coli* host chaperone protein was partially purified alongside the RyR1 regions which suggests the chaperonin may assist in folding the RyR1 region and may be doing so in such a way that also prevents maltose from accessing the active site on MBP. It also further suggests the recombinant protein has limited solubility.

The protein RyR1$_{(2091\text{-}2708)}$ appeared to be subjected to protease digestion by an *E. coli* host protease. The recombinant protein has a theoretical molecular mass of 120 KDa, but when analysed by SDS-PAGE the protein was shown to have a molecular mass of approximately 90 KDa. Mass spectrometry analysis of the protein further confirmed this idea where only the RyR1 amino acids 2091-2452 along with the MBP tag were identified. This protease digestion is likely taking place within the cell and as a result the event cannot be inhibited by the addition of a protease inhibitor, as the cells still need to have active proteases to grow and proliferate and create the amino acids required for the expression of the recombinant protein. As the region was soluble and could be partially purified it was selected for further purification.

The next problem was the protease digestion to separate the HD1 from its purification tag. The MBP tagged proteins pMALp2g$_{(2091\text{-}2490)}$ and pMALp5x $_{(2091\text{-}2490)}$ could not be digested while bound to the amylose resin. However, they could be digested following elution from the resin, which suggests the resin may be preventing the specific protease from accessing its recognition site between the purification tag and the HD1.

While the expressed and partially purified HD1 may have formed a multimeric structure and potentially soluble aggregate, this was not confirmed. Interestingly, this putative structure

may be stable enough to withstand the harsh conditions of SDS-PAGE. Which first required the denaturation of the protein in loading dye containing SDS and beta-mercaptoethanol and was then heated to 100 ° C. This was noted in figure 3.6 and appendix 2.6 in which a protein with a mass of approximately 200 kDa was confirmed by mass spectrometry to correspond to the HD1 and the MBP tag, while the tagged HD1 was shown experimentally to have a mass of 90 KDa. If this is the case it is interesting to note that the MBP tag was functional and it is likely that any multimeric state was due to interactions between HD1, leaving MBP in a functionally active condition. However, it seems a population of the recombinant protein exists in which MBP is able to bind amylose or dextrin but is unable to release it when exposed to elution buffer. This may suggest a population of the recombinant protein exists in which the MBP is only partially functional which may result from the formation of a multimeric state. The formation of a multimeric state may also explain why the HD1 did not elute from the amylose or dextrin resins, for the protein to elute all MBP tags bound to the resin would need to be released from the resin. Should even one tag still remain bound it could tether the entire multimeric structure to the resin.

As well as featuring an MBP tag the expressed protein also had a $His_{(6)}$ tag, so that a Ni NTI affinity column could be utilised in an attempt further purify the $RyR1_{(2091-2708)}$. The tagged HD1 however, did not interact with the column to a large enough extent to justify utilising this purification method. This suggests the $His_{(6)}$ tag is shielded from interacting with the immobile phase of the column by either the MBP tag or the HD1.

When ion exchange chromatography was performed in an attempt to further purify the $RyR1_{(2091-2708)}$, it was noted the HD1 eluted from the column with biphasic distribution. This could result from the protein existing in solution in different populations each with their own unique chemical and physical properties. As RyR1 is a homotetramer, it is possible that the expressed protein could also be in different multimeric states. In an attempt to identify a population of the tagged HD1 which could be utilised for further purification each of these potential populations were subjected to protease digestion by TEV. This was carried out to determine if a population that could be digested to completion which would be favoured for further purification over a population that could not be digested. However, no proposed population of $RyR1_{(2091-2708)}$ could be completely digested, which suggests that even if the

RyR1 region exists in solution in range of different populations, all have a TEV recognition site with limited access.

The idea that $RyR1_{(2091-2708)}$ had formed a multimeric structure was further confirmed following size exclusion chromatography. In this case the tagged HD1 passed through the size exclusion column at a faster rate compared to proteins with a larger molecular mass (figure 3.12). This suggests the recombinant protein has a larger surface area than its molecular mass would suggest. Other proteins with a smaller molecular mass also eluted in the same fractions which may suggest these proteins may interact with the RyR1 region. As their identity was not confirmed, the exact reason for their presence in solution is unknown. The elution of the tagged HD1 as a single peak suggests the protein, while potentially existing in different populations, each has a consistent surface area.

When hydrophobic interaction chromatography was trialled to further purify the HD1, the pressure within the column drastically increased and no protein was eluted from the column. This likely suggests that as the salt concentration was decreased the protein bound to the column may have precipitated within the column. This could have resulted from the increased NaCl concentration of 1 M used in the buffer. This was used to immobilise the protein on the column potentially denaturing the recombinant protein. As the salt concentration decreased, while still keeping protein in solution, the HD1 may have begun to refold and ultimately adopted an insoluble aggregated structure. The increased salt concentration could have also affected the interaction between the HD1 and the *E. coli* host chaperonin. Without the physical interaction with the chaperonin the RyR1 region may have lost its stability in solution and eventually dropped out of solution forming an aggregated structure. As the aggregate began to form it may have pulled the surrounding proteins out of solution causing the precipitate to expand throughout the column.

Because $RyR1_{(2091-2708)}$ could not be purified following dextrin, Ni NTA, ion exchange, size exclusion chromatography and hydrophobic interaction chromatography, efforts to obtain a pure protein were halted.

The N-terminal domain of RyR1 did not appear to form an interaction with the HD1 during *in vitro* binding assays. This does not rule out an interaction in the context of full length RyR1. The results from expression suggest that the HD1 is cleaved by protease digestion by an *E. coli* host protease. This is thought to occur surrounding the amino acid arginine 2452, an amino acid shown to form a hydrogen bond with serine 174 of the N terminal domain. Therefore, the interface between the two domains may not be complete. Host protease digestion of the HD1 may also allow the recombinant protein to adopt a non-native structure allowing more freedom of movement surrounding the newly created C-terminal end. This may limit the interaction between the two domains. The binding interface between the NTD and HD1 is comprised predominantly of loop regions, which typically have freedom of movement until non-covalent interactions cause the region to adopt a more ordered structure. Because the N-terminal domain was also expressed in isolation from the rest of RyR1, the loop regions are likely to have more freedom of movement in comparison to the native protein where they could be fixed in place by the surrounding RyR1 domains and as such are less likely to be in the exact position to interact with the predominantly alpha helical HD1. The potential multimeric structure of the HD1 could also have affected the interaction of the two recombinantly expressed proteins, where the binding site of the NTD may be taken up by another HD1. The presence of purification tags on both proteins may have also been the cause of the lack of interaction, where the tags could interfere with the interaction.

3.4 Chapter summary

A functionally significant region of RyR1 was cloned for recombinant expression which included the region corresponding to the RyR1 amino acids 2091-2708. The region was shown to be soluble following expression in an *E. coli* host and could be partially purified using batch purification when the maltose binding protein purification tag was exploited. The RyR1 region was likely subjected to protease digestion by an *E. coli* host protease and as a result only a truncated region could be detected during the purification process. Other proteins were enriched alongside the RyR1 region and included a chaperonin protein which may indicate that the expressed protein is unstable or insoluble. The region was subjected to other purification techniques including size exclusion, anion exchange and hydrophobic interaction

chromatography. The region could not be purified to an extent acceptable for any biochemical analysis or crystallisation trials to be performed and as a result the intended structural characterisation could not be performed.

4. *In silico* characterisation of MH pathogenic RyR1 variants.

4.1 Introduction

The RyR1 HD1 (amino acids 2091-2708) could not be purified following recombinant expression, therefore variants within this region could not be structurally characterised by X-ray crystallography. Instead, pathogenic variants within the HD1 were analysed *in silico* to assess the utility of this approach for pathogenicity prediction. The protein visualisation software PyMOL was used to assess pathogenic variants and infer why a functional change in RyR1 has taken place.

The rabbit RyR1 has been structurally characterised by cryo electron microscopy with an overall resolution of 3.8 Å in both the open and closed states (9). Two separate structures of the channel were published in the open conformation, one in the ryanodine bound state and one in the Ca^{2+}, ATP and caffeine bound state. In the closed state the channel was purified in the absence of ATP and in the presence of EGTA. Two further structures were also published, in the presence of either Ca^{2+} or ATP in the closed but primed conformation. The primed conformation refers to a conformational change in the cytosolic region of RyR1 but with the channel pore closed. A hypothesis was proposed that the protein adopts this conformation in preparation for a final stimulus resulting in channel opening (9). For all structures the resolution was highest surrounding the pore of the channel, where specific amino acid side chains could be identified. The resolution decreased at the extremities of the protein tetramer and while in many cases amino acids could be identified by side chain, certain regions of the channel could only be identified by secondary structure. As a general rule, the farther the region was laterally from the centre of the channel the more difficult the region was to identify with high resolution. The HD1 amino acids 2479 - 2734 could only be identified by amino acid backbone where the alpha helical secondary structure could be visualised. This lack of resolution limits any attempted mapping of potential structural changes induced by a pathogenic variant.

The ryanodine receptor was shown to consist of large rigid domains which are likely to move relative to each other during channel opening, from the closed conformation potentially in the primed state and then to the open conformation. A large and noticeable conformational change is predicted to occur in the cytoplasmic region of the channel, ultimately resulting in a change in conformation of the transmembrane region. This change is thought to cause the amino acid ile 4938 (NM_000540.2) to be rotated out of the pore allowing Ca^{2+} ions to migrate through the channel. This amino acid is therefore thought to act as a hydrophobic plug preventing the passage of Ca^{2+} through the channel. Once the amino acid has been repositioned Ca^{2+} would be free to migrate down its concentration gradient into the sarcoplasm.

RyR2 has also been characterised by cryo EM, the overall structure of the protein was very similar to RyR1. The NTD, helical domains, central domain and channel domain share a high amino acid identity between the two isoforms and have very similar structures (98, 99). Disease linked variants were mapped to the structure of RyR2 and a mechanism by which the variant alters RyR2 function was proposed based on the functional characteristics of each variant (100). Two general rules were proposed to explain a functional change in RyR2 resulting from a specific variant. 1) Variants located on the surface may disrupt interactions between RyR and its modulators. 2) Variants within the centre of the protein were thought to affect the interactions between domains which ultimately lead to an alteration in RyR2 function (100).

The second rule further confirmed initial proposals of how certain variants may cause a disease state in either RyR1 or 2. Following the structural characterisation of RyR domains by X-ray crystallography and mapping of variants onto the structure it was noted that a number of variants were located at the extremities of domains and did not affect the structure of the domain itself (101). It was proposed these variants were likely to affect interdomain interactions and thus cause a disease state.

4.2 *In silico* characterisation of MH pathogenic variants

The amino acid numbering in this chapter refers to the rabbit RyR1, accession number P11716. The Protein Data Bank identity 5TB1 was used to visualise the channel in the closed state and 5TAM was used to view the channel in the open state, where the channel was purified in the presence of Ca^{2+}, ATP and caffeine. All variants studied in this chapter have been confirmed as pathogenic for MH-susceptibility and are listed in table 4.1. This chapter represents a proof of principle study on the ability of using *in silico* analysis to predict potentially pathogenic structural changes in RyR1.

Rabbit amino acid and pathogenic variant	Corresponding human amino acid and variant	Pathogenic effect	Reference for function
Arg 2163 Cys	Arg 2163 Cys	MH	(71, 72, 102)
Arg 2163 His	Arg 2163 His	CCD/MH	(30, 72)
Val 2168 Met	Val 2168 Met	MH	(71)
Thr 2206 Met	Thr 2206 Met	MH	(102, 103)
Arg 2336 His	Arg 2336 His	MH	(11)
Ala 2350 Thr	Ala 2350 Thr	MH	(102)
Arg 2355 Trp	Arg 2355 Trp	MH	(11)
Gly 2375 Ala	Gly 2375 Ala	MH	(102)
Ala 2428 Thr	Ala 2428 Thr	MH	(104)
Gly 2434 Arg	Gly 2434 Arg	MH	(102, 105)
Arg 2435 His	Arg 2435 His	CCD/MH	(102)
Arg 2452 Trp	Arg 2452 Trp	MH	(60)
Arg 2454 Cys	Arg 2454 Cys	MH	(102)
Arg 2454 His	Arg 2454 His	MH	(102)
Arg 2458 Cys	Arg 2458 Cys	MH	(102)
Arg 2458 His	Arg 2458 His	MH	(102)

Table 4.1. Summary of the pathogenic amino acid variants that were used for *in silico* analysis. The first column represents the amino acid variant with respect to the rabbit RyR1 numbering (p11716.B). The second column is the corresponding human amino acid (NM_000540.2) change that has been confirmed as being pathogenic. The third column summarises the disease associated with the variant. The fourth column contains references that confirm the pathogenicity of each variant.

4.2.1 Arg 2163

Located on an alpha helix in the helical domain 1, the arg 2163 side chain projects into a pocket between three alpha helices forming a hydrogen bond with the backbone of the residue ser 1729 and leu 2201 in the open state of the channel. However, in the closed state,

arg 2163 forms only a hydrogen bond with ser 1729 (figure 4.1). Serine 1729 is within an adjacent domain called the junctional solenoid, which is the RyR1 domain linked to the binding of FKBP12. As a hydrogen bond forms between these two residues it strongly suggests that arg 2163 plays an important role in the interaction between the two domains.

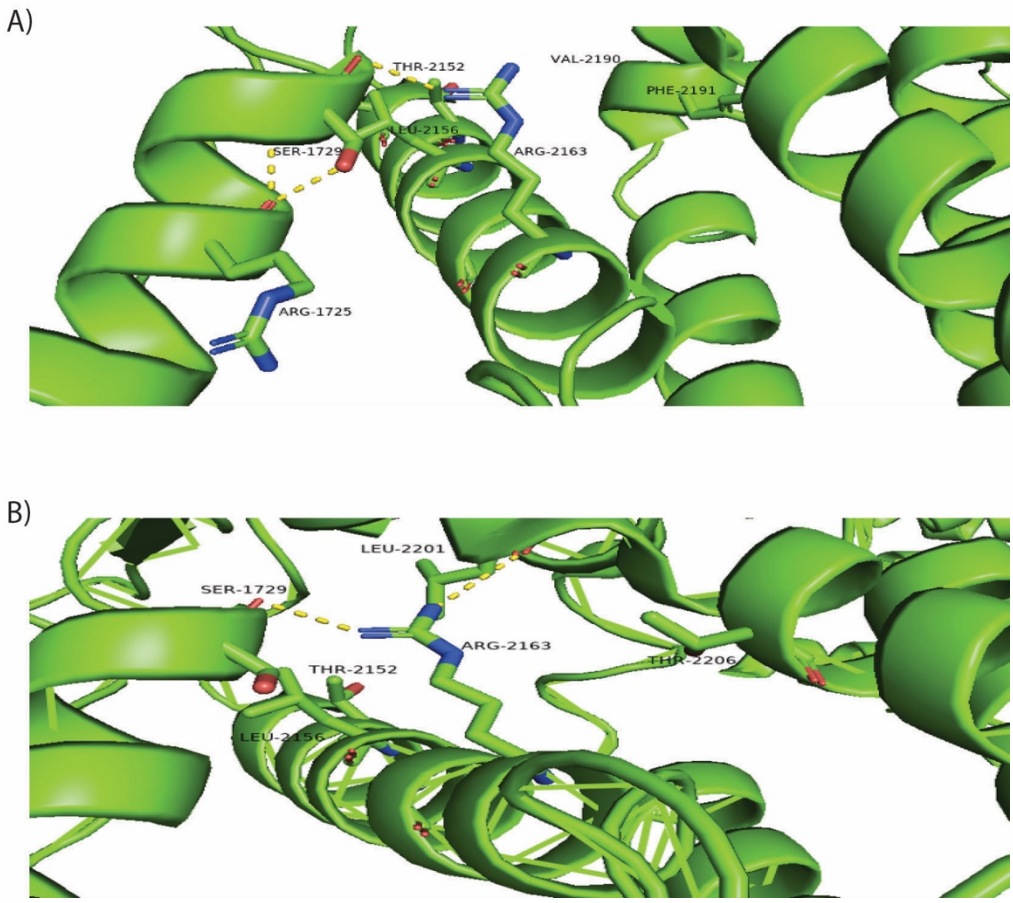

Figure 4.1. Figure depicting the structure of arg 2163 in the closed state A) and open state B). Amino acids have been identified by three letter code; hydrogen bonds have been represented by a broken yellow line. Numbering refers to the rabbit RyR1 and the structure was produced using PyMOL version 2.4.0a0, the PDB ID 5TB1 was used to model the closed state, the PDB ID 5TAM was used to model the open state.

The introduction of the cysteine residue was not predicted to clash with any other amino acid (figure 4.2). The introduction of the variant lead to the loss of the H bonds in both the open and closed states.

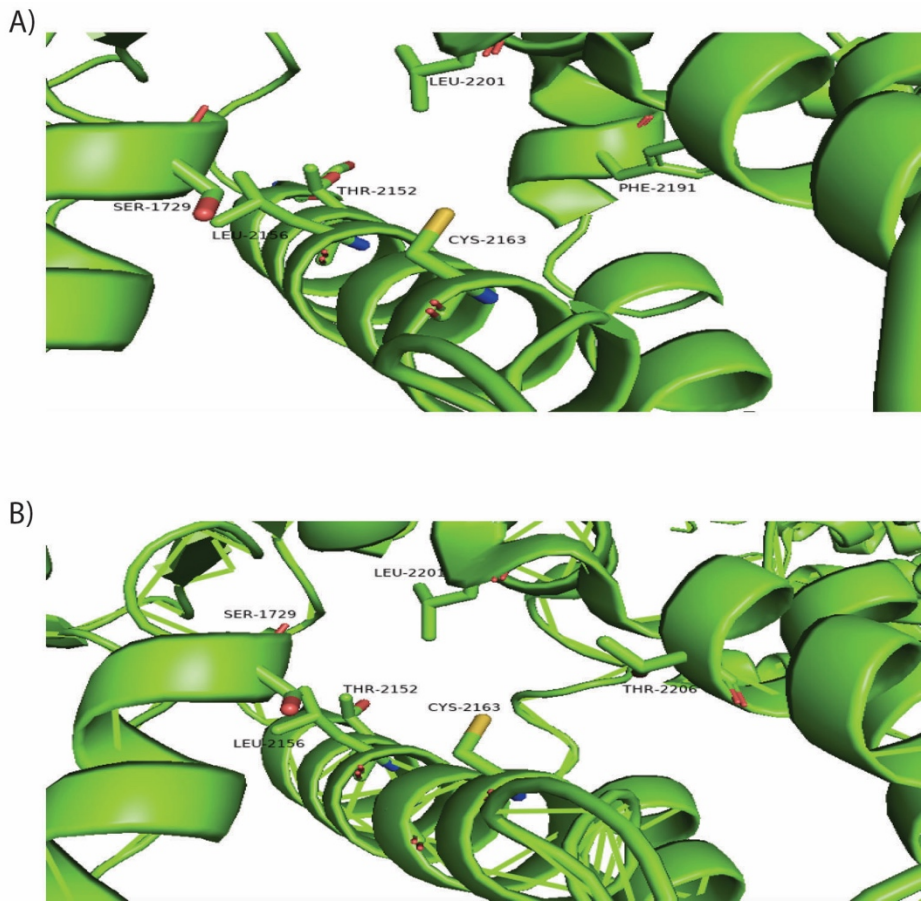

Figure 4.2. Predicted structural changes resulting from the arg 2163 cys variant. A) the closed state. B) the open state. Amino acids have been identified by three letter code. Numbering refers to the rabbit RyR1 and the structure was produced using PyMOL version 2.4.0a0, the PDB ID 5TB1 was used to model the closed state, the PDB ID 5TAM was used to model the open state.

The arg 2163 cys variant has been functionally characterised in both dyspedic myotubes (71, 72) and stably expressing HEK 293 cells (102). When myotubes were exposed to 10 mM caffeine the peak release of Ca^{2+} was similar to that of WT (72), however at lower concentrations the variant was shown to have an increased response to caffeine compared to a WT control (71). Cells expressing the variant were also shown to release Ca^{2+} at rest (72); in this case the cells would undergo oscillations of Ca^{2+} release which were not visible in cells expressing WT RyR1. This phenomenon was also observed in other cell lines expressing MH and CCD linked variants including the variants thr 4636 ala, tyr 4795 cys, arg 2435 leu, thr 4826 ile, arg 615 cys, Δglu 2348. Cells expressing the arg 2163 cys variant had an increased number of oscillations compared to other variants, however both the open duration of the channel and the peak Ca^{2+} release was lower compared to other variants. Despite the

constant fluctuations in RyR1 opening there was no change in the overall cytosolic Ca^{2+} concentration. Together with the similar response to 10 mM caffeine compared to WT these data suggest no change in the amount of Ca^{2+} stored in the SR (72). When ryanodine binding was used to characterise the opening probability of the variant following its expression in myotubes both the variant containing and WT channels behaved very similarly in activating Ca^{2+} concentrations, between 10 nM and 10 µM, where the EC_{50} for both proteins was the same (71). In contrast the variant channel had a weaker response to the inhibition by both Ca^{2+} (between 400 µM – 2 mM) and Mg^{2+} (between 0.3 and 10 mM) where higher concentrations of the antagonists were required to achieve the same level of inhibition as WT (71). Interestingly, when a similar experiment was performed following the expression of RyR1 in HEK293 cells opposing results were noted (102). The variant containing channel expressed in HEK 293 cells was more sensitive to Ca^{2+} activation compared to WT RyR1, however similar inhibition by Ca^{2+} was noted, which could suggest CICR could be responsible for the premature Ca^{2+} release. Alternatively, the conflicting results could be due to RyR1 being expressed in different cell lines. The dyspedic myotubes express a number of other proteins typically expressed in skeletal muscle and as a result these proteins may affect the regulation of RyR1 and may also be present following the preparation of RyR1 containing microsomes for analysis. HEK 293 cells do not express these proteins and as a result RyR1 would be in isolation (106, 107). RyR1 could also be subjected to different post-translational modifications in different cell lines, something which is common for other proteins (108). Differences in the systems used to characterise the binding of ryanodine could have also had an effect on the results which may ultimately result in the conflicting results reported for the effects of Ca^{2+}.

Taken together, these results suggest that the variant causes destabilisation of the channel in the closed state which allows the channel to open and close without stimulation. This could indicate the hydrogen bond that forms between arg 2163 and ser 1729 is essential in stabilising the closed and / or primed conformations. While the variant appears to destabilise the channel leading to Ca^{2+} release at rest the exact mechanism by which this takes place cannot be determined using the currently available data. In addition, while the variant appears to cause a Ca^{2+} leak into the cytosol at rest, the amount that passes through the channel is not likely to be substantial as it does not appear to have a significant effect on the

SR stores. The leak may result from a channel that is easily activated, or from a channel that is difficult to inhibit compared to WT. While PyMOL did not predict structural hinderance would be caused by the cysteine substitution, (which would strongly suggest a conformational change would take place), the presence of the thiol group at the expense of a positive charge may lead to a conformational change or at the very least lead to a lack of stability in the closed state, potentially due to fewer H-bonds. The variant has been implicated in an alteration in regulation by Ca^{2+} (71, 102). As the arg 2163 residue is not in close proximity to either the high or low affinity Ca^{2+} binding sites, there is a possibility that long range structural changes may take place which may ultimately affect the binding of Ca^{2+} or the propagation of the resulting conformational change throughout the channel. The variant is located at the interface between the HD1 and the junctional solenoid so the loss of the hydrogen bond that links the two domains could have a significant effect on how the two domains move relative to each other during the opening of the channel (9). The loss of this bond and the eventual destabilisation of the domain interface could also cause the channel to favour the open state, leading to the Ca^{2+} leak at rest, and under MH-inducing conditions lead to the mass release of Ca^{2+} from the SR. The presence of the variant could also have an effect on the primed conformation as it appears that binding of Ca^{2+} is enough to open the channel. The binding of Ca^{2+} to WT RyR1 is predicted to cause the channel to adopt the primed conformation, and the subsequent binding of ATP to cause the channel to open (9). The variant may introduce an instability or a structural change in the primed conformation that causes the channel to transition directly to the open state without binding ATP.

The onset of MH in patients with the Arg 2163 Cys variant may stem from an RyR1 that can leak Ca^{2+} at rest, a process which is exacerbated following exposure to triggering agonists (72). This mechanism the onset of MH has been previously proposed for other RyR1 variants (109). While an exact mechanism by which this takes place has yet to be determined, the argument could be made that the variant will cause the channel to be easily activated or that the channel is more difficult to inhibit. Determining the structure of the variant containing channel in the context of the full length RyR1 would provide more in-depth insight into the mechanism by which this takes place. A structure in the Ca^{2+} and or Mg^{2+} bound state would determine the conformation that the channel adopts following the binding of each ion, which in turn would provide a greater understanding of the opening characteristics of this particular

channel. It must also be kept in mind that the number of variant-containing subunits within the tetramer could also have an effect on the mechanism by which RyR1 opens and closes. Six possible combinations of the variant-containing tetramer could be produced when expressed in a heterozygous host, each of which could have their own unique functional properties (110, 111).

A pathogenic histidine variant has also been identified at residue 2163 in both CCD and MH-susceptible individuals (72). Structural hinderance with a clash with amino acid serine 1729 was predicted to occur when the variant was modelled using PyMOL in both open and closed conformations (figure 4.3).

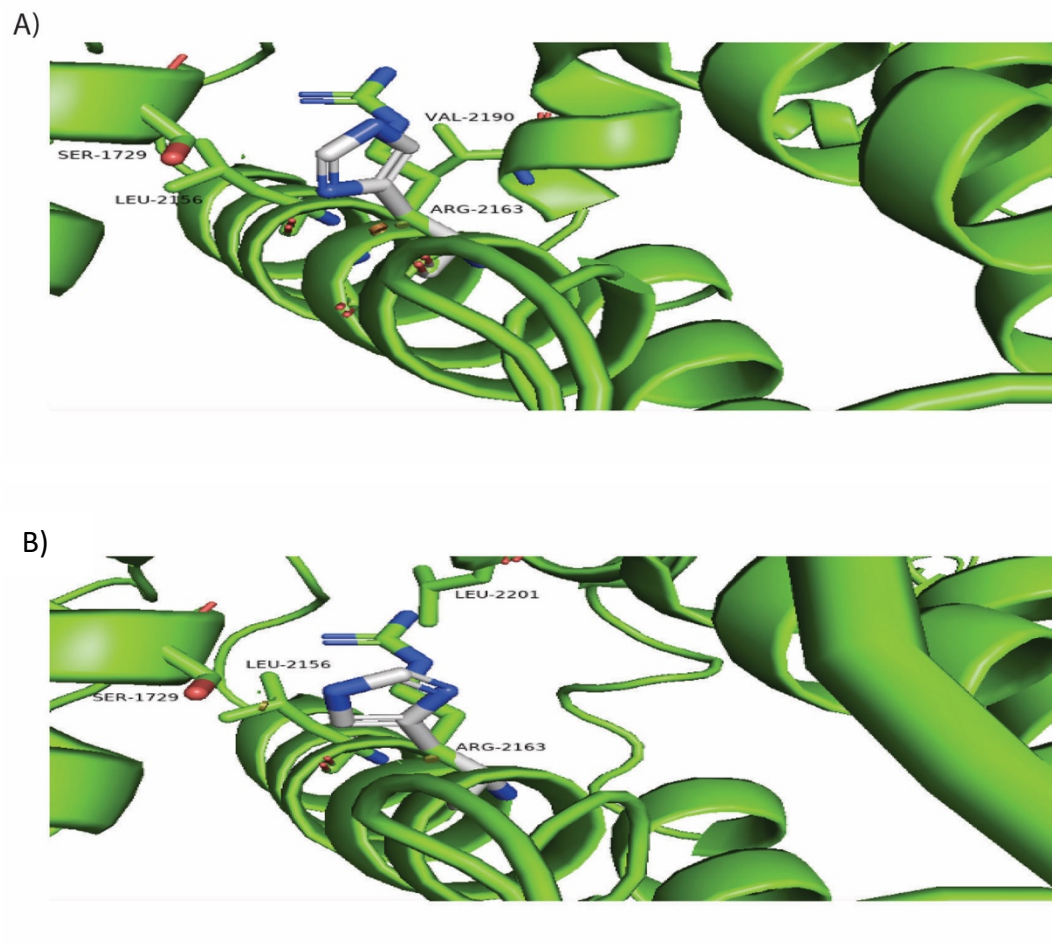

Figure 4.3. Modelling of the R2163H variant. A) Modelling of the R2163H variant in the closed state. B) Modelling of the R2163H variant in the open state. Numbering refers to the rabbit RyR1 and the structure was produced using PyMOL version 2.4.0a0, the PDB ID 5TB1 was used to model the closed state, the PDB ID 5TAM was used to model the open state.

The presence of the histidine variant has a more pronounced effect on the closed conformation compared to the cysteine variant previously described (72). In functional studies, the histidine containing channel also underwent oscillations but the opening of RyR1 was more frequent ultimately resulting in an increased cytosolic concentration of Ca^{2+} (72). Variant-containing cells exposed to 10 mM caffeine were shown to have a decreased response to the agonist with less Ca^{2+} released from the SR in comparison to WT RyR1 (72). This likely results from the continual leak of Ca^{2+} across the SR membrane, depleting stores leading to the muscle weakness characteristic of CCD. Because of the continual leak, a Ca^{2+} concentration gradient could not be maintained across the SR and as such there would be very little available Ca^{2+} for release into the cytosol following the activation of RyR1. The his variant was also shown to have an increased response to voltage stimulation compared to WT (72), with the channel opening at lessor voltage stimulation compared to WT. This is likely due to the leaky nature of the channel that is more prone to opening than WT. Peak release of Ca^{2+} in the his variant was diminished compared to WT RyR1 further supporting the suggestion that the SR stores were depleted prior to stimulation (72). This observation provides further support for the suggestion that SR Ca^{2+} store depletion may be the mechanism underlying CCD. The histidine variant was also shown to be more prone to Ca^{2+} activation compared to WT RyR1 and the arg 2163 cys variant (102). The increased Ca^{2+}-induced activation may explain the continual Ca^{2+} leak from the SR due to the high cytosolic concentration of Ca^{2+} surrounding the SR membrane. Loss of the hydrogen bond with ser 1729 in the closed conformation and the presence of the larger histidine residue which also causes a structural hinderance likely causes the channel to favour the open state which is exaggerated by the binding of Ca^{2+} to the high affinity binding site on RyR1. As it appears the binding of Ca^{2+} may be enough to open the channel in the absence of other ligands it is likely the presence of the his variant causes RyR1 to transition through the primed conformation and into the open state without the need for other stimuli.

A patient is diagnosed as being MHS by IVCT or CHCT if the measured contracture strength exceeds a defined threshold (112). *In vitro* studies have shown that cells expressing the arg 2163 cys variant will release lesser amounts of Ca^{2+} compared to a WT control, which potentially explains the muscle weakness observed in some patients (72). The same studies

have also shown that the variant-containing cells release Ca^{2+} at lower concentrations of agonists compared to an MHN control, supporting hypersensitivity. It is likely that sufficient Ca^{2+} can be released from the SR at lower agonist concentrations to induce muscle contractions above the threshold to be consistent with MH. The leaky nature of the channel is once again a potential explanation for this and it is accepted that the channel can easily transition from the closed state into the open state (72). The presence of MH-inducing agonists is likely to exaggerate this effect ultimately leading to further Ca^{2+} release.

Once again, a structure of the full-length RyR1 containing the arg 2163 his variant could provide further insight into the mechanism by which the channel is causing both MH and CCD. A structure in the Ca^{2+} bound state, would provide insight into whether the channel is able to transition directly into the open state following the binding of Ca^{2+}.

4.2.2 Val 2168

Valine 2168 is located on a loop region between two alpha helices and is in close proximity to the amino acid arg 615, (arg 614 in human RyR1, accession number NM_000540.2) of the same subunit in both the open and closed states of the channel (figure 4.4). Interestingly the arg 614 cys variant has also been shown to be pathogenic for MH, highlighting the potential importance of the interaction between the HD1 and the N terminal domain, in which the arg 615 cys is located, in the regulation of RyR1. The introduction of the methionine variant was predicted to clash with arg 615 in both the open and closed states.

A)

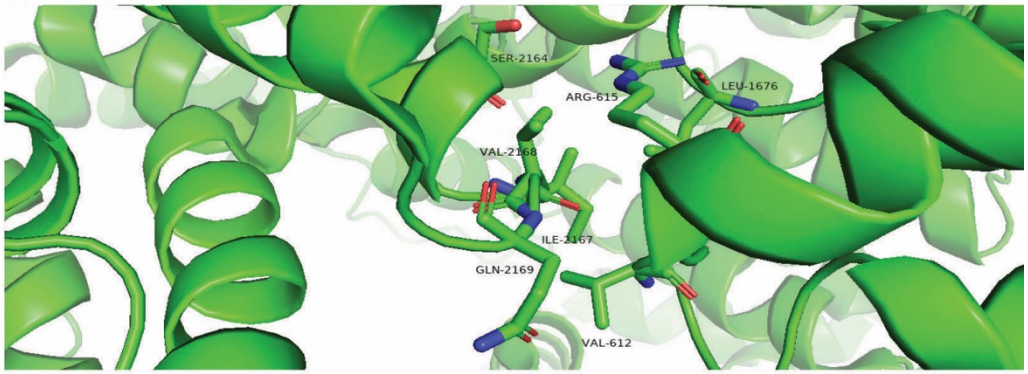
SER-2164
ARG-615
LEU-1676
VAL-2168
ILE-2167
GLN-2169
VAL-612

B)

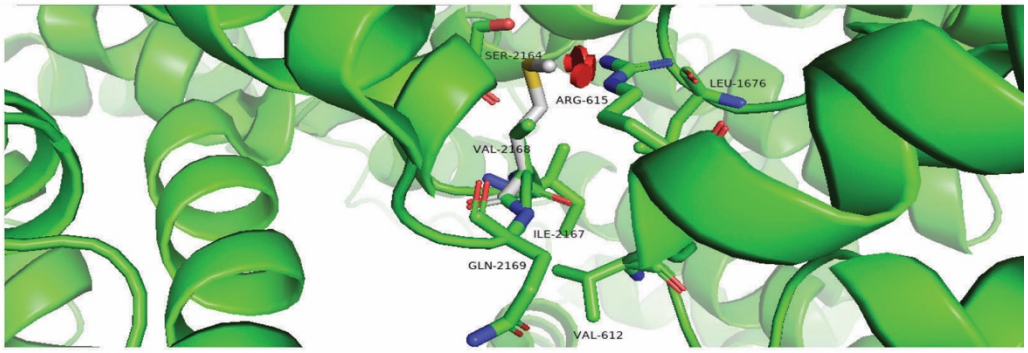
SER-2164
LEU-1676
ARG-615
VAL-2168
ILE-2167
GLN-2169
VAL-612

C)

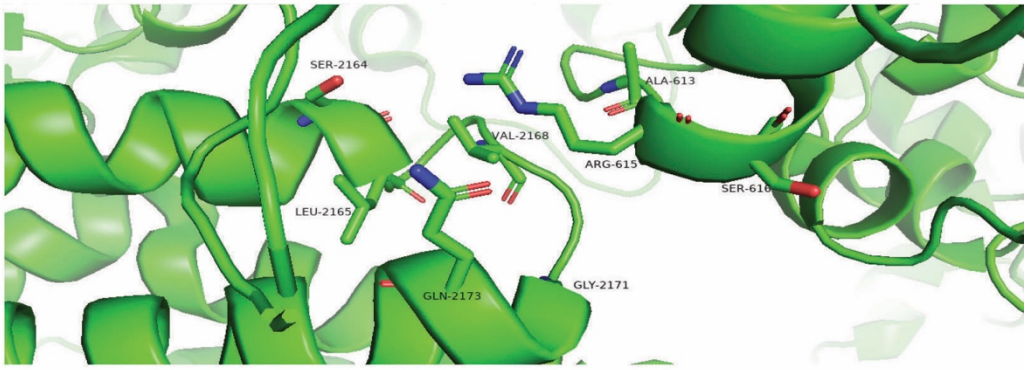
SER-2164
ALA-613
VAL-2168
ARG-615
SER-616
LEU-2165
GLN-2173
GLY-2171

D)

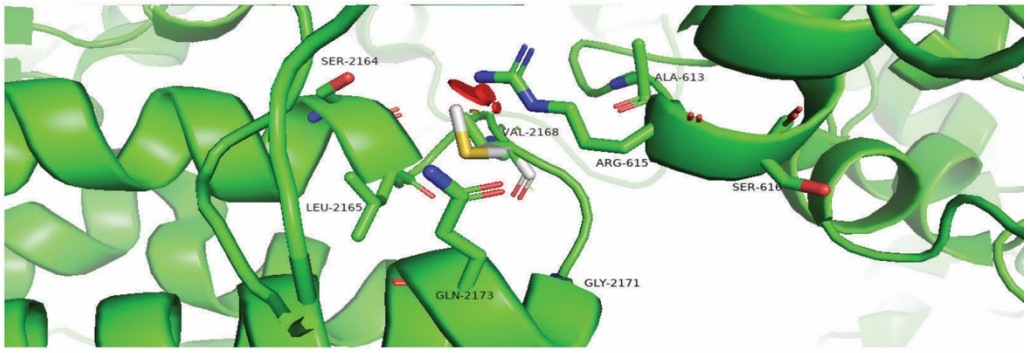
SER-2164
ALA-613
VAL-2168
ARG-615
SER-616
LEU-2165
GLN-2173
GLY-2171

Figure 4.4. Modelling Val 2168 Met in the closed and open states of RyR1. A) Depiction of the region surrounding val 2168 in the closed state of RyR1. B) Predicted structural clashes after modelling the val 2168 met variant have been highlighted by red disks. C) Depiction of the region surrounding val 2168 in the open state of RyR1. D) Predicted structural clashes after modelling the val 2168 met variant have been highlighted by red disks. Numbering refers to the rabbit RyR1 and the structure was produced using PyMOL version 2.4.0a0. The PDB ID 5TB1 was used to model the closed state, while the PDB ID 5TAM was used to model the open state.

Val 2168 met was functionally characterised in dyspedic myotubes which were loaded with fluo 4 (71). The variant-containing cell lines had an increased release of Ca^{2+} response to the agonists KCl, caffeine and 4-CmC compared to a wild type control. The binding of ryanodine in comparison to a WT control was also assessed in this study. The val 2168 met variant had an increased K_I with respect to both Ca^{2+} and Mg^{2+} compared to a wild type control. The EC_{50} for the binding of Ca^{2+} at activating concentrations (between 10 nM and 10 µM) was the same for WT and the variant-containing channel. This suggests that the increased Ca^{2+} release from the SR may result at least in part from a decreased inhibition of RyR1 by both Ca^{2+} and Mg^{2+} allowing RyR1 to remain open longer.

The presence of the methionine variant and the resulting structural hinderance likely leads to a structural change which expands beyond the HD1 into the adjacent N-terminal domain thus resulting in a hypersensitive channel consistent with the MH phenotype. The reduced inhibition by both Ca^{2+} and Mg^{2+} (71) suggests the variant may have far reaching structural changes affecting the binding sites of both of these ions, reducing their affinity for the channel. Alternatively, the variant could prevent the propagation of the resulting conformational change in RyR1 following the binding of the ion, resulting in reduced inhibition.

Considering the effects of Ca^{2+} and Mg^{2+}, it is possible that an MH reaction in patients with the val 2168 met variant results from a channel that is more likely to remain in the open state after opening. An increased open duration of the channel could result in an increased release of Ca^{2+} into the cytosol leading to an MH episode. In addition, structural characterisation of

the channel in both the Ca^{2+} and Mg^{2+} bound states in comparison to WT would highlight any functional differences between WT and mutant channel.

4.2.3 Thr 2206

Thr 2206 is located on an alpha helix and is in close proximity to other helices within the same subunit in both the open and closed states (figure 4.5). Thr 2206 is in close proximity to the amino acid arg 2163, located on an adjacent alpha helix. The mutation of arg 2163 to either cys or his has been confirmed as being MH pathogenic. As two amino acids with the potential of causing MH are located in close proximity to each other it highlights the importance of the local region in the overall function or regulation of RyR1. When the pathogenic 2206 methionine variant was modelled it was shown to clash with leu 2166 in both the open and closed states.

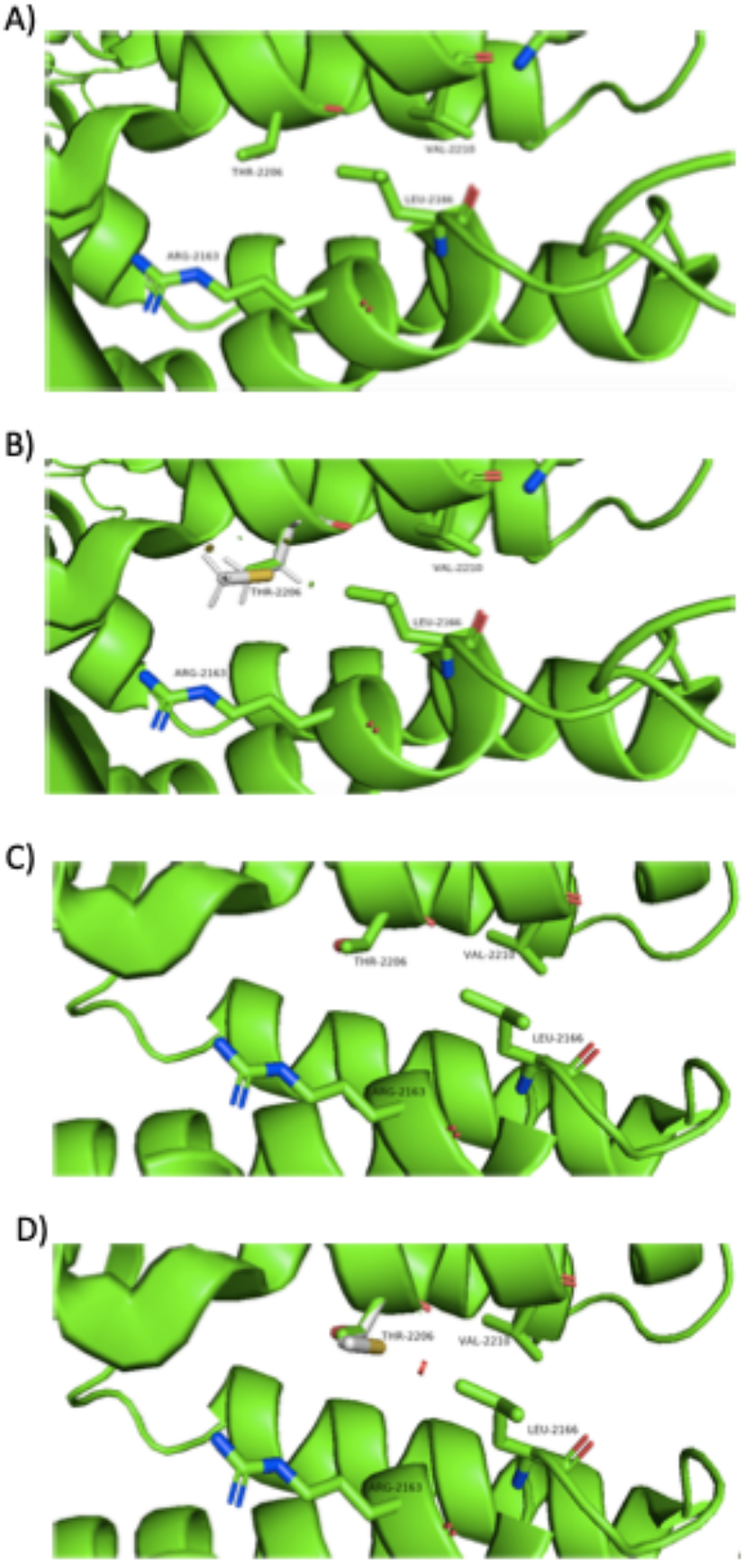
A)
THR-2206
VAL-2210
LEU-2166
ARG-2163
B)
THR-2206
VAL-2210
LEU-2166
ARG-2163
C)
THR-2206
VAL-2210
LEU-2166
ARG-2163
D)
THR-2206
VAL-2210
LEU-2166
ARG-2163

Figure 4.5. Structural modelling of the MH pathogenic variant thr 2206 met variant. A) structural modelling of the 2206 in the closed state. B) structural modelling of the 2206 in the open state. C) Structural hinderances following the introduction of the methionine variant in the closed state. D) Structural hinderances following the introduction of the thr2206met variant in the open state. Numbering refers to the rabbit RyR1 and the structure was produced using PyMOL version 2.4.0a0, the PDB ID 5TB1 was used to model the closed state, the PDB ID 5TAM was used to model the open state.

Functional characterisation of the thr 2206 met variant was carried out in stably expressing HEK 293 cells (102). Cells expressing the variant were shown to have a lower overall release of Ca^{2+} following exposure to 10 mM caffeine compared to wild type, however the EC_{50} for caffeine release was significantly lower. Cells expressing the thr 2206 met variant were also shown to have an increased resting cytosolic [Ca^{2+}] compared to WT and a diminished resting ER Ca^{2+} level. This suggests that the variant RyR1 is leaking Ca^{2+} into the cytosol. While a Ca^{2+} leak appears to occur, the extent of this does not seem to be large enough to cause CCD as the variant has yet to be identified in CCD patients.

When ryanodine binding was used to monitor the open probability of the channel it was shown that at rest the variant-containing channel was more likely to open compared to WT, but the open probability was much less than the CCD causative arg 2168 his variant (102). To monitor the effect of CICR on the opening of the channel, the channel was exposed to increasing levels of Ca^{2+} (102). The variant-containing channel was shown have a decreased K_A, half the concentration of Ca^{2+} required to induce maximal RyR1 opening, and increased A_{max}, the total number of RyR1 channels open, at activating levels of Ca^{2+} compared to WT, suggesting that the variant-containing channel is more prone to CICR compared to WT. The variant containing channels also had an increased K_I, half the concentration of Ca^{2+} required to inhibit RyR1, compared to WT indicating the variant is more difficult to inhibit compared to WT RyR1.

The methionine residue was shown to cause a structural hinderance when modelled in PyMOL which is likely to cause a conformational change. Methionine is also different chemically to threonine having a thiol group compared to the polar group of threonine which

can also have an effect on the structure of the protein. The structural implications of the variant may be changes in local environment, as well as structural changes propagating through the local domain into surrounding domains and / or changes in interdomain interactions. While thr 2206 is not in close proximity to a Ca^{2+} binding site, the methionine variant has an effect on the channels function following the binding of the Ca^{2+} suggesting a longer range structural change may take place.

The onset of MH with respect to the thr 2206 met variant under inducing conditions may result from binding of Ca^{2+} as the channel transitions from the closed state through the primed state into the open state. The high Ca^{2+} concentrations surrounding the SR membrane following the opening of an RyR1 channel may stimulate opening of neighbouring RyR1 channels, ultimately leading to mass Ca^{2+} release into the cytosol. The increased K_I of the variant-containing RyR1 also suggests that the channel does not easily close (102). Both of these factors could lead to an increased open duration of the channel and prolonged Ca^{2+} release from the SR. To further confirm this suggestion, the variant containing RyR1 could be structurally characterised in both Ca^{2+} free and Ca^{2+} bound states, where in each case it the effect of the variant on the structure could be determined.

4.2.4 Arg 2336

Arg 2336 is located on an alpha helix with the side chain projecting towards another helix. In the open state of the channel the side chain of arg 2336 forms a hydrogen bond with the amino acid back bone of the residue leu 2332 and ala 2428 (figure 4.6). These H-bonds were not detected in the closed state of the channel which is an indication the amino acid is more likely to play a role in the formation or stability of the open state.

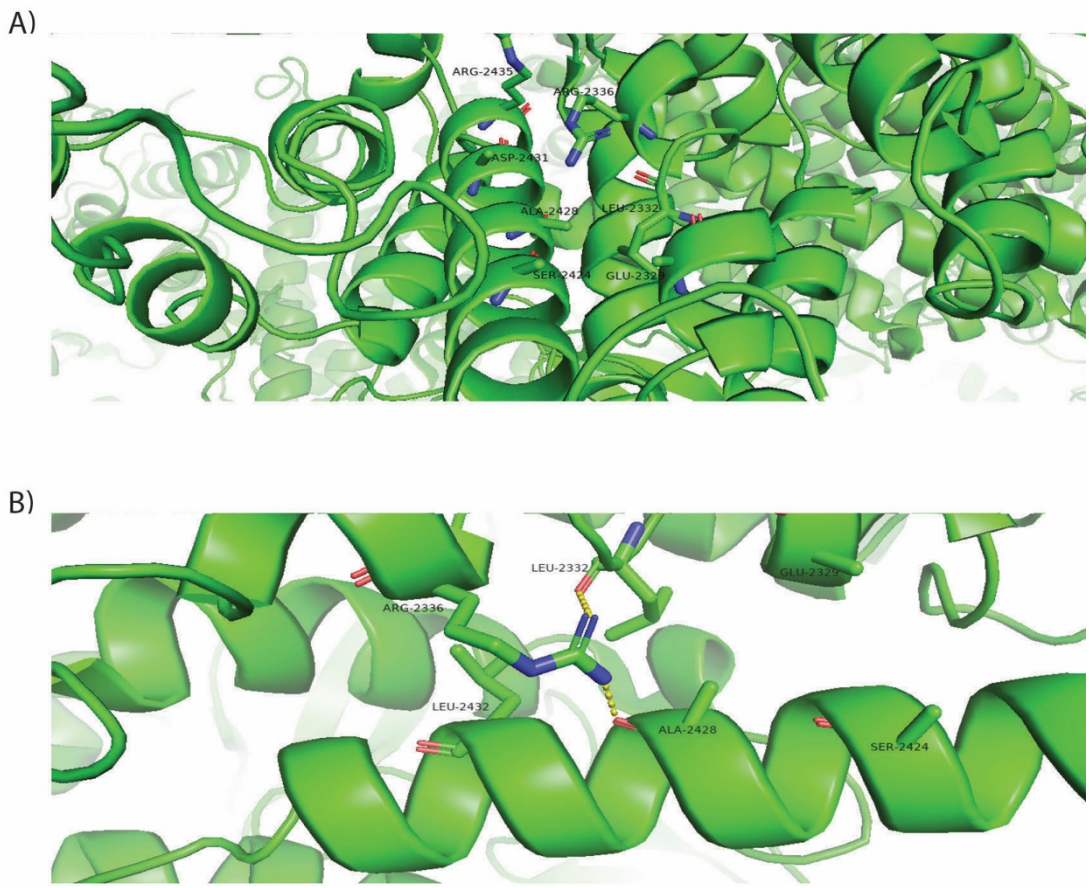

Figure 4.6. Structural modelling of arg 2336 in the A) closed state and B) open state of the RyR1. Hydrogen bonds have been highlighted by broken yellow lines. Numbering refers to the rabbit RyR1 and the structure was produced using PyMOL version 2.4.0a0. The PDB ID 5TB1 was used to model the closed state and the PDB ID 5TAM was used to model the open state.

The MH pathogenic histidine 2336 variant was predicted to clash with arg 2435 and phe 2340 in the closed state, and with the amino acids leu 2332, leu 2432 and ala 2428 in the open state (figure 4.7).

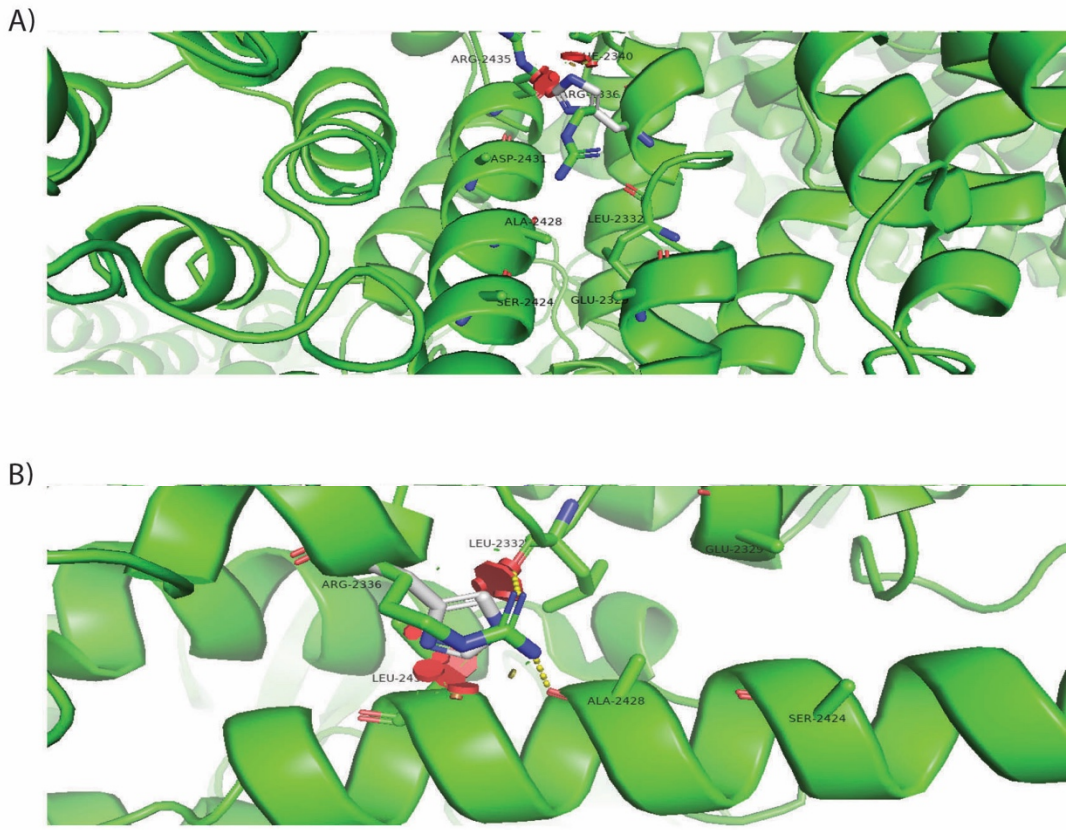

Figure 4.7. Predicted structural hinderance of the arg 2336 his variant A) in the closed state and B) in the open state. Numbering refers to the rabbit RyR1 and the structure was produced using PyMOL version 2.4.0a0. The PDB ID 5TB1 was used to model the closed state and the PDB ID 5TAM was used to model the open state.

This variant was functionally characterised in stably expressing HEK293 cells (11). The cells were shown to have an increased response to caffeine compared to cells expressing WT RyR1, where a significantly decreased EC_{50} for caffeine was noted for the variant. As yet the variant has not been functionally characterised using ryanodine, limiting discussion on open characteristics. However, the structural hindrance and the decreased EC_{50} for caffeine in a cell based assay may be sufficient to explain the hypersensitivity of RyR1 bearing this variant *in vivo*. While a statement cannot be made about the transition of the variant between the closed, primed and open states at rest and in the presence of Ca^{2+} as has been suggested for other variants discussed in this chapter, the arg 2336 his variant may have similar effects. The structural hinderance and loss of hydrogen bonding caused by the variant could result in a structural change which likely propagates through the HD1 and more than likely has an impact on the interaction between HD1 and the adjacent N-terminal domain or Jsol.

4.2.5 Ala 2350

The ala 2350 is located on an alpha helix. In the closed and open state of the channel the residue projects towards a pocket formed between an adjacent loop region where the amino acid is in close proximity to serine 2345 (figure 4.8).

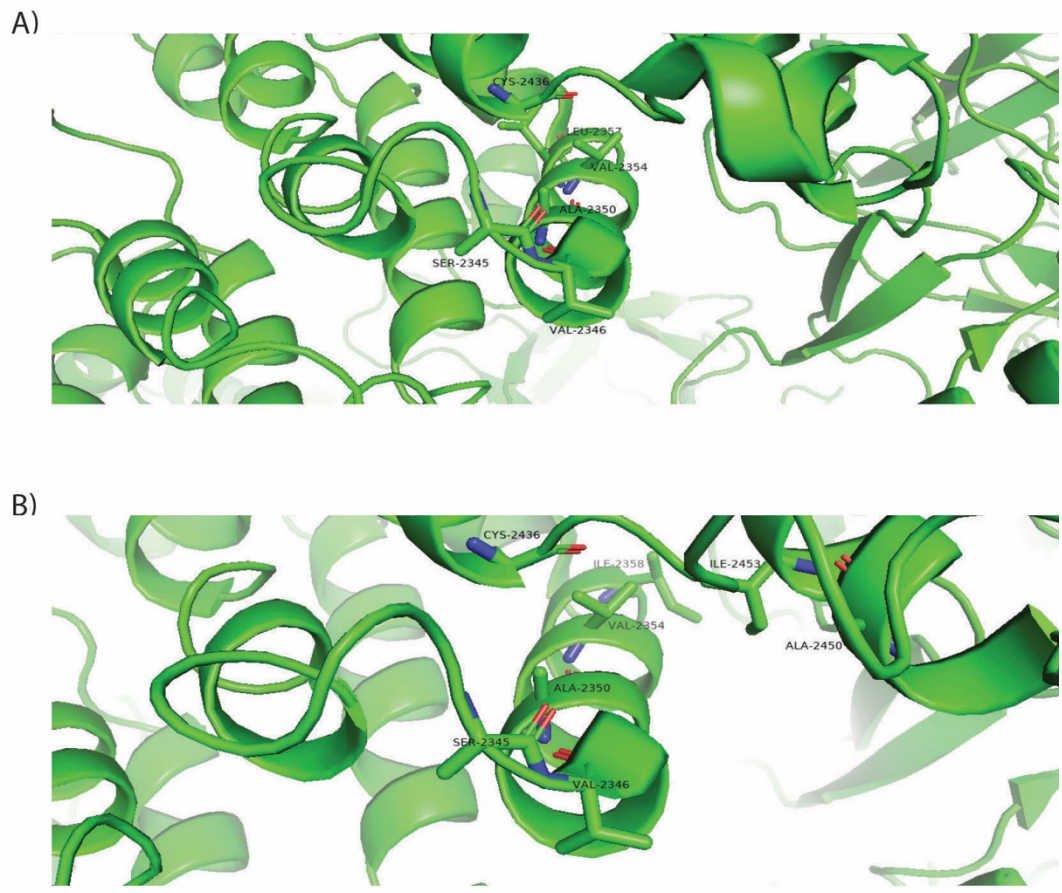

Figure 4.8. Structural modelling of the RyR1 residue ala 2350. A) Closed state. B) Open state. Numbering refers to the rabbit RyR1 and the structure was produced using PyMOL version 2.4.0a0. The PDB ID 5TB1 was used to model the closed state and the PDB ID 5TAM was used to model the open state.

There was no predicted structural hinderance noted in either the closed or open states when the MH pathogenic threonine 2350 variant was modelled using PyMOL (figure 4.9).

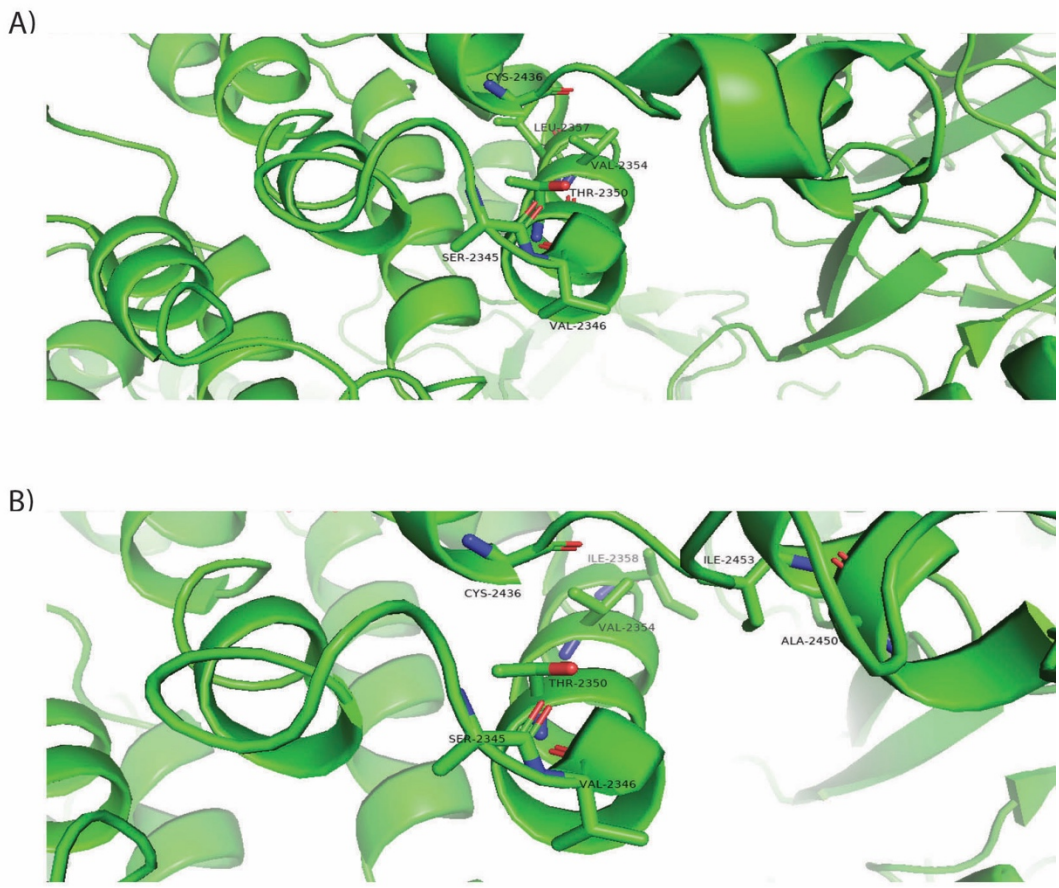

Figure 4.9. Structural modelling of the MH pathogenic ala 2350 thr. A) Thr 2350 in the closed state. B) Thr 2350 in the open state. Numbering refers to the rabbit RyR1 and the structure was produced using PyMOL version 2.4.0a0. The PDB ID 5TB1 was used to model the closed state and the PDB ID 5TAM was used to model the open state.

Stably expressing HEK293 cells were used to functionally characterise the ala 2350 thr variant (102). The cells were shown to have a decreased EC_{50} for caffeine compared to WT, an increased resting cytosolic Ca^{2+} concentration compared to WT and a decreased resting ER Ca^{2+} concentration. Ryanodine binding assays suggested that the variant-containing channels had both a decreased K_A and increased K_I for Ca^{2+}. Indicating the variant containing channels are more prone to opening in the presence of Ca^{2+} (between 10 nM and 10 µM) and less prone to inhibition by Ca^{2+} (Between 400 µM and 2 mM). Taken together, these data suggest that the variant may aid transition of the channel from the primed conformation to the open state following the binding of Ca^{2+}. Ca^{2+} has a weaker inhibitory effect on the variant-containing channel compared to WT suggesting that the channel is less likely to transition from the open state back to either the primed or closed states. As Ca^{2+} is the only agonist required to open the channel the variant on its own may destabilise the primed state in such a way that causes

the channel to transition between the two states independent of other agonists like ATP. As a structural hinderance was not predicted to occur for the ala 2350 thr variant, it is likely the introduction of a polar threonine residue may cause a structural change or instability of the local region leading to a change in RyR1 function.

With respect to the onset of MH, the agonist dependent prolonged release of Ca^{2+} from the ER resulting from the ala 2350 thr variant likely results from an instability created in the primed conformation, where the variant-containing channel may more easily transition into the open state. The decreased inhibition by Ca^{2+} also suggests the channel is less likely to transition from the open state to a closed conformation, further suggesting the variant causes a destabilisation, of the closed or primed state. However, this statement can only be made for Ca^{2+} as the effects of other agonists and antagonists have not been characterised. As RyR1 was expressed in HEK293T cells, there is also the possibility the channel was not subjected to specific post-translational modifications, or the effects of regulatory proteins that would be present in skeletal muscle and which may have an effect on the channels function.

4.2.6 Arg 2355

Arg 2355 is located on an alpha helix with the side chain projecting into a cleft created in the external regions of RyR1 (figure 4.10). This residue does not form an interaction with any other amino acids within RyR1, but may act to form an interaction with other ligands on the cytosolic face of RyR1.

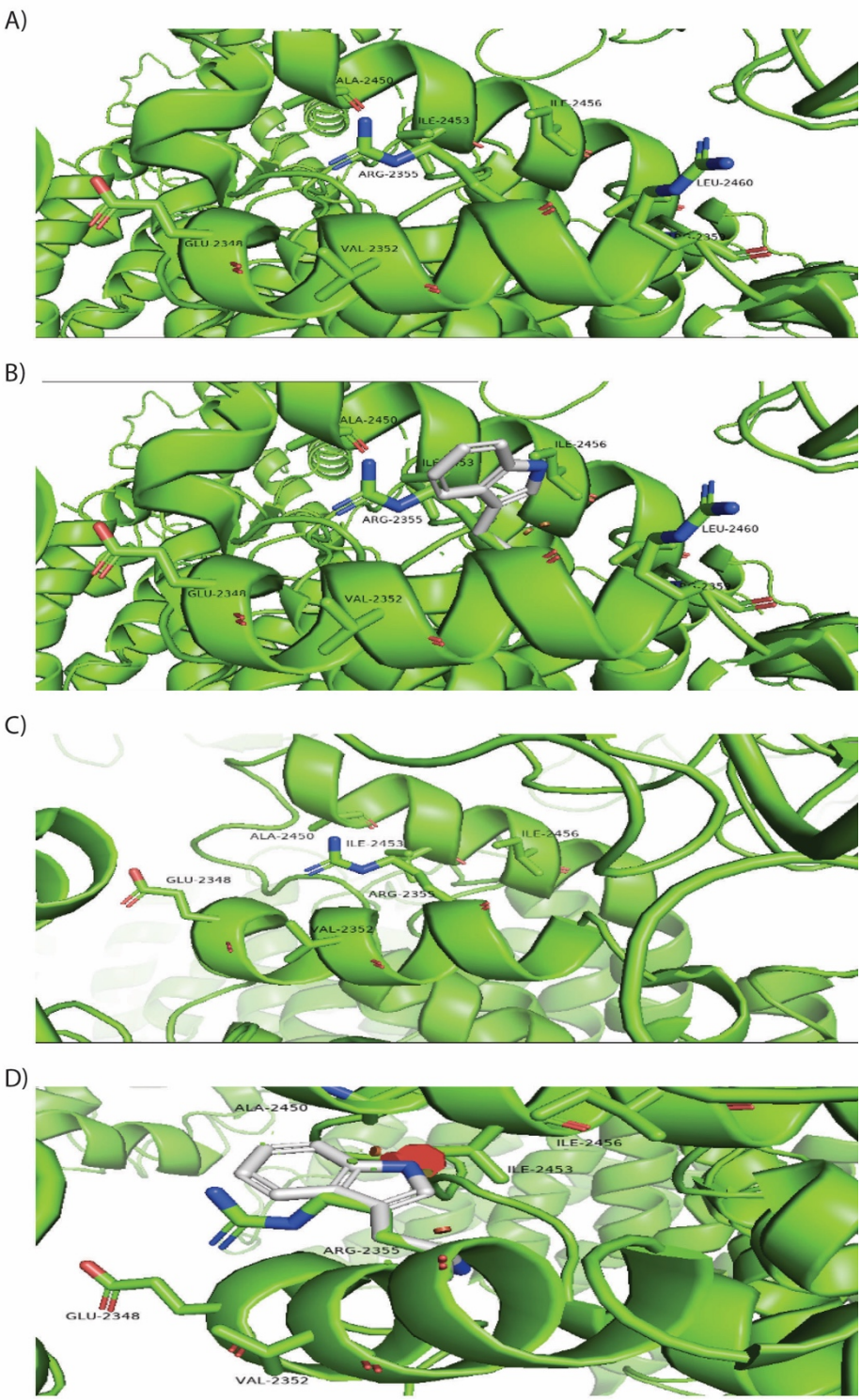

Figure 4.10. Structural modelling of the MH-pathogenic variant arg 2355 trp. A) Arg 2355 in the closed state. B) predicted structural hinderances with trp 2355 in the closed state of RyR1. C) Arg 2355 in the open state. D) Predicted structural hinderances of the trp 2355 in the open state of RyR1. Numbering refers to the rabbit RyR1 and the structure was produced using PyMOL version 2.4.0a0. The PDB ID 5TB1 was used to model the closed state and the PDB ID 5TAM was used to model the open state.

When the MH pathogenic 2355 tryptophan variant was modelled it did not appear to clash with any other amino acids in the closed state. However, in the open state the variant was predicted to clash with ile 2453 located on an adjacent alpha helix (figure 4.10).

The variant was functionally characterised in stably expressing HEK293 cells in the presence of the agonist caffeine (11) and shown to have a decreased EC_{50} compared to WT. As yet the variant has not been functionally characterised by ryanodine binding, limiting discussion on its potential functional effects. However, it is likely given the proximity to other variants within the HD1, that this variant plays a similar role in the onset of MH to other variants within the HD1. Structural hinderance produced by the histidine variant may induce a conformational change that ultimately effects the structure of the HD1 and likely its interaction with surrounding domains causing the channel to favour the open state. Whether or not this effect results from a channel that is easily activated or has a reduced inhibition cannot yet be proposed given the paucity of functional data.

4.2.7 Gly 2375

Gly 2375 is located at the edge of an alpha helix where the secondary structure transitions into a loop region (figure 4.11). The lack of a large side chain, in many cases, can aid in the protein structure adopting a tight bend to allow transition between a structured and non-structured region. It is likely that glycine 2375 is playing this role in RyR1.

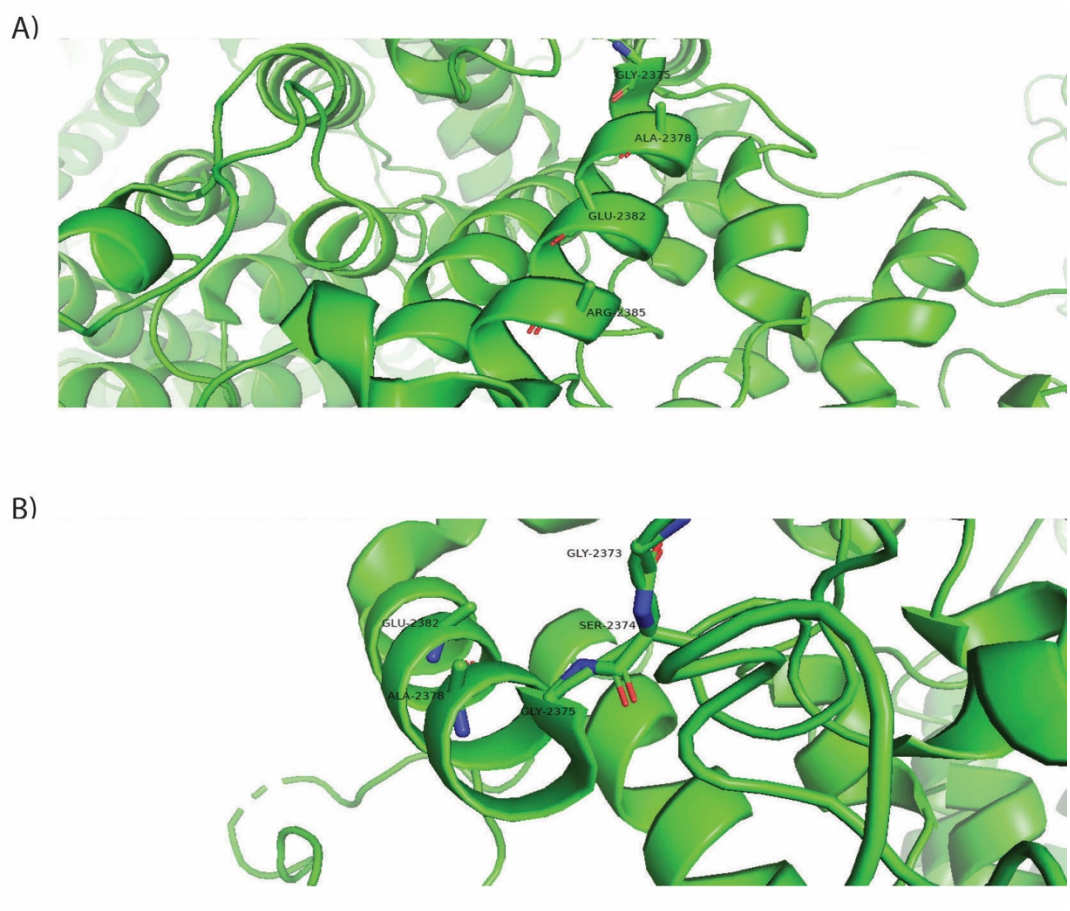

Figure 4.11. Structure of RyR1 surrounding gly 2375. A) The closed state of RyR1. B) The open state of RyR1. Numbering refers to the rabbit RyR1 and the structure was produced using PyMOL version 2.4.0a0. The PDB ID 5TB1 was used to model the closed state and the PDB ID 5TAM was used to model the open state.

When the MH pathogenic alanine variant was modelled in PyMOL no structural hinderance was predicted (figure 4.12). The difference in the side chains between glycine and the pathogenic alanine is not substantial but the addition of a -CH_3 group may be enough to restrict the tight bend required to make the transition from an alpha helix to an unstructured loop region. As a result, the variant may have a greater effect on the secondary structure of the local region than can be predicted using PyMOL. This could potentially cause a large effect on the tertiary structure of RyR1 which may be propagated from HD1 through to adjacent domains of RyR1.

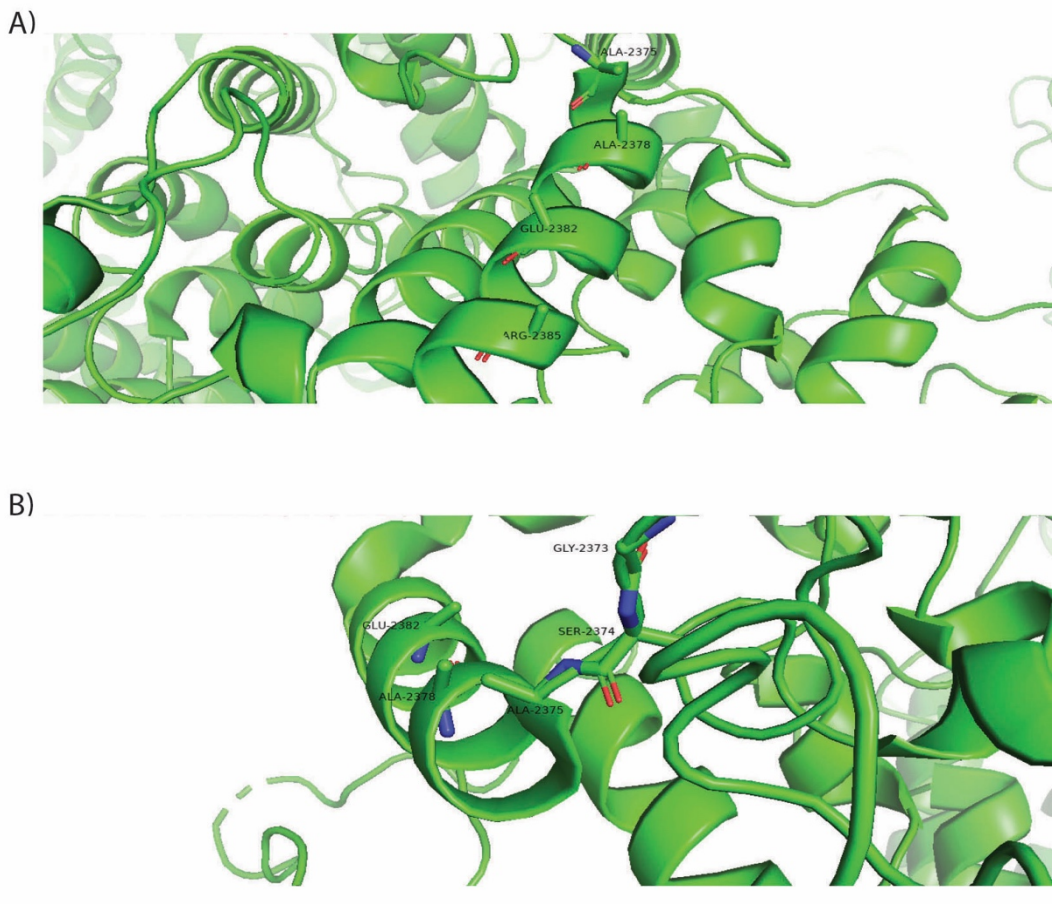

Figure 4.12. Structural modelling of the MH-pathogenic variant gly 2375 ala. A) The closed state. B) The open state. Numbering refers to the rabbit RyR1 and the structure was produced using PyMOL version 2.4.0a0. The PDB ID 5TB1 was used to model the closed state and the PDB ID 5TAM was used to model the open state.

Gly 2375 ala was functionally characterised in stably expressing HEK293 cells and exhibited a decreased EC_{50} compared to the WT RyR1 in response to the agonist caffeine (102). The variant was shown to have an elevated cytosolic Ca^{2+} concentration compared to WT coupled with a decreased concentration of Ca^{2+} within the ER compared to WT. Ryanodine binding was used to characterise the opening characteristics of the channel in the presence of Ca^{2+}. The variant-containing channel was shown to have a similar response to Ca^{2+} compared to WT at activating Ca^{2+} concentrations. However, Ca^{2+} has an increased K_I with respect to the variant compared to WT, suggesting the channel was more difficult to inhibit compared to WT (102). The increased cytosolic Ca^{2+} concentration in cells expressing the gly 2375 ala variant suggests the RyR1 channel is leaky and can open without the need for external stimulation and independent of Ca^{2+}. Further ryanodine binding assays exploring alternative

agonists to include calmodulin and ATP could provide a greater insight into this mechanism. To confirm the variant was causing RyR1 to open in the presence of the agonist, the variant containing channel would have to bind ryanodine at lower agonist concentrations compared to a WT control. It is likely the leakiness of the channel is playing a role, in part, in the onset of MH under inducing conditions, where following the exposure to an MH-inducing anaesthetic the channel is more likely to favour the open state. The lack of inhibition by Ca^{2+} is also likely to play a strong role in the onset of MH where the channel remains open for a longer duration of time. However, other factors including post-translational modification specific to muscle and the presence of other binding partners cannot be ruled out due to functional analysis being carried out in non-muscle cell line.

4.2.8 Ala 2428

Alanine 2428 is located on an alpha helix with it's the side chain projecting towards another alpha helix in both the open and closed states (figure 4.13).

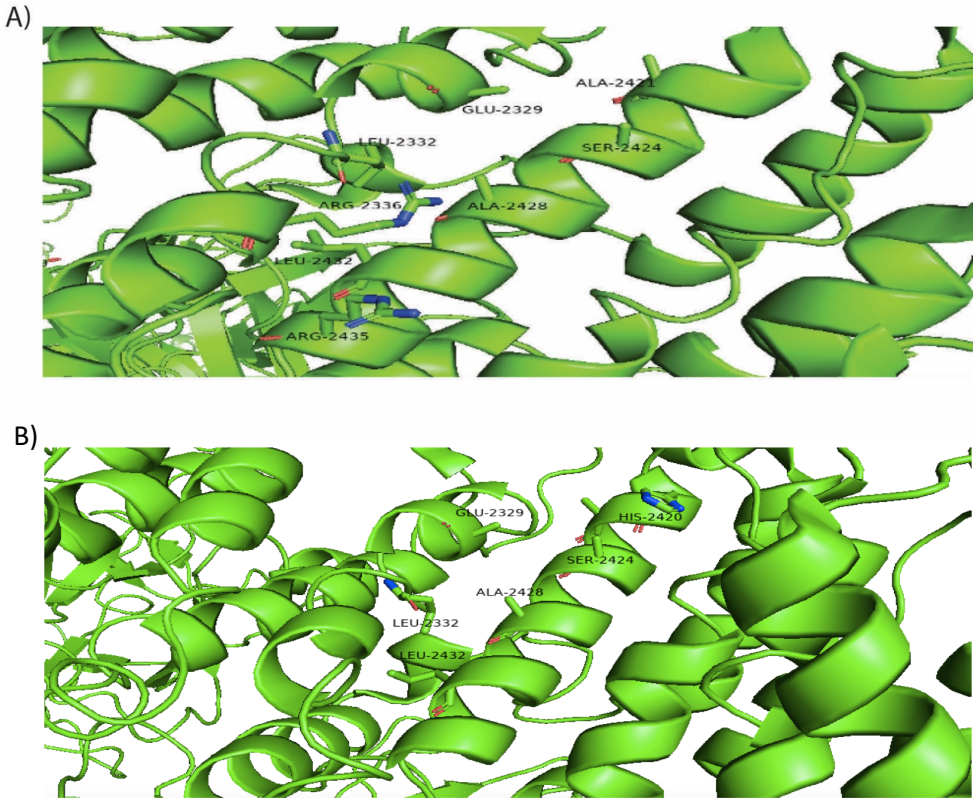

Figure 4.13. Structural modelling of the residue ala 2428. A) Closed state. B) Open state. Numbering refers to the rabbit RyR1 and the structure was produced using PyMOL version 2.4.0a0. The PDB ID 5TB1 was used to model the closed state and the PDB ID 5TAM was used to model the open state.

When the pathogenic threonine variant was modelled in PyMOL the side chain was predicted to interfere with the adjacent residues leu 2332, arg 2336 and ser 2424 in the closed states, and to clash with ser 2424 and arg 2336 in the open state (figure 4.14). Threonine's polar uncharged side chain is in close proximity to the positively charged residue arg 2336. While the variant was predicted to clash with this amino acid the two may form a hydrogen bond with each other which could have further structural implications within the tetramer. Using only modelling within a single subunit to predict downstream effects of introduced variants in a protein such as RyR1, highlights the limitations of *in silico* analysis.

.

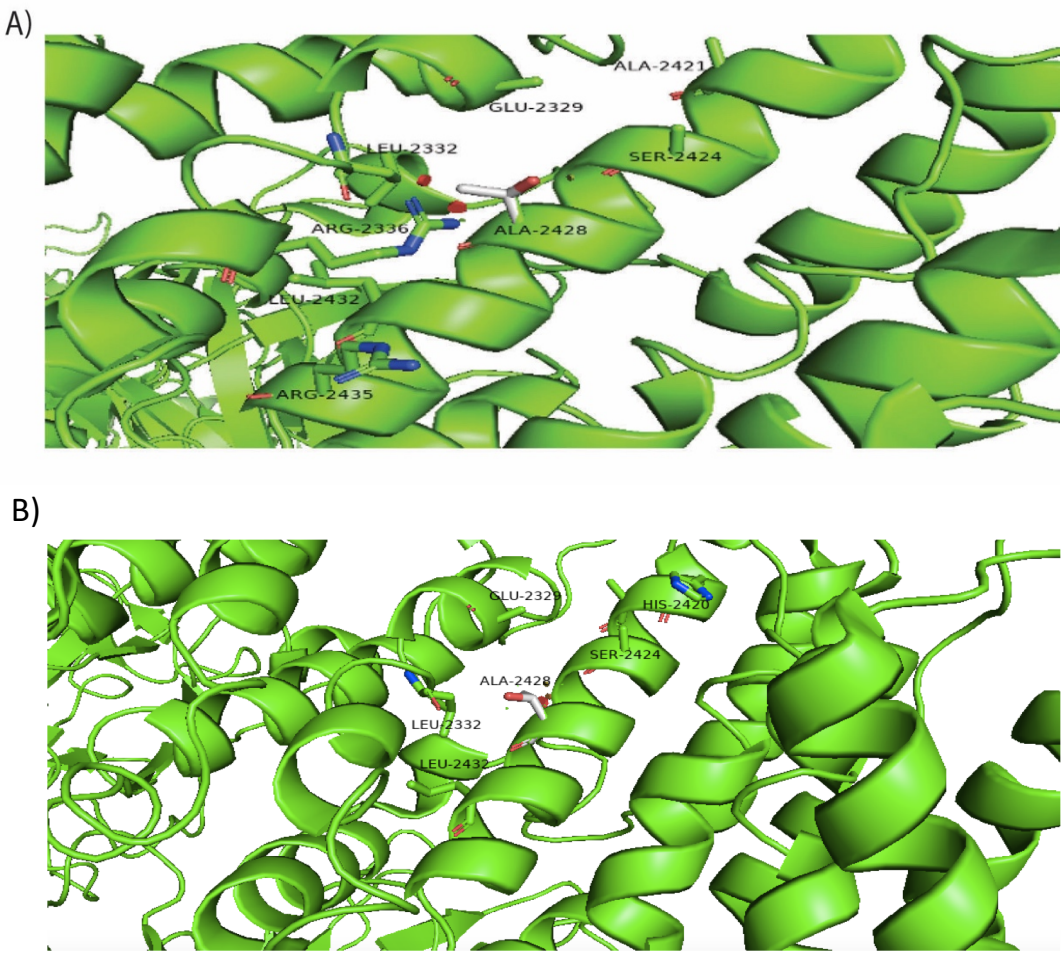

Figure 4.14. Structural modelling of the ala 2428 thr. A) Structural hinderances resulting from the thr 2428 variant in the closed state. B) Predicted structural change of the closed state of RyR1 resulting from the thr 2428 residue. C) Modelling of the structural hinderances resulting from the thr 2428 variant in the open state. D) Predicted structural change of the open state of RyR1 resulting from the thr 2428 variant. Numbering refers to the rabbit RyR1 and the structure was produced using PyMOL version 2.4.0a0. The PDB ID 5TB1 was used to model the closed state and the PDB ID 5TAM was used to model the open state.

The ala 2428 thr variant was determined to be pathogenic for MH by segregation analysis but as yet no functional insight has been provided into the variants mechanism of causing MH (104). To further understand the mechanism by which this variant causes MH, functional studies would need to be performed. Experiments including cell based Ca^{2+} release assays in response to agonists, measuring resting Ca^{2+} levels and ryanodine binding assays using microsomal preparations in the presence of different agonists may provide further perspective on how the variant results in MH under triggering conditions.

4.2.9 Gly 2434

Gly 2434 is located on an alpha helix and projects towards an adjacent alpha helix. It is difficult to make an analysis of the local region surrounding the glycine residue, as the particular region surrounding this residue was not well resolved during structural characterisation, where a number of amino acid side chains could not be identified and as such were labelled as being unknown (UNK) (figure 4.15) (9). The lack of resolution in the local region highlights the freedom of movement this particular region of the HD1 has in the context of the full length RyR1. This further highlights the need for a high resolution crystal structure of the HD1 in which variants can be introduced and structurally characterised by X-ray crystallography or modelled *in silico*.

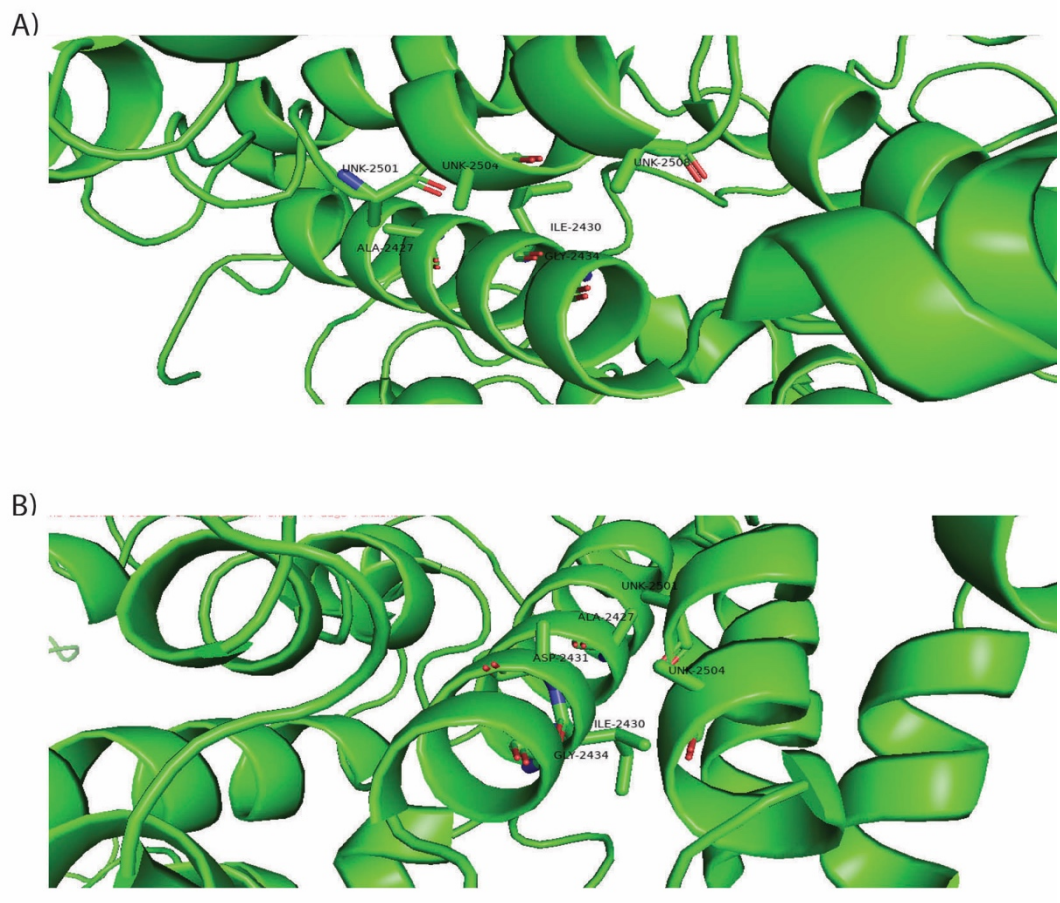

Figure 4.15. Structural modelling of the RyR1 residue gly 2434. A) The closed state of RyR1. B) The open state of RyR1. Numbering refers to the rabbit RyR1 and the structure was produced using PyMOL version 2.4.0a0. The PDB ID 5TB1 was used to model the closed state and the PDB ID 5TAM was used to model the open state.

While the pathogenic arginine residue at this position could be modelled and the resulting structural hinderance caused by the introduction of the comparatively large and polar side chain could be visualised, a true prediction of the structural clashes could not be performed due to the unknown nature of the surrounding amino acids (figure 4.16).

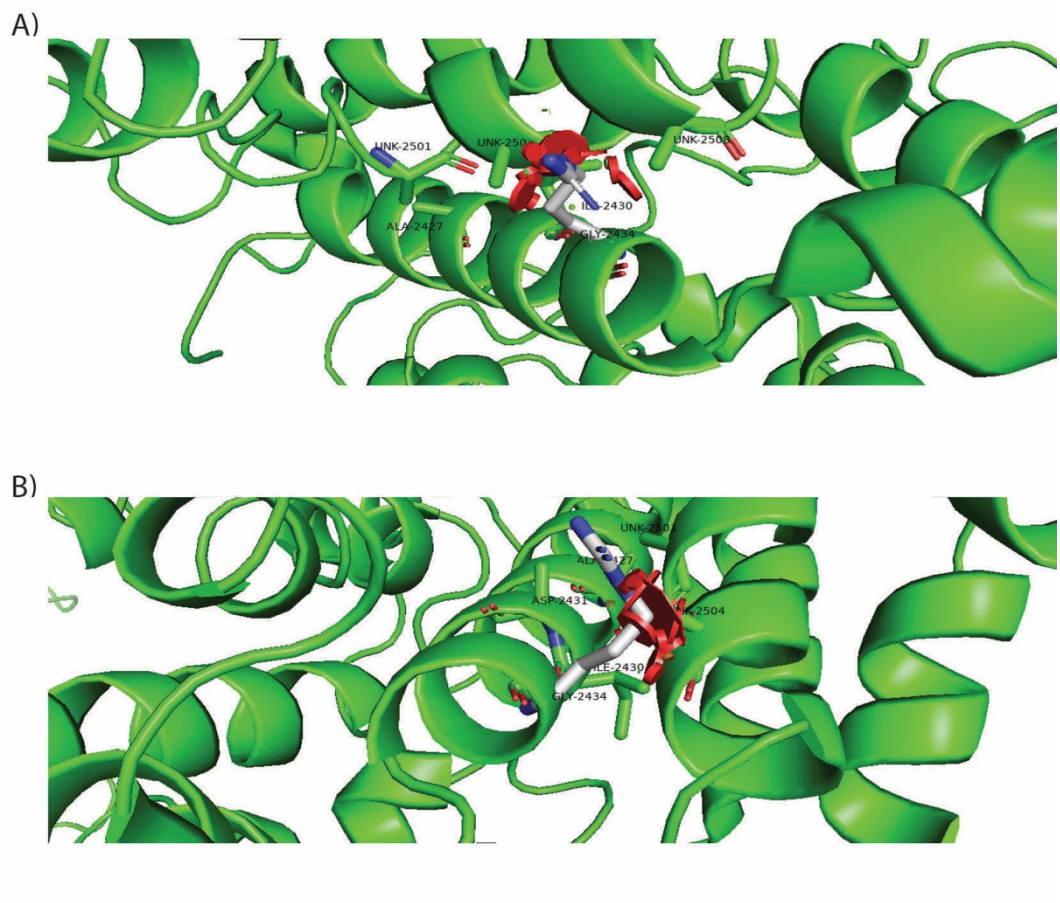

Figure 4.16. Predicted structural clashes resulting from the introduction of the gly 2434 arg variant. A) the closed state. B) The closed state. Structural hinderances are highlighted by red disks. Numbering refers to the rabbit RyR1 and the structure was produced using PyMOL version 2.4.0a0. The PDB ID 5TB1 was used to model the closed state and the PDB ID 5TAM was used to model the open state.

The variant was functionally characterised following the extraction of SR membrane vesicles from a skeletal muscle biopsy (105) as well as following expression in stably expressing HEK293 cells (102). RyR1 in both cases was shown to have a decreased EC_{50} with respect to caffeine compared to a WT control. Ryanodine binding was also used to characterise RyR1 function in the presence of different Ca^{2+} concentrations. SR vesicles containing the variant extracted from both tissue types were also shown to have a lower K_A and an increased K_I for Ca^{2+} compared to a WT control, which suggests the channel should open following exposure to lower Ca^{2+} concentrations and be less likely to be inhibited at inhibitory Ca^{2+}concentrations. The ability of calmodulin to inhibit RyR1 was also characterised by ryanodine binding assays following the extraction of SR membrane vesicles from skeletal

muscle (105). It was shown the variant-containing channel had a decreased inhibition compared to WT.

The presence of the arginine variant likely results in a structural change in RyR1 within the HD1. It is possible the alpha helix in which the arginine residue resides and the adjacent helix in which the structural hinderance occurs will both adopt a new orientation. This may result in the propagation of the conformational change throughout the HD1 having an effect on the interaction of HD1 with adjacent domains.

It has been shown that arg 2434 variant leads to an increased activation of RyR1 by CICR (102, 105), which is possibly due to destabilisation of the primed state, in which the variant containing channel transitions from the closed state through the primed state and into the open conformation following the binding of Ca^{2+}. The increased K_I of Ca^{2+} for the variant-containing channel suggests the channel has a lower affinity for Ca^{2+} compared to WT RyR1, which could suggest long range structural changes may take place affecting the low affinity Ca^{2+} binding site. The gly 2434 arg variant is not in close proximity to the low affinity Ca^{2+} binding site, indicating that the variant may cause a long range conformational change which decreases the binding affinity of Ca^{2+}.

Calmodulin has been previously shown to interact with the HD1 of RyR2 (37). Due to the high amino acid identity shared between RyR1 and RyR2 it is likely that calmodulin also interacts with the HD1 of RyR1. The decreased inhibitory effect of calmodulin in the gly 2434 arg variant could result from more direct structural changes. It must be kept in mind that the SR vesicles used in the experiments summarised here were extracted from skeletal muscle tissue and so were heterozygous for the variant. As such, one of 6 combinations of RyR1 can exist, each with a different combination of WT and variant-containing subunits, each of which could have individual calmodulin binding characteristics depending on the number of variant-containing subunits present in the tetramer. The onset of MH under inducing conditions in patients with the gly 2434 arg variant is likely to result from a channel that is able to open easily. The associated mechanism could be through destabilisation of the primed conformation, coupled by a reduced inhibition by both Ca^{2+} and calmodulin, which ultimately encourages the channel to open for longer periods of time compared to WT. Structural characterisation of the gly

2434 arg variant, particularly in the Ca^{2+} bound and calmodulin bound state, would provide more insight into the mechanism by which the variant causes MH.

4.2.10 Arg 2435

Arg 2435 is located on an alpha helix and projects into a cleft within the external reaches of the HD1 (figure 4.17). In the closed state the residue does not form any hydrogen bonds, however in the open state a hydrogen bond forms between the side chain of arginine and the backbone of phe 2340.

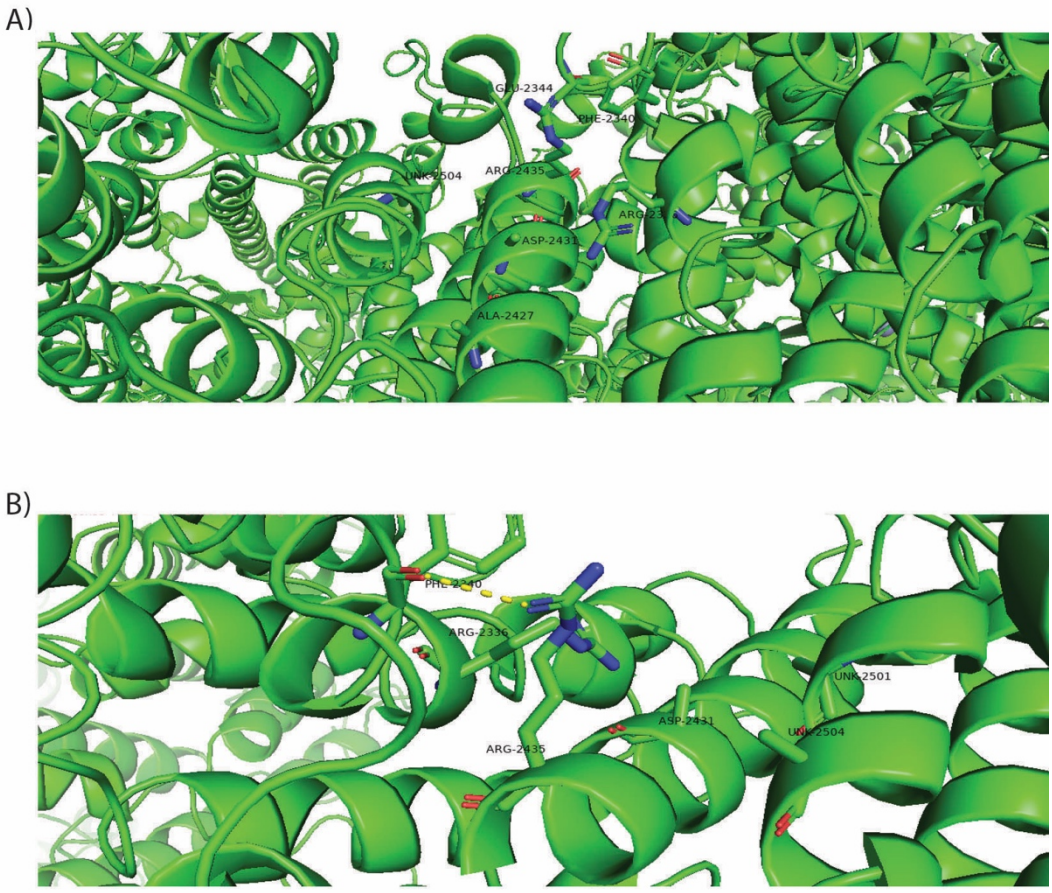

Figure 4.17. Structural modelling of the RyR1 residue arg 2435. A) The closed state of RyR1. B) The open state of RyR1. Numbering refers to the rabbit RyR1 and the structure was produced using PyMOL version 2.4.0a0. The PDB ID 5TB1 was used to model the closed state and the PDB ID 5TAM was used to model the open state.

No structural hinderance was shown to occur when the his variant, pathogenic for CCD was modelled in the closed state, however, in the open state the histidine side chain was shown to clash with the adjacent residue aspartic acid 2431 (figure 4.18).

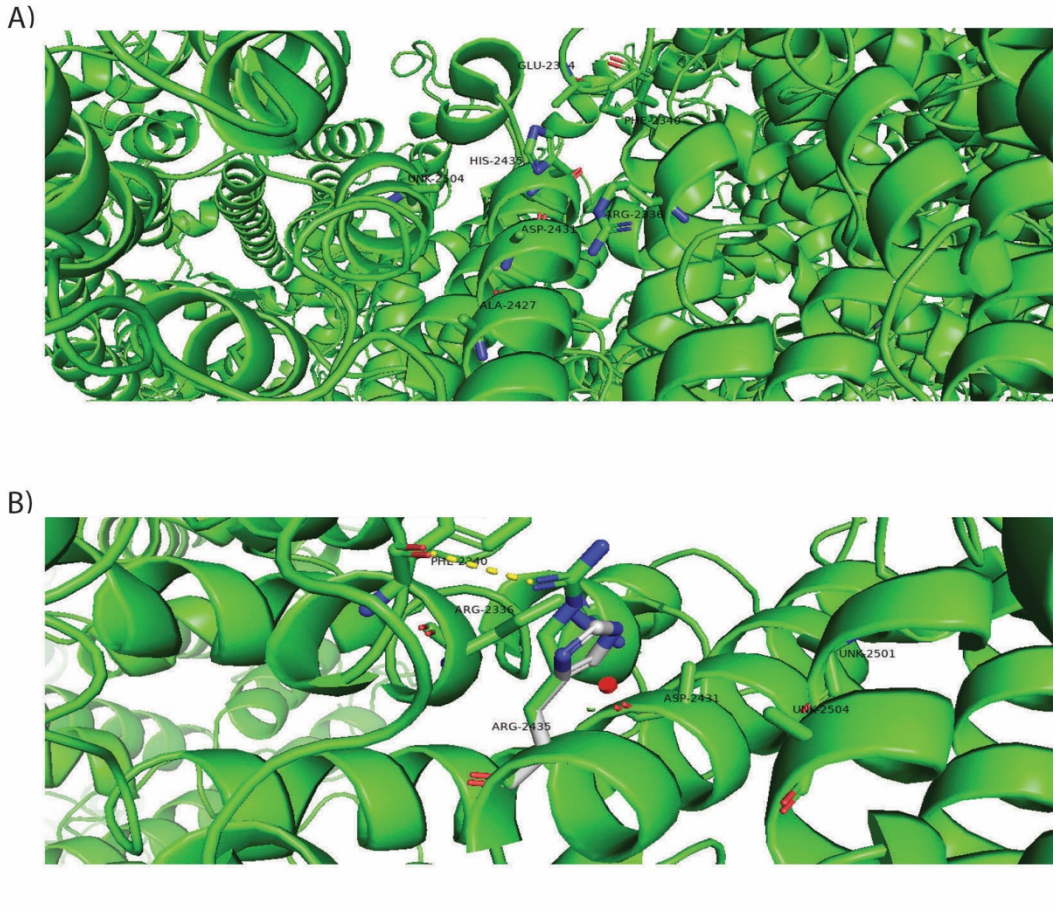

Figure 4.18. Structural modelling of the MH-pathogenic arg 2435 his variant. A) Modelling of his 2435 in the closed state. B) Predicted structural hinderances resulting from the his 2435 in the open state of RyR1. Red disks represent structural hinderances. Numbering refers to the rabbit RyR1 and the structure was produced using PyMOL version 2.4.0a0. The PDB ID 5TB1 was used to model the closed state and the PDB ID 5TAM was used to model the open state.

The CCD variant has been functionally characterised in stably expressing HEK293 cells (102). During the functional characterisation it was shown the cells had a decreased maximum release of Ca^{2+} from the ER following exposure to 10 mM caffeine compared to WT. Coupled with having a lower ER Ca^{2+} concentration and elevated cytoplasmic Ca^{2+} suggests that the channel may be continually leaking Ca^{2+} across the SR membrane. This was supported by ryanodine binding assays, where at resting levels of Ca^{2+}, the variant-containing channel had a significantly increased binding potential compared to WT, which suggests the channel

favours the open state at rest. When Ca^{2+} concentrations were increased it was shown that the variant-containing channel had a decreased K_A and increased K_I for Ca^{2+} and an increased A_{max} compared to WT. This suggests the channel may be more prone to CICR compared to WT and may be the reason for the decreased ER Ca^{2+} concentration compared to WT and ultimately the CCD phenotype. The reduced muscle tension used to diagnose the patient with CCD may stem from the depleted ER stores leading to a reduced Ca^{2+} release into the cytosol following stimulation. The presence of the variant is likely to destabilise the primed state of the channel. After binding of Ca^{2+} the transition from the closed state through the primed conformation and to the open conformation may be favoured. This mechanism has been proposed for the variants arg 2163 cys, arg 2163 his, thr 2206 met, and ala 2350 thr. This mechanism appears to be enhanced for the arg 2435 his variant as the K_A for the variant is not just decreased compared to WT, but it is significantly decreased compared to the other MH pathogenic variants suggesting that the channel is more prone to CICR compared to the previously described variants (102). The Ca^{2+} released from the SR may play a role in a feed forward mechanism, as the Ca^{2+}concentration surrounding the SR following release is high, which in turn can further activate other RyR1 channels prolonging the depletion of Ca^{2+} from the SR. Due to the propensity of the variant to cause the channel to favour the open state, there is a possibility that the variant, as well as destabilising the primed state, has an effect on the closed conformation. In this case the variant may cause a structural change that propagates through the channel aiding the binding of Ca^{2+} to the high affinity binding site. The 2435 his variant may also cause a destabilisation in the closed conformation that acts to induce a pseudoprimed conformation where the binding of Ca^{2+} or another agonist may lead to the opening of the channel. To further understand the function of the variant, electrophysiology could be used to monitor the transition of the channel between the closed and open states at rest in the context of either a single channel or the whole cell. Results of such experiments may provide further insight into the ability of the variant-containing channel to open and close without external stimuli. Ryanodine binding assays could also be used, in the presence of other RyR1 agonists and antagonists, to determine if these have an effect on the opening and closing characteristics of the variant-containing channel compared to WT.

4.2.11 Arg 2452

Arg 2452 forms a hydrogen bond with the amino acid back bone of serine 175 within the N-terminal domain of an adjacent subunit in both the open and closed states (figure 4.19). This interaction is likely to be important in stabilising the two subunits and may play a role in the movement of the two domains with respect to each other during opening of the channel, where the arginine residue could act as a pivot point allowing the two domains to move relative to each other.

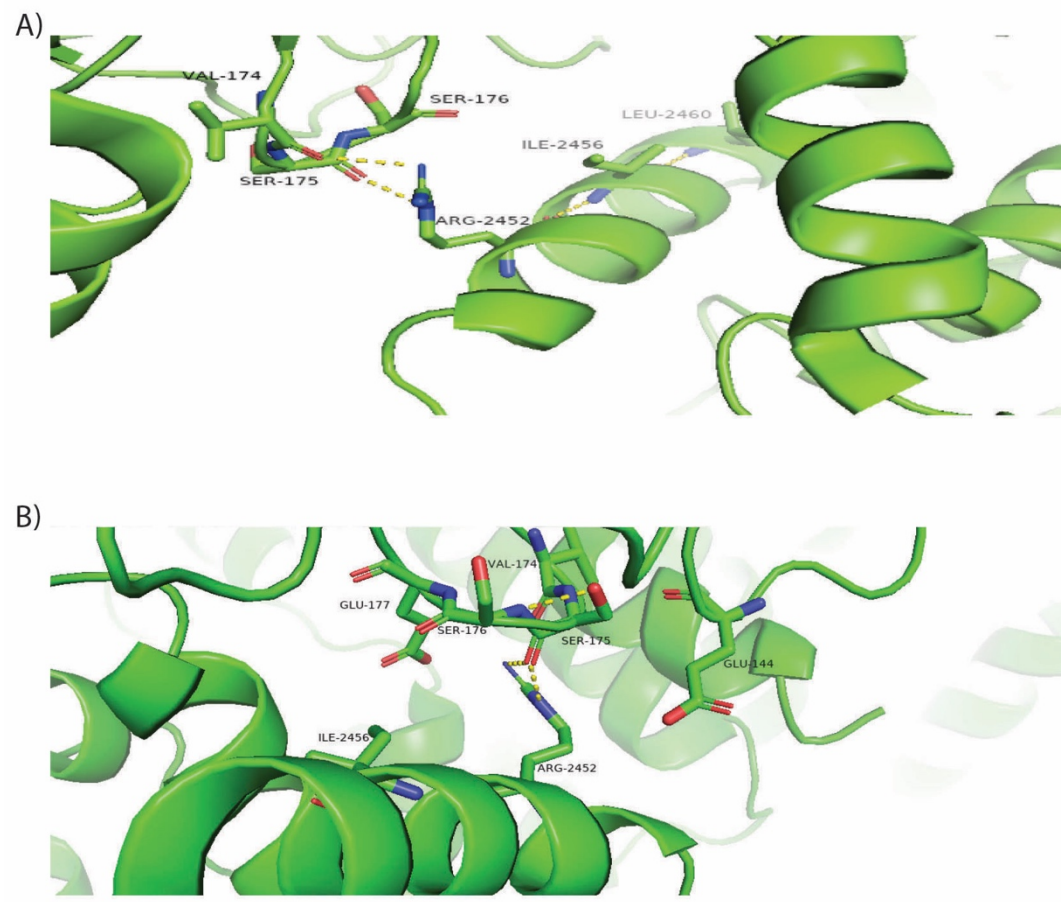

Figure 4.19. Structural modelling of the RyR1 residue arg 2452. A) The closed state of RyR1. B) The open state of RyR1. Numbering refers to the rabbit RyR1 and the structure was produced using PyMOL version 2.4.0a0. The PDB ID 5TB1 was used to model the closed state and the PDB ID 5TAM was used to model the open state.

When the pathogenic trp variant was modelled, the large bulky residue did not clash with any other amino acids in the closed state (figure 4.20). However, in the open state the trp residue was shown to clash with ser 175 and glu 144. The hydrogen bond between the two subunits was lost in both open and closed states when arg was replaced by trp.

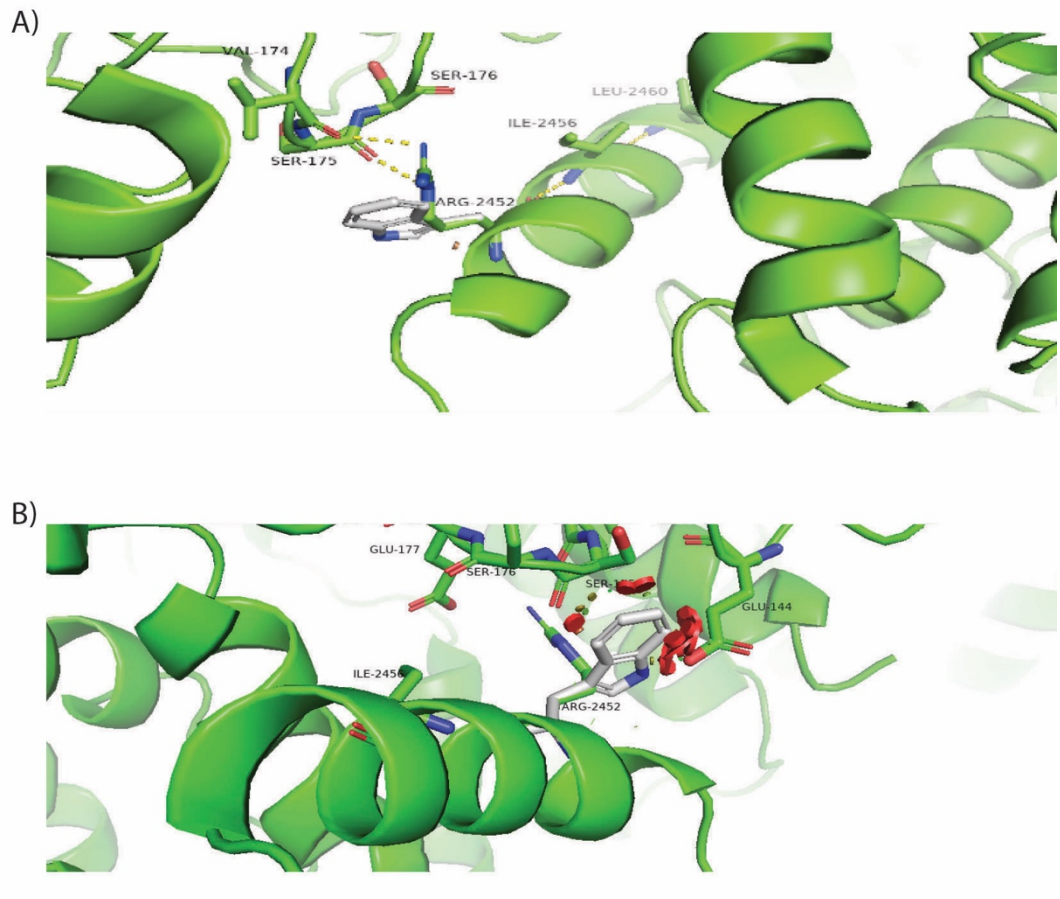

Figure 4.20. Predicted structural hinderance resulting from the introduction of the MH-pathogenic trp 2452 variant. A) the closed state of RyR1. B) the open state of RyR1. Red disks represent structural hinderances. Numbering refers to the rabbit RyR1 and the structure was produced using PyMOL version 2.4.0a0. The PDB ID 5TB1 was used to model the closed state and the PDB ID 5TAM was used to model the open state.

The arg 2452 trp variant has been functionally characterised in transiently transfected HEK 293 cells and primary myotubes (60). In both systems, the variant was shown to have a decreased EC_{50} for 4-CmC compared to WT control. An exact mechanism for the onset of MH for this variant cannot be proposed as ryanodine binding has not been performed to date. The location of the variant at the interface between the HD1 and the N-terminal domain and

resulting structural hinderance strongly suggests a structural change may occur but whether this effects the HD1, N-terminal domain or both is currently unknown.

Performing ryanodine binding assays in the presence of RyR1 specific agonists and antagonists may help to provide further insight into the mechanism by which the variant-containing channel results in MH. These experiments could determine whether the channel is more prone to opening compared to WT or if the channel is more difficult to inhibit the results of which could assist in determining the mechanism by which the variant results in MH.

4.2.12 Arg 2454

Two MH pathogenic variants, cys and his, have been identified at the residue 2454. Arginine 2454 is located on the same alpha helix as the 2452 residue (figure 4.21). However, the arg side chain projects towards the core of its own subunit.

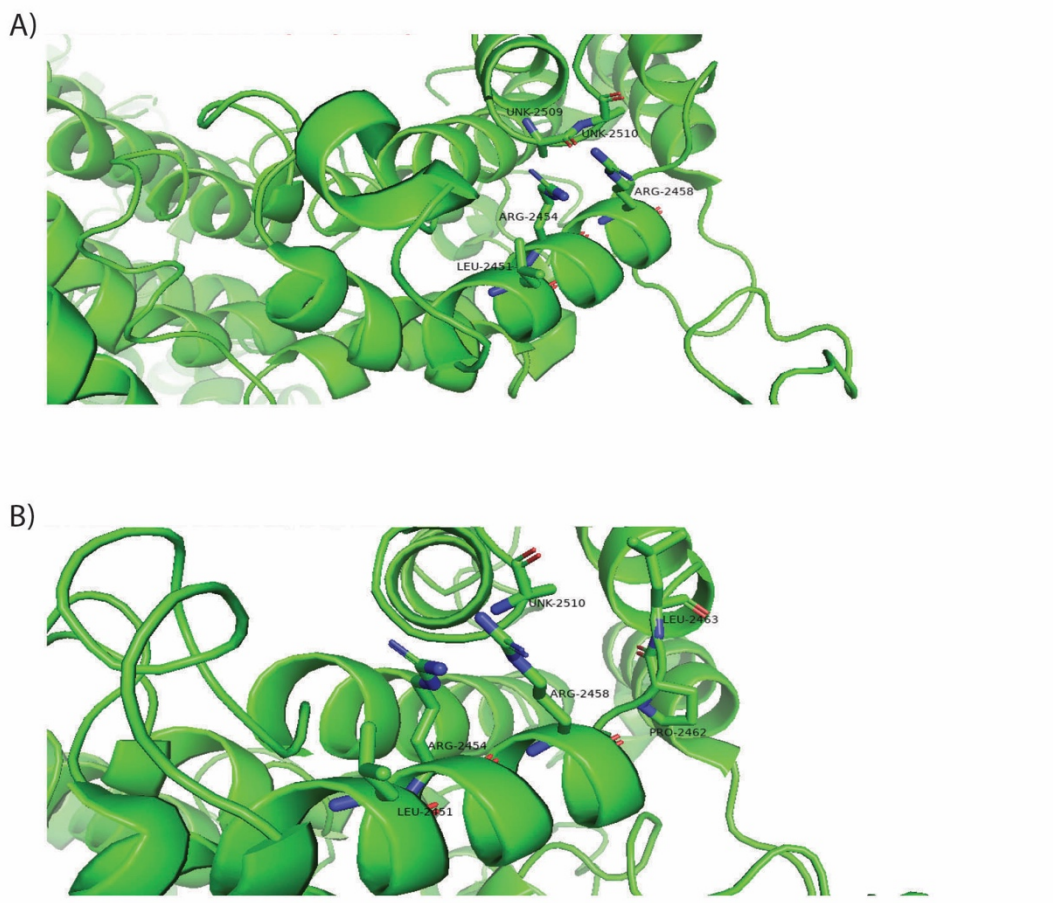

Figure 4.21. Structural modelling of the RyR1 residue arg 2454. A) The closed state of RyR1. B) The open state of RyR1. Numbering refers to the rabbit RyR1 and the structure was produced using PyMOL version 2.4.0a0. The PDB ID 5TB1 was used to model the closed state and the PDB ID 5TAM was used to model the open state.

No structural hinderance was predicted to occur for the cys variant in either the open or closed conformations (figure 4.22). Any change in function is likely due to the replacement of a large positively charged amino acid for a smaller polar amino acid. A change in the local chemistry may occur, but as there are unknown amino acids in the local region it is difficult to make further predictions on possible structural effects of this variant.

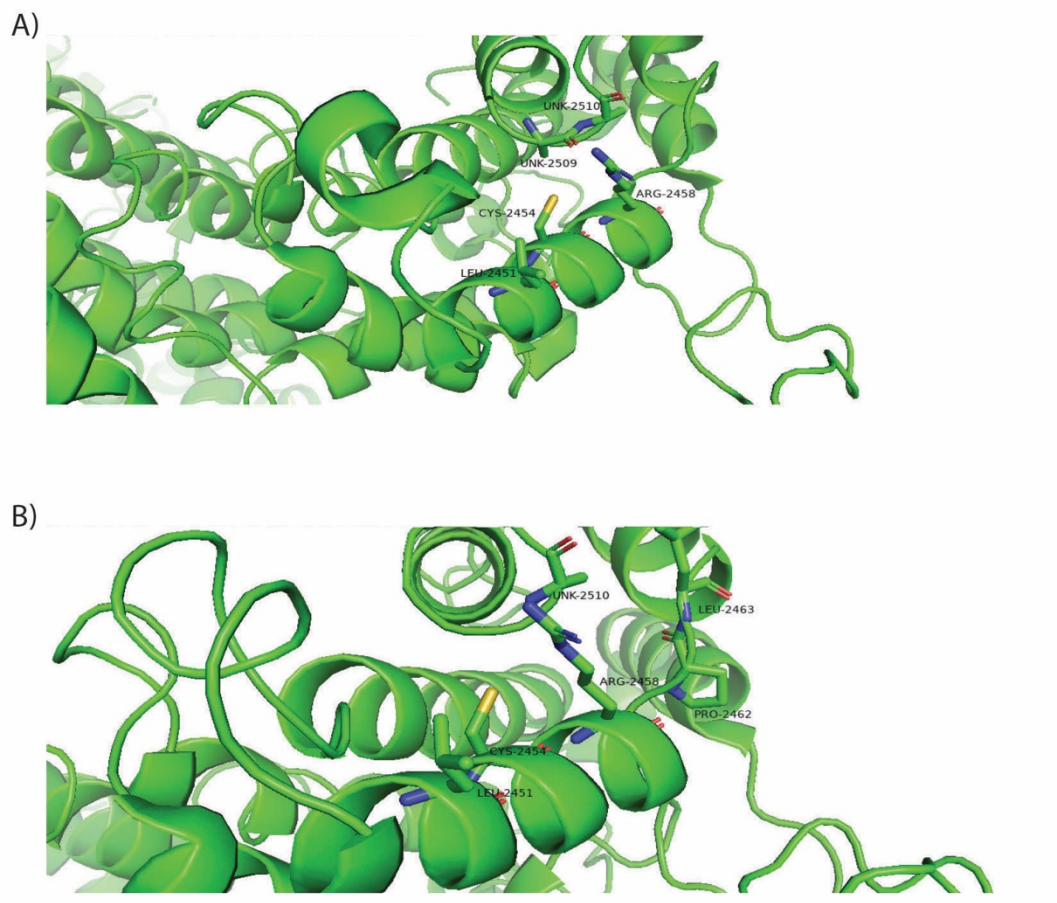

Figure 4.22. Structural modelling of the MH-pathogenic arg 2454 cys variant. A) Modelling of the variant in the closed state. B) modelling of the variant in the open state. Numbering refers to the rabbit RyR1 and the structure was produced using PyMOL version 2.4.0a0. The PDB ID 5TB1 was used to model the closed state, while the PDB ID 5TAM was used to model the open state.

When the histidine variant was modelled in PyMOL a structural hindrance was predicted to occur between the amino acids arg 2458 and the unknown amino acid 2509 (figure 4.23).

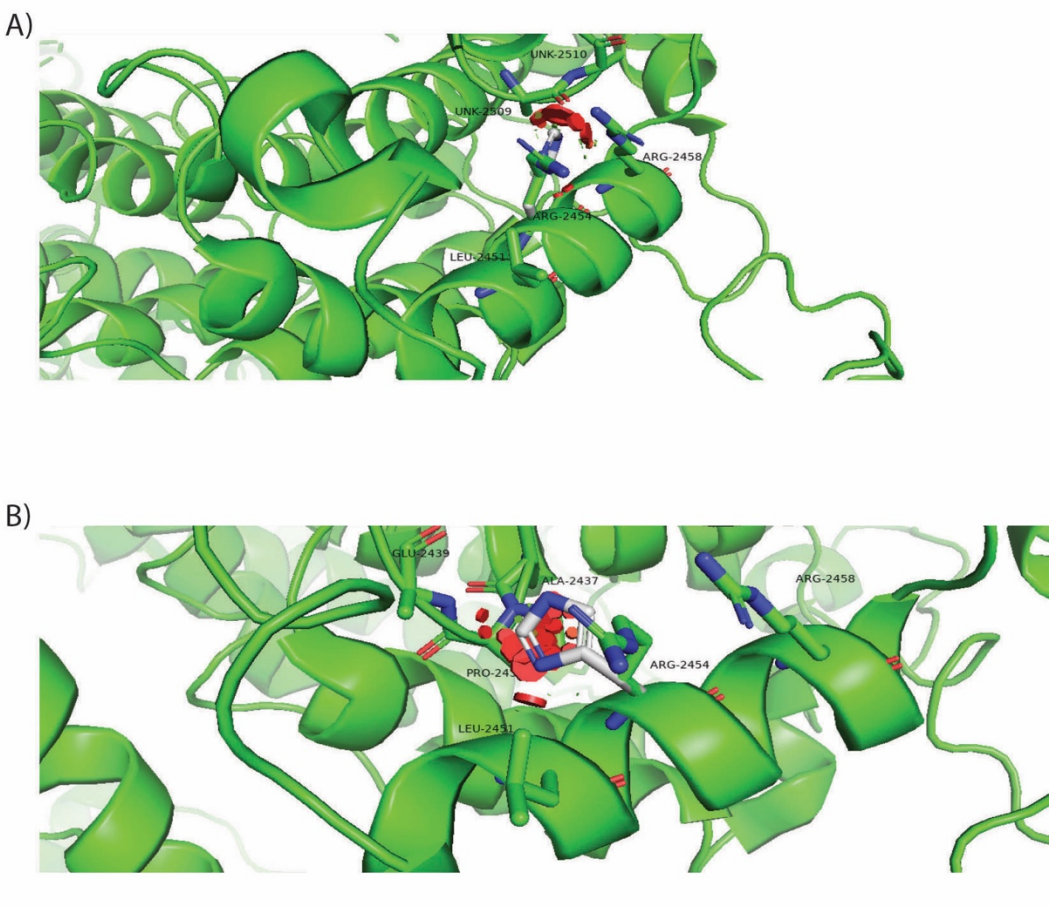

Figure 4.23. Structural modelling of the MH-pathogenic arg 2454 his variant. A) The closed state of RyR1. B) The open state of RyR1. Red disks represent structural hinderances. Numbering refers to the rabbit RyR1 and the structure was produced using PyMOL version 2.4.0a0. The PDB ID 5TB1 was used to model the closed state, while the PDB ID 5TAM was used to model the open state.

Both variants have been functionally characterised in stably expressing HEK293 cells (102), where both were shown to have a significantly decreased EC_{50} compared to WT following exposure to caffeine. This represents a defining indication that the variants are pathogenic for MH.

Interestingly, the mechanism by which the cysteine variant can result in MH is likely to be different to that previously described for a number of variants in this chapter. During ryanodine binding assays it was shown that the variant had very similar binding characteristics to that of WT at both rest and in the presence of activating Ca^{2+} (102). This suggests that CICR may not be involved in the onset of MH. The variant was shown to have an increased K_I for Ca^{2+} compared to WT, suggesting the channel is more difficult to inhibit compared to WT. This

variant is more likely to result in MH due to prolonged opening of RyR1 leading to the mass release of Ca^{2+}. The variant is more likely to either stabilise the open conformation or prevent the transition from the open state back to a closed conformation. Ryanodine binding assays were only performed at rest or in the presence of Ca^{2+} and as a result a more in depth mechanism cannot be proposed. The variant could still destabilise the closed or primed conformation, however it may do so via a mechanism that has not yet been explored and may result following the binding of ATP or apo-calmodulin for example. Differences in the inhibition characteristics following the binding of Mg^{2+} and calmodulin could also be explored to further characterise the variant.

The histidine variant at position 2454 was shown to have an increased ryanodine binding potential compared to WT at resting [Ca^{2+}], suggesting that the arg 2454 his variant is more prone to opening compared to the cys variant at the same site (102). The K_A for Ca^{2+}, while being lower compared to WT, was still much higher compared to the MH / CCD pathogenic variants arg 2163 his and arg 2435 his (102). This suggests that while the arg 2454 his variant may cause the channel to leak, it appears to be less prone to doing so compared to other variants. In this case, the argument could be made that CICR and the destabilisation of the primed conformation may result in MH. However, like the cysteine variant another mechanism that has yet to be explored could also be the cause of MH.

4.2.13 Arg 2458

Two amino acid variants (his and cys) of arg 2458 have been classified as being MH pathogenic (102). Arg 2458 is on the same alpha helix as the functionally important arg 2452 and arg 2454 residues. Like arg 2454, the arg 2458 side chain projects into the core of the HD1 and is predicted to form a hydrogen bond with unknown amino acid 2510 in the closed state, however this bond is not present in the open state of the channel (figure 4.24). This suggests that arg 2458 may play a role in stabilising the closed state of the channel. As the bond is not present in the open state it suggests a structural change within this region during opening of the channel.

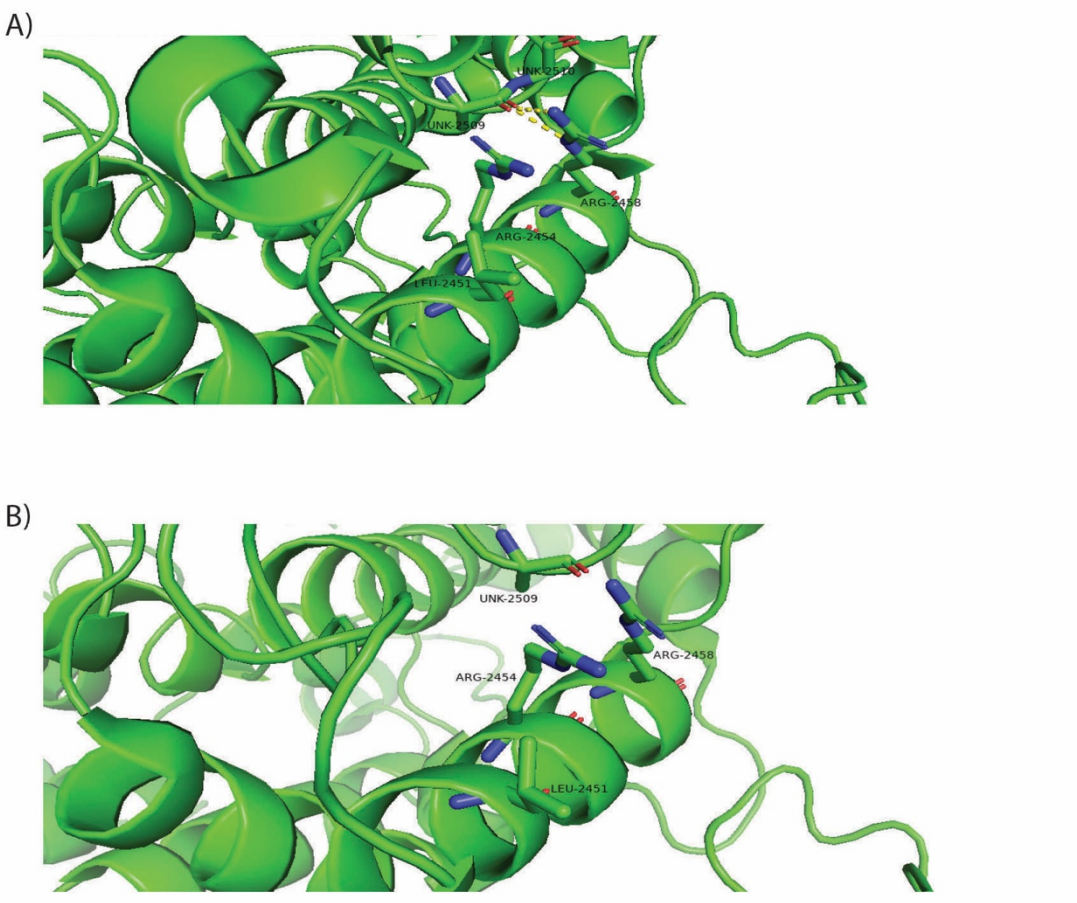

Figure 4.24. Structural modelling of the RyR1 residue arg 2458. A) The closed state. B) The open state. Numbering refers to the rabbit RyR1 and the structure was produced using PyMOL version 2.4.0a0. The PDB ID 5TB1 was used to model the closed state, while the PDB ID 5TAM was used to model the open state.

No structural hinderance was predicted to occur in either the open or closed state when the cysteine variant was modelled using PyMOL (figure 4.25). It is possible that a change in RyR1 function results from a large positively charged amino acid being substituted for a smaller polar amino acid. The loss of the hydrogen bond may also destabilise the channel. As unknown 2510 is located on an unstructured loop region the loss of the hydrogen bond may provide this amino acid and those surrounding it with greater degrees of freedom. As a number of amino acids in the local region were unassigned it is difficult to predict further roles the variant might play in RyR1 function.

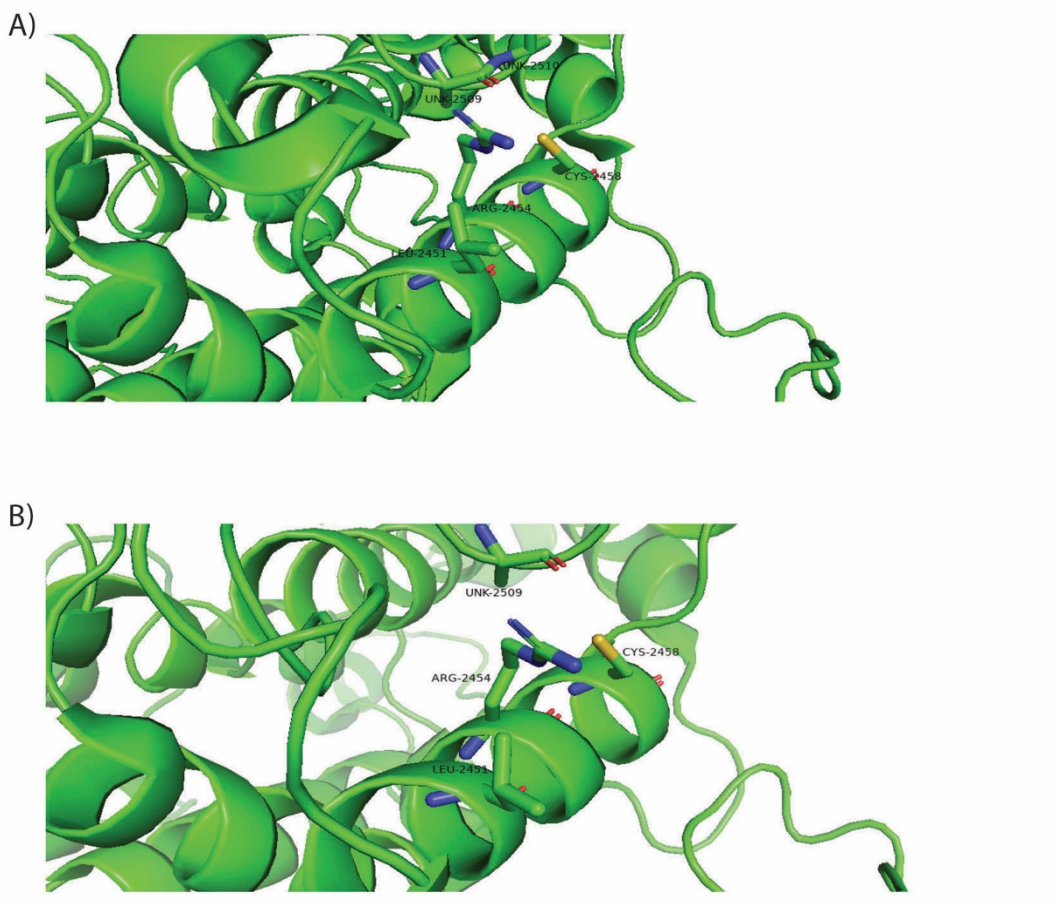

Figure 4.25. Structural modelling of the of the RyR1 residue cys 2458. A) The closed state. B) The open state. Numbering refers to the rabbit RyR1 and the structure was produced using PyMOL version 2.4.0a0. The PDB ID 5TB1 was used to model the closed state, while the PDB ID 5TAM was used to model the open state.

No structural hinderance in either the open or closed state was detected for the his variant at position 2458 (figure 4.26). Once again, a number of amino acids in the local region surrounding the variant were unassigned during the initial structural characterisation of the protein. It is possible that a clash may occur between one or more of these amino acids. The hydrogen bond formed between the arginine residue and unknown 2510 in the closed state was lost during the introduction of the variant with possible destabilisation of the structure. The substitution of a positively charged amino acid for a smaller polar amino acid is also likely to have a functional consequence.

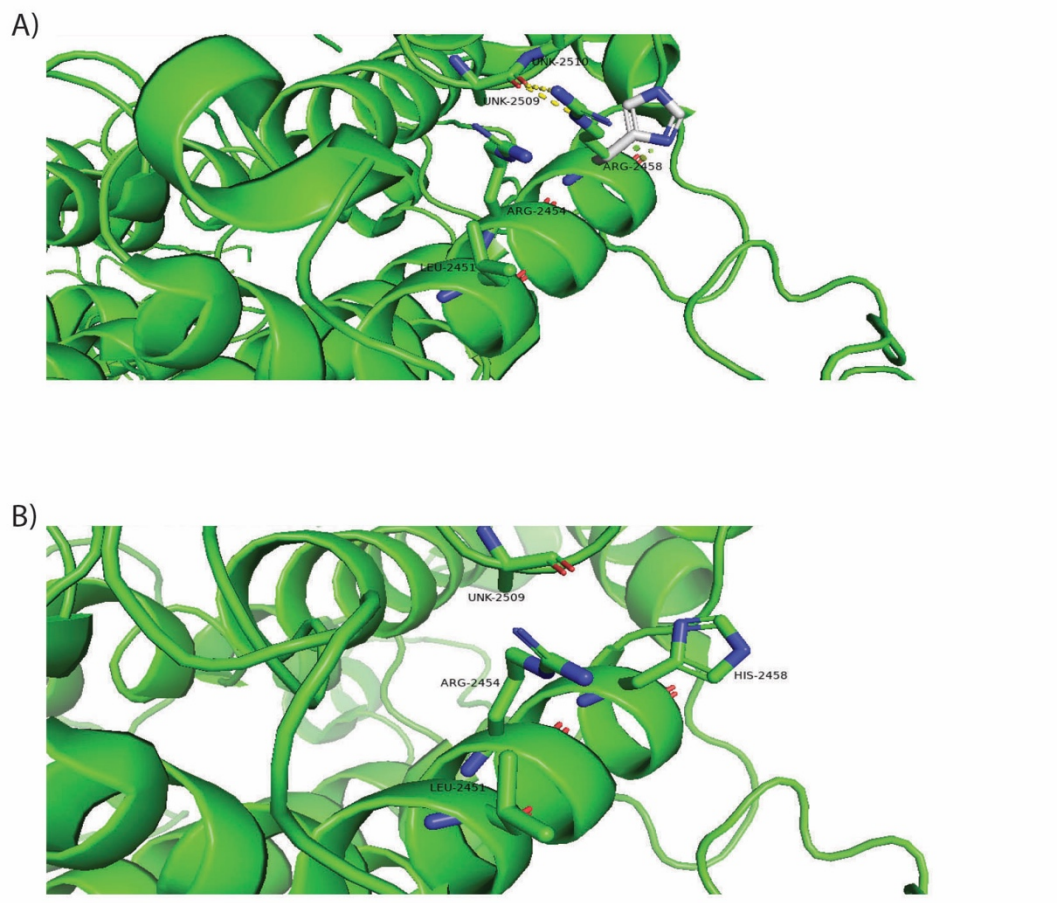

Figure 4.26. Structural modelling of the MH-pathogenic arg 2458 his variant. A) The closed state. B) The open state. Numbering refers to the rabbit RyR1 and the structure was produced using PyMOL version 2.4.0a0. The PDB ID 5TB1 was used to model the closed state, while the PDB ID 5TAM was used to model the open state.

The cysteine and histidine variants had similar effects when functionally characterised in stably expressing HEK293 cells (102). Both had a reduced EC_{50} for caffeine compared to cells expressing the WT RyR1. An elevated resting [Ca^{2+}] was also detected for cells expressing either variant, which was accompanied by a reduced ER Ca^{2+} concentration. When ryanodine binding assays were performed in the presence of Ca^{2+} there was little difference between WT RyR1 and either variant at resting levels of Ca^{2+}. When Ca^{2+} levels were increased to both activating and inhibitory concentrations it was noted that neither variant-containing RyR1s was significantly different to WT RyR1. Indicating that neither CICR nor altered Ca^{2+} inhibition is the cause of MH with respect to these two variants.

Neither variant was predicted to induce a structural hinderance when modelled in PyMOL and as a result it is likely the onset of MH in patients with the variants results from a change in amino acid chemistry in the local region. Ryanodine binding assays were used to functionally characterise the variants, where the open probability of the channel was monitored in the presence of increasing Ca^{2+} concentrations (102). It was noted that CICR was not the cause of MH. Therefore, MH with respect to the variants arg 2458 cis and arg 2458 his must result from a mechanism independent of Ca^{2+}. Further functional analysis of the variant needs to performed in order to address other potential mechanisms that may explain the MH phenotype. Ryanodine binding assays in the presence of other agonists, for example ATP or apo-calmodulin, could be performed to analyse the opening characteristics of RyR1 comparing the variant-containing channel to WT. A decreased K_A would suggest the variant containing channel is more prone to opening compared to WT. The same assay could also be performed in the presence of antagonists, for example Ca^{2+} bound calmodulin and Mg^{2+} to show changes in the inhibition of the variant containing channel in comparison to WT. An increase in K_I would suggest the channel is more difficult to inhibit and may explain the increased Ca^{2+} release characteristic of an MH episode.

Concluding remarks

MH pathogenic variants within the HD1 have been modelled *in silico.* In each case the variant could be modelled within the local region and a potential structural change was proposed. In many cases it is likely that the variants can induce a structural and functional change in RyR1 via a mechanism that is distant from the variant (81). This is consistent with the previously proposed hypothesis that MH pathogenic variants have a structural effect on the surrounding domains which ultimately is the cause of MH under inducing conditions (101). The proposed structural changes have been shown in many cases to affect the opening characteristics of RyR1 following the binding of Ca^{2+} (71, 102). This may result from a destabilisation of the closed or primed conformations which causes the channel to be more prone to opening following the binding of Ca^{2+}. In other cases, the variant may stabilise the open state or may lower the affinity for Ca^{2+} at the low affinity binding site making it more difficult to inhibit channel opening. In either situation, the channel is likely to be in the open state for longer

periods of time and the associated prolonged Ca^{2+} release may result in an MH episode. To further understand the role that each variant plays in the onset of MH, ryanodine binding assays could be performed in the presence and absence of different agonists and antagonists, to include ATP, ADP, calmodulin or Mg^{2+}. Where the ability for different concentrations of these agonists and antagonists to open or close the channel can be compared to a WT control, any differences in K_A, A_{max} or K_I could provide further insight into the role the variant may play in the onset of MH. To gain a further understanding of how each variant can result in MH, the variant containing RyR1 would need to be structurally characterised by cryo EM. Determining the structure of the variant containing RyR1 in the presence of agonists or antagonists to include Ca^{2+}, ATP, calmodulin and Mg^{2+} would provide further insight into the mechanism by which the variant causes MH, particularly if the variant has been previously shown to be functionally different to WT following the binding of the ligand. Any changes in local structure induced by the variant could be examined along with any long range structural implications, which may have an effect on either the binding of the ligand or the resulting conformational change following its binding.

5. The use of immortal myoblast cell lines for functional characterisation of RyR1 variants

5.1 Introduction

5.1.1 Myoblasts

Structure-function relationships of RyR1 could not be carried out using protein regions expressed in *E. coli*, therefore an alternative system was investigated. Myoblasts are primary cells that can be extracted from a muscle tissue sample. The cells can be cultured and following the removal of serum from the media can be induced to differentiate into myotubes (113). Myotubes represent intact muscle to a certain extent, in that they express both the ryanodine receptor and DHPR along with other proteins involved in the regulation of Ca^{2+} homeostasis within muscle cells. Myotubes can be induced to release Ca^{2+} from the SR following exposure to RyR1 agonists in a concentration-dependent manner making them a useful tool for the functional characterisation of RyR1. Myotubes do not contain optimally formed terminal cisternae, a critical feature in EC-coupling and the rapid release of Ca^{2+} from the SR following stimulation, thus human cultured myotubes are also a non-contractile cell line. However, the cells release Ca^{2+} from the SR in response to the RyR1 specific agonist 4-C*m*C and caffeine, or after depolarisation by K^{+}. In addition, myotube cell lines from mice or humans are often used for the characterisation of Ca^{2+} homeostasis and RyR1 variants (113). In a constantly dividing somatic cell, telomers, caps at the ends of chromosomes that maintain chromosomal integrity, will constantly shorten (114). The eventual loss of telomers will cause the cell to enter replicative senescence as part of the cell's normal life span. Myoblasts therefore, have a limited lifespan and cannot undergo more than approximately 50 doublings before entering senescence (115). This feature of primary myoblasts limits their long term use in functional analysis. Immortalised myoblasts, on the other hand, provide a renewable resource for repeated assays over a longer time period, because they have been manipulated to express telomerase.

The protein human telomerase reverse transcriptase (hTERT) protein in combination with an RNA component, which provides the template for telomere repeat synthesis, is used to maintain telomer length in cells. hTERT reverse transcribes the RNA template creating the missing DNA fragment on the newly transcribed DNA strand, which is then incorporated into the genome, preserving the telomer length in the cell. While myoblasts do not express hTERT under native conditions, they do express the RNA component of the enzyme. The hTERT cDNA has been previously introduced into primary myoblasts using a retroviral transduction system (114). Expression of hTERT helps to maintain telomeres and has been shown to allow the cells to survive and proliferate in culture for an additional 50 doublings compared to primary myoblasts (115). The expression of hTERT alone is not sufficient to immortalise the cells however, as processes other than telomere shortening cause the cells to enter cell cycle arrest (115). The overexpression of a second protein, cyclin dependent kinase 4 (CDK4), has been shown to help maintain the cell cycle and ensure the cells make the transition from the G1 to the S phase (figure 5.1). The over expression of CDK4 has been shown to prevent cell cycle arrest ensuring the cell cycle continues and the cells continue to proliferate in culture (116). Cells shown to express both of these proteins have been reported to proliferate in culture for 125 days. Although they eventually enter senescence and die with continual passaging, this will occur significantly later than their primary counterparts (115).

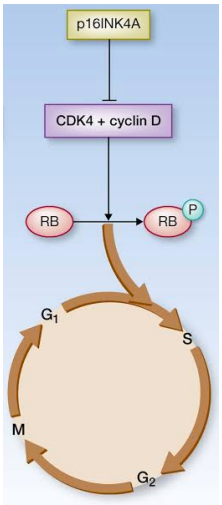

Figure 5.1. Figure summarising the cell cycle and the regulation performed by CDK4. P16INK4A represents the protein p16. RB represents the protein retinoblastoma. The individual stages of the cell cycle S, G2 M and G1 have all been represented. Figure taken from (117), no permission required to use figure.

5.1.2 CRISPR / Cas 9

The ability to generate immortalised myoblast cells from patient muscle tissue would provide the necessary cells for subsequent manipulation for functional characterisation of RyR1 variants. Specifically, the clustered regularly interspaced short palindromic repeats (CRISPR)/Cas 9 system could be used to introduce specific nucleotide changes into the genome of immortalised myoblasts. After differentiation into myotubes, these edited cells could be used to study the function of the introduced variant in close to physiological conditions, particularly if a single allele is modified, which would more closely represent malignant hyperthermia which is inherited in a heterozygous manner. The site specific genome editing tool CRISPR/Cas 9 has recently been adopted in a number of studies to knock out genes or introduce specific variants into a genome (118). The ribonucleoprotein Cas 9, an endonuclease, is used *in vivo* in prokaryotes to digest viral DNA following infection. The RNA component of the enzyme is used to target the enzyme to the invading viruses' DNA which is then digested to protect the cell from infection. The mechanism by which Cas 9 digests DNA at a specific site has been exploited in recent years to modify eukaryotic genomes. In this case the RNA component of the complex must be designed to target a specific region of the genome. Once digested the host cell will repair the break. Under physiological conditions cells will exploit the non-homologous repair mechanism, with the consequent introduction of an insertion/deletion (indel) in the local region surrounding the lesion leading to an alteration in the expressed protein (figure 5.2). The introduction of an indel is a random event which can result in an alteration of the reading frame, leading to the expression of a nonsense protein. If the reading frame is maintained an alteration in the length of the protein may take place which can have an effect on the structure and/or function of the protein. The homology directed repair (HDR) mechanism can also be utilised to repair the double stranded break. This is a controlled process using a repair template to introduce a single point mutation. In this case the reading frame of the protein is maintained with the expressed protein having a single amino acid change.

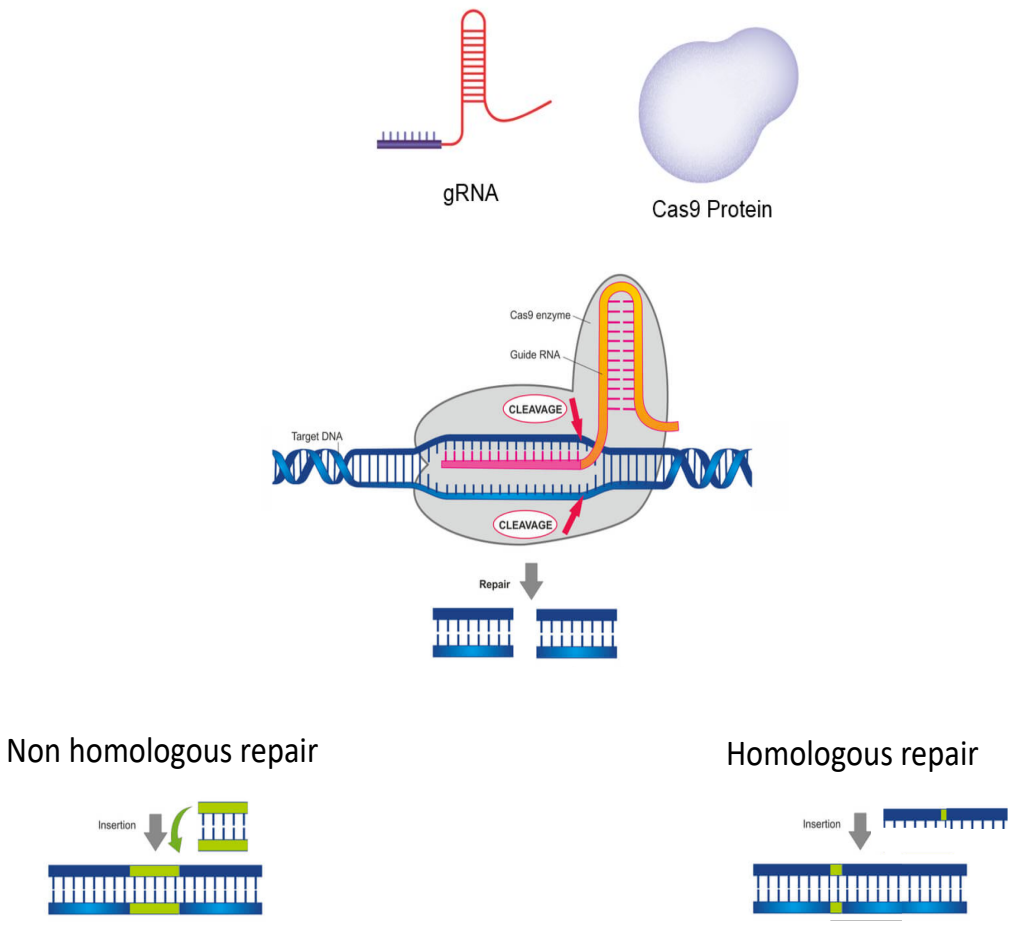

Figure 5.2. General diagram of how Cas 9 in combination with a guide RNA can lead to the digestion of a host cell genome and the two repair mechanisms. Figure adapted from (119) no permission required to use figure.

The CRISPR/Cas 9 system could be used to either introduce a variant into a MHN cell line or be used to remove a potentially pathogenic variant from a cell line derived from an MH susceptible patient. Subsequent functional analysis of both edited cell lines could be used to demonstrate that a single pathogenic variant is both necessary and sufficient to result in MH. Due to the number of manipulations required, primary myoblasts cannot be used for CRISPR/Cas 9 gene editing, as they are likely to enter senescence before the procedure could be completed. Having immortal cell lines produced from patients in which specific variants can either be introduced or removed would be a significant advance in furthering the use of diagnosis by DNA screening. Variants could be introduced and functionally characterised in a system where the only difference between cell lines is the specific variant. This approach would limit the effect of a patients genetic background on the Ca^{2+} release characteristics. To

this end, patient-derived primary myoblasts were isolated and immortalised to provide cell lines that could be used for CRISPR/Cas 9 editing and subsequent characterisation of MH-associated variants.

Patient derived cells provide the perfect host for the modification and characterisation of specific variants. Where the variant can be introduced into cells extracted from an MHN family member, any change in Ca^{2+} homeostasis in the modified cell line can be attributed to the introduced variant. However, no change in function may suggest another familial variant is the cause for the disorder. Conversely, a suspected MH linked variant could be removed from an MHS cell line returning the genome back to wild type and again functional analysis could be used to confirm the consequence of the variant. Both approaches could be utilised in the characterisation of variants to increase the number of DNA tests and decrease the number of IVCTs accordingly. This chapter describes the immortalisation of primary myoblasts isolated from muscle biopsy samples, followed by their initial characterisation. The muscle samples were extracted from two MH negative individuals (patient I.D numbers 2332 and 2342) and one patient diagnosed with CCD who was confirmed as being MH-susceptible by IVCT (patient I.D number 2338). None of these patients have variants in *RYR1*. The RyR1 amino acid variant his 4833 tyr has been previously shown to be pathogenic for malignant hyperthermia and is prevalent in the New Zealand MH susceptible population (10). CRISPR/Cas 9 gene editing was used in an attempt to introduce the his 4833 tyr variant into a patient derived immortal myoblast cell line. As this variant is known to be pathogenic for MH, it would make a useful positive control for subsequent analysis of uncharacterised variants.

5.2 Results

5.2.1 Extraction of Primary myoblasts from muscle tissue

Muscle biopsies were obtained from patients undergoing a normal diagnostic procedure for susceptibility to MH. Use of surplus tissue for research purposes was obtained by informed consent with approval from the Health and Disabilities Ethics Committees 19/NTB/18. Myoblasts were prepared using the pre-plating method from muscle biopsies taken from

three separate individuals. This process involves the extraction of a mixture of primary myoblasts and fibroblasts from mechanically and enzymatically disrupted muscle tissue (2.2.10.6). These primary cells were resuspended in growth medium and transferred to a 10 cm cell culture dish. As fibroblasts attach to the plastic surface more readily than myoblasts do, the fibroblasts were selectively removed over the course of two hours by successively transferring the cell suspension to two new plates allowing the majority of the fibroblasts to attach to the plate surface of the first two plates. The third plate should then contain predominantly myoblasts. The myoblasts were then allowed to establish and form colonies over several days. The number of colonies formed was different between samples extracted from different patients. This is most likely due to the fact that several hundred viable cells were extracted from one patient and fewer than 100 were extracted from another. Using as much muscle tissue as possible (approximately 2-4 grams) to prepare cells usually ensured a significant number of cells was extracted from the tissue. However, other variables may have affected the number of cells extracted, including the age of the patient and the time lapsed from the biopsy being taken to cell extraction. The muscle tissue was stored in unsupplemented cell culture media on ice which may have also had an effect on cell viability. This parameter was unable to be controlled as all muscle tissue used was only available after completion of the diagnostic IVCT carried out at Palmerston North hospital.

Magnetic activated cell sorting (MACS) was trialled to isolate myoblasts. This process involves the labelling of myoblasts with an antibody specific to a myocyte cell surface antigen, CD82. The antibody is conjugated to a magnetic bead which allows for the immobilisation of the cells onto a specific column (Miltenyi biotec MS column) for later elution. All non-labelled cells (fibroblasts, that do not express CD82) should pass through the column unimpeded, while myogenic cells expressing CD82 should bind. Following elution from the column, the myoblasts were grown in culture, but fewer cells attached to the plate surface and began to form colonies using this method compared to the pre-plating method (table 5.1).

Patient I.D	Number of cells, pre-plating	Total number of cells following MACS	Number of cells in flow through	Number of cells following elution
2275	254	89	47	42
2288	356	71	44	27

Table 5.1. Table summarising the number of cells extracted from the pre-plating method and MACS from two separate patients. N=2 in each case, with numbers representing the average of both extractions.

MACS requires the cells to be incubated in PBS for an extended period of time where the cells are subjected to a number of incubations, wash and centrifugation steps which may have led to cell death. Following the extraction of cells using the pre-plating method, cells can be quickly suspended in medium and placed within an incubator. These conditions may be more favourable for cell growth as the cells have an immediate nutrient-rich and warm environment which may explain why a higher number of cells survived the pre-plating method. Once cells had been isolated, immortalisation methods were trialled starting with a lentiviral transduction system.

5.2.2 Preparation of a lentivirus vector for expression of human telomerase

Lentiviral particles have the potential to transduce both actively dividing and non-dividing cells. This was preferred over a retroviral system, which has been utilised by other research groups, as retroviral systems can transduce only dividing cells (114). The cDNA corresponding to hTERT, cloned into a pBABE retroviral vector, was PCR amplified and subcloned into the lentiviral transfer vector, pLENTI CMV (appendix 3.2.2). The presence of the hTERT cDNA was initially confirmed by restriction endonuclease digestion, using Xba1 and Sal1, to yield two bands of 8545 bp and 3450 bp in size corresponding to the entire vector back bone and hTERT cDNA respectively (figure 5.3). The presence of the cDNA was further confirmed by Sanger sequencing of the entire coding region which also confirmed that no PCR-induced variants were present in the cDNA.

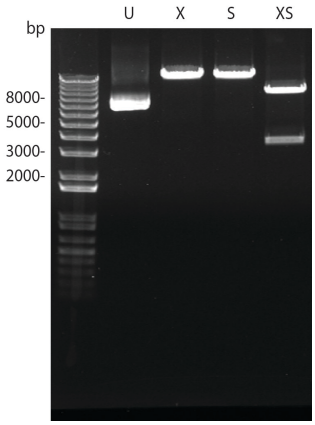

Figure 5.3. Restriction endonuclease digestion confirming the identity of the pLENTI hTERT vector. U represents uncut vector DNA. X represents the vector DNA digested with Xba1. S represents the vector DNA digested with Sal1. XS the vector DNA digested with both Xba1 and Sal1. The 1Kb+ Plus DNA ladder was used to estimate the sizes of DNA. DNA was separated by 0.7 % agarose gel electrophoresis for one hour at 90 mV in 1 x TAE. DNA was stained with 0.5 µg/mL ethidium bromide and visualised under UV light using the image lab 5.1 software. The 1 kB plus DNA size standard was to used estimate the size of DNA fragments.

The pLENTI CMV CDK4 vector had been prepared previously in a similar manner. Confirmation of this clone was also performed by restriction endonuclease digestion (figure 5.4) using the enzymes Xba1 and Sal1 rendering two bands with the sizes of 8033 bp and 909 bp representing the vector backbone and CDK4 cDNA respectively. Sanger sequencing confirmed the correct sequence.

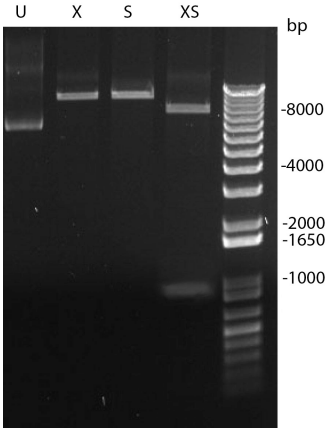

Figure 5.4. Restriction endonuclease digestion confirming the identity of the pLENTI CDK4 vector. U represents uncut vector DNA. X represents the vector DNA digested with Xba1. S represents the vector DNA digested with Sal1. XS the vector DNA digested with both Xba1 and Sal1. The 1Kb+ Plus DNA ladder was used to estimate the sizes of DNA. DNA was separated by 0.7 % agarose gel electrophoresis for one hour at 90 mV in 1 x TAE. DNA was stained with 0.5 µg/mL ethidium bromide and visualised under UV light using the image lab 5.1 software. The 1 kB plus DNA size standard was to used estimate the size of DNA fragments.

After confirming the identity of the cloned hTERT and CDK4 cDNAs by Sanger sequencing, lentiviral particles were produced using HEK293T cells as the host cell line.

5.2.3 Production of lentiviral particles and transduction of primary myoblasts

To optimise the transduction process, viral particles were produced which contain the cDNA for green fluorescent protein (GFP) so that transduced cells could be visualised over non-transduced cells. To produce viral particles HEK293T cells were transiently transfected with three lentiviral vectors: transfer plasmid which houses the GFP cDNA, the packaging and envelope plasmids, psPAX2 and VSV-G respectively, as described in methods section 2.2.11.1. Each vector provides an essential component for the production of live lentiviral particles for secretion into the growth medium (figure 5.5). Medium was collected, viral titre determined and used to infect a myoblast target cell.

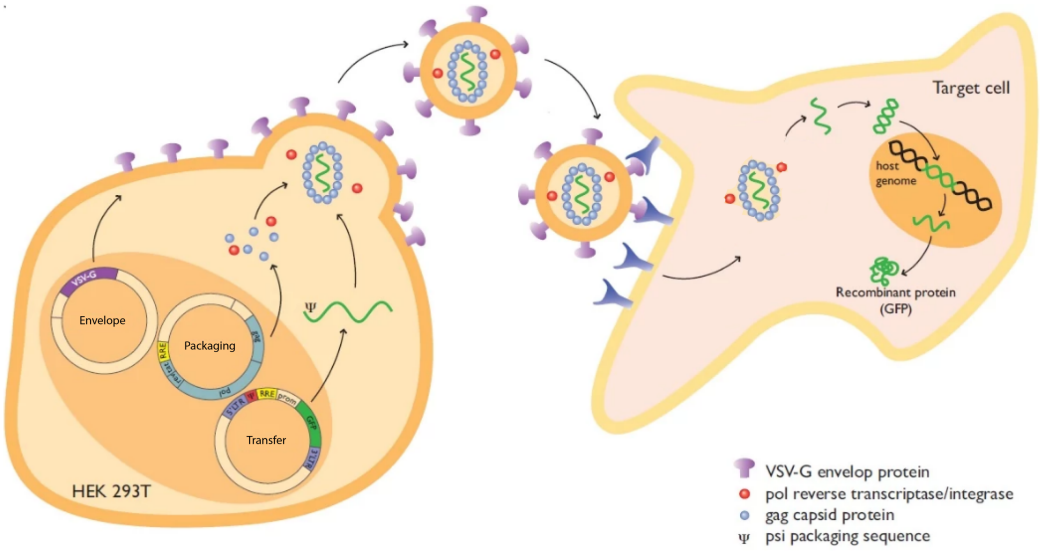

Figure 5. 5. Schematic diagram summarising the production of lentivirus particles and the infection of a target cell. Figure adapted from (120), no permission required to use figure.

After collection, the concentration of viral particles was determined using reverse transcriptase PCR specific to lentiviral DNA where genomic concentration was converted to an infectious titre. The concentration of GFP viral particles was determined by comparing the crossing points of amplicons containing the virus with the crossing points of the control samples provided with the kit of known concentration (figure 5.6).

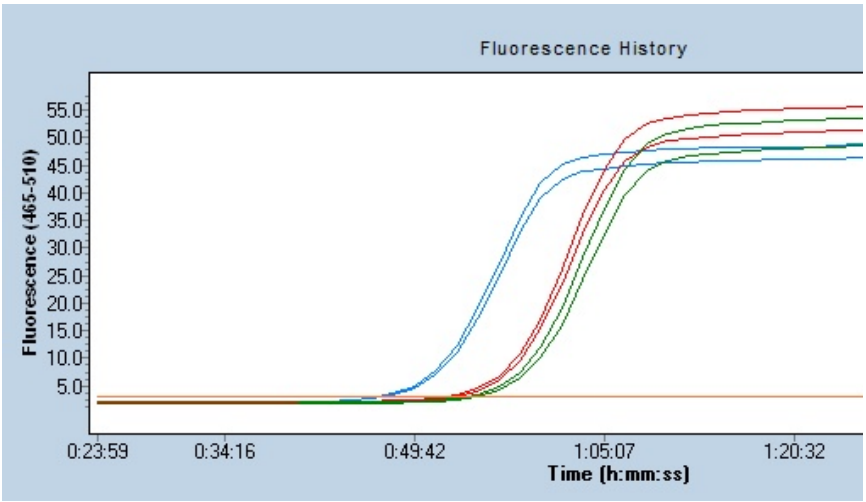

Figure 5.6. Reverse transcriptase quantitative PCR confirming the production of lentivirus particles. The blue lines represent the amplification of standard 1. The red lines represent the amplification of GFP containing viral particles. Green lines represent the amplification of the second standard. The orange line represents the no template control.

Viral particles containing GFP cDNA were consistently produced at a concentration of approximately 1.5 x 10^7 IU/mL.

To assess the efficiency of lentiviral transduction, a cell culture containing commercially purchased HMCL 7304 immortal myoblasts was grown to the approximate confluences of 30, 50 and 70 % in 10 cm tissue culture dishes. The cells, at each level of confluence, were transduced with known concentrations of lentivirus containing the cDNA for GFP. Viral particles were either diluted directly following production and used to infect the myoblast cell lines or concentrated following the protocol described in section 2.2.11.2.

The expression of GFP, following transduction, was detected using an inverted fluorescence microscope where the number of cells expressing GFP was visualised over cells not expressing GFP (table 5.2).

approximate confluence of myoblasts	concentration of lentivirus (IU/mL)	volume of virus (µL)	Number of cells expressing GFP	Percentage of cells expressing GFP
30	$1x10^3$	200	0	0
30	$1x10^5$	200	2	0.04
30	$1x10^7$	200	10	0.2
30	$1x10^8$	200	7	0.15
50	$1x10^3$	200	0	0
50	$1x10^5$	200	7	0.07
50	$1x10^7$	200	25	0.25
50	$1x10^8$	200	21	0.21
70	$1x10^3$	200	0	0
70	$1x10^5$	200	0	0
70	$1x10^7$	200	15	0.1
70	$1x10^8$	200	19	0.16

Table 5.2. Summary of the number of myoblasts expressing GFP following transduction with lentivirus particles

The percentage of transduced cells was low in all combinations of cell confluence and viral concentration. The optimal conditions for successful transduction was chosen as 50 % confluence using a viral titre of at least $1x10^7$.

The GFP cDNA was incorporated into the genome of the myoblasts alongside the cDNA encoding an antibiotic resistance gene, allowing for the selection of transduced cells over non-transduced cells. In this case two separate lentiviral particles were produced; one containing hygromycin resistance and one containing neomycin resistance. To determine the appropriate concentrations of hygromycin and geneticin, a neomycin analogue, both non-transduced and transduced cells were exposed to different concentrations of each antibiotic and the time to kill non-transduced cells was then measured (table 5.3).

A)

Hygromycin Concentration (µg/mL)	Days until total cell death
5	N/A
10	14
25	10
50	6
100	3
200	2

B)

Geneticin Concentration (µg/mL)	Days until total cell death
20	N/A
50	12
100	10
200	5
400	1
500	1

Table 5. 3. Table summarising the time taken for the antibiotics A) hygromycin and B) geneticin to kill myoblasts.

The concentrations 25 µg/mL and 100 µg/mL were selected for hygromycin and geneticin respectively, as roughly 10 days was required to kill all non-transduced cells. At lower concentrations some cells were still able to survive in culture or took a prolonged time period to die and at higher concentrations cell death was rapid with the risk that the antibiotic would overpower the resistance marker, killing transduced cells. Both hygromycin and geneticin act as antibiotics by inhibiting protein translation, therefore high concentrations may not kill the cells but it may add additional stress decreasing cell viability.

The transduction was repeated, using patient extracted cells grown to a confluence of 50 % in a 10 cm cell culture dish and transduced with lentiviral particles containing GFP at the concentrations of either $1x10^7$ or $1x10^8$ IU/mL. For this experiment, two separate lentiviral particles were produced; one containing hygromycin resistance and one containing neomycin resistance. Following transduction, the cells expressing GFP were visualised using an inverted fluorescence microscope (figure 5.7).

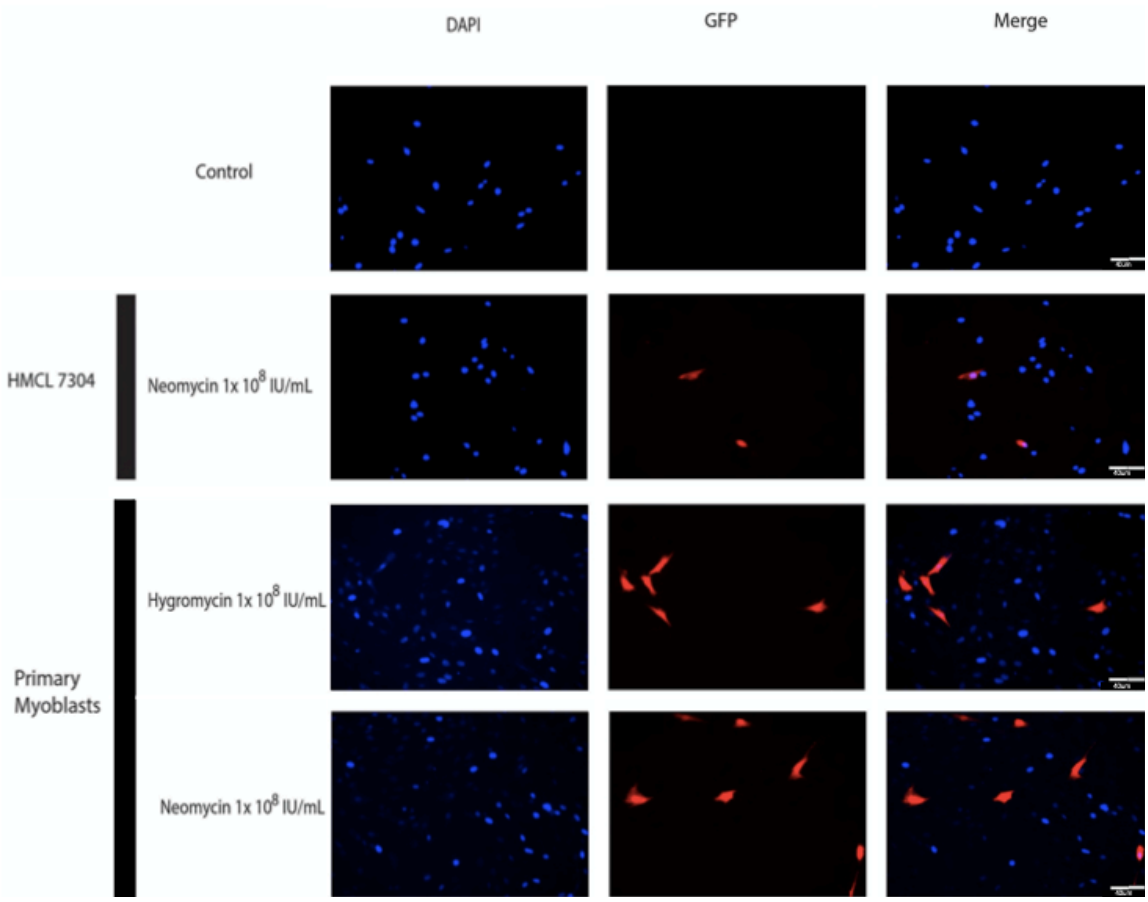

Figure 5.7. Expression of GFP in transduced primary myoblasts. Nuclei were stained with DAPI shown in blue. GFP is highlighted in red. The third column shows a merged image. The first row represents non-transduced cells and the following rows have been identified by cell name either HMCL 7304 or primary myoblasts, neomycin and hygromycin represent different antibiotic resistance markers transduced alongside GFP, the viral titre has been represented. The size bar indicates 40 µm. Images were taken using the Olympus IX83-based Multidimensional Imaging Platform.

The extent of transduction in the patient extracted cell cultures was similar to that of the pure, commercially purchased myoblast culture. This suggests that regardless of the identity of the cells, efficiency of transduction is similar. At the point of visualisation, the cells were also exposed to either the antibiotic hygromycin or geneticin (G418) depending on the virus the cells were transduced with to select for transduced cells over non-transduced cells. Following the death of primary cells and the propagation of transduced cells the expression of GFP was again determined (figure 5.8). After selection, more than 80 % of the cells expressed GPF.

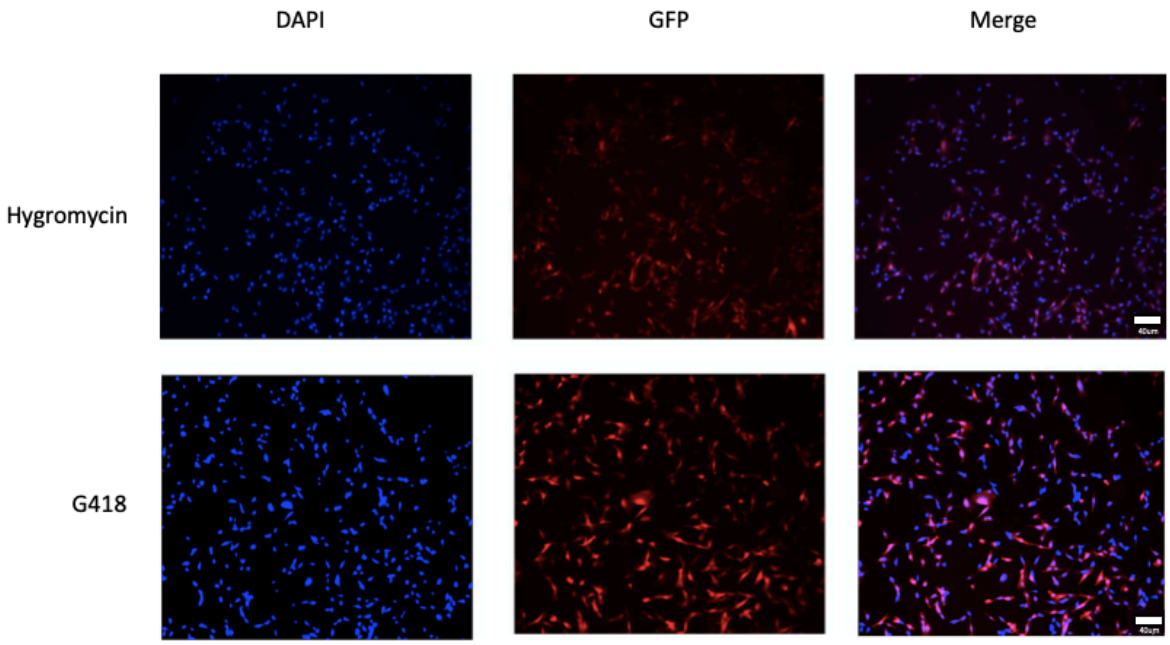

Figure 5.8. The expression of GFP in transduced myoblasts following antibiotic selection. The antibiotic the cells were selected in is indicated. The size bar indicates 40 µm. Images were taken using the Olympus IX83-based Multidimensional Imaging Platform

Not all cells were shown to express GFP, suggesting that not all cells visualised had been transduced. These cells may have survived selection if the concentration of the antibiotic was too low or cells in the surrounding area may have degraded the antibiotic allowing non-transduced cells to survive. The cells that did not appear to express GFP were isolated cells, surrounded by cells that can express GFP, so it is possible the cells were still in the process of dying, as they had not formed a colony.

These results show that myoblasts can be transduced with lentiviral particles, however, the transduction efficiency was very low. To increase the rate of transduction the product ViraDuctin™ was trialled. ViraDuctin™ is a propriety formulation for lentiviral transduction. The kit has been optimised to increase the interaction between the virion and target cells. ViraDuctin™ has been previously shown to increase transduction rates in primary cells. To test the efficiency of the kit, primary myoblasts were transduced with lentivirus containing the GFP cDNA with and without ViraDuctin™. While the high percentage of transduction rates advertised by the manufacturers were not achieved, the rate still increased by 500 % (table 5.4). ViraDuctin™ was used for all subsequent transductions.

	Average	SEM	P Value
Percentage of cells expressing GFP without ViraDuctin™	0.3	0.0758	
Percentage of cells expressing GPF, when treated with ViraDuctin™	1.5	0.144	0.0045

Table 5.4. Table summarising the percentage of primary myoblasts transduced by lenti virus treated with ViraDuctin™. N=3 the two tailed student's t-test was used to compare the two results with a result of <0.05 considered to be statistically significant.

Following transduction, cells were again subjected to selection with 25 µg/mL hygromycin where the expression was used to visualise transduced cells over non transduced cells (figure 5.9). Again, almost all were shown to express GFP, indicating the transduction and selection was successful.

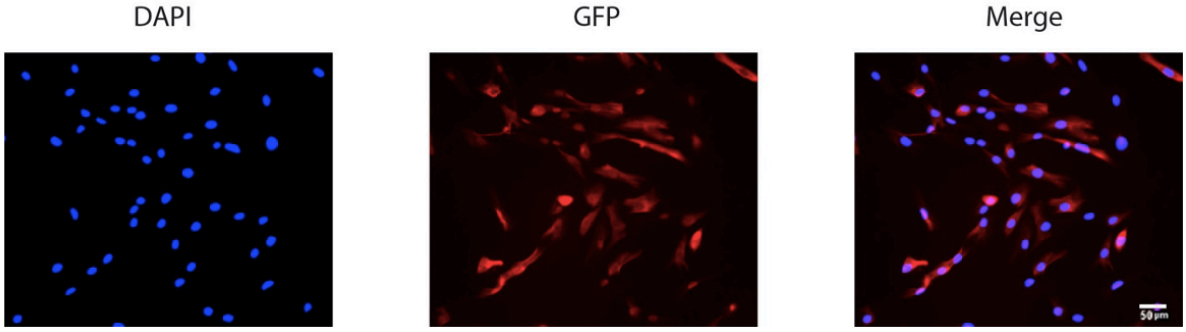

Figure 5.9. The expression of GFP in transduced myoblasts following antibiotic selection. Transduced cells were selected for in 25 µg/mL hygromycin for 10 days before visualisation. The size marker represents 50 µm. Images were taken using the Olympus IX83-based Multidimensional Imaging Platform.

After optimising the transduction of primary myoblasts utilising lentiviral particles containing the GFP cDNA, efforts were made to immortalise myoblasts using lentiviral particles containing the cDNA for hTERT and CDK4.

5.2.4 Immortalisation of primary myoblasts using lentivirus

HEK293T cells were transfected with the vectors required to produce hTERT or CDK4 lentivirus. Viral particles were collected, and the presence of virus was determined using reverse transcriptase PCR specific to lentiviral particles. Viral particles containing the cDNA for CDK4 were produced very effectively. However, viral particles containing human telomerase cDNA were consistently produced at concentrations approximately six-fold lower than for CDK4 (figure 5.10, table 5.5)

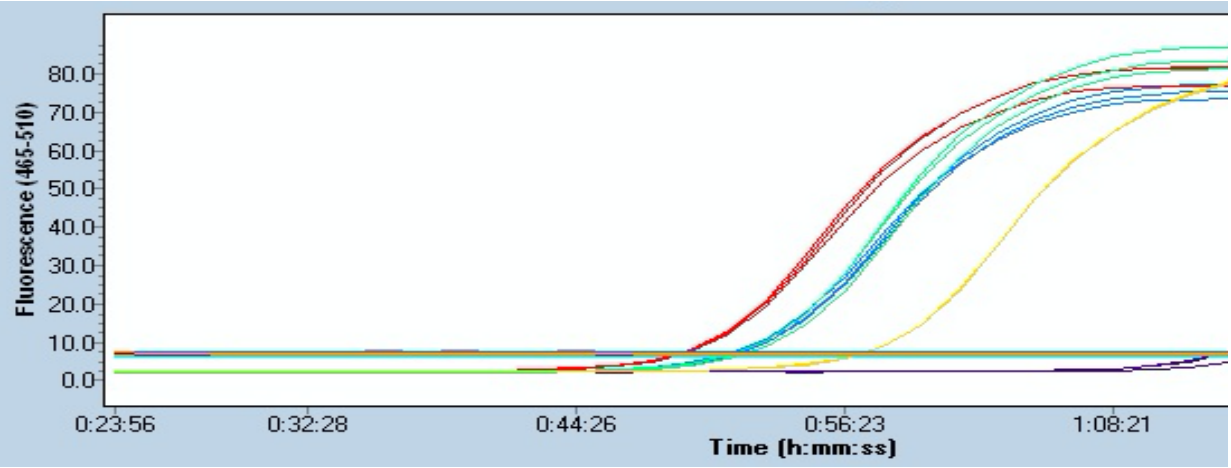

Figure 5.10. Reverse transcriptase quantitative PCR confirming the production of Lentivirus particles. Red represents positive control 1, blue represents positive control 2, cyan represents CDK4, yellow represents hTERT. Purple represents growth media collected from non-transformed HEK293T cells. Orange represents a no template control.

Name of virus/cDNA	Average	SEM	P-value
hTERT	2.5×10^{6}	2.7	
CDK4	1.5×10^{7}	71.5	0.031

Table 5.5. Table summarising approximate concentrations of virus produced in HEK293T cells. N=7 the two tailed student's t-test was used to compare the results and a P-value <0.05 was considered to be statistically significant.

The length of the human telomerase cDNA, 3450 base pairs, exceeds the maximum DNA length for efficient lentiviral packaging of approximately 3000 base pairs and may be the reason for the lower titre. CDK4 viral particles were consistently produced to a relatively high concentration of 1.5×10^{7}. Freshly extracted primary myoblasts were grown to a confluence of approximately 50 % and transduced with either the human telomerase or the CDK4

lentivirus at a concentration of 1 x 10^7 IU/mL. The hTERT virus had to be concentrated using the method outlined in section 2.2.11.2. Following transduction, the cells were subjected to antibiotic selection with either hygromycin or geneticin respectively. Cells transduced with the CDK4 virus exhibited a comparable cell death to that of the cells transduced with the GFP virus indicating very comparable transduction efficiency was achieved. However, a larger amount of cell death was detected for cells transduced with the human telomerase virus and a significantly lower number of cells survived selection (table 5.6).

Patient number	% of cells transduced with hTERT	SEM	% of cells transduced with CDK4	SEM	P-value
2332	0.1	0.00165552	0.9	0.04714045	0.0002
2338	0.2	0.00873053	0.8	0.07071068	0.0023
2342	0.1	0.00504058	0.4	0.04951618	0.0075

Table 5.6. Table summarising the transduction rates of patient extracted myoblasts using hTERT or CDK4. N=3 the student's unpaired t-test was used to compare transductions rates of the percentage of cells transduced with hTERT to the percentage of cells transduced with CDK4. a P-value <0.05 was considered to be statistically significant.

It is interesting to note that primary cells could not be transduced with both hTERT and CDK4 lentiviral particles at the same time. This may be due to the low transduction rate where it was unlikely one cell would be transduced with both viruses. To immortalise the cells, myoblasts were initially transduced with hTERT virus, to ensure the early expression of human telomerase reverse transcriptase, in an attempt to preserve telomere integrity as early as possible. Following selection, the cells were then transduced with CDK4 viral particles and again subjected to selection. Cells able to survive in both antibiotics were regrown and subjected to MACS purification to obtain a pure myoblast sample. When MACS was performed on an established cell culture, approximately 80 % of the cells survived the purification process. Because more cells were subjected to the labelling and purification process, a greater number of cells were able to survive and quickly began to divide in medium

as compared to cells freshly extracted from a muscle biopsy. Of the cells that survived the purification process, approximately 30 % of the cells flowed through the column. The remaining 70 % were initially immobilised and were subsequently eluted from the column. This indicates the primary cell culture was mixed as would be expected from the pre-plating method or some myoblasts were not labelled and as a result passed through the column.

It is interesting to note that cells extracted from different patients had different rates of transduction (table 5.6). In addition, the longer the cells were grown in culture the less likely the cells were able to be transduced (table 5.7). There is a significant decrease in transduction rate between days 7 and 10 (P-value 0.01664 and 0.001) confirming the importance of an early transduction in the immortalisation process. There was no significant difference between in transduction rates between days 14 and 21 (P-value 0.35105 and 0.9975) indicating that beyond 14 days of growth there is no change in transduction rate.

Patient number	Days after extraction cells were transduced	% of cells transduced with hTERT	SEM	P-value in comparison to day 7	P-value in comparison to day 10	P-value in comparison to day 14
2332	7	0.1	0.0017			
	10	0.05	0.123	0.01664		
	14	0.01	0.080	0.00022	0.17814	
	21	0	0	0.0001	0.00674	0.35105
2338	7	0.2	0.0087			
	10	0.03	0.0042	0.0001		
	14	0.03	0.0045	0.0002	0.0000	
	21	0.01	0.0044	0.0001	0.0975	0.9975

Table 5.7. The percentage of cells transduced with hTERT lentivirus depending on days in culture prior to transduction. N=3, the one way ANOVA test was used to compare the percentage of cells transduced on days 7, 10, 14 and 21, a P-value <0.05 was considered to be statistically significant.

In an attempt to increase the efficiency of the transduction process, cells freshly extracted from muscle biopsy tissue, were suspended in media containing viral particles prior to being plated. In this experiment the number of primary cells exposed to virus was unknown and being a mixture of cells, the number of myoblasts within was also unknown. However, the

concentration of virus present within the media and incubation periods prior to selection could be controlled. Transduction of freshly extracted myoblasts was carried out in growth medium containing viral particles expressing GFP in the presence of ViraDuctin^{TM}. While the percentage of cells transduced could not be determined, cells resembling myoblasts were transduced, and formed colonies. After approximately seven days of growth, when the cells reached 80 % confluence, antibiotic selection was performed to identify transduced cells over non-transduced cells where approximately 10 colonies of cells survived selection after each transduction. When this method was repeated utilising the CDK4 lentivirus the same results were observed where approximately 10 cells were transduced following extraction. In contrast, only one or two colonies survived selection using the hTERT virus.

The most successful method for lentiviral immortalisation of myoblasts first required the growth of the primary cell culture to approximately 50 % confluence followed by transduction with $1x10^7$ IU/mL of hTERT lentivirus. Following selection and regrowth of cells to 50 % confluence the cells were then transduced with $1x10^7$ IU/mL of CDK4 lentivirus. This method was followed for subsequent lentiviral-based immortalisation. The process was still inefficient where the transduction efficiency for both hTERT and CDK4 lentiviral particles was low with each virus having an approximate transduction rate of 0.1 and 0.7 respectively (Table 5.6). The selection and regrowth phase took approximately 3-4 weeks to progress to completion. The cells would have progressed through many doublings during the process of immortalisation, which may have affected their viability. Alternative methods exist for the introduction of specific cDNA into cells and these could be trialled as an alternative. These include the use of different plasmids to produce viral particles or lipophilic reagents for transfection or electroporation.

5.2.5 Immortalisation of myoblasts using nucleofection

One alternative method to introduce hTERT and CDK4 for immortalisation of myoblasts is nucleofection. Nucleofection is an electroporation-based transfection method which requires the disruption of the cell membrane and nuclear membrane using proprietary reagents. The

process is very harsh and can reduce cell viability. When the vectors are introduced into the nucleus of the cell, they have the potential to be incorporated into the genome by non-homologous recombination, creating a stable cell line. The recombination process is non-specific and has a very low rate of incorporation. To initially assess cell viability and nucleofection efficiency, the previously immortalised myoblast cell line, HMCL 7304, was subjected to nucleofection with the vector pLENTI GFP containing hygromycin resistance. During the nucleofection process approximately half of the cells died but, of those that survived approximately 99 % of the cells expressed GFP (table 5.8)(figure 5.11).

Cell line	Percentage of cells expressing GFP
HMCL 7304	99 %

Table 5.8. Percentage of cells expressing GFP following nucleofection.

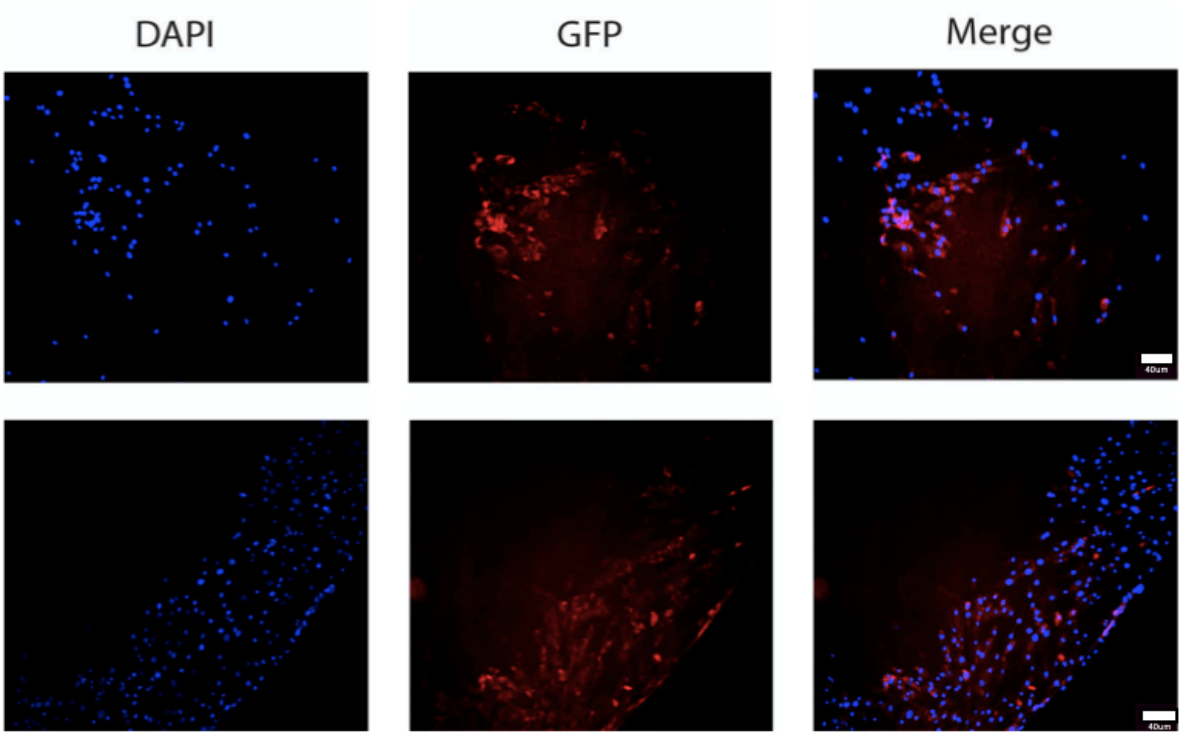

Figure 5.11. GFP expression following nucleofection of HMCL 7304 cells. Images taken from two separate attempts have been presented. Cells were visualised 48 hours after nucleofection and the expression of the protein was monitored using an inverted fluorescence microscope at 10 x magnification. The size marker represents 40 µm.

At the point of visualisation, the cells were also subjected to antibiotic selection. Some cells died during selection, however the majority of the cells that attached to the surface of the plate survived and within 4 days had formed colonies. After approximately 10 days the cells

stalled in growth, and over the following five days the cells began to die and within another 10 days all cells were dead. This suggested that integration into the genome had not occurred. As the cells were not able to propagate the vector, continual cell division would lead to its dilution. With time, the cells would not have enough copies of the vector present to lead to sufficient expression of the resistance marker, leading to cell death. The lack of cell viability following selection is not a result of the harsh conditions associated with the electroporation as cells that were not subjected to selection proliferated in solution. This exercise suggests nucleofection is not a viable alternative to lentiviral transduction in the immortalisation of myoblasts. No other attempts were made to optimise this system and the lentiviral system was used to immortalise cells for all further experiments. The primary cell culture subjected to immortalisation was a mixed culture containing both myoblasts and a proportionally smaller number of fibroblasts. Prior to the functional characterisation of each cell line efforts were made to confirm the identity of the cells within the culture.

5.2.6 Confirming the identity of immortal myoblasts

To determine if the cells immortalised by lentiviral transduction were in fact myoblasts, the cells were fixed with paraformaldehyde and labelled with an antibody against the myogenic marker desmin, a filamentous protein which tethers the nuclear membrane via the Z-disk to the plasma membrane. A Trit C conjugated secondary antibody was used to visualise desmin. The expression of desmin in immortal cells was compared to that of primary, non-transduced, cells extracted from the same patient (figure 5.12)

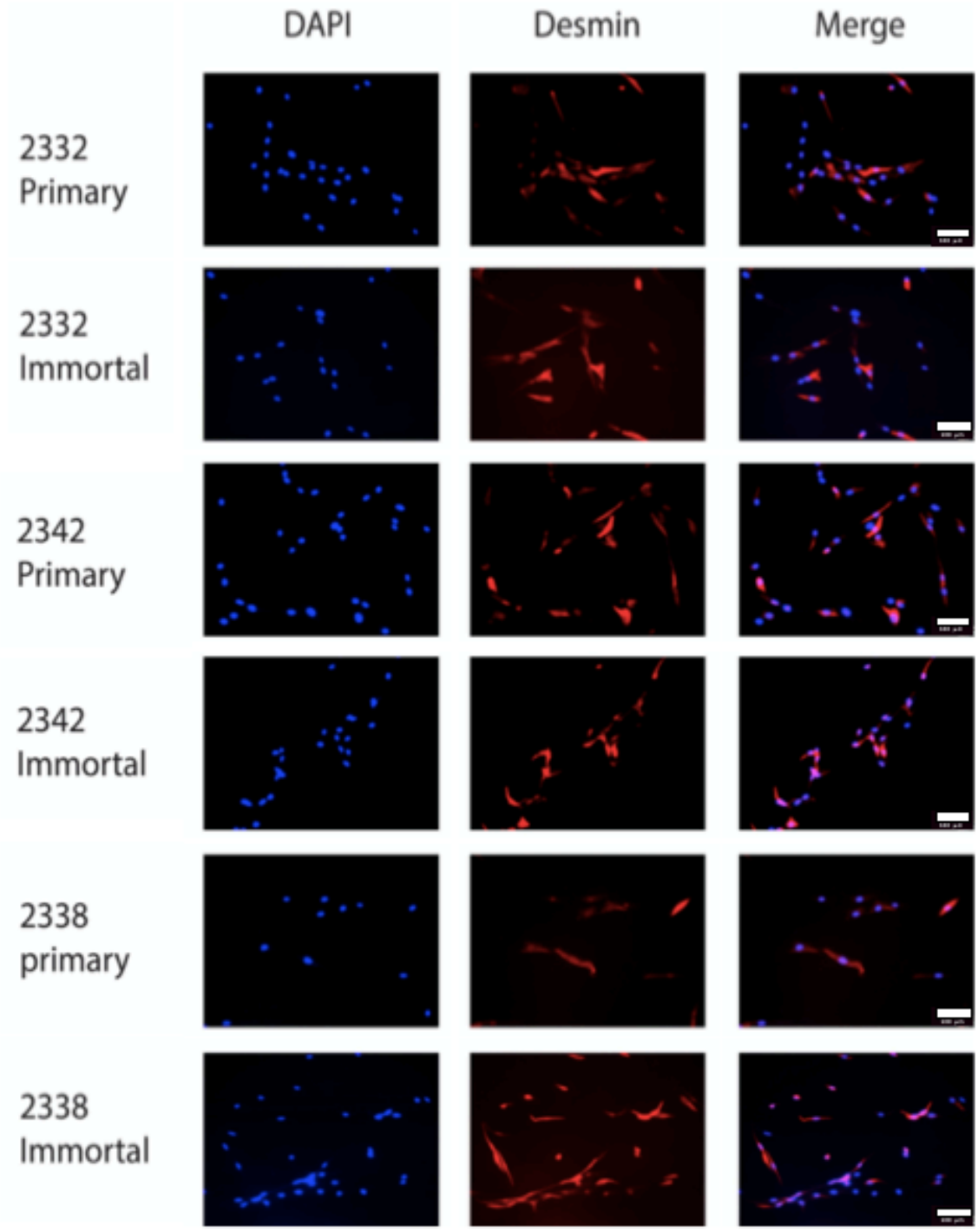

Figure 5.12. An example of the fluorescent staining of myoblasts showing the expression of the protein desmin. DAPI was used to stain the nuclei (blue). A Trit C conjugated antibody was used to detect desmin (red). Merge shows overlay of the two images. Images were taken using the Olympus IX83-based Multidimensional Imaging Platform at 20 x magnification. The individual patients have been represented by code number with both primary and immortal cells being represented. The size marker represents 100 µm.

Patient number	Percentage of primary cells expressing desmin	Percentage of immortal cells expressing desmin
2332	85	100
2342	91	100
2338	78	100

Table 5.9. Summary of the number of cells expressing desmin in either primary or immortal cell lines

Desmin was detected in cells purified from all patients (table 5.9). In some cases, the cells had begun to differentiate or had at least formed an attachment to an adjacent cell. A small percentage of primary cells contained no detectable desmin. The cells visualised in figure 5.12 were not subjected to purification steps to enrich for myoblasts, therefore other cells which do not express desmin may have also been present in the cell culture. During the immortalisation process the cells had been subjected to magnetic activated cell sorting. Myoblasts were therefore enriched following this step and desmin was detected in all cells suggesting the purification process was successful. While the myoblasts survived selection, and in theory should also express hTERT, ensuring the function of the enzyme is important to determine if the cells are in fact immortalised.

5.2.7 Determining telomere length

Quantitative PCR was used to determine telomere length following the transduction of myoblasts. Primers specifically designed to the telomeres were used for the amplification of genomic DNA. As the telomeres consist of a repeating DNA sequence, TTAGGG, PCR cannot be used to estimate the overall length of the telomeres, however quantitative PCR can be used to determine the relative number of telomere repeats in comparison to a single copy gene. Primers specific to the telomeres were designed replicating those published by Cawthon 2002 (121). The primers were designed to limit the formation and amplification of primer dimers (figure 5.13). Both primers, Tel 1 and Tel 2, each contain specific nucleotide mismatches which would still allow annealing of the primer to genomic DNA, however this

would limit the binding of the primers to each other. The 5' end of Tel 1 was modified to include 5 Ts to prevent the amplification of the primer pairs should a primer dimer form.

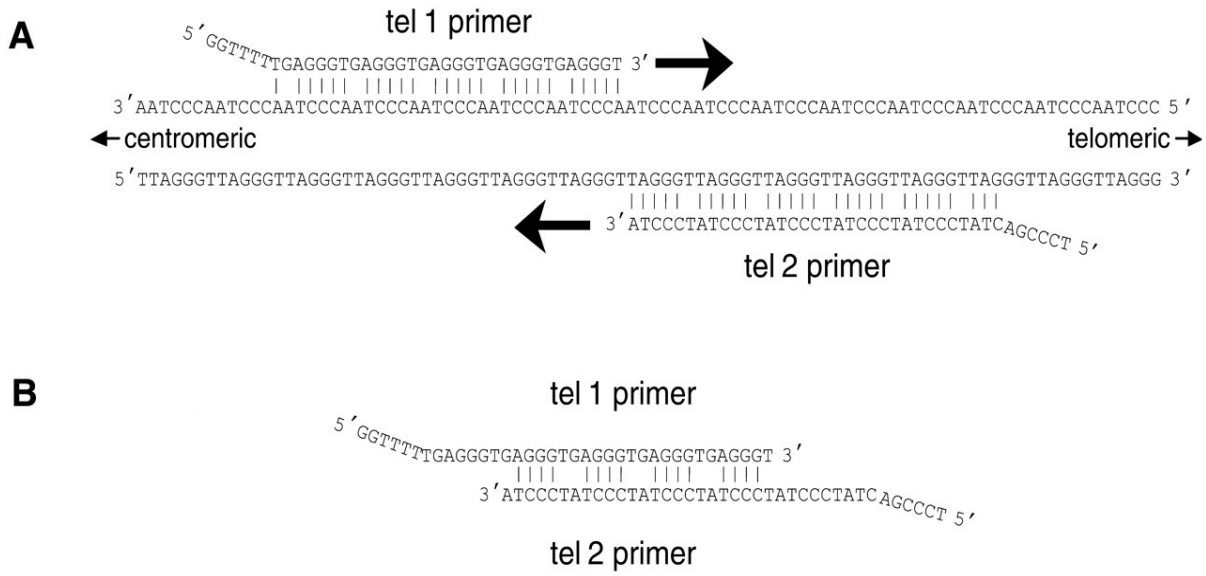

Figure 5.13. Schematic representation of the primers used for the amplification of telomere repeat regions. A) figure depicting the binding of the primers to genomic DNA. B) Figure depicting the binding formation of primer pairs.

A single copy gene, interferon beta 1 (IFNB1), was used as a reference to determine the relative telomere length. Following PCR amplification of the telomere region and INFB1 the crossing points of each sample were calculated. The crossing point is a representation of the telomere length; the longer the telomere repeat region the lower the crossing point is expected to be. In comparison, amplification of the IFNB1 gene should occur later and have a crossing point with a higher number, and hence the relative number of telomere repeats can be estimated.

A standard curve was established to determine the efficiency of both the INFB1 (figure 5.14) primers and the telomere-specific primers. The initial establishment of a standard curve was performed using genomic DNA purified from myoblasts, as a template, with the Roche 480 HRM master mix. The Cp values were plotted against the log of the template DNA concentration and the Lightcycler® 480 Software was used to determine the amplification efficiency. An efficiency of 1.987 was determined for the INFB1 primers which indicates the

amount of DNA in each well is doubling with each cycle, as expected for specific well matched primers.

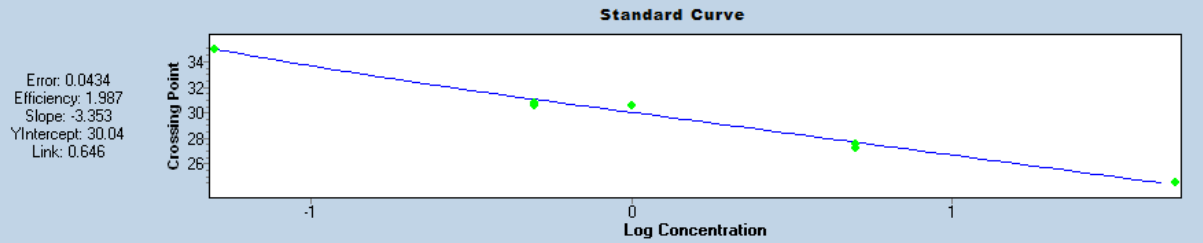

Figure 5.14. Standard curve depicting the efficiency of amplification using the INFB1 primers.

No amplification was observed while determining the efficiency of the telomere repeat region using the Roche 480 HRM master mix. As an alternative, the Ssofast Evagreen (Bio-Rad) master mix was used to amplify the genomic DNA, giving an efficiency of 10.94. An efficiency this high is an indication that the amplification is increasing at a rate of 10 each cycle (figure 5.15). As the maximum efficiency for PCR amplification is 2, an efficiency of 10 suggests non-specific amplification has occurred.

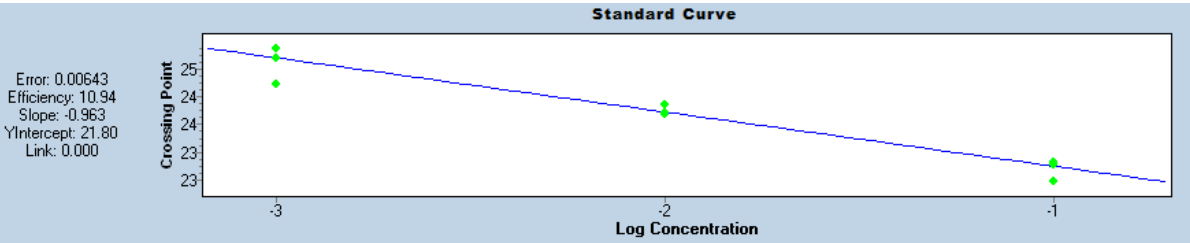

Figure 5.15 Standard curve depicting the efficiency of amplification of the telomere repeat primers.

The telomere repeat region located at the end of each chromosome consists of the DNA sequence TTAGGG repeated multiple times (figure 5.16). Therefore, the primers designed to this region have the potential to form a large number of possible PCR products. The PCR products will all contain multiple binding sites for the primers in the following cycles. As a result, genomic DNA cannot be used as a template to determine the efficiency of the telomere-specific primers.

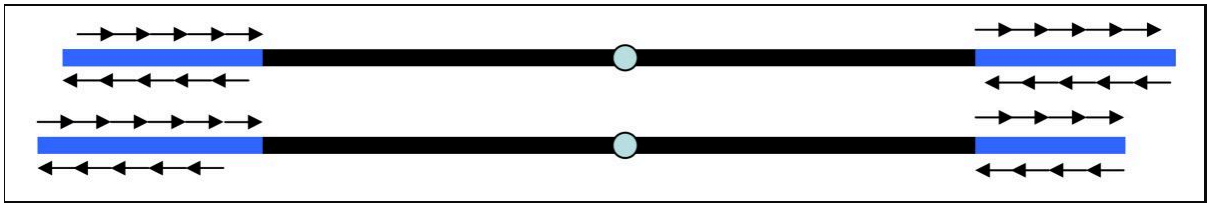

Figure 5.16. Schematic representation of the telomere repeat region and primer binding sites. Black represents the genomic DNA. Blue represents the telomeric region, arrows represent possible primer binding sites.

To overcome this problem a telomere repeat oligonucleotide $(TTAGGG)_{14}$ was used as a template to determine primer efficiencies as in previous studies (122). Initial PCRs were performed replicating the previously used conditions and an efficiency of 1.543 was determined (figure 5.17).

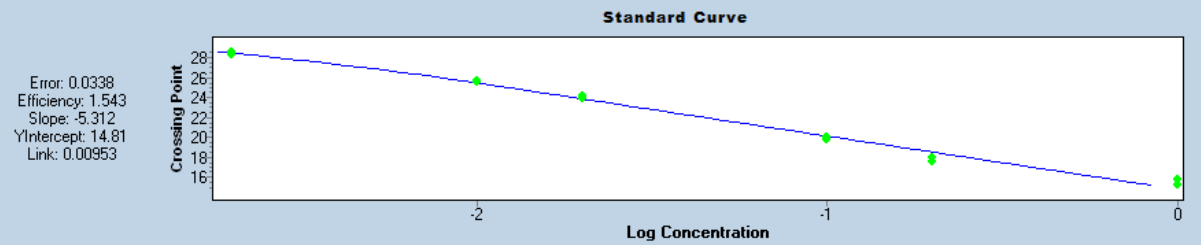

Figure 5.17. Standard curve determined after performing PCR using the telomere repeat oligo as a DNA template.

Altering one primer concentration with respect to another has been previously shown to aid in the amplification of the telomere region (121). The concentrations 270 nM Tel 1 and 900 nM Tel 2 were trialled and an efficiency of 1.850 was achieved (figure 5.18).

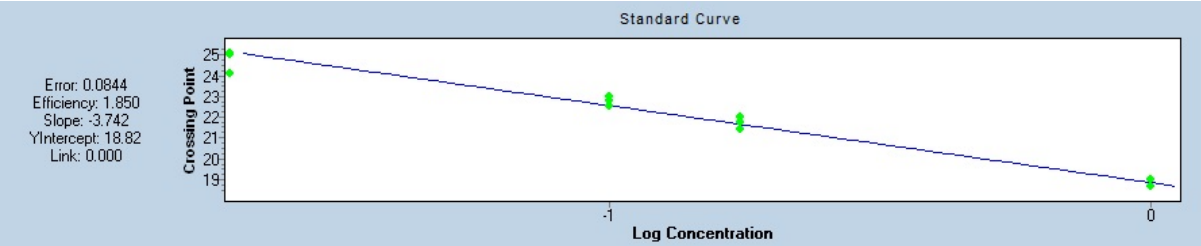

Figure 5.18. Standard curve determined after performing PCR using the telomere repeat oligo as a DNA template.

After achieving an efficiency of 2 +/- 10 % for both primer pairs a qPCR was performed using each primer pair separately with 35 ng of genomic DNA. The Cp value was determined for each sample and compared to each other using the following calculation.

1. Extract Cp values from Roche output.

2. Calculate $\Delta Cp = Cp_{Tel} - Cp_{INFB1}$ for each sample.

3. Calculate Tel/INFB1 ratio ($=2^{-\Delta Cp}$) for each sample.

Using genomic DNA as a template for the PCR, it was noted the PCR amplified two-three cycles prior to the no template control (figure 5.19). While the primers were designed to inhibit the formation and amplification of primer dimers it is possible that this still occurred.

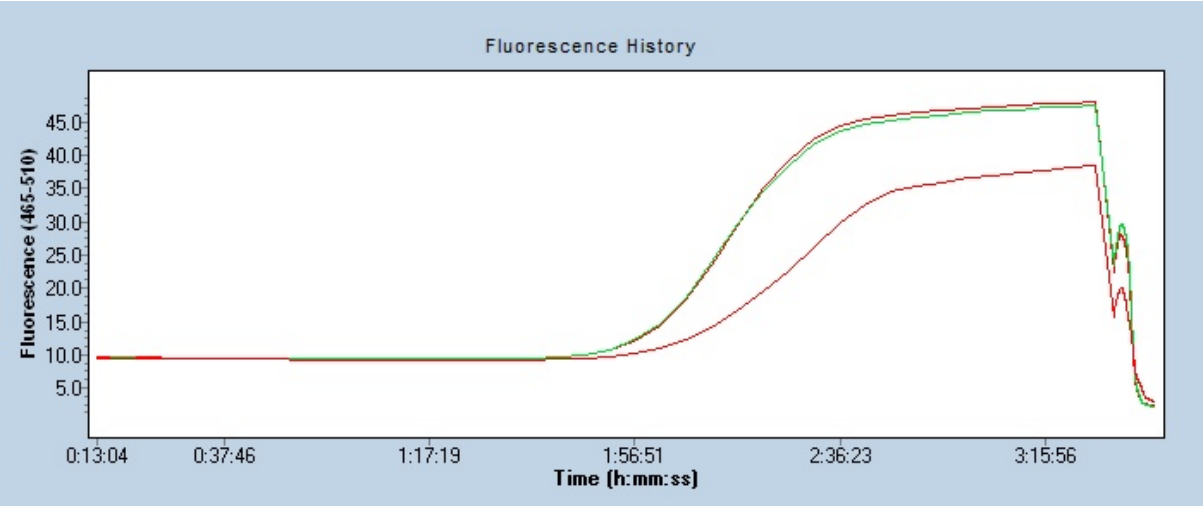

Figure 5.19. Amplification of genomic DNA using telomere repeat specific primers. The sample containing genomic DNA has been shown in green. The sample containing no template DNA is shown in red.

The difference in length of the passage 2 cells compared to the passage 6 cells was statistically insignificant (43.71 vs 35.75, p value 0.1009). The expression of hTERT had no significant effect on the length of the telomere.

Cell	Relative telomere length (n=3)	SEM	P-value
Primary cells, passage 2 day 14	43.71	2.2	
Primary cells, passage 6 day 32	35.75	2.4	0.1009
hTERT transduced, day 21	37.67	1.6	0.1187
hTERT and CDK4 transduced, day 32	34.53	2.5	0.0922

Table 5.10. Table depicting the relative telomere length in primary and immortal myoblast cell lines. N=3 refers to the number of biological replicates. The student's t-test was used to compare the relative telomere length of passage 2 day 14 samples to all other samples, a value <0.05 was considered to be statistically significant.

During the PCR the no template control consistently amplified 3 cycles later than the DNA containing samples using the telomere primers, suggesting the amplification of primer dimers. The consistent amplification of the DNA containing samples may have resulted from the amplification of genomic DNA along with the primer dimers greatly effecting the results, and may explain the statistically insignificant results obtained.

5.2.8 Myoblast differentiation

The ryanodine receptor is expressed only following the differentiation of myoblasts into myotubes. After the removal of serum (described in section 2.2.10.8) from the medium the cells began to differentiate. Primary myoblasts appeared to be fully differentiated in approximately 7 days, while immortalised myoblasts took approximately 2 weeks to differentiate. A difference in morphology of the myotubes was observed between primary and immortal myotubes including the previously immortalised HMCL 7304 cell line (figure 5.20). The primary myotubes typically extended beyond the field of view of the microscope where immortal myotubes were seldom visualised extending beyond the field of view of the microscope. Primary myotubes were also heavily branched in structure, while the immortal myotubes did not form obvious branched structures. The immortal myotubes produced in this study where consistent in morphology with the commercially purchased HMCL 7304 cell line. When the HMCL 7304 were previously characterised it was shown the cells were able to form large branched structures similar to those produced by primary myotubes in this study

(114). While the protocol for differentiation was identical, these structures could not be replicated in this current research. Nevertheless, both primary and immortalised myoblasts were able to differentiate and form myotubes.

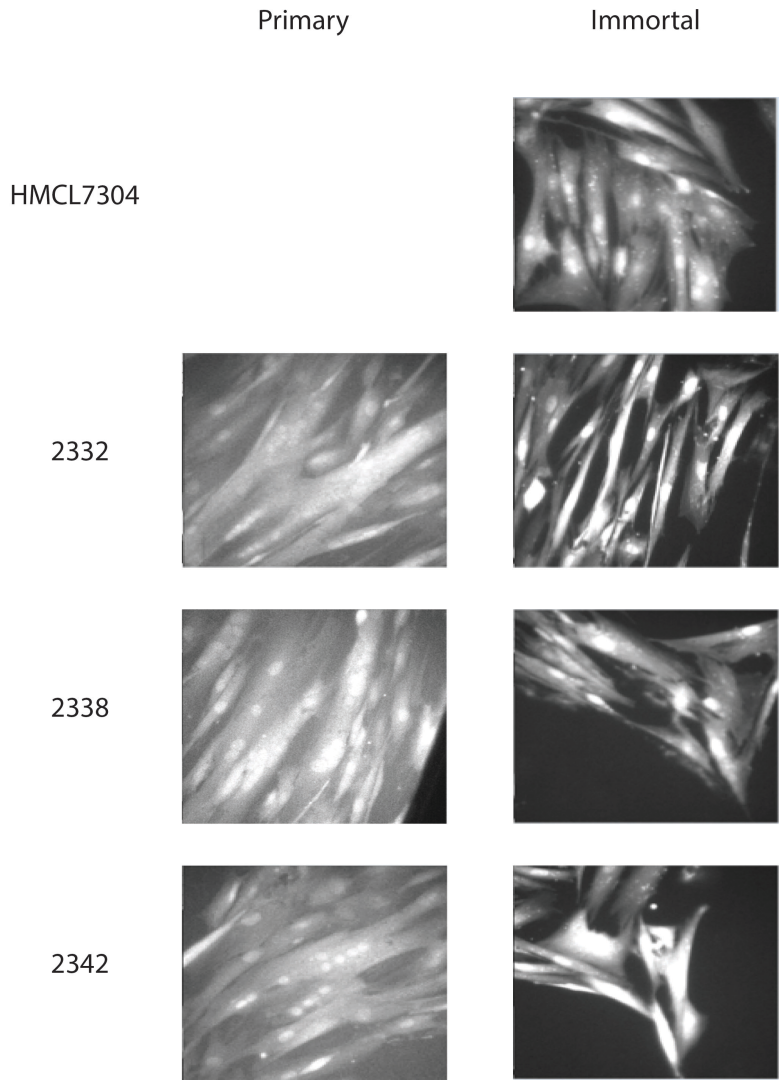

Figure 5.20. Comparison of myotubes produced from primary and immortal cells. Images were taken following the differentiation of myoblasts into myotubes, cells were labelled with 0.5 µM fura 2 AM. The cells were excited at 340 and 380 nm and emission intensity at 510 nm was measured. Presented is the fluorescence emission ratio of 340/380 nm. Cell lines were identified by name, HMCL-7304, or by code number. Cells were visualised using an Olympus IX81 fluorescence microscope at 40 x magnification.

The immortalisation process used is not a true immortalisation, but it drastically extends the life of cells in culture (115). However, the cells may still enter growth arrest if they are subjected to prolonged growth or stress in culture. During the lentiviral immortalisation

process the cells were grown in culture continuously for approximately four weeks. The cells may have aged to an extent that they are no longer able to differentiate to the same extent as the lower passage number primary cells extracted from the same patient.

To determine if both primary and immortal myoblasts had differentiated, the expression of myogenic markers myosin heavy chain, atrogen 1, myostatin and Pax 7 was assessed by reverse quantitative PCR. Myosin heavy chain is a protein within the thick filaments involved in the contraction of skeletal muscle. Atrogen 1 is a protein involved in the atrophy of skeletal muscle. Myostatin is a protein involved in stalling the growth of skeletal muscle. Pax7 is a transcription factor involved in the specification and maintenance of muscle stem cells, the down regulation of expression of Pax7 precedes differentiation of the cells into mature muscle cells. Eleven primer pairs were designed to amplify cDNA produced from myotubes corresponding to these four genes (appendix 3.1) as described in methods section 2.2.13. An initial PCR was performed, and conditions were optimised to produce a single amplicon of the expected size. Single products were produced from the primer pairs myostatin 1, atrogen 1 and myosin heavy chain 1 (appendix 3.5). The PCR could not be optimised for any of the Pax 7 primer pairs. The efficiency of amplification of primer pairs that could amplify a single product of the expected size was determined (Figure 5.21). Primers were also designed to amplify the reference gene acidic ribosomal phosphoprotein P0 (36B4) which is a non-myogenic protein and should be consistently expressed despite the differences in morphology of the two cell lines. Only primer pairs that gave an amplification efficiency of 2 +/- 10 % were used to determine changes in relative gene expression.

Myosin heavy chain 1

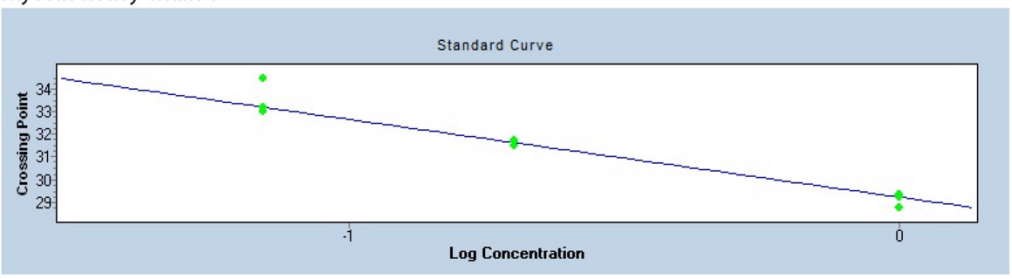

Efficiency 2.129

Atrogen 1

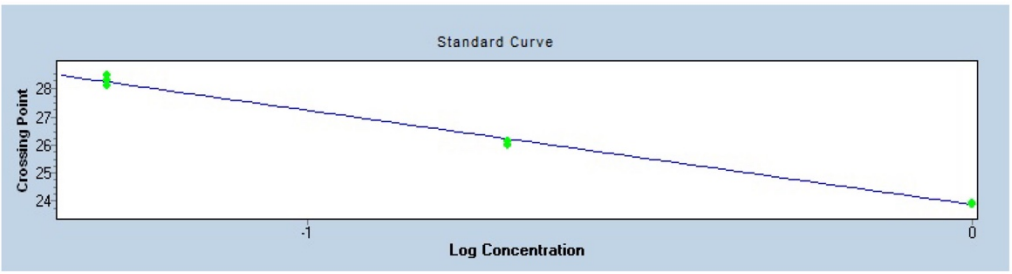

Efficiency 1.973

Myostatin 1

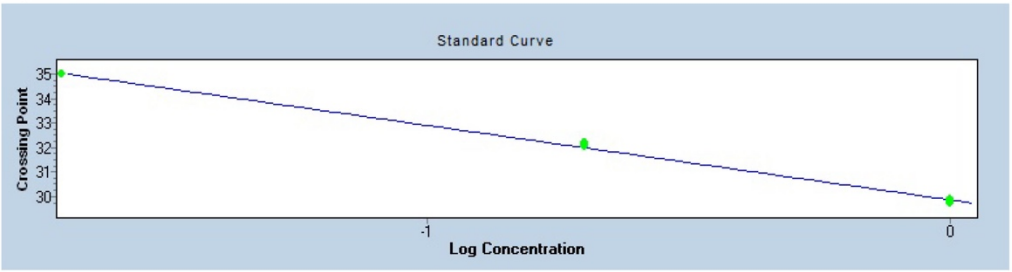

Efficiency 2.114

36B4

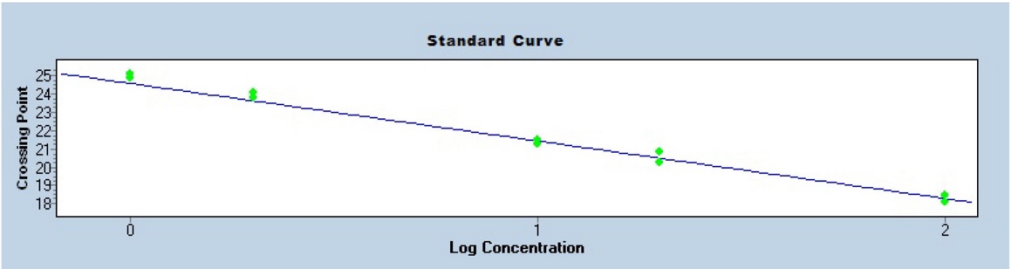

Efficiency 2.093

Figure 5.21. Standard curve depicting the efficiency of amplification of the primer pairs myosin heavy chain 1, atrogen 1, myostatin 1, and 36B4.

Upon formation of myotubes, RNA was extracted from the cells and the relative expression of the genes myostatin, myosin heavy chain and atrogen were assessed compared to the

reference gene 36B4 as summarised in methods section 2.2.13.3. The student's t-test was used to compare the results. It is interesting to note there was a significant increase in the expression of myostatin and atrogen (P value 0.0001 and 0.005 respectively) in the immortal cell line compared to the primary cell line (figure 5.22) but there was no significant change in the expression of myosin heavy chain (P value 0.4391).

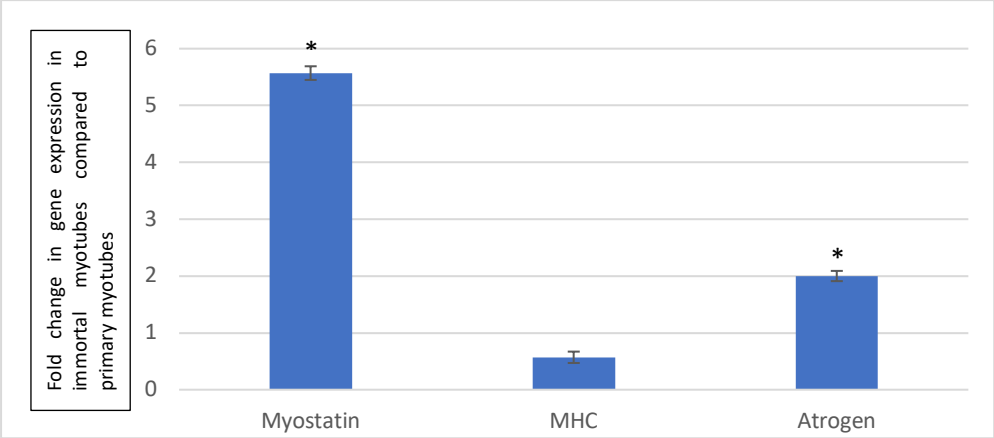

Figure 5.22. Relative gene expression comparing primary and immortal myotubes produced from patient 2342. Cells were grown in Hams F10, 20 % FBS, 4 % pen/strep and differentiated into myotubes using DMEM, 2 % horse serum, 4 % pen/strep. Relative levels of expression for each gene were determined in comparison to the reference gene 36B4. Presented are the results produced from three biological replicates. Error bars are represented by SEM. The two tailed student's t-test was used to compare the results and a P-value <0.05 was considered to be statistically significant. A * refers to results that are significantly different P value >0.05.

The consistent expression of the myosin heavy chain gene is an indication that both the primary and immortal cell lines are able to differentiate into myotubes. However, the increased expression of the myostatin and atrogen genes may explain the smaller size of the immortal myotubes compared to the primary myotubes. The expression of the myostatin gene may cause the cell to stall in growth, preventing the formation of large tube like structures, while the expression of atrogen would cause the cells to decrease in size.

The myosin heavy chain protein is expressed only following the differentiation of myoblasts into myotubes. Therefore, western blotting was carried out in an attempt to confirm expression of myosin heavy chain and therefore the differentiation of myoblasts (figure 5.23 A), appendix 3.3). A western blot was also performed on protein extracted from non-

differentiated myoblasts, to confirm that myosin heavy chain is only expressed following differentiation.

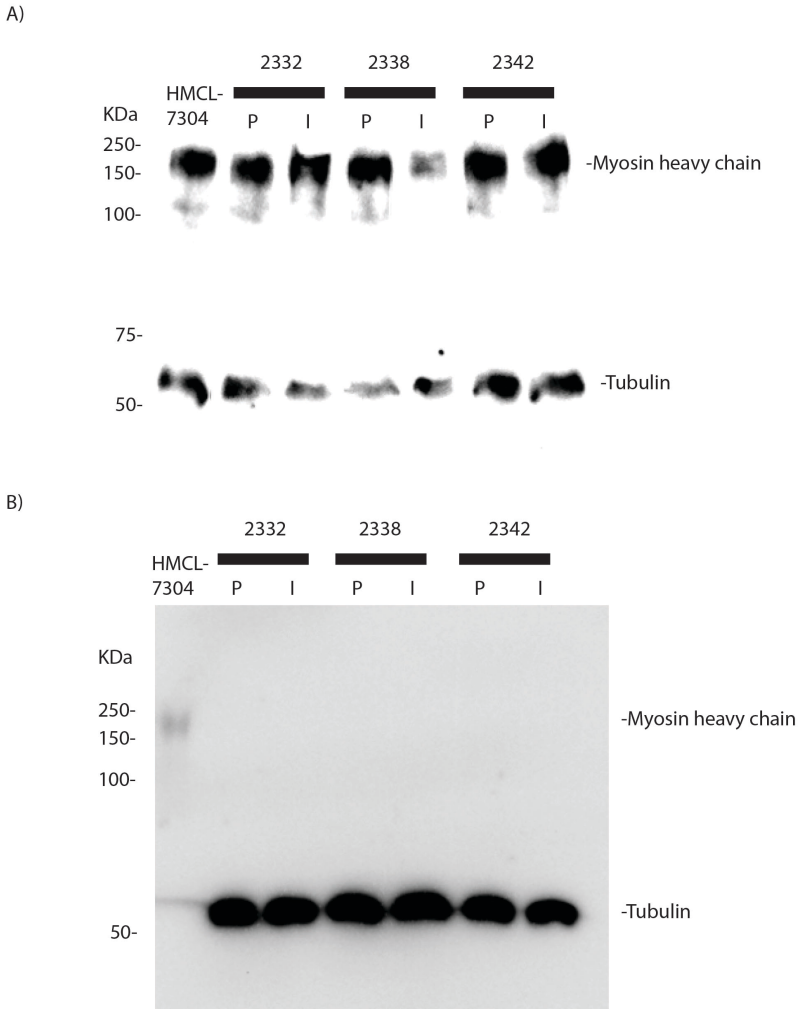

Figure 5.23. Western blot analysis confirming the expression of myosin heavy chain in primary and immortal myotubes. A) Expression of myosin heavy chain in differentiated myotubes. HMCL-7304 refers to protein extracted from differentiated HMCL-7304 cells. B) Expression of myosin heavy chain in myoblasts. HMCL-7304 acts as a positive control for the myosin heavy chain antibody and refers to protein extracted from differentiated HMCL-7304 myotubes. Individual patient samples have been identified by number. P refers to protein extracted from primary cells and I refers to protein extracted from immortal cells. Proteins were separated by 7 % SDS polyacrylamide gel electrophoresis at 120 mV for ninety minutes and transferred to an immobilon membrane at 35 amps for 16 hours. Primary antibodies specific to tubulin and myosin heavy chain were used to detect the protein, a horse radish peroxidase conjugated secondary antibody was used to visualise the proteins.

Despite the differences in morphology noted between primary and immortal myotubes both cell types expressed myosin heavy chain, indicating that the cells had indeed differentiated. The detection of both myosin heavy chain and tubulin was low in both immortal and primary myotubes. The contrast in figure 5.23 A) was adjusted to allow the easy viewing of the bands, and a non-adjusted figure has been presented in appendix 3.4. Due to weak detection of both tubulin and myosin heavy chain the relative expression of the protein could not be determined quantitatively. The detection of tubulin was more noticeable in myoblasts when the same amount of protein was loaded into a gel as noted in figure 5.23 B). Due to time constraints the western blot could not be optimised to obtain a clearer or more consistent figure. No myosin heavy chain was detected in non-differentiated cells supporting the idea that the cells following differentiation the cells had formed myotubes. The protein seems to have been expressed to the same extent in all cell lines, except for immortal cells prepared from patient 2338 where the detection of myosin heavy chain was lower compared to the other cell lines. This may be due to the poor detection of the protein or a loading error. The image in figure 5.23 is a representation of six attempts at performing the western blot, where the detection of both myosin heavy chain and tubulin was low in the case of all differentiated cells. When the expression of tubulin was compared in both differentiated and non-differentiated cells (figure 5.23 B) the amount of tubulin was visibly lower in differentiated cells despite consistent amounts of protein being loaded into each well.

Having demonstrated differentiation of myoblasts into myotubes, the next stage was to compare function. As function can be assessed by measuring Ca^{2+} release via RyR1, it was necessary to show that myotubes expressed RyR1. Therefore, the primary and immortalised cells were fixed in paraformaldehyde and labelled with antibodies against RyR1 and the SR membrane protein, protein disulphide isomerase (PDI) to ensure the correct localisation of RyR1 within the cell (figure 5.24).

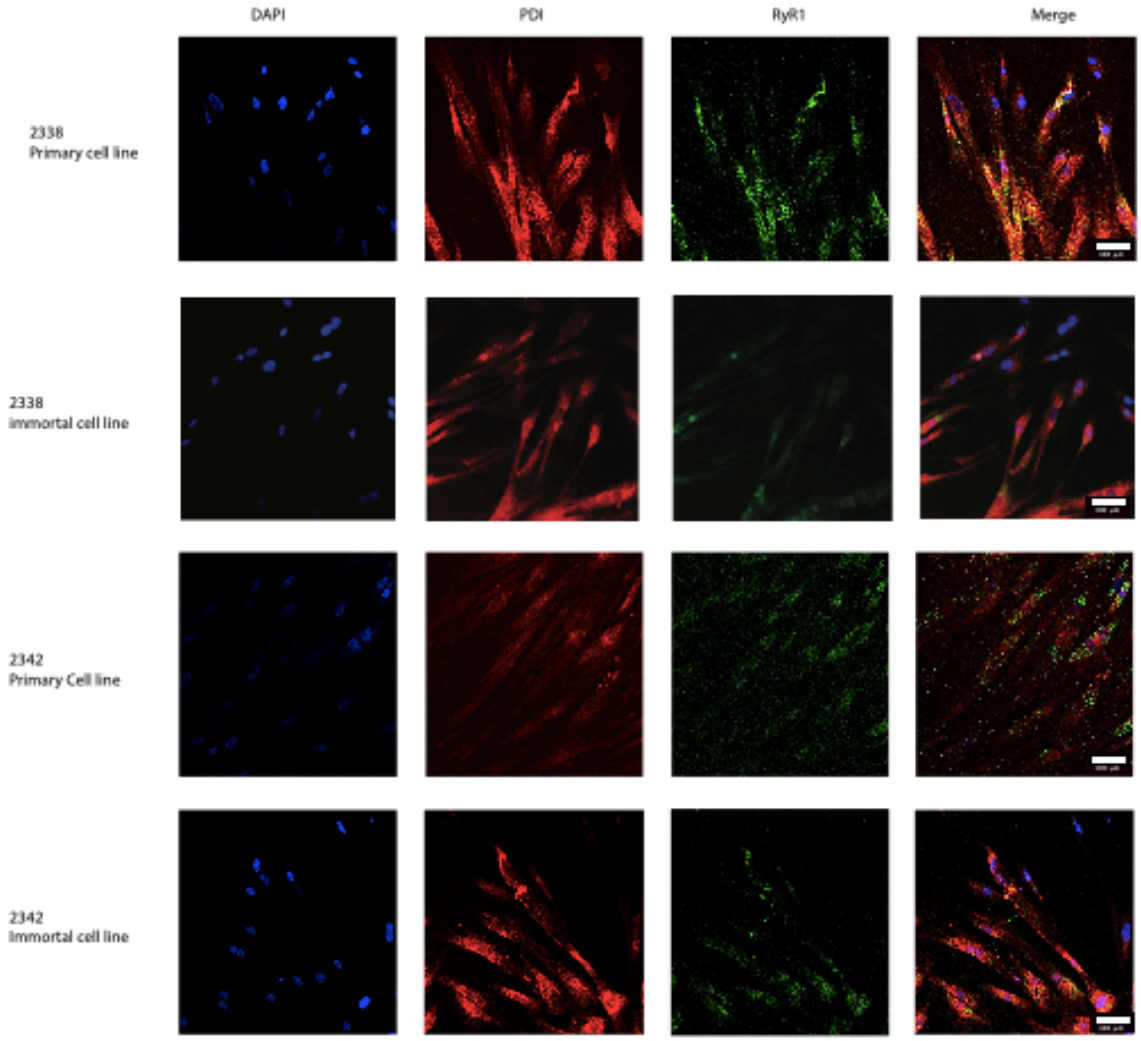

Figure 5.24. Immunofluorescent staining of myotubes confirming the expression of RyR1 in primary and immortal myotubes. Nuclei were stained with DAPI represented in blue. A Trit C conjugated antibody was used to detect PDI represented in red, a Fit C conjugated antibody was used to detect the ryanodine receptor represented in green. Merge shows the overlay of the three images. The size marker represents 50 µm.

Differentiated myotubes, characterised by being branched and multinucleated were identified in both immortal and primary cell cultures and were shown to express RyR1 which colocalised with PDI. Immortalised cell lines once again formed smaller tube structures compared to the primary cells. Some cells did not stain for RyR1, suggesting incomplete differentiation. These cells appeared to be mononucleated and were smaller compared to large branched myotubes.

Western blot analysis was also performed to further ensure the expressed RyR1 was of the correct size and integrity following expression and was expressed in approximately equal amounts in each cell line (figure 5.25). The detection of tubulin was again low, however RyR1 was readily detected.

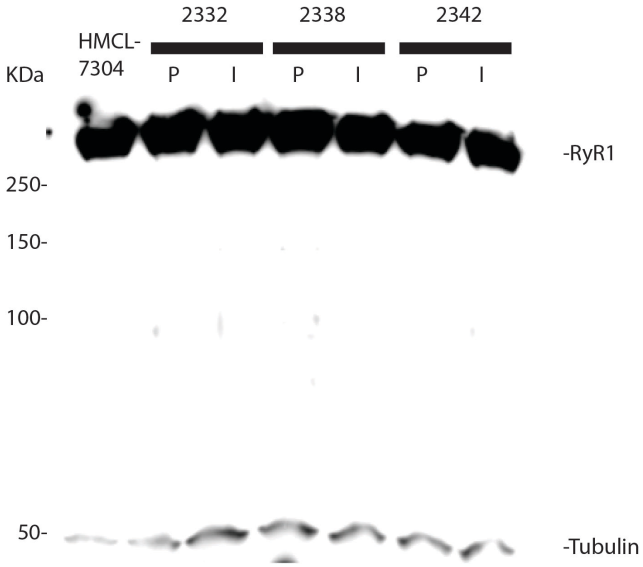

Figure 5.25. Western blot analysis confirming the expression of RyR1 in primary and immortal myotubes. The lane labelled HMCL-7304 refers to protein extracted from HMCL 7304 myotubes. Cells prepared from patients have been identified by number, P refers to primary cells, I refers to immortal cells. Proteins were separated by 7 % SDS polyacrylamide gel electrophoresis at 120 mV for ninety minutes and transferred to an immobilon membrane at 35 amps for 16 hours. Primary antibodies specific to tubulin and RyR1 were used to detect each protein, a horse radish peroxidase conjugated secondary antibody was used to visualise the proteins.

5.2.9 Functional characterisation of immortal myotubes

Having confirmed expression of RyR1 in immortalised myoblasts, Ca^{2+} homeostasis was assessed in, both primary and immortal myotubes using a Ca^{2+} release assay. The cells were labelled with the Ca^{2+} sensitive fluorescent dye fura 2-AM. Once fura 2-AM enters the cell, the acetoxymethyl (AM) group is removed by cellular esterases and the deesterified fura 2 is able to bind Ca^{2+}. Fura 2 can be excited by two separate wavelengths 340 nm and 380 nm both with an emission wavelength of 510 nm. In the Ca^{2+} bound state the emission intensity at 510 nm increases when excited at 340 nm, while the emission intensity decreases when excited at 380 nm. The 340 nm/380 nm ratio is a means of measuring increases in cytosolic

Ca^{2+} concentration that is independent of dye concentration, where a rise in fluorescence at 340 nm will always be accompanied by a decrease in 380 nm. Changes in the fluorescence ratio upon exposure to the RyR1 agonist 4-CmC were monitored and primary cells were compared to their immortal counterparts. The change in fluorescence at each concentration of 4-CmC was expressed as a relative change compared to the maximal change detected at 1200 µM 4-CmC (figure 5.26). The maximum concentration of 1200 µM 4-CmC had been previously determined experimentally (123).

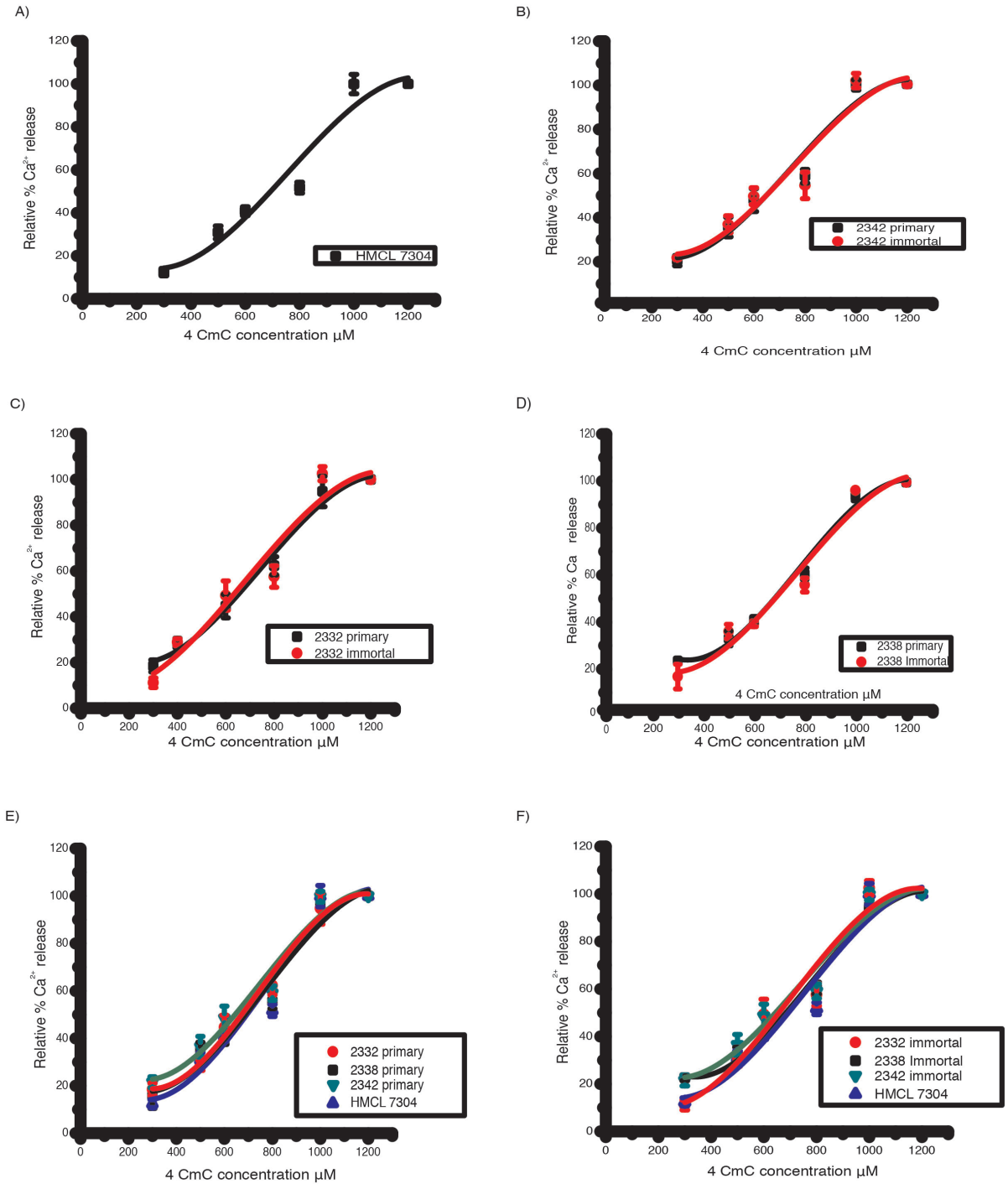

Figure 5.26. Curves showing Ca^{2+} release in primary and immortalised myotubes in response to the RyR1 agonist 4-CmC. A) Ca^{2+} release in the HMCL 7304 cell line. B) Ca^{2+} release in myotubes from patient 2342, the response from primary cells has been represented in black and immortal cell have been represented in red. C) Ca^{2+} release in myotubes from patient 2332. D) Ca^{2+} release in myotubes from patient 2338. E) Ca^{2+} release in all primary cells compared to HMCL 7304. F) Ca^{2+} release in all immortalised cell lines. N=9, error bars represent SEM.

Patient number	EC_{50}	SEM	P. value compared to the HMCL 7304 cell line	P. value comparing primary and immortal cell lines
2342 Primary	642	8.99	0.0935	
2342 Immortal	643	7.72	0.0985	0.9206
2332 Primary	661	6.02	0.2246	
2332 Immortal	633	7.35	0.0586	0.0588
2338 Primary	671	9.03	0.9013	
2338 Immortal	673	9.90	0.7862	0.8606
HMCL 7304	675	11.89		

Table 5.11. EC_{50} values following the Ca^{2+} release assays. Cell lines have been identified by patient number and either primary or immortal. The EC_{50} values for each cell line have been stated along with the SEM. Two P. values have been stated, one compared to the HMCL 7304 cell line, and one comparing primary and immortal cell lines produced from the same patient. A P. value <0.05 was considered to be statistically significant.

There was no significant difference in the Ca^{2+} release characteristics or EC_{50} values between primary and immortal cell lines produced from the same patient (table 5.11) suggesting that despite differences in morphology between immortal and primary myotubes there was no difference in the Ca^{2+} release between the two cell lines. There was also no significant difference in the Ca^{2+} release characteristics between primary and immortal cell lines extracted from different patients. One patient, 2338, previously shown to have central core disease (CCD) had been confirmed to be MHS by *in vitro* contracture test. Screening by next generation screening revealed no variants in *RYR1* or *CACNA1S* (gene encoding the DHPRα_{1s} subunit) or other genes with a potential role in MH susceptibility. No significant difference in EC_{50} values was detected in these cells compared to the MHN cell lines with respect to the specific RyR1 agonist 4-CmC (table 5.11). This suggests that MH susceptibility as assessed by IVCT in this patient results via a mechanism independent of an RyR1 process which therefore cannot be characterised using 4-C*m*C as an agonist. This observation highlights the complexities in both MHS and CCD phenotypes and the non-specific nature of the IVCT, which is a characterisation of skeletal muscle contraction, a multiple step process, in response to halothane and caffeine. Response of myotubes to 4-CmC monitors only a single step in the muscle contraction process, which is the flow of Ca^{2+} across the SR in response to RyR1 opening. Should a variant occur in a protein that does not directly affect this step any potential effect cannot be measured using this system. Nevertheless, these experiments

confirm that RyR1 is functional in response to 4-CmC in immortalised myotubes and there is no significant difference in their response compared to primary myotubes.

5.2.10 Myotube depolarisation

As myotubes are excitable cells, depolarisation can also be used to demonstrate function in immortalised myotubes. Decreasing the Na^+ concentration while simultaneously increasing K^+ concentration in the buffer surrounding the myotubes causes the cell membrane to depolarise. This leads to the activation of the DHPR and the resulting opening of RyR1, with subsequent Ca^{2+} release from the SR. The activation of Ca^{2+} release from the SR in this case is not an RyR1-specific process as other proteins are involved, however, it has been used to characterise RyR1 variants in previous studies (71, 124). It has been previously shown that different variants have different responses to K^+ exposure with some cell lines exhibiting a hypersensitive response to K^+ when compared to WT. Other variants show no effect on the amount of Ca^{2+} released from the SR, however the cells had a prolonged return to resting levels. Different variants may behave differently in response to depolarisation, or the differences in cell function may result from differences in the systems used to characterise variants in other laboratories. The effect of K^+ was tested using patient derived cell lines. Both primary and immortal myoblasts were differentiated into myotubes and labelled with fura 2-AM. Primary myotubes were exposed to [K^+] ranging from 5 mM to 100 mM to determine the maximum concentration of K^+ that will lead to release of Ca^{2+} from the SR. This range was based on results published in previous studies where 60 mM had been shown to elicit a maximal response (71). Consistent with other published work 60 mM K^+ was shown to cause the greatest response while 5 mM was the lowest concentration to have a measurable response (figure 5.27). Only three attempts at establishing a defined concentration gradient of K^+ to release Ca^{2+} from the SR could be performed before the microscope used to monitor changes in fluorescence ceased to function and as a result further work could not be performed. The results presented in figure 5.25 are preliminary and further optimisation would need to be performed at a later date.

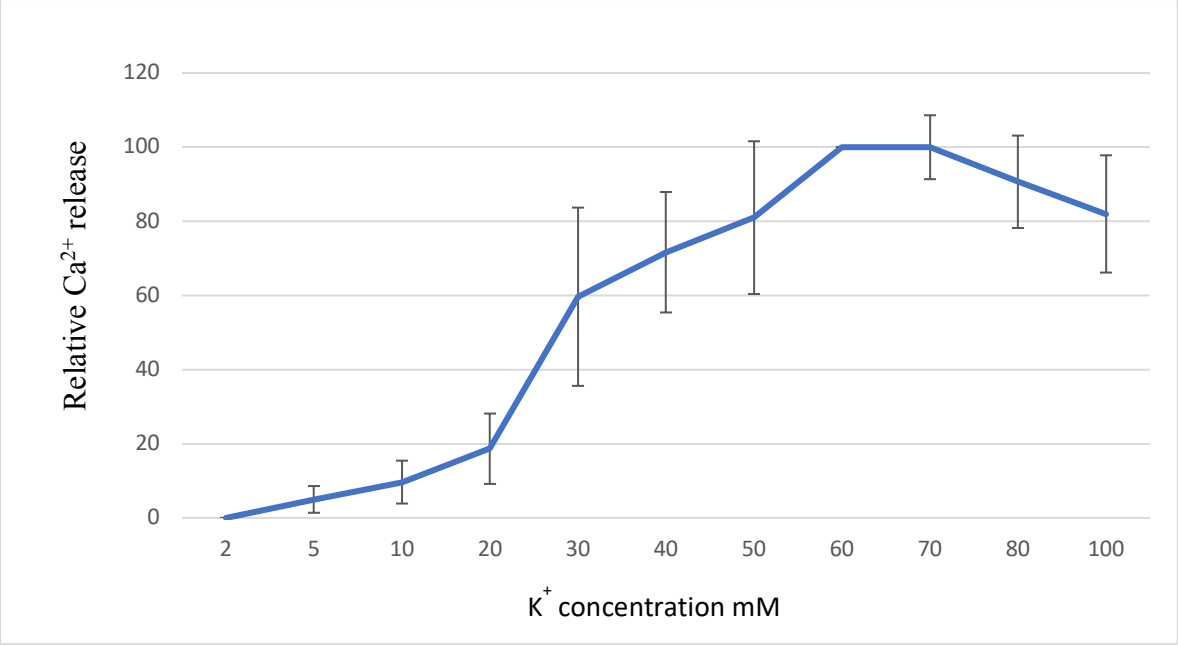

Figure 5.27. Graph depicting the relative Ca^{2+} release from the SR in response to the agonist K^+. The cells used in this experiment were in primary myotubes produced from patient 2338. The presented results are a representation of the Ca^{2+} release assays performed on three technical replicates. Error bars represent SEM.

It is interesting to note that when myotubes were labelled with 1 µM Fura 2-AM at 37 °C for an hour and the cells were exposed to K^+ of any concentration small and defined regions of the cell lost fluorescence (figure 5.28).

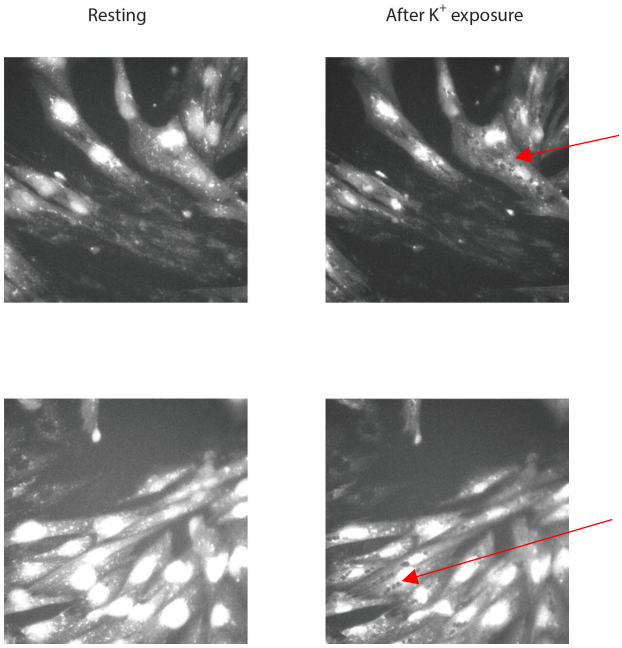

Figure 5.28. Figure depicting HMCL 7304 myotubes before and after exposure to 60 mM KCl. Cells at rest are presented in the left panel and following exposure to KCl on the right. Cells were labelled with 1 µM fura 2 AM and were excited with the wavelengths 340 and 380 nm and emission intensity was measured at 510 nm. Presented is the fluorescence associated with 340/380 nm emission ratio. The characteristic loss of fluorescence has been indicated by red arrows. Cells were visualised using Olympus IX81 fluorescence microscope (40 x magnification).

While it could not be confirmed in the current study, previous studies have shown that following the depolarisation of cells, mitochondria, in response to a high cytosolic Ca^{2+} and K^+ concentrations will actively transport Ca^{2+} from the matrix into the cytosol (125). This is a process that is thought to be involved in the cell's preparation for death. Mitochondria contain esterases and are able to cleave the AM unit from fura 2-AM, and as a result the mitochondria can be readily labelled with the dye. The labelling of the mitochondria could only take place if the cytosol was overloaded with the dye, overwhelming cytosolic esterases. Esterified fura-2 could therefore continue to pass into the mitochondria. Decreasing the concentration of fura 2-AM used to label the cells to 0.5 µM and loading the cells for only 30 minutes at room temperature prevented this phenomenon from being visualised. This suggests the organelle is no longer being labelled with the dye. Should Ca^{2+} be released from the mitochondria in response to K^+ this will still occur, however the localised loss in fluorescence will not have an effect on the fluorescence of the cells and as a result will not affect the data obtained during the assay. Due to an equipment failure in the fluorescence

microscope used to monitor Ca^{2+} release an image was not captured confirming the maintenance of fluorescence using these conditions.

It is very interesting to note that primary myotubes had a very rapid response to K^+. Ca^{2+} homeostasis was altered very quickly and would return to the resting state relatively quickly. Cells immortalised by lentivirus did not respond to K^+ (appendix 3.4.1). This may result from the cells inability to form large myotubes, where proteins required for the release of Ca^{2+} from the SR in response to K^+ may not be expressed. Due to equipment failure this work was unable to be completed.

5.2.11 Caffeine induced Ca^{2+} release

Caffeine is another agonist that can be used to induce Ca^{2+} release from the SR. Like K^+, caffeine is not an RyR1 specific agonist however caffeine is able to form an interaction with RyR1 causing it to favour the open state (9). To determine the maximum caffeine concentrations required to release Ca^{2+} from the SR, primary myotubes were exposed to caffeine concentrations ranging from 0.5 mM – 15 mM, a window of concentrations accepted in other studies to be optimal for Ca^{2+} release (69, 71, 126). Ten mM caffeine was shown to be the minimum concentration required to release maximal Ca^{2+} from the SR, this is consistent with other studies and 0.5 mM caffeine was the lowest concentration to give a measurable response (figure 5.29) (11, 71). Only 4 attempts at establishing a concentration response of caffeine to functionally analyse Ca^{2+} release from the SR could be performed before equipment failure occurred, preventing the further optimisation of this assay. Further work will need to be performed to establish the optimal range of caffeine concentrations required to functionally characterise RyR1 variants.

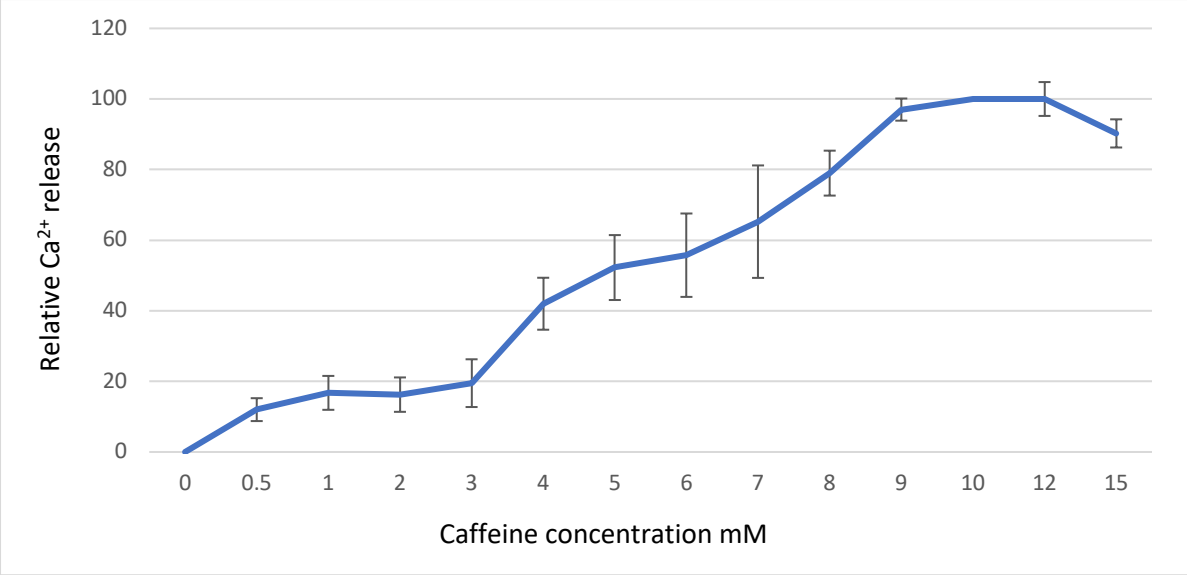

Figure 5.29. Graph depicting the relative Ca^{2+} release from the SR in response to the agonist caffeine. The cells used in this experiment were in primary myotubes produced from patient 2338. The presented results are a representation of the Ca^{2+} release assays performed on four technical replicates, as such error bars were not presented for any data point.

Similar to K^+, it is interesting to note the cells immortalised by lentivirus did not respond to caffeine while the primary cells had a strong and predictable response (appendix 3.4.2). Again, due to equipment failure this work was unable to be completed. Nevertheless, functional analysis of variants should be able to be achieved using 4-CmC as the RyR1 agonist.

The immortalisation process requires the cells to be grown continually in culture for up to 4 weeks first requiring the transduction of cells with a single virus and following selection, transduction with a second virus. While the cells now express human telomerase and CDK4 and will not enter cellular senescence resulting from telomere shortening or cell cycle arrest they are not truly immortal. The cells are still subject to other control mechanisms outside of the expression of hTERT and CDK4 and can still enter arrest resulting from these processes. The extended time the cells were grown in culture prior to performing the Ca^{2+} release assays may be the reason why the immortalised cell lines did not behave as expected during Ca^{2+} release following exposure to K^+ and caffeine. The time taken to immortalise the cells cannot be altered as it is limited to transduction and selection rates. Since the medium the cells are grown in can be altered and may aid in growth and differentiation of myoblasts, some changes were made to the growth conditions as discussed in the next section.

5.2.12 Optimising myoblast growth conditions.

Dexamethasone is a corticosteroid medication which has been shown previously to aid in the growth of myoblasts in culture. It has been accepted that corticosteroids generally induce skeletal muscle atrophy by increasing the rate of protein catabolism and decreasing the rate of protein synthesis. However, growing primary myoblasts in the presence of dexamethasone in culture has been shown to aid in the proliferation and subsequent differentiation of these cells (127). Previous studies have suggested, that in the presence of the drug, myoblasts become more efficient during metabolism, shifting from predominantly anaerobic metabolism to more oxidative methods and following the removal of dexamethasone and FBS from the medium the cells differentiated into larger myotubes compared to cells not exposed to the drug (127, 128). There is evidence to suggest that having dexamethasone in the growth medium is more beneficial in the long term proliferation of myoblasts in culture than simply transducing myoblasts with human telomerase and CDK4 (115). While the expression of these proteins should increase the life span of the cells beyond that of primary cells by preventing the cells from entering senescence, from either telomere shortening or cell cycle arrest, the presence of dexamethasone has been suggested to further encourage cell proliferation.

Exposing myoblasts to dexamethasone for a period of 96 hours prior to differentiation has been previously shown to alter gene expression in the resulting myotubes. The expression of the myogenic marker myosin heavy chain was up regulated, while there was a decrease in the expression of genes linked with atrophy; atrogen, myostatin and pax7 (127). As described previously immortal myoblasts appear to form smaller myotubes than do primary cells and do not release Ca^{2+} in response to either K^{+} or caffeine stimulation. Exposing the immortalised cell lines to dexamethasone prior to differentiation may aid in the formation of larger myotubes making them a more viable cell line for the characterisation of RyR1 variants. This was trialled and expression of myosin heavy chain, atrogen and myostatin was measured to test the cellular response to dexamethasone treatment.

To determine if dexamethasone treatment would increase the efficiency of differentiation in immortal myotubes, conditions previously published were recreated in which primary and immortal myoblasts prepared from patient 2342 were grown in either complete Hams F10 or complete Hams F10 containing 10 µM dexamethasone for 96 hours prior to differentiation (127). The time to differentiate was not noticeably different in the dexamethasone treated cells and there were no obvious differences in the morphology between the treated myotubes and non-treated myotubes (table 5.12, Figure 5.30). However, the increased time to differentiate and the different morphology still occurred between immortal and primary cell lines in the presence of dexamethasone.

Patient ID 2342	Time to differentiate (days)	SEM
Non-treated primary	6	0
Dexamethasone treated primary	6	0
Non-treated immortal	14	0
dexamethasone treated immortal	14	0

Table 5.12. Comparison of time to differentiate in cells treated with and without dexamethasone. N=3.

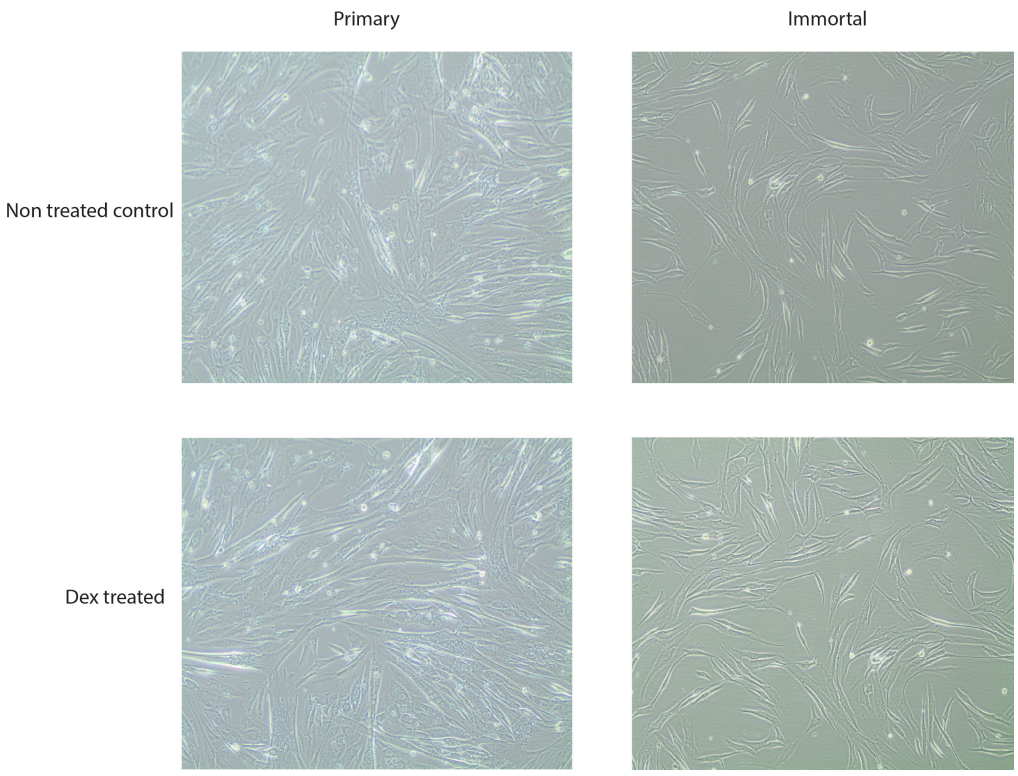

Figure 5.30. Myotube morphology following treatment in dexamethasone. Myoblasts extracted from patient 2342 were in grown medium containing 10 µM dexamethasone for 96 hours prior to differentiation. The non-treated cells were not exposed to dexamethasone. Figures were produced using an Olympus CKX41 microscope using the cell sense standard software (10 x magnification).

Upon formation of myotubes RNA was extracted from the cells and the relative expression of the genes myostatin, myosin heavy chain and atrogen were assessed compared to the reference gene 36B4 summarised in methods section 2.2.13.3. The student's t-test was used to compare the results. There was very little change in gene expression of any of the three genes following exposure to dexamethasone. The primary cells were 10 days old and differentiated very quickly in the presence and absence of dexamethasone. There was no significant difference in the expression of myostatin or myosin heavy chain with P-values of 0.48 and 0.24 respectively. There was, however, a significant decrease in the expression of atrogen in treated cells (P-value 0.0031) (figure 5.31). Dexamethasone had no significant effect on the expression of any of the three genes in immortal myotubes. This differs from previous research which suggests the presence of dexamethasone would have a more significant effect on the expression of these genes, leading to a decrease in their expression

(127). This may have been due to the fact the cells took, in both cases, two weeks to differentiate. During this time any initial effect the drug had on the cells may have been lost.

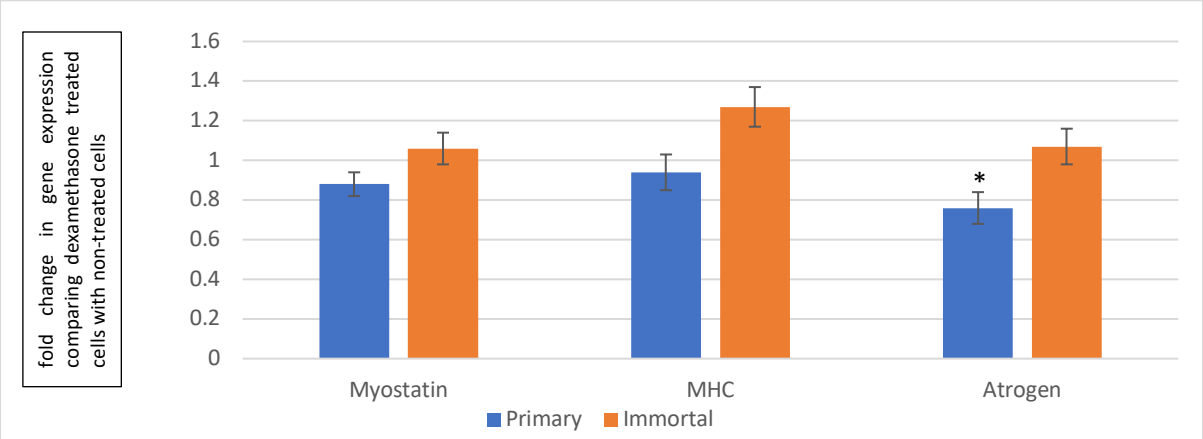

Figure 5.31. Relative gene expression in primary and immortal myotubes produced from patient 2342 comparing dexamethasone treated and untreated cells. The relative change in gene expression in primary cells following treatment is presented in blue and immortal cells in orange. Cells were exposed to 10 µM dexamethasone 96 hours prior to differentiation. Relative levels of expression for each gene were determined in comparison to the reference gene 36B4. Presented are the results produced from three biological replicates. Error bars are represented by SEM. A * refers to results that are significantly different, P value <0.05.

Western blot analysis was performed to monitor any changes in the expression of myosin heavy chain at the protein level following treatment with dexamethasone (figure 5.32). Comparison of expression could only be performed qualitatively due to the low detection of both myosin heavy chain and myosin but, there was no obvious difference in the detection of the protein in the case of dexamethasone treated and non-treated cells which is an indication the treatment of the drug does not have an effect on the translation of myosin heavy chain.

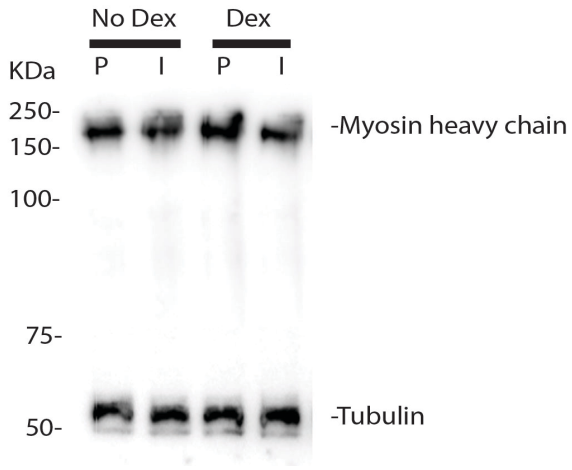

Figure 5.32. Western blot analysis of the expression of myosin heavy chain following the treatment with dexamethasone in cells produced from patient 2342. P refers to primary cells, I refers to immortal cells. Proteins were separated by 7 % SDS polyacrylamide gel electrophoresis at 120 mV for ninety minutes and transferred to an immobilon membrane at 35 amps for 16 hours.

Due to equipment failure, Ca^{2+} homeostasis in response to RyR1 agonists has not yet been assessed in dexamethasone treated cells.

In summary, immortalised myoblasts appeared to have similar properties as the primary myoblasts, but took longer to differentiate and did not respond to K^+ and caffeine. Immortalised myotubes did however, respond to 4-CmC potentially providing a functional assay to assess RyR1 variants in an optimised myotube experimental system. This preliminary work provided a starting point for trialling gene editing to insert a known MH pathogenic variant into an immortalised myoblast cell line isolated from an MHN patient.

5.2.13 CRISPR / Cas 9 modification of immortal myoblasts

A commercially available CRISPR/Cas 9 cDNA and custom designed guide RNAs were purchased from Resolving Images to introduce the c.14497C>T (p. his 4833 tyr) variant into an immortalised patient derived myoblast cell line. Three separate pLENTI Cas 9 vectors were provided, each of which contained a unique guide sequence to direct the Cas 9 nuclease to different positions of the human genome surrounding the nucleotide c.14497C. Three separate guides had been designed to increase the chances of obtaining effective targeting

and digestion. A single stranded DNA repair template containing the c.14497C>T was also purchased from Resolving Images.

To confirm if each guide sequence could lead to Cas 9 digestion of the host genome, immortal myoblasts produced from patient 2342 (MHN myoblasts lacking the familial variant) were nucleofected with each guide vector individually, which would then lead to the expression of Cas 9 along with the guide leading to the digestion of the genome. Nucleofection was selected to introduce the vector into the cells as it was previously shown in section 5.2.5 to lead to a 100 % transfection rate despite being quite harsh for the cell line. The introduction of the vector into the cells is important along with the expression of Cas 9 and guide RNA but integration into the genome is not necessary and unwanted. For this experiment a repair template was not included in the nucleofection mixture, so any cleavage by Cas 9 would be repaired by the non-homologous repair mechanism and an indel should be introduced into the genome if targeting and digestion were successful. Following the nucleofection, the cells were grown to confluence in complete Hams F10 and genomic DNA was extracted from the cells. The T7 endonuclease assay was used to determine if any indels had been created in the genome as described in methods section 2.2.14.3. As T7 endonuclease will digest a heteroduplex, the genomic DNA surrounding the Cas 9 target site was PCR amplified, melted and re-annealed to create heteroduplex DNA fragments (figure 5.33). A T7 digested DNA would suggest that Cas 9 was able to digest the host cell's DNA and the cells non-homologous repair mechanism had been utilised to repair the break. If no digestion was detected it is an indication there is an absence of a heteroduplex and therefore inability of Cas 9 to digest the target site.

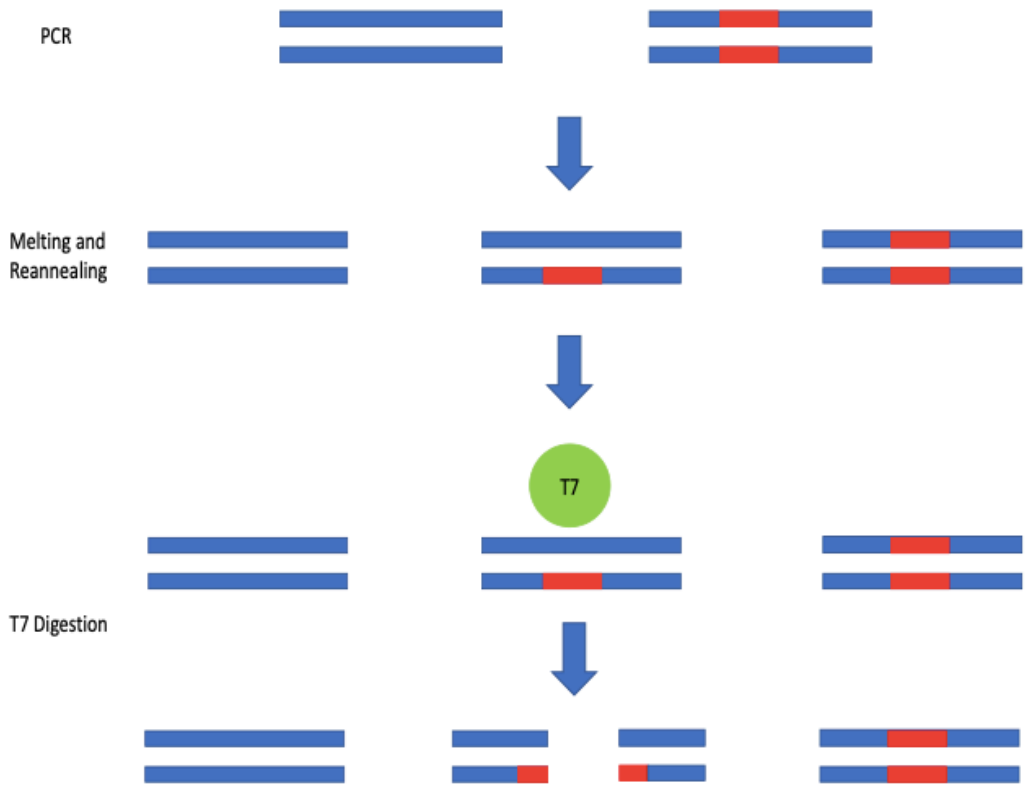

Figure 5.33. Schematic diagram summarising the PCR amplification of genomic DNA, the creation of heteroduplex and the digest of resulting heteroduplex by the T7 endonuclease. Genomic DNA is represented in blue. Red represents an indel.

As a control to ensure the T7 endonuclease was functional, genomic DNA extracted from a patient containing a known heterozygous 14 base pair deletion in *RYR1* was PCR amplified surrounding the deletion. The resulting heteroduplex, after melting and reannealing was also digested with the T7 endonuclease. A PCR product of 672 bp was expected from this control and following the digestion of the heteroduplex bands the size of 672, 550 and 122 base pairs were expected to be seen (figure 5.34). A PCR product free from indels of 668 bp was expected for the cells subjected to Cas 9 digestion. If non-homologous repair had taken place this size was expected to be different as the process is non-specific and the length of the PCR product will depend on how the cells repair the break. In the case of the heteroduplex formed following Cas 9 digestion, two bands were visible prior to digestion, one of the expected size of the non-modified amplicon 668 bp and one close to 800 bp suggesting an insertion may have been introduced. Following the T7 endonuclease digest of the heteroduplex, assuming the non-modified PCR product had annealed to a modified product, three separate bands

were expected to be seen following gel electrophoresis. Non-modified DNA should give bands of 668, 550 and 118 base pairs, in addition to bands of other sizes assuming modification had taken place. The bands of the size 668 and 550 base pairs were visible on the gel however the smaller, 118 bp band, could not be seen due to the low DNA concentration where the DNA could not be visualised on the gel. The band of approximately 800 bp in length was no longer present following the digest being replaced by a weak smear of DNA. This is a strong indication the band represented was a heteroduplex and had been digested. A band of approximately 600 bp was also visible following digestion and may represent a digestion product of this proposed heteroduplex. T7 digest products were visible for all three guide sequences using both myoblasts, with several bands smaller than 550 bp apparent for target 1. A control digestion of non-modified DNA was also performed to confirm that the T7 endonuclease could only digest a heteroduplex. In this case non modified DNA surrounding the CRISPR target site was PCR amplified melted and reannealed and incubated with T7. The band following digestion was weaker which may suggest some digestion took place (figure 5.34 B). The decreased DNA concentration may result from non-specific digestion by T7 endonuclease, variants may have been introduced in the PCR products during amplification which also allowed for the formation of a heteroduplex and ultimately the digestion by T7 endonuclease.

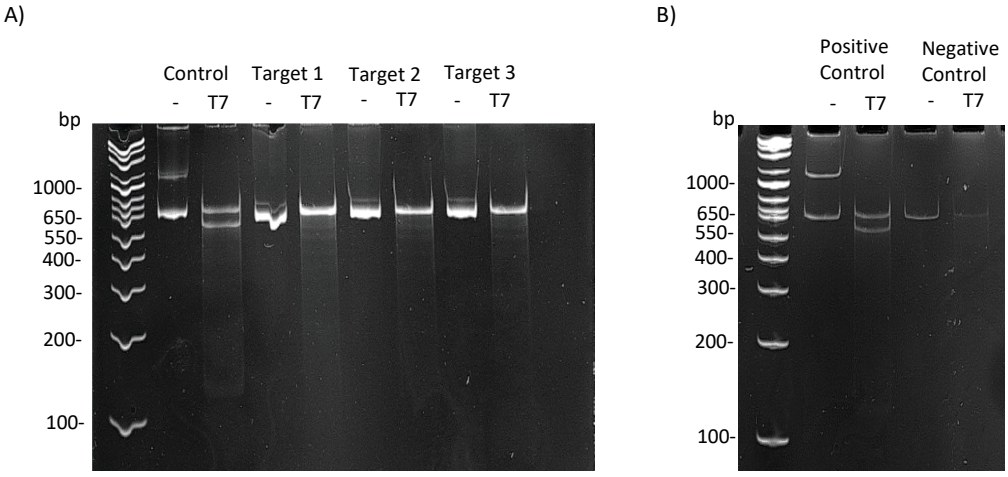

Figure 5.34. T7 endonuclease assay confirming the modification of genomic DNA for each guide sequence. A) T7 digestion of modified DNA. Control, indicates the heteroduplex formed from DNA with a known deletion. The targets for each guide sequence have been identified by number. A – sign indicates a nondigested control, lanes titled T7 indicate the heteroduplex following digestion. B) Control digestion of non-modified DNA. Positive control indicates the heteroduplex formed

from DNA with a known deletion, Negative control indicates non modified DNA. DNA was separated by 10 % acrylamide gel electrophoresis in TAE buffer at 120 mV for one hour and stained in ethidium bromide and visualised under UV light using the Uvitec Uvidoc HD6.

The majority of the DNA visible on the gel corresponded to the band of 668 bp in length suggesting a large proportion of the DNA extracted from the cell culture was in the non-modified state or at least did not form a heteroduplex following the PCR. This suggests a low modification rate in nucleofected cells. This may result from poor efficiency of nucleofection of the vector or inefficient expression of Cas 9 or guide targeting this region of the genome. Nevertheless, the results of this experiment suggest that all three of the guide RNAs target the correct site for modification.

To perform the modification of the host cell genome leading to the site-specific introduction of the c.14497C>T variant, immortal myoblasts prepared from patient 2342 were nucleofected with each Cas 9 guide vector individually along with the single stranded DNA repair template. Cells were regrown to confluence and single cell cultures were then established. Initially cells were suspended in growth medium and dispensed into wells of a 96 well plate at a rate of approximately one cell per three wells in an attempt to obtain single clones. Wells in which a single cell was identified each exhibited a range of growth characteristics. In many cases a colony formed as expected. In some cases, however, a single cell would attach to the plate surface and a colony began to form, but then die following several divisions. In other cases, after several divisions the cells within the colony would spontaneously differentiate; at which time the cells would stop dividing and the colony would no longer continue to grow and would eventually die. Myoblasts seemed to grow best when around other myoblasts and grow particularly well at higher confluence. Being at such a low confluence may have had a severe adverse effect on the cells resulting from lack of specific growth factors secreted by the cells to aid in the formation of colonies. Nevertheless, some clonal growth did occur using this selection method.

Genomic DNA was extracted from each cell culture that was able to grow and populate the whole well. High-resolution amplicon melting (HRM) was used to screen each culture for the

presence of the variant, as described in method section 2.2.14.4. A control wild type and c.14497T heterozygote were included as controls (figure 5.35).

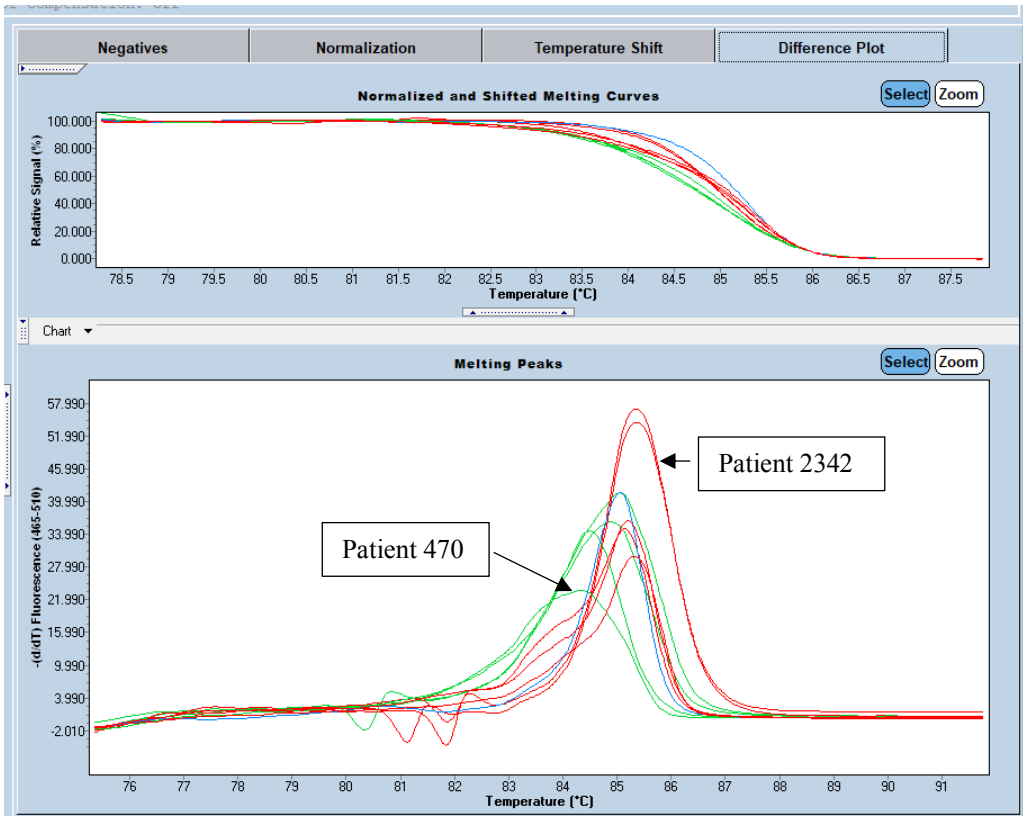

Figure 5.35. Melting curves following high resolution amplicon melting. Curves coloured in red are representative of the non-modified control, patient 2342, or have melting peaks consistent with it. Curves coloured in green are representative of the positive control, patient 470, containing the c.14497 C>T variant or have melting peaks consistent with it. The curve coloured in blue was not grouped with either the negative or positive controls and therefore has different melting properties compared to the two controls.

Approximately 5 % of colonies subjected to screening had melting peaks consistent with the positive control. Several of these cultures had two melting peaks, one consistent with the non-modified control and one that matched the positive control which may result from either a polyclonal culture or one copy of the genome being modified. Some cell samples had a peak that was inconsistent with either control, which may suggest the presence of an indel repaired by the non-homologous repair mechanism.

Sanger sequencing confirmed the presence of the variant in the case of all samples with a melting peak consistent with the positive control. Both the variant and the wild type were identified in the samples with two melting peaks (figure 5.36). Only the variant was detected in the samples with the single peak consistent with the positive control suggesting that either both copies of the genome were modified or allele drop out may have also occurred during the PCR. Allele drop out likely occurred in the case of the positive control (patient 470). This patient is known to be heterozygous for the variant and in this case two peaks would be expected during melt curve analysis. Sanger sequencing also suggested the sole presence of the c.14997C>T variant further supporting this hypothesis. Allele drop out can be caused by a SNP at one or other primer annealing sites or DNA secondary structures in the template. As the assay for the c.14997C>T variant is validated and routinely used successfully for allele discrimination, it is unlikely that either of these reasons account for allele drop-out in this PCR. All cells positively identified as containing the variant were cultured for further growth including those thought to be heterozygous and those thought to be homozygous.

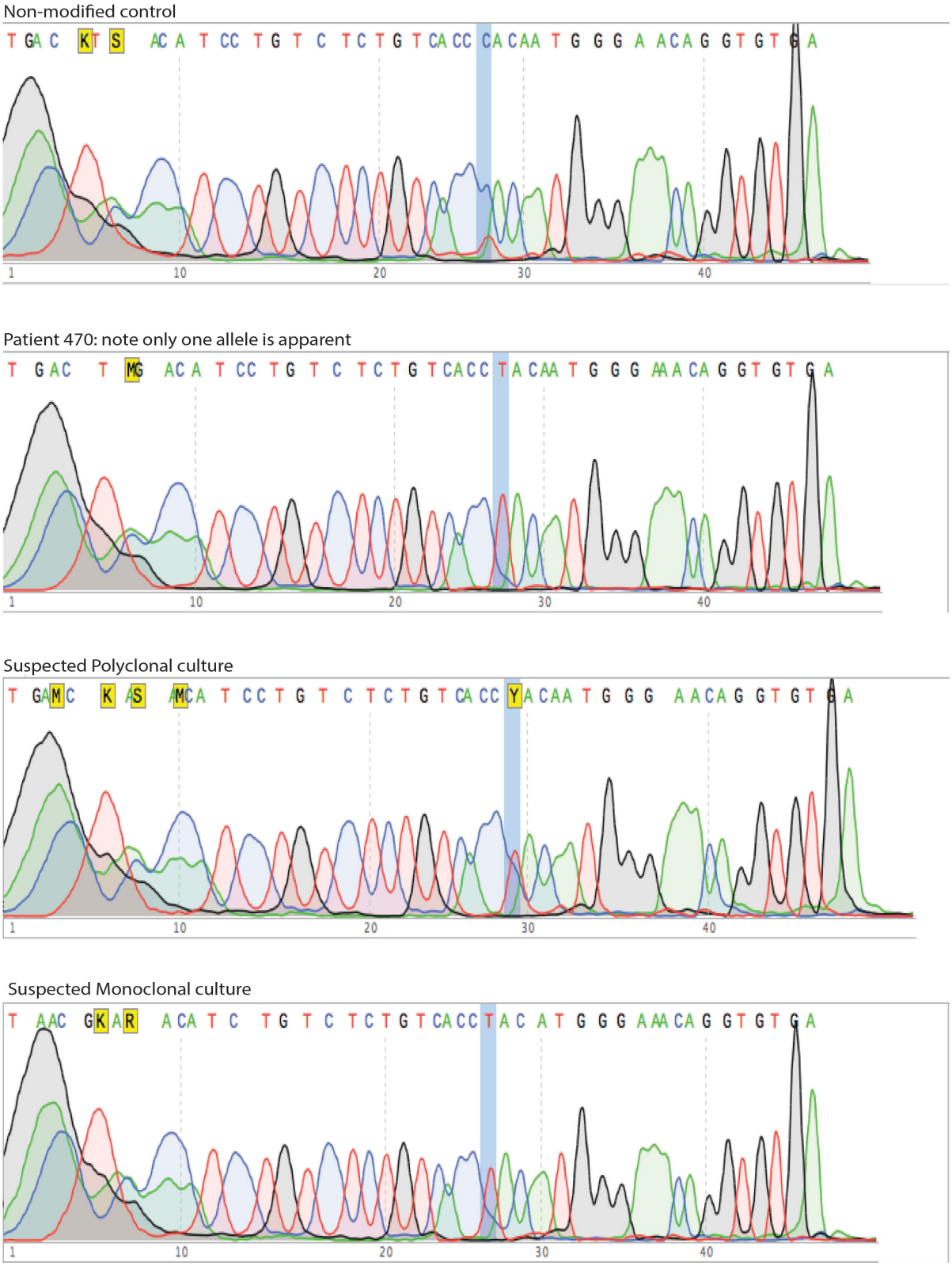

Figure 5.36. Sequencing results confirming the presence of the c.14497 C>T variant in immortal modified myoblasts.

The low efficiency of modification is consistent with the low rate of digestion seen in the T7 assay, suggesting that Cas 9 is unable to efficiently modify the genome in this particular region. For a modification to take place a cell first needed to be nucleofected with the Cas 9 guide vector, both Cas 9 and the RNA needed to be expressed and form the ribonucleoprotein complex along with subsequent cleavage of DNA. The repair template also needed to be present and be utilised to repair the break to ensure homology-directed repair would occur. The repair template was single stranded DNA, which can be degraded by host nucleases. The cells were nucleofected with both the Cas 9 vector containing the guide sequence and the repair template simultaneously, to ensure the repair template was present as soon as the break was created to minimise the formation of indels following nucleofection. As no modification was detected it is more likely that Cas 9 was unable to digest the genome than the repair template being degraded, but the latter cannot be ruled out. In either case, low modification efficiencies are not uncommon and these results suggest successful introduction of a site directed variant (129-131).

Following trypsin treatment of cells for the extraction of DNA for screening none of the cells shown to contain the variant survived the regrowth stage. An aliquot of the cells was separated from the cells destined for DNA extraction and was added to a new well of a 96 well plate and fresh growth medium was added to the well. Either the cells would not attach to the plate surface or the cells would quickly die. Because of this no further analysis could be performed. While evidence of editing was clear, mixed cultures cannot be ruled out. To improve single cell selection, a second method for the growth and selection of single cell colonies was trialled as an alternative. Potentially modified cells were grown on a 10 cm tissue culture dish at a density of approximately 20 cells per dish. Following the formation of colonies, a cloning ring was placed around the colony and the cells were trypsin treated. The cells released from the plate surface were transferred to a well of a six well plate, the cells were re-grown and DNA was extracted from the cells upon reaching confluence. The c.14497C>T variant could not be identified during screening by HRM in cells grown by this method. However, the cells did attach to the surface of the 6 well plate and did repopulate the well quickly and following trypsin treatment for DNA extraction the cell kept for maintenance did survive and behaved as expected. It is therefore possible that editing is deleterious to the myoblasts and only unedited cells can survive.

5.3 Discussion

Myoblasts have been immortalised in previous studies using a retroviral transduction protocol for the introduction of hTERT and CDK4 (114, 115). More recent studies suggest the use of lentivirus (132). The protocols for the transduction in all cases are limited in their description of the process and as such it is unknown if the exact conditions were replicated in this study. Most studies do not make reference to the concentration of viral particles, the number of cells or the duration the cells were exposed to the virus. The rates of transduction observed in this thesis were consistent with the rates transduction rates reported by others (132). Further informal discussions with other researchers it seems the number of cells transduced in the research described in this thesis was a fair representation of a typical transduction.

There was a difference in the morphology of primary and immortal myotubes noted in this research. The myotubes produced had a morphology consistent with the commercially produced and well characterised HMCL 7304 cell line. The HMCL 7304 cell line has been previously shown to form large branched like myotube structures similar to what was noted for the primary myotubes produced in the current study but this could not be replicated (114). The HMCL 7304 cells were a gift from another research group and the exact age of the cells is unknown and it is very likely the cells had undergone a number of doublings in the time between the original image was taken and the images taken for this thesis. The increased age of the cells is a plausible reason for lack of full differentiation.

Due to the low transduction rate the myoblasts were grown in culture for approximately 4 weeks from the time they were extracted from muscle tissue until the time they were immortalised. Adding additional growth time to prepare the myoblasts for differentiation and for the preparation of stocks for long term storage in liquid nitrogen the cells were approximately 6 weeks old by the time analysis could be performed. This is approximately the same time taken for primary myoblasts to enter senescence of 50 days (115). Myoblasts transduced with hTERT and CDK4 have been shown to grow and divide in culture for 110 days,

which should suggest the cells produced in the current research are within their growth window (115). Previously produced immortal myoblasts have been shown to differentiate, and were where shown to express the myogenic markers myosin heavy chain, desmin and pax 7 to the same level as the parental primary mortal myoblast cell line (115), which contradicts the results seen in this thesis. The time to immortalise the myoblasts was not stated in the publication nor the age of the cells prior to differentiation. At the point of differentiation the primary and immortal myoblasts may have been grown in culture for the same amount of time. If this was the case, a difference in gene expression may not be expected as the cells are the same age. The primary and immortal myoblasts produced in this research were 2 and 6 weeks old respectively at the point of differentiation. Any difference in gene expression may result from the difference in age of the cells. However, the immortalisation process may have also had an effect. During the integration of DNA by the lentiviral process, the hTERT and CDK4 cDNA were supposedly incorporated randomly into transcriptionally active regions of the genome. As a result deleterious alterations in gene expression may have occurred that could affect both growth and differentiation. To accurately determine the exact region of the genome in which hTERT and CDK4 incorporated, monoclonal cell lines would need to be established over an extended period for subsequent genome analysis. As shown in the later stages of this chapter during the selection of monoclonal cell lines following CRISPR modification, the establishment of monoclonal cell lines was both difficult and time consuming process. Moreover, most of the cells did not survive. It was therefore not deemed viable to explore the use of monoclonal cultures for identification of integration sites. Transcriptomic analysis has gone on to show no significant change in gene expression between primary and immortal myoblasts (133). However, once again the publication did not indicate specifics about the preparation of the cells for transduction nor the age of the cells prior to differentiation before transcriptomic analysis. Should age matched myoblasts have been used to extract RNA similar patterns of gene expression may be expected, however if the age of the cells were different, as was the case for this thesis, it suggests the methods utilised for myoblast transduction and growth used in this thesis need to be optimised to better represent the protocols used by others.

In an attempt to understand why a change in morphology had occurred after immortalisation, the expression of myogenic markers was compared between primary and immortal

myotubes. There was a significant increase in the relative expression of the genes myostatin and atrogen but no change in the expression of myosin heavy chain. The expression of the protein myosin heavy chain was monitored by western blot analysis however the detection of the protein was poor and relative levels of the protein could not be determined. The levels of the proteins myostatin and atrogen proteins were not monitored, so it cannot be confirmed if the changes in gene expression were reflected at the protein level. However, the changes in gene expression observed are an indication that the cells were undergoing atrophy and this is a potential cause for the decreased size of the immortal myotubes compared to the primary myotubes.

Both primary and immortal myotubes responded in a similar fashion to 4-C*m*C, where the cells released Ca^{2+} from the SR into the cytosol following exposure to the agonist. This suggests the expressed RyR1 is functional in both cell lines. The use of other agonists, on the other hand, was not so clear cut. As expected, primary myotubes responded to both caffeine and K^+, in which Ca^{2+} was released from the SR. However, no measurable change in cytosolic Ca^{2+} was observed in immortal myotubes in response to either caffeine or K^+. The proposed lack of differentiation in immortal myotubes may lead to changes in expression of other genes, including those encoding proteins involved in CICR which ultimately lead to a lack of Ca^{2+} release through RyR1. While no change in cytosolic Ca^{2+} was measured when immortal myotubes were exposed to K^+ it was interesting to note that small and isolated regions of the cells lost fluorescence. Mitochondria will depolarise in the preparation for cell death and while not confirmed, this may have been what occurred (125). Decreasing the concentration of fura-2, loading time and incubation temperature stopped this from being visualised, but cell death may still have been signalled. Fura-2 can only pass through a membrane if it has an AM group, this is removed as the dye enters the cell by cytosolic esterases. The increased concentration of the dye may have overwhelmed the cytosolic esterases and allowed the dye to pass into organelles to include mitochondria. Alternatively, membrane integrity may have been compromised in immortalised myoblasts, allowing the de-esterified dye to readily diffuse into the mitochondria.

Immortalised myotubes, including the HMCL 7304 cell line, have been previously shown to release Ca^{2+} from the SR in response to both caffeine and K^+ (114). However, this could not

be replicated in this thesis research. When the HMCL 7304 cell line was initially characterised, the cells were shown to form large branched structures reminiscent of the primary myotubes reported in this thesis (114). The formation of these large tube-like structures could not be replicated and may be the reason for the lack of response to both agonists.

Previous studies have suggested that exposing the cells to dexamethasone prior to the differentiation of the myoblasts could aid in the differentiation process (127). It has previously been shown that exposure to dexamethasone would lead to a decrease in the expression of the proteins myostatin and atrogen (127). In the research described in this thesis a significant decrease in the expression of atrogen was noted when primary cells were exposed to dexamethasone, but no significant change was noted for myostatin. The primary cells were quite low in passage number, and as such may have had a low expression of the two genes initially, which may have masked the effect of dexamethasone. There was no significant change in gene expression of any gene analysed in the immortal myotubes. As the cells took 14 days to differentiate, any initial effect of the dexamethasone may have been lost. Cells exposed to dexamethasone were not functionally characterised in this study and as a result it is unknown if there was any effect on Ca^{2+} release characteristics. It has been previously suggested that constant exposure to dexamethasone at the myoblast stage is essential for the prolonged growth of myoblasts in culture (115). While it was not trialled in this thesis research, this is something that could be further explored and may aid in the differentiation of the myoblasts or their prolonged growth and viability in culture.

The c.14997C>T variant was successfully introduced into immortalised myoblasts by CRISPR / Cas 9 modification. The presence of the variant was confirmed by HRM and DNA sequencing, following the extraction of DNA from potential monoclonal cultures. Unfortunately, the cell lines that were shown to contain the variant could not be grown to confluence and further characterisation was not possible. Cell senescence may have resulted from the advanced age of the cells, as following immortalisation the cells were approximately 4 weeks old. The further growth of the cells in preparation for Ca^{2+} assays and later CRISPR / Cas 9 modification and single cell selection added a further 15 days of growth. Therefore, it is possible that the cells may have entered replicative senescence due to prolonged growth in culture. During the re-growth of the cells, after DNA extraction, the cells were seeded at low density. Having

insufficient cells in culture could lead to a lack of growth factors being released causing the cells to stall in growth, eventually leading to senescence. If a colony did form, in some cases the cells would begin to differentiate and as such no longer divide. Myoblasts, when in close proximity can self-differentiate despite not being in differentiation media. For this work to be repeated with a better chance of success, optimal growth, proliferation and subsequent differentiation conditions will need to be determined. If possible, methods to speed up the immortalisation process may also be beneficial.

5.4 Chapter summary

Cell lines from three separate individuals were immortalised using a lentiviral transduction system. These cells were transduced with the cDNA encoding the proteins human telomerase and cyclin dependent protein kinase 4. The presence of myoblasts in the cell lines was confirmed by immunofluorescent staining with an antibody specific to the myogenic marker desmin. The activity of the expressed protein human telomerase was indirectly assessed by quantitative PCR of telomere length. The results obtained from the assay indicated that low passage primary cells had slightly longer telomeres compared to immortal cells, however the assay itself is flawed as primer-dimers were likely forming during the assay which would have affected the results. It may have been more efficient and informative to measure the expression of hTERT before and after immortalisation and over a time course of cell proliferation.

Both primary and immortal myoblasts were successfully differentiated into myotubes and were confirmed to express RyR1 by both immunofluorescence and western blot analysis. Primary myotubes formed large, branched structures while immortal myotubes were comparatively smaller and less branched. Immortal myotubes were multinucleated indicating the cells had differentiated at least to some extent. As both primary and immortal cell lines expressed RyR1 they were able to release Ca^{2+} from the SR in response to the RyR1 specific agonist 4-C*m*C. Primary myotubes could respond to the general Ca^{2+} release agonists caffeine

and K^+ although only a few assays could be performed before equipment failure prevented the continuation of this work. Immortal myoblasts on the other hand did not respond to either caffeine or K^+. This may result from the cells not fully differentiating as compared to the primary cell lines leading to a lack of specific protein expression. While it was not confirmed this could include the DHPR subunits or any of the other proteins involved in receiving and transmitting the Ca^{2+} release signal to RyR1. Reverse transcriptase quantitative PCR was used to determine any differences in gene expression between primary and immortal cells of three muscle specific genes, myosin heavy chain, atrogen and myostatin. There was no significant change in the expression of myosin heavy chain. Interestingly immortal cells had an increased expression of the genes myostatin and atrogen. Both of these proteins are associated with atrophy of skeletal muscle cells, which may explain the reduced size of the immortal myotubes.

The drug dexamethasone was trialled to determine its ability to aid in the differentiation of myoblasts however no significant change in differentiation was visualised. The drug did not appear to have any effect on the size of myotubes formed. Primary myoblasts treated with dexamethasone showed a decrease in the expression of the gene atrogen which may indicate that the drug is having a positive effect on the differentiation of the cells. There was no significant change in gene expression in immortal myoblasts treated with dexamethasone. This may result from the cells taking two weeks to differentiate where any effect the drug initially had on the cells may have been lost.

The MH pathogenic variant c.14997C>T was introduced into an immortalised patient-derived cell line using CRISPR / Cas 9 and a specific repair template. HRM was initially used to screen for the variant and its presence was later confirmed using Sanger sequencing. Of the cells shown to contain the variant most were shown to be heterozygous. HRM revealed two peaks for some samples suggesting the presence of the variant on one allele while the other remained unmodified. While it was not confirmed, the presence of polyclonal cultures cannot be ruled out. In some samples, single peaks were evident and may suggest the cells were homozygous where both alleles were modified, or allele drop out had occurred during the PCR and only the variant containing allele had been amplified. The latter was more likely to be the case because the positive control in this experiment appeared homozygous for the

variant. The patient from which the standard DNA sample had been extracted was previously confirmed as being heterozygous for the variant.

In summary, CRISPR/Cas 9 gene editing was shown to be successful however cell viability remains an issue and needs to be explored further and rectified before reattempting CRISPR/Cas 9 gene editing. Given the problems with functional characterisation of the immortalised cell lines, it simply may not be feasible to pursue CRISPR/Cas 9 editing of myoblasts. The primary myoblasts will not survive long enough for CRISPR/Cas 9 editing to be effective and the apparent lack of viability of immortalised cell lines may preclude this method being used for characterisation of *RYR1* variants. While a less physiological system, HEK293 cells expressing *RYR1* variants has proven effective in functional characterisation (60, 102). In the long term, it may be more efficient to focus on streamlining this more established method for any subsequent characterisation of new genetic variants.

6. Future directions

6.1 Recombinant expression of the RyR1 helical domain 1

As $RyR1_{(2091-2708)}$ expressed in this study could not be purified to a level required for crystallography or biochemical assays, no structural or functional characterisation could be performed. The recombinantly expressed $RyR1_{(2091-2708)}$ was not able to be efficiently digested with the protease TEV, separating the MBP and $His_{(6)}$ purification tags from the RyR1 region. The use of a different protease may aid in the improvement of the digestion. This would require recloning the RyR1 region into a new vector containing the same tags with a different protease recognition site. Examples of other proteases include factor Xa, human rhino virus 3C protease or enterokinase (134-136). Alternative solubility or purification tags could also be trialled which may aid in the purification of the recombinant protein, an example of alternative tags and a general purification protocol for each in presented in table 6.1.

Tag	Matrix for enrichment	Elution
Small Ubiquitin-like modifier	Ni-NTA	Imidazole
Galactose binding protein	Galactose	Galactose
Streptavidin	Biotin	Biotin

Table 6.1. Example of solubility and purification tags that could be used to purify recombinant proteins.

At the point of purification, the secondary structure of the protein should be characterised by circular dichroism to ensure the protein is comprised predominantly of alpha helices consistent with the domain within the full-length rabbit RyR1 (9). Crystallisation trials could then be performed providing that sufficient purified protein can be obtained. Initially a general screen could be used (for example those sold by Hampton research (137)). When general conditions of crystallisation are established, a more specific screen could be performed to optimise the process. Crystal formation could be characterised by crush tests and the ability of the crystals to diffract X-rays. The structure of the RyR1 region could then be determined using the Australian synchrotron by interpreting the diffraction pattern after

exposing the crystals to X-rays. Nucleotide variants, both pathogenic and MH-associated, could then be introduced into the expression vector by site directed mutagenesis. The purification and structural characterisation could be replicated for the variant containing protein, however further optimisation may need to be performed for these proteins. Should a structure be determined for both the wild type and variant the structure of each could be compared and the structural alterations caused by the variant could be determined. The crystal structure could also be docked to the previously determined cryo-EM structure of rabbit RyR1 (9). This would be particularly interesting for variant containing structures, as any structural change present in the HD1 could be visualised in the context of the full-length channel, and an explanation for the functional consequence of the variant could be proposed.

The soluble RyR1 region could also be characterised biochemically in a number of ways. The interaction between the recombinantly expressed RyR1 N-terminal domain could be characterised. Pull down assays similar to those described in section 3.3.8 could be repeated with a suitable construct. The ability of the expressed HD1 to interact with calmodulin could also be characterised in a similar manner as the calmodulin cDNA is available in an expression vector. Bio-Layer Interferometry could also be used to characterise the interaction between the HD1 and potential protein interactors (138) by immobilising the RyR1 region on a probe and exposure to a sufficiently purified potential binding partner or ligand. The potential interaction between the two could then be measured. The potential ATP binding characteristics of the region could be characterised, where the purified protein could be exposed to a labelled, non-hydrolysable ATP analogue (139). Analogues are commercially available and have specific light absorption and emission properties when in contact with a protein. Monitoring fluorescence intensity at these specific wavelengths at increasing concentrations of the analogue could provide an insight into function of the domain. The ability of MH-pathogenic variants within the HD1 to affect these biochemical properties could be characterised to provide an insight into the mechanism by which the variant causes MH.

As cryo electron microscopy has been utilised to characterise rabbit RyR1, a similar system could be used to characterise MH pathogenic variants. Due to the high amino acid identity shared between human RyR1 and rabbit or mouse RyR1, CRISPR/Cas9 could be used to introduce MH pathogenic variants into the genome of these organisms creating animal MH

models. These organisms have been previously subjected to CRISPR/Cas 9 modification for the characterisation of genes other then *RYR1* in the context of a whole organism (140-143). The full-length RyR1 could be purified from these organisms and the channel could be structurally characterised in a manner as previously reported for the rabbit RyR1. It must be kept in mind that a number of mice would need to be euthanised to obtain the 100 g of skeletal muscle tissue required to purify RyR1 (9) and as such obtaining ethical approval to do this work may be difficult. As a result, the use of rabbit as a host may be a more viable option. In this case RyR1 could be purified in the presence of protein and ligand modifiers as well as relevant *in vivo* modifications. A system such as this would eliminate any alterations in protein structure that may result from recombinant systems. Knock in mice have been produced containing RyR1 variants (67-69), therefore the process could be followed using muscle extracted from these organisms as a proof of principle.

6.2 Establishing immortal myoblast cell lines

Due to equipment failure in the fluorescence microscope used to analyse Ca^{2+} release in response to agonists, assays could not be completed for either caffeine or K^{+}. To further understand the role these agonists play with respect to RyR1 variants, replacement components need to be installed onto the microscope and the assays would need to be optimised for the new system and software.

The immortalisation of myoblasts using a lentiviral system was chosen as both dividing and non-dividing cells can be infected but it is an inefficient process, requiring the growth of cells in culture for 4 weeks. Utilising a different system may be able to improve the efficiency of the process. Retrovirus is commonly used in other laboratories for this process and may be a useful alternative to trial (114, 116). Retroviral particles can only infect dividing cells, which may be an advantage as non-dividing and senescent cells would be excluded at the infection step. Adenovirus has been successfully used to transduce myoblasts and could also be trialled (144). However, this once again is typically non-integrative and a selectable marker would need to be introduced alongside hTERT and CDK4 to ensure integration. While viral transduction methods are reported to be more efficient for myoblasts, it may also be worth

exploring lipophilic transfection systems including a selectable marker to ensure genome integration (144).

Alternative methods exist for determining telomere length. Probe based assays can also be used, which would first require the extraction of a large amount of DNA from a cell culture (145). The genomic DNA is then digested with restriction endonucleases that have a very high number of recognition sites within the genome. Southern blotting using a labelled probe specific for telomeres could be used to detect the telomeres. This method could provide an insight into the average telomere length within the DNA sample and can be used to directly compare different samples. Being able to monitor telomere length after immortalisation would assist in development of optimal methods for growth and maintenance of immortal cells.

Exposing both primary and immortal cells to 10 µM dexamethasone 96 hours prior to differentiation did not lead to a change in the morphology of the myotubes. Other studies have suggested that growing the cells perpetually in 1 µM dexamethasone is beneficial for the prolonged growth of myoblasts in culture (115). The immortalisation could be repeated with new myoblast cell lines exposing them to the lower dexamethasone concentration, where once again changes in the expression of the genes myostatin, myosin heavy chain and atrogen could also be monitored to compare differentiation in the different cell lines. Different growth medium and/or growth factors could also be trialled to improve differentiation of the myoblasts. A new process has recently been proposed for the differentiation of primary myoblasts [personal communication with Sophie Burling, 2020]. This requires the differentiation of myoblasts in neurobasal-A-based medium which has 14 growth factors / supplements / cytokines more directed at the differentiation of neural cells. The medium was first utilised in the differentiation of myoblasts in an attempt to recognise the relationship between muscle and nerve cells. The differentiation of myoblasts in this medium, free from serum, has resulted in cells that are visibly striated and form organised myofibers. These myofibers can also visibly contract in response to caffeine, which may indicate the cells have reached a level of maturity that will be more suitable for measuring Ca^{2+}-release from the SR in response to depolarisation and 4-C*m*C than as described in chapter 5.

6.3 CRISPR / Cas 9 modification of an immortalised myoblast cell line

CRISPR Cas 9 was trialled in an attempt to streamline the production of specific variants within a physiologically relevant system which could have been used for functional characterisation leading to the expansion of the MH genetic test. Two bottlenecks in the production of modified cells were identified in this study, the first being the overall modification of cells. During the T7 assay it was noted Cas9 was unable to efficiently digest the genome of immortalised myoblasts. The targeting of Cas 9 to the genome is dependent on the guide RNA sequence, therefore trialling different guide sequences may aid in the targeting of the enzyme. Modified Cas 9 enzymes have been reported to increase the modification potential of the enzyme. One such example requires the use of a recombinantly expressed Cas 9 linked to a cytosine deaminase (146). In this case the Cas 9 needs to contain a variant which makes it partially active, so that it is unable to create a double-strand break in the genome, however it can still create a single-strand break. Cytosine nucleotides within the R-loop, created when Cas 9 binds to the opposing DNA strand, can then be subjected to deamination creating uracil. To avoid the back conversion of the uracil to cytosine the Cas 9 enzyme also needs to be linked to a uracil glycosylase inhibitor. The selective nicking of the non-modified strand by Cas 9 will bias the repair mechanism towards the production of the A - T variant (147). The use of this process is unique in that it can only be used to create a C - T variant, however no repair template is required. A C - T variant was desired in this study and as such the system could be trialled to produce the his 4833 tyr variant. A drawback of this system is that it will be impossible to control which cytosine residues within the R-loop will be subjected to modification. The c.14997C residue subjected to modification in this study is proceeded by two other cytosine residues, and there are two others in close proximity and as such other, non-desired, variants are likely to be introduced. However other *RYR1* variants may be more suited for this approach.

The second bottle neck was the selection of modified cells over non-modified cells which was a very time consuming and inefficient process. It was difficult to keep the myoblasts alive following passage for screening. Alternative modification methods have recently been

implemented to make the selection process more efficient. For example, long repair templates have been used to introduce selection markers like green fluorescent protein into the genome alongside the variant or to knock out a gene (148, 149). The c.14497C residue is in close proximity to a splice site in the genomic DNA. The long repair template could introduce the GFP or an antibiotic selection marker cDNA into the myoblast genome within the intron under control of its own promoter. As long as the splice sites are maintained the selectable marker should not be introduced into the RyR1 coding region. Modified cells could then be selected as the selection marker should be expressed at the myoblast stage, before RyR1 is expressed. After confirming the variant has been introduced into the genome, the cells could be differentiated into myotubes at which stage the mRNA of the selectable marker would be spliced out. Just because cells express the selectable marker does not necessarily mean the cells have been modified, however this method would markedly reduce the number of cells to screen.

Off target effects of the CRISPR modification will also need to be taken into account. Potential alternative targets for the Cas 9 and guide can be predicted and these regions can be sequenced, however whole genome sequencing would be a more accurate method for determining whether off-target effects have occurred (150-152). In both cases the DNA sequence from both non-modified and modified cells would need to be compared.

Following the incorporation of the c.14997C>T variant into the genome of the myoblasts the cell line and the incorporated variant would need to be characterised in comparison to the non-modified cell line to determine whether the variant has an effect on Ca^{2+} homeostasis. This could be performed using the upgraded fluorescence microscope following optimisation of the process. Alternative methods including electrophysiology could also be trialled, in which single channel studies or whole cell patch clamp could be utilised where RyR1 is characterised either following purification from a cell or within a cell respectively. Protocols for both methods have been established and have been used to successfully characterise the flow of Ca^{2+} ions across the SR which can be translated into RyR1 function (73, 74). Should the myotubes display a functional alteration consistent with a pathogenic variant, it would confirm that CRISPR/Cas 9 is a viable method in the characterisation of MH-linked variants. At this point previously uncharacterised variants could be introduced into a patient derived

myoblast cell line and functionally characterised by this method, increasing the number of RYR1 variants available for genetic screening to determine MH-susceptibility. The ability to use CRISPR/Cas 9 to change a causative variant back to wild type would also be extremely useful. Functional analysis showing normal responses to agonists of such an edited myotube would provide proof that a single RyR1 variant is both necessary and sufficient to result in MH-susceptibility. Such a result would pave the way towards acceptance of using DNA based tests to predict an MHN phenotype, without needing a muscle biopsy. This would drastically improve diagnosis of MH-susceptibility, a major aim of much MH research in the foreseeable future.

7. Concluding remarks

The RyR1 HD1 corresponding to the amino acids 2091-2708 was recombinantly expressed in an *E. coli* host. The protein was shown to be soluble and could be partially purified from the cell lysate exploiting the maltose binding protein purification tag. However, further separation techniques failed to purify the protein to a level required for crystallisation trials. As a result, MH pathogenic variants could not be structurally characterised. Because of this the variants were characterised *in situ*, using the full-length rabbit RyR1 structurally determined by cryo electron microscopy. Many of the pathogenic variants resulted in a change in the side chain chemistry of the amino acid, and many also resulted in structural hinderance both of which have the potential to lead to a structural alteration in the local region of RyR1 and as a result may go on to cause MH in these susceptible patients.

Primary myoblasts extracted from three separate patients were immortalised using lentiviral transduction for the cDNA encoding the proteins hTERT and CDK4. Both immortal and primary myoblasts were differentiated where it was shown that immortalised cells adopt a different morphology compared to the primary cells and also took a significantly longer time to differentiate. Both cells express the myogenic proteins myosin heavy chain and RyR1, indicating that both cell lines had differentiated. When functionally characterised both primary and immortal cell lines responded to the RyR1 agonist 4-C*m*C and had an indistinguishable response to the agonist. However only primary cells could respond to K^+ or caffeine, both of which are not specific for RyR1. The reason for this lack of response has yet to be determined. Changes in gene expression of myogenic proteins was also compared between primary and immortalised cell lines where immortal cells had an increased expression of the atrophy markers atrogen and myostatin, potentially explaining the different morphology of the cells.

CRISPR/Cas9 was used to introduce the MH pathogenic *RYR1* variant c.14977C>T into an immortal myoblast cell line for subsequent functional characterisation as a positive control. Cells lines were screened by high resolution amplicon melting for introduction of the variant

and then confirmed by Sanger sequencing. Cell lines shown to contain the variant did not survive the selection process and as a result further functional characterisation of the introduced variant could not be performed. Nevertheless, this proof of principle study suggests that CRISPR/Cas 9 can be used to edit patient-derived myoblasts and provide a starting point for optimisation of the system.

8. Reference list

1. P. M. Hopkins, *et al.* European malignant hyperthermia group guidelines for investigation of malignant hyperthermia susceptibility. *British Journal of Anaesthesia* **115**, 531-539 (2015).
2. N. Pollock, E. Langton, K. Stowell, C. Simpson, N. McDonnell. Safe duration of postoperative monitoring for malignant hyperthermia susceptible patients. *Anaesthesia and Intensive Care* **32**, 502-509 (2004).
3. H. Rosenberg, N. Pollock, A. Schiemann, T. Bulger, K. Stowell, Malignant hyperthermia: a review. *Orphanet Journal of Rare Diseases* **10** (2015).
4. Anonymous. Diagnostic mutations. Retreived from https://www.emhg.org /diagnostic-mutations (2020).
5. Anonymous. Histology of muscle. Retreived from http://faculty.etsu.edu/. (2020)
6. R. Araya, *et al.* Dihydropyridine Receptors as Voltage Sensors for a Depolarization-evoked, IP3R-mediated, Slow Calcium Signal in Skeletal Muscle Cells. *The Journal of General Physiology* **121** (2003).
7. K. Jurkatprott, T. McCarthy, F. Lehmannphorn. Genetics and pathogenesis of malignant hyperthermia. *Muscle and Nerve* **23**, 4-17 (2000).
8. V. Sorrentino, P. Pompeo. Ryanodine receptors: how many, where and why? *Trends in Biochemical Sciences* **14** 98-103 (1993).
9. A. Georges *et al.* Structural basis for gating and activation of RyR1. *Cell* **167**, 145-157 (2016).
10. K. Sato, N. Pollock, K. Stowell. Functional studies of *RYR1* mutations in the skeletal muscle ryanodine receptor using human *RYR1* complementary DNA. *Anesthesiology* **112**, 1350-1354 (2010).
11. A. Merritt, *et al.* Assessing the pathogenicity of *RYR1* variants in malignant hyperthermia. *British Journal of Anaesthesia* **4**, 533-543 (2017).
12. R. Robinson, D. Carpenter, M. Shaw, J. Halsall, P. Hopkins. Mutations in *RYR1* in malignant hyperthermia and central core disease. *Human Mutation* **27**, 977-989 (2006).
13. K. N. Northab, *et al.* Approach to the diagnosis of congenital myopathies. . *Neuromuscular Disorders* **24**, 3193-3204 (2004).
14. R. Brislin, M. Theroux. Core myopathies and malignant hyperthermia susceptibility: a review. *Paediatric Anaesthsia* **23**, 834-841 (2013).
15. N. Monnier, *et al.* Null mutations causing depletion of the type 1 ryanodine receptor *RYR1* are commonly associated with recessive structural congenital myopathies with cores. *Human Mutation* **29**, 670-678 (2008).
16. H. Zhou, *et al.* Epigenetic allele silencing unveils recessive *RYR1* mutations in core myopathies. *The American Journal of Human Genetics* **79**, 859-868 (2006).
17. Y. Cui, *et al.* A dihydropyridine receptor α1s loop region critical for skeletal muscle contraction is intrinsically unstructured and binds to a SPRY domain of the type 1 ryanodine receptor. *The International Journal of Biochemistry & Cell Biology* **41**, 677-686 (2009).

18. R. Weiss, *et al.* Functional analysis of the R1086H malignant hyperthermia mutation in the DHPR reveals an unexpected influence of the III-IV loop on skeletal muscle EC coupling. *American Journal of Physiology* **287**, 1094-1102 (2004).
19. J. Eltit, *et al.* Malignant hyperthermia susceptibility arising from altered resting coupling between the skeletal muscle L-type Ca^{2+} channel and the type 1 ryanodine receptor. *Proceedings of the National Academy of Sciences of the United States of America* **109**, 7923-7928 (2012).
20. A. Polster, S. Perni, H. Bichraoui, K. Beam. Stac adaptor proteins regulate trafficking and function of muscle and neuronal L-type Ca^{2+} channels. *Proceedings of the National Academy of Sciences of the United States of America* **112**, 602-606 (2015).
21. E. J. Horstick, *et al.* Stac3 is a component of the excitation–contraction coupling machinery and mutated in Native American myopathy. *Nature Communications* **4** (2013).
22. J. Linsley, *et al.* Congenital myopathy results from misregulation of a muscle Ca^{2+} channel by mutant Stac3. *Proceedings of the National Academy of Sciences of the United States of America* **114**, 228-236 (2016).
23. W. Chen, *et al.* Reduced threshold for store overload-induced Ca^{2+} release is a common defect of RyR1 mutations associated with malignant hyperthermia and central core disease. *Biochemical Journal* **474**, 2749-2761 (2017).
24. M. Porta, *et al.* Coupled gating of skeletal muscle ryanodine receptors is modulated by Ca^{2+}, Mg^{2+}, and ATP. *American Journal of Phsiology* **303**, 682-697 (2012).
25. D. Laver, T. Baynes, A. Dulhunty. Magnesium Inhibition of Ryanodine-Receptor Calcium Channels: Evidence for Two Independent Mechanisms. *The Journal of Membrane Biology* **156**, 213-229 (1997).
26. O. Popova, M. Baker, T. Tran, T. Le, I. Serysheva. Identification of ATP-binding regions in the RyR1 Ca^{2+} release channel. *Public Library of Science* **7**, 48725 (2012).
27. S. Qi-An *et al.* Oxygen-coupled redox regulation of the skeletal muscle ryanodine receptor-Ca^{2+} release channel by NADPH oxidase 4. *Proceedings of the National Academy of Sciences of the United States of America* **108**, 16098-161103 (2011).
28. R. Chaube, *et al.* Regulation of the skeletal muscle ryanodine receptor/Ca^{2+}-release channel RyR1 by S-palmitoylation. *Journal of Biological Chemistry* **289**, 8612-8619 (2014).
29. P. Aracena, G. Sánchez, P. Donoso, S. Hamilton, C. Hidalgo. S-Glutathionylation Decreases Mg2+ Inhibition and S-Nitrosylation Enhances Ca^{2+} Activation of RyR1 Channels. *Journal of Biological Chemistry* **278**, 42927-42935 (2003).
30. P. Aracena-Parks, *et al.* Identification of cysteines involved in S-nitrosylation, S-glutathionylation, and oxidation to disulfides in ryanodine receptor type 1. *Journal of Biological Chemistry* **281**, 40354-40368 (2006).
31. T. Oda, *et al.* Oxidation of ryanodine receptor (RyR) and calmodulin enhance Ca release and pathologically alter, RyR structure and calmodulin affinity. *Journal of Molecular and Cellular Cardiology* **85** (2015).
32. C. Moore, J. Zhang, S. Hamilton. A Role for Cysteine 3635 of RyR1 in Redox Modulation and Calmodulin Binding. *Journal of Biological Chemistry* **274**, 36831-36834 (1999).
33. J. Zhang, *et al.* Oxidation of the skeletal muscle Ca^{2+} release channel alters calmodulin binding. *American Journal of Physiology* **276**, 46-53 (1999).

34. Z. Yuchi, *et al.* Crystal structures of ryanodine receptor SPRY1 and tandem-repeat domains reveal a critical FKBP12 binding determinant. *Nature Communications* **6** (2015).
35. S. Reiken, *et al.* PKA phosphorylation activates the calcium release channel (ryanodine receptor) in skeletal muscle. *Journal of Cell Biology* **160**, 919-928. (2003).
36. J. Suko *et al.* Phosphorylation of serine 2843 in ryanodine receptor-calcium release channel of skeletal muscle by cAMP-, cGMP- and CaM-dependent protein kinase. *Biochimica et Biophysica Acta (BBA) - Molecular Cell Research* **1175**, 193-206 (1993).
37. D. Gong, *et al.* Modulation of cardiac ryanodine receptor 2 by calmodulin. *Nature* **572**, 347-351 (2019).
38. L. Xu, A. Gomez, D. Pasek, G. Meissner, N. Yamaguchi. Two EF-hand motifs in ryanodine receptor calcium release channels contribute to isoform-specific regulation by calmodulin. *Cell Calcium* **66**, 62-70 (2017).
39. D. MacLennan, W. Chen. Store overload-induced Ca^{2+} release as a triggering mechanism for CPVT and MH episodes caused by mutations in RYR and CASQ genes. *The Journal of Physiology* **587**, 3113-3115 (2009).
40. E. Sanchez, *et al.* Phosphorylation of human calsequestrin: implications for calcium regulation. *Molecular and Cellular Biochemistry* **353** (2011).
41. K. Lewis, L. Ronish, E. Rios, C. Kang. Characterization of two human skeletal calsequestrin mutants implicated in malignant hyperthermia and vacuolar aggregate myopathy. *Journal of Biological Chemistry* **290**, 28665-28674 (2015).
42. M. Dainese, *et al.* Anesthetic-and heat-induced sudden death in calsequestrin-1-knockout mice. *Federation of American Societies for Experimental Biology* **23**, 1710-1720 (2009).
43. L. Wei, E. Gallant, A. Dulhunty, N. Beard. Junctin and triadin each activate skeletal ryanodine receptors but junctin alone mediates functional interactions with calsequestrin. *The International Journal of Biochemistry & Cell Biology* **41**, 2214-2224 (2009).
44. J. Lee, *et al.* Negatively charged amino acids within the intraluminal loop of ryanodine receptor are involved in the interaction with triadin. *Journal of Biological Chemistry* **279**, 6994-7000 (2003).
45. G. Avila, J. O'Brien, R. Dirksen. Excitation–contraction uncoupling by a human central core disease mutation in the ryanodine receptor. *Proceedings of the National Academy of Sciences of the United States of America* **98**, 4215-4220 (2001).
46. N. Beard, *et al.* Phosphorylation of skeletal muscle calsequestrin enhances its Ca^{2+} binding capacity and promotes its association with junctin. *Cell Calcium* **44**, 363-373 (2008).
47. Y. Wang, *et al.* Altered stored calcium release in skeletal myotubes deficient of triadin and junctin. *Cell Calcium* **45**, 29-37 (2009).
48. J. D. Fessenden, W. Feng, I. N. Pessah, P. D. Allen. Amino Acid Residues Gln4020 and Lys4021 of the Ryanodine Receptor Type 1 Are Required for Activation by 4-Chloro-m-cresol. *Journal of biological chemistry* **281**, 21022-21031 (2006).
49. T. AnhTa, I. Pessah, T. Yang, P. Allen. Functional defects in six ryanodine receptor isoform-1 (RyR1) mutations associated with malignant hyperthermia and their impact on skeletal excitation-contraction coupling. *Journal of Biological Chemistry* **278**, 25722-25730 (2003).

50. T. Murayama, *et al.*, Genotype–phenotype correlations of malignant hyperthermia and central core disease mutations in the central region of the RyR1 channel. *Human Mutation* **37**, 1231-1241 (2016).
51. V. Sorrentino, P. Volpe. Ryanodine receptors: how many, where and why? . *Trends in Pharmacological Sciences* **14**, 98-103 (1993).
52. M. Cacheux, *et al.* Interplay between Triadin and Calsequestrin in the Pathogenesis of CPVT in the Mouse. *Molecular Therapy* **28**, 171-179 (2020).
53. K. Kujala, *et al.* Cell Model of Catecholaminergic Polymorphic Ventricular Tachycardia Reveals Early and Delayed Afterdepolarizations. *Public Library of Science One* **7** (2012).
54. X. Xu, *et al.* Decreased affinity of calmodulin binding to RyR2 may cause leaky channel in CPVT-associated mutation: insight from RyR2 R2474s/+ knock-In mouse model. *Circulation* **118** (2008).
55. D. Jiang, *et al.* Enhanced store overload–induced Ca^{2+} release and channel sensitivity to luminal Ca^{2+} activation are common defects of RyR2 mutations linked to ventricular tachycardia and sudden death. *Circulation Research* **97**, 1173-1181 (2005).
56. B. Gray, *et al.* A novel heterozygous mutation in cardiac calsequestrin causes autosomal dominant catecholaminergic polymorphic ventricular tachycardia. *Heart Rhythm* **13**, 1652-1660 (2016).
57. E. Kim, *et al.* Characterization of human cardiac calsequestrin and its deleterious mutants. *Journal of Molecular Biology* **373**, 1047-1057 (2007).
58. H. Rosenberg, J. Antognini, S. Muldoon. Testing for Malignant Hyperthermia. *Anesthesiology* **96**, 232-237 (2002).
59. T. Murayama, *et al.* Genotype–Phenotype Correlations of Malignant Hyperthermia and Central Core Disease Mutations in the Central Region of the RyR1 Channel. *Human Mutation* **37**, 1231-1241 (2016).
60. C. Roesl, K. Sato, A. Schiemann, N. Pollock, K. Stowell. Functional characterisation of the R2452W ryanodine receptor variant associated with malignant hyperthermia susceptibility. *Cell Calcium* **56**, 195-201 (2014).
61. J. Zeuthen. Epstein-Barr virus (EBV), lymphocytes and transformation. *Journal of Cancer Research and Clinical Oncology* **106**, 1-11 (1983).
62. T. Girard, *et al.* B-lymphocytes from malignant hyperthermia-susceptible patients have an increased sensitivity to skeletal muscle ryanodine receptor activators. *Journal of biological chemistry* **276**, 48077-48082 (2001).
63. M. Broman, *et al.* Mutation screening of the *RYR1* cDNA from peripheral B-lymphoytes in 15 Sweedish malignant hyperthermia index cases *British Journal of Anaesthesia* **102**, 642-649 (2009).
64. C. Neville, N. Rossenthal, M. McGrew, N Bogdanova, S. Hauschka. Skeletal muscel cultures. *Methods in Muscle Biology* **52**, 85-116 (1998).
65. X. Guo, *et al. In vitro* differentiation of functional human skeletal myotubes in a defined system. *Royal Society of Chemistry* **2**, 131-138 (2014).
66. L. Golini, *et al.* Junctophilin 1 and 2 proteins interact with the L-type Ca^{2+} channel dihydropyridine receptors (DHPRs) in skeletal muscle. *Journal of biological Chemistry* **286**, 43717-43725 (2011).
67. M. Chelu, *et al.* Heat- and anesthesia-induced malignant hyperthermia in an RyR1 knock-in mouse. *Journal of the Federation of American Societies for Experimental Biology* **20**, 329-330 (2005).

68. B. Yuen, *et al.* Mice expressing T4826I-RyR1 are viable but exhibit sex- and genotype-dependent susceptibility to malignant hyperthermia and muscle damage. *Federation of American Societies For Experimental Biology* **26** (2011).
69. T. Yang, *et al.* Pharmacologic and functional characterization of malignant hyperthermia in the R163C RyR1 knock-in mouse. *Anesthesiology* **105**, 1164-1175 (2006).
70. I. Basic, Z. Tadic., V. Lackovic, A. Gomercic. Stress syndrome: Ryanodine receptor (*RYR1*) gene in malignant hyperthermia in humans and pigs. *Periodicum Biologorum* **99**, 313-317 (1997).
71. T. Yang, T. Ta, I. Pessah, P. Allen. Functional defects in six ryanodine receptor isoform-1 (RyR1) mutations associated with malignant hyperthermia and their impact on skeletal excitation-contraction coupling. *Journal of Biological Science* **278**, 25722-25730 (2003).
72. R. Dirksen, G. Avila. Distinct effects on Ca^{2+} handling caused by malignant hyperthermia and central core disease mutations in RyR1. *Biophysical Journal* **87**, 3193-3204 (2004).
73. G. Avila, E. H. Lee, C. Perez, P. Allen, R. Dirksen. FKBP12 binding to RyR1 modulates excitation-contraction coupling in mouse skeletal myotubes. *Journal of Biological Chemistry* **278**, 22600-22608 (2003).
74. C. Manno, *et al.* Altered Ca^{2+} concentration, permeability and buffering in the myofibre Ca^{2+} store of a mouse model of malignant hyperthermia. *The Physiological Journal* **591**, 4439-4457 (2013).
75. L. Kimlicka, K. Lau, C. Tung, F. V. Petegem. Disease mutations in the ryanodine receptor N-terminal region couple to a mobile intersubunit interface. *Nature Communications* **4** (2013).
76. K. Lau, F. V. Petegem. Crystal structures of the ryanodine receptor SPRY2 domain. *Biophysical Journal* **108** (2015).
77. Z. Yuchi, *et al.* Crystal structures of ryanodine receptor SPRY1 and tandem-repeat domains reveal a critical FKBP12 binding determinant. *Nature Communications* **6** (2015).
78. K. Lau, F. V. Petegem. Crystal structures of wild type and disease mutant forms of the ryanodine receptor SPRY2 domain. *Nature Communications* **5** (2014).
79. Z. Yuchi, K. Lau, F. V. Petegem. Disease mutations in the ryanodine receptor central region: crystal structures of a phosphorylation hot spot domain. *Structure* **20**, 1201–1211 (2012).
80. M. L. Bannister, *et al.* Malignant hyperthermia mutation sites in the Leu2442–Pro2477 (DP4) region of RyR1 (ryanodine receptor 1) are clustered in a structurally and functionally definable area. *Biochemical Journal* **401**, 333-339 (2007).
81. P. AntonioLobo, F. V. Petegem. Crystal Structures of the N-Terminal Domains of Cardiac and Skeletal Muscle Ryanodine Receptors: Insights into Disease Mutations. *Structure* **17**, 1505-1514 (2009).
82. RCBS, Protein Data Bank. (Accessed 2020).
83. S. Reiken, *et al.* PKA phosphorylation activates the calcium release channel (ryanodine receptor) in skeletal muscle. *Journal of Cell Biology* **160**, 919-928 (2003).
84. Q. Sun, B. Wang, M. Miyagi, D. Hess, J. Stamler. Oxygen-coupled redox regulation of the skeletal muscle ryanodine receptor/Ca^{2+} release channel (RyR1). *Journal of Biological Chemistry* **288**, 22962-22971 (2013).

85. P. Aracena, G. Sánchez, P. Donoso, S. L. Hamilton, C. Hidalgo. S-glutathionylation decreases Mg^{2+} inhibition and S-nitrosylation enhances Ca^{2+} activation of RyR1 channels. *Journal of Biological Chemistry* **278**, 42927-42935. (2003).
86. A. Merritt, *et al.* Assessing the pathogenicity of *RYR1* variants in malignant hyperthermia. *British Journal of Anaesthesia* **118** (2017).
87. Blayney L, *et al.* ATP interacts with the CPVT mutation-associated central domain of the cardiac ryanodine receptor. *Biochimica et Biophysica Acta- General Subjects* **1830**, 4426-4432 (2013).
88. S. Paytubi, *et al.* ABC50 Promotes Translation Initiation in Mammalian Cells. *Journal of Biological Chemistry* **284**, 24061-24073 (2009).
89. C. Loveday, *et al.* Germline mutations in RAD51D confer susceptibility to ovarian cancer. *Nature Genetics* **43**, 879-882 (2011).
90. C. Vonrhein, H. Bonisch, G. Schafer, G. E. Schulz. The structure of a trimeric archaeal adenylate kinase. *Journal of Molecular Biology* **282**, 167-179 (1998).
91. A. Lavie, *et al.* Crystal structure of yeast thymidylate kinase complexed with the bisubstrate inhibitor P1-(5‘-adenosyl) P5-(5‘-thymidyl) pentaphosphate (TP5A) at 2.0 Å resolution: implications for catalysis and AZT activation. *Biochemisrty* **37**, 3677-3686 (1998).
92. T. Stehle, G. E. Schulz. Refined structure of the complex between guanylate kinase and its substrate GMP at 2·0 Å resolution. *Journal of Molecular Biology* **224**, 1127-1141 (1992).
93. M. Samsó, W. Feng, I. Pessah, P. Allen. Coordinated movement of cytoplasmic and transmembrane domains of RyR1 upon gating. *Public Library of Science* **7**, 980-995 (2009).
94. S. Ludtke, I. Serysheva, S. Hamilton, W. Chiu. The pore structure of the closed RyR1 channel. *Structure* **13**, 1203-1211 (2005).
95. H. Tegel, S. Tourle, J. Ottosson, A. Persson. Increased levels of recombinant human proteins with the Escherichia coli strain Rosetta(DE3). *Protein Expression and Purification* **69**, 159-167 (2010).
96. J. Stephens. Characterisation RyR1 variants linked to malignant hyperthermia. *Master’s thesis, Massey University, Palmerston North, New Zealand* (2016).
97. G. Fischer, F. Schmid. The mechanism of protein folding. Implications of *in vitro* refolding models for de novo protien folding and translocation in the cell *Perspectives in Biochemistry* **29**, 2205-2212 (1989).
98. M. Brohus, *et al.* Ca^{2+}-dependent calmodulin binding to cardiac ryanodine receptor (RyR2) calmodulin-binding domains. *Biochemical Journal* **476**, 193-209 (2019).
99. W. Peng, *et al.* Structural basis for the gating mechanism of the type 2 ryanodine receptor RyR2. *Science* **354** (2016).
100. J. Xionga, *et al.* Pathogenic mechanism of a catecholaminergic polymorphic ventricular tachycardia causing-mutation in cardiac calcium release channel RyR2. *Journal of Molecular and Cellular Cardiology* **117** (2018).
101. L. Kimlicka, K. Lau, C. Tung, F. VanPetegem. Disease mutations in the ryanodine receptor N-terminal region couple to a mobile intersubunit interface. *Nature Communications* **4** (2013).
102. T. Murayama, *et al.* Genotype–phenotype correlations of malignant hyperthermia and central core disease dutations in the central region of the RyR1 channel. *Human Mutation* **37**, 1231-1241 (2016).

103. l. Galli, *et al.* Mutations in the *RYR1* gene in Italian patients at risk for Malignant Hyperthermia: evidence for a cluster of novel mutations in the C-terminal region. *Cell Calcium* **32**, 143-151 (2002).
104. H. Rueffert, D. Olthoff, C. Deutrich, C. D. Meinecke, U. G. Froster. Mutation screening in the ryanodine receptor 1 gene (*RYR1*) in patients susceptible to malignant hyperthermia who show definite IVCT results: identification of three novel mutations. *Anaesthesiologica Scandinavica* **46**, 692-698 (2002).
105. J. Lopez, V. Kaura, C. Diggle, P. Hopkins, P. Allen. Malignant hyperthermia, environmental heat stress, and intracellular calcium dysregulation in a mouse model expressing the p.G2435R variant of RyR1. *British Journal of Anaesthesia* **121**, 953-961 (2018).
106. X. Zhao, *et al.* Increased store-operated Ca^{2+} entry in skeletal muscle with reduced calsequestrin-1 expression. *Biophysical Journal* **99**, 1556-1564 (2010).
107. D. Rossi, *et al.* Distinct regions of triadin are required for targeting and retention at the junctional domain of the sarcoplasmic reticulum. *Biochemical Journal* **458**, 407-417 (2014).
108. B. Garcia, C. Thomas, N. Kelleher, C. Mizzen. Tissue-specific expression and post-translational modification of histone H3 variants. *Journal of Proteome Research* **10**, 4225-4236 (2008).
109. J. Stephens *et al.*, Functional analysis of *RYR1* variants linked to malignant hyperthermia. *Temperature* **3**, 328-339 (2016).
110. R. Robinson, *et al. RYR1* mutations causing central core disease are associated with more severe malignant hyperthermia *in vitro* contracture test phenotypes. *Human Mutation* **20**, 88-97 (2002).
111. M. Brini, *et al.* Ca^{2+} signaling in HEK-293 and skeletal muscle cells expressing recombinant ryanodine receptors harboring malignant hyperthermia and central core disease mutations. *Journal of Biological Chemistry* **280**, 15380-15389 (2005).
112. P. M. Hopkins, *et al.* European Malignant Hyperthermia Group guidelines for investigation of malignant hyperthermia susceptibility. *British Journal of Anaesthesia* **115**, 531-539 (2015).
113. E. Estève, *et al.* A malignant hyperthermia–inducing mutation in RyR1 (R163C): alterations in Ca^{2+} entry, release, and retrograde signaling to the DHPR. *Journal of General Physiology* **135**, 619-628 (2010).
114. O. Rokach, *et al.* Establishment of a human skeletal muscle-derived cell line: biochemical, cellular and electrophysiological characterization. *Biochemical Journal* **455**, 169-177 (2013).
115. C. Zhu, *et al.* Cellular senescence in human myoblasts is overcome by human telomerase reverse transcriptase and cyclin-dependent kinase 4: consequences in aging muscle and therapeutic strategies for muscular dystrophies. *Aging Cell* **6**, 515-523 (2007).
116. S. Donna, *et al.* Telomerase Can Extend the Proliferative Capacity of Human Myoblasts, but Does Not Lead to Their Immortalization. *molecular cancer research* **1**, 643-653 (2003).
117. M. Dickinson. Molecular pathways: CDK4 inhibitors for cancer therapy. *American Association for Cancer Research* **20**, 3379-3383 (2014).

118. C. Provenzano, *et al.* CRISPR/Cas9-mediated deletion of CTG expansions recovers normal phenotype in myogenic cells derived from myotonic dystrophy 1 patients. *Nucleic Acids* **9**, 337-348 (2017).
119. C. R. Fernandez. CRISPR cas9: the gene editing tool changing the world. Retreived from https://www.labiotech.eu/in-depth/crispr-cas9-review-gene-editing-tool. (2020)
120. InvivoGen. Invivogen insight inovation within reach. retreived from https://www.invivogen.com/sites/default/files/invivogen/old/docs/Insight_201004.pdf (2010).
121. R. Cawthon. Telomere measurement by quantitative PCR. *Nucleic Acids Research* **30**, 47 (2002).
122. N. O'Callaghan, M. Fenech. A quantitative PCR method for measuring absolute telomere length. . *Biological Procedures* **13** (2011).
123. R. Parker. Functional consequences of RyR_1 variants. **Doctoral dissertation, Massey University, Palmerston North, New Zealand** (2019).
124. T. Yang, P. Allen, I. Pessah, J. Lopez. Enhanced excitation-coupled calcium entry in myotubes is associated with expression of RyR1 malignant hyperthermia mutations. *Journal of Biological Chemistry* **282**, 37471-37478 (2007).
125. J. Keelan, O. Vergun, M. Duchen. Excitotoxic mitochondrial depolarisation requires both calcium and nitric oxide in rat hippocampal neurons. *The Journal of Physiology* **1**, 797-813 (1999).
126. T. Murayama, *et al.* Divergent activity profiles of type 1 ryanodine receptor channels carrying malignant hyperthermia and central core disease mutations in the amino-terminal region. *Public Library of Science* **10** (2015).
127. D. Han, W. Yang, T. Kao. Dexamethasone treatment at the myoblast stage enhanced C2C12 myocyte differentiation. *International Journal of Medical Sciences* **14**, 434-443 (2017).
128. J. Nehlin, M. Just, A. Rustan, M. Gaster. Human myotubes from myoblast cultures undergoing senescence exhibit defects in glucose and lipid metabolism. *Biogerontology* **12**, 349-365 (2011).
129. J. Song, *et al.* RS-1 enhances CRISPR/Cas9- and TALEN-mediated knock-in efficiency. *Nature Communications* **7**, 10548 (2016).
130. X. Ren, *et al.* Enhanced specificity and efficiency of the CRISPR/Cas9 system with optimized sgRNA parameters in drosophila. *Cell Reports* **9**, 1151-1162 (2014).
131. L. Baena-Lopez, C. Alexandre, A. Mitchell, L. Pasakarnis, J. Vincent. Accelerated homologous recombination and subsequent genome modification in Drosophila. *Development* **140**, 4818-4825 (2013).
132. G. Stadler, *et al.* Establishment of clonal myogenic cell lines from severely affected dystrophic muscles - CDK4 maintains the myogenic population. *Skeletal Muscle* **1** (2011).
133. M. Thorley, *et al.* Skeletal muscle characteristics are preserved in hTERT/cdk4 human myogenic cell lines. *Skeletal Muscle* **6** (2016).
134. New Engalnd Biolabs. Factor Xa protease. Retreived from https://international.neb.com/products/p8010-factor-xa-protease#Product%20Information. (2020)
135. Merck, HRV-3C Protease. Retreived from https://www.sigmaaldrich.com/catalog/product/sigma/sae0045?lang=en&region=NZ&gclid=EAIaIQobChMIgrrShovw7gIVxL2WCh2CPwh9EAAYASAAEgJTovD_BwE. (2020)

136. Merck, Enterokinase from bovine intestine. Retreived from https://www.sigmaaldrich.com/catalog/product/sigma/e4906?lang=en&region=NZ. (2020).
137. Hampton Research, Crystallization screens. Retreived from https://hamptonresearch.com/cat-1.html. (2020).
138. ForteBio. Fast quantitation of proteins antibodies using the BLItz system retreived from https://www.fortebio.com/sites/default/files/en/assets/app-note/fast-quantitation-of-proteins-and-antibodies-using-blitz-system.pdf. (2019)
139. C. Bagshaw. ATP analogues at a glance. *Journal of Cell Science* **114**, 459-460 (2001).
140. Q. Lv *et al.*, Efficient Generation of Myostatin Gene Mutated Rabbit by CRISPR/Cas9. *Scientific Reports* **6** (2016).
141. T. Sui, Y. Siang, D. Liu, T. Liu, L. Xu, Y. Gao, L. Lai, Z. Li, R. Han. A novel rabbit model of Duchenne muscular dystrophy generated by CRISPR/Cas9. *Disease Models and Mechanisms* doi: 10.1242/dmm.032201 (2018).
142. K. Carroll, *et al.* A mouse model for adult cardiac-specific gene deletion with CRISPR/Cas9. *Proceedings of the National Academy of Sciences* **113**, 338-343 (2015).
143. M. Hashimoto, T. Takemoto. Electroporation enables the efficient mRNA delivery into the mouse zygotes and facilitates CRISPR/Cas9-based genome editing. *Scientific Reports* **5** (2015).
144. P. Campeau, P. Chapdelaine, S. Seigneurin-Venin, B. Massie, J. Tremblay. Transfection of large plasmids in primary human myoblasts. *Gene Therapy* **8**, 1387-1394 (2001).
145. A. Montpetit, *et al.* Telomere length: a review of methods for measurement. *Nursing Research* **63**, 289-299 (2015).
146. J. L. Doman, A. Raguram, G. A. Newby, D. R. Liu. Evaluation and minimization of Cas9-independent off-target DNA editing by cytosine base editors. *Nature Biotechbology.* (2020).
147. A. C. Komor, Y. B. Kim, M. S. Packer, J. A. Zuris, D. R. Liu. Programmable editing of a target base in genomic DNA without double-stranded DNA cleavage. *Nature* **533**, 420-424 (2016).
148. Z. Wu, *et al.* CRISPR/Cas9 mediated GFP knock-in at the MAP1LC3B locus in 293FT cells is better for bona fide monitoring cellular autophagy. *Biotechnology Journal* **13** (2018).
149. H. Kina, T. Yoshitani, K. Hanyu-Nakamura, A. Nakamura. Rapid and efficient generation of GFP-knocked-in Drosophila by the CRISPR-Cas9-mediated genome editing. *Development, Growth and Differentiation* **61** (2019).
150. Y. Dong *et al.* Genome-wide off-target analysis in CRISPR-Cas9 modified mice and their offspring. *Genes, Genomes, Genetics* **9**, 3645-3651 (2019).
151. K. Anderson, *et al.* CRISPR off-target analysis in genetically engineered rats and mice. *Nature Methods* **15**, 512-514 (2018).
152. C. Smith, *et al.* Whole-genome sequencing analysis reveals high specificity of CRISPR/Cas9 and TALEN-based genome editing in human iPSCs. *Cell Stem Cell* **15**, 12-13 (2014).
153. F. Madeira, *et al.* The EMBL-EBI search and sequence analysis tools APIs in 2019. *Nucleic Acids Research* **47**, 363-641 (2019).

9. Appendices

Appendix 1. Sequence alignment of RyR1 and RyR2 highlighting MH and CPVT pathogenic variants.

```
RyR1            -MGDAEGEDEVQFLRTDDEVVLQCSATVLKEQLKLCLAAEGFGNRLCFLEPTSNAQNVPP
RyR2            MADGGEGEDEIQFLRTDDEVVLQCTATIHKEQQKLCLAAEGFGNRLCFLESTSNSKNVPP
                  ...*****:*************:**: *** *****************.***::****

RyR1            DLAICCFVLEQSLSVRALQEMLANTVEAG------------VESSQGGGHRTLLYGHAIL
RyR2            DLSICTFVLEQSLSVRALQEMLANTVEKSEGQVDVEKWKFMMKTAQGGGHRTLLYGHAIL
                **:** ********************* .            ::::***************

RyR1            LRHAHSRMYLSCLTTSRSMTDKLAFDVGLQEDATGEACWWTMHPASKQRSEGEKVRVGDD
RyR2            LRHSYSGMYLCCLSTSRSSTDKLAFDVGLQEDTTGEACWWTIHPASKQRSEGEKVRVGDD
                ***::* ***.**:**** *************:********:******************

RyR1            IILVSVSSERYLHLSTASGELQVDASFMQTLWNMNPICS--RCEEGFVTGGHVLRLFHGH
RyR2            LILVSVSSERYLHLSYGNGSLHVDAAFQQTLWSVAPISSGSEAAQGYLIGGDVLRLLHGH
                :************** ..*.*:***:* ****.: **.*  .. :*:: **.****:***

RyR1            MDECLTISPADS-DDQRRLVYYEGGAVCTHARSLWRLEPLRISWSGSHLRWGQPLRVRHV
RyR2            MDECLTVPSGEHGEEQRRTVHYEGGAVSVHARSLWRLETLRVAWSGSHIRWGQPFRLRHV
                ******:...:  ::*** *:*******..*********.**::*****:*****:*:***

RyR1            TTGQYLALTEDQGLVVVDASKAHTKATSFCFRISKEKLDVAPKRDVEGMGPPEIKYGESL
RyR2            TTGKYLSLMEDKNLLLMDKEKADVKSTAFTFRSSKEKLDVGVRKEVDGMGTSEIKYGDSV
                ***:**:* **:.*::::* .**..*:*:* ** *******. :::*:***..*****:*:

RyR1            CFVQHVASGLWLTYAAPDPKALRLGVLKKKAMLHQEGHMDDALSLTRCQQEESQAARMIH
RyR2            CYIQHVDTGLWLTYQSVDVKSVRMGSIQRKAIMHHEGHMDDGISLSRSQHEESRTARVIR
                *::*** :****** : * *::*:* ::::**::*:******.:**:*.*:***::**:*:

RyR1            STNGLYNQFIKSLDSFSGKPRGSGPPAGTALPIEGVILSLQDLIIYFEPPSEDLQHEEKQ
RyR2            STVFLFNRFIRGLDALSKKAKAS----TVDLPIESVSLSLQDLIGYFHPPDEHLEHEDKQ
                **  *:*:**:.**::* *.:.*     . ****.* ******* **.**.*.*:**:**

RyR1            SKLRSLRNRQSLFQEEGMLSMVLNCIDRLNVYTTAAHFAEFAGEEAAESWKEIVNLLYEL
RyR2            NRLRALKNRQNLFQEEGMINLVLECIDRLHVYSSAAHFADVAGREAGESWKSILNSLYEL
                .:**:*:***.*******:.:**:*****:**::*****:.**.**.****.*:* ****
```

```
RyR1            LASLIRGNRSNCALFSTNLDWLVSKLDRLEASSGILEVLYCVLIESPEVLNIIQENHIKS
RyR2            LAALIRGNRKNCAQFSGSLDWLISRLERLEASSGILEVLHCVLVESPEALNIIKEGHIKS
                **:******.*** ** .****:*:*:************:***:****.****:*.****

RyR1            IISLLDKHGRNHKVLDVLCSLCVCNGVAVRSNQDLITENLLPGRELLLQTNLINYVTSIR
RyR2            IISLLDKHGRNHKVLDVLCSLCVCHGVAVRSNQHLICDNLLPGRDLLLQTRLVNHVSSMR
                ************************:********.** :******:*****.*:*:*:*:*

RyR1            PNIFVGRAEGTTQYSKWYFEVMVDEVTPFLTAQATHLRVGWALTEGYTPYPGAGEGWGGN
RyR2            PNIFLGVSEGSAQYKKWYYELMVDHTEPFVTAEATHLRVGWASTEGYSPYPGGGEEWGGN
                ****:* :**::**.***:*:***.. **:**:********* ****:****.** ****

RyR1            GVGDDLYSYGFDGLHLWTGHVARPVTSPGQHLLAPEDVISCCLDLSVPSISFRINGCPVQ
RyR2            GVGDDLFSYGFDGLHLWSGCIARTVSSPNQHLLRTDDVISCCLDLSAPSISFRINGQPVQ
                ******:**********:* :**.*:**.**** .:**********.********* ***

RyR1            GVFESFNLDGLFFPVVSFSAGVKVRFLLGGRHGEFKFLPPPGYAPCHEAVLPRERLHLEP
RyR2            GMFENFNIDGLFFPVVSFSAGIKVRFLLGGRHGEFKFLPPPGYAPCYEAVLPKEKLKVEH
                *:**.**:*************:*************************:*****:*:*::*

RyR1            IKEYRREGPRGPHLVGPSRCLSHTDFVPCPVDTVQIVLPPHLERIREKLAENIHELWALT
RyR2            SREYKQERTYTRDLLGPTVSLTQAAFTPIPVDTSQIVLPPHLERIREKLAENIHELWVMN
                 :**::* .   .*:**: .*::: *.* **** **********************.:.

RyR1            RIEQGWTYGPVRDDNKRLHPCLVDFHSLPEPERNYNLQMSGETLKTLLALGCHVGMADEK
RyR2            KIELGWQYGPVRDDNKRQHPCLVEFSKLPEQERNYNLQMSLETLKTLLALGCHVGISDEH
                :** ** ********** *****:* .*** ********* ***************::**:

RyR1            AEDNLKKTKLPKTYMMSNGYKPAPLDLSHVRLTPAQTTLVDRLAENGHNVWARDRVGQGW
RyR2            AEDKVKKMKLPKNYQLTSGYKPAPMDLSFIKLTPSQEAMVDKLAENAHNVWARDRIRQGW
                ***::** ****.* ::.******:***.::***:* ::**:****.********: ***

RyR1            SYSAVQDIPARRNPRLVPYRLLDEATKRSNRDSLCQAVRTLLGYGYNIEPPDQEPSQVEN
RyR2            TYGIQQDVKNRRNPRLVPYTLLDDRTKKSNKDSLREAVRTLLGYGYNLEAPDQDHAARAE
                :*.  **:  ********* ***: **:**:*** :***********:*.***: :   :

RyR1            QSR--CDRVRIFRAEKSYTVQSGRWYFEFEAVTTGEMRVGWARPELRPDVELGADELAYV
RyR2            VCSGTGERFRIFRAEKTYAVKAGRWYFEFETVTAGDMRVGWSRPGCQPDQELGSDERAFA
                 .    :*.*******:*:*::*********:**:*:*****:**  :** ***:** *:.

RyR1            FNGHRGQRWHLGSEPFGRPWQPGDVVGCMIDLTENTIIFTLNGEVLMSDSGSETAFREIE
RyR2            FDGFKAQRWHQGNEHYGRSWQAGDVVGCMVDMNEHTMMFTLNGEILLDDSGSELAFKDFD
                *:*.:.**** *.* :**.**.********:*:.*:*::******:*:.***** **::::
```

```
RyR1            IGDGFLPVCSLGPGQVGHLNLGQDVSSLRFFAICGLQEGFEPFAINMQRPVTTWFSKGLP
RyR2            VGDGFIPVCSLGVAQVGRMNFGKDVSTLKYFTICGLQEGYEPFAVNTNRDITMWLSKRLP
                :****:****** .***:::*:*:***:*:::*:*******:****:* :* :* *:** **

RyR1            QFEPVPLEHPHYEVSRVDGTVDTPPCLRLTHRTWGSQNSLVEMLFLRLSLPVQFHQHFRC
RyR2            QFLQVPSNHEHIEVTRIDGTIDSSPCLKVTQKSFGSQNSNTDIMFYRLSMPIECAEVFSK
                **  ** :* * **:*:***:*:.***:::*:::::***** .:::* ***:*::  : *

RyR1            TAGATPLAPPGLQPPAEDEARAAEPDPDYENLRRSAGGWSEAENGKEGTAKEGAPGGTPQ
RyR2            TVAGGLPGAGLFGPKNDLEDYDADSDFEVLMKTAHGHLVPDRVDKDKEATKP--------
                *...   ..  : *  : *   *:.* :       .   .:  : .: ::*

RyR1            AGGEAQPARAENEKDATTEKNKKRGFLFKAKKVAMMTQPPATPTLPRLPHDVVPADNRDD
RyR2            ------------EFNNHKDYAQEKPSRLKQRFLLRRTKPDYSTSHSARLTEDVLADDRDD
                           * :  .:  :::   :* : :   *:*  :.: .    : * **:***

RyR1            PEIILNTTTYYYSVRVFAGQEPSCVWAGWVTPDYHQHDMSFDLSKVRVVTVTMGDEQGNV
RyR2            YDFLMQTSTYYYSVRIFPGQEPANVWVGWITSDFHQYDTGFDLDRVRTVTVTLGDEKGKV
                 ::::::*:*******:*.****: **.**:*.*:**:* .***.:**.****:***:*:*

RyR1            HSSLKCSNCYMVWGGDFVSPGQQGRISHTDLVIGCLVDLATGLMTFTANGKESNTFFQVE
RyR2            HESIKRSNCYMVCAGESMSPGQGR--NNNGLEIGCVVDAASGLLTFIANGKELSTYYQVE
                *.*:* ****** .*: :****    .:..* ***:** *:**:** ***** .*::***

RyR1            PNTKLFPAVFVLPTHQNVIQFELGKQKNIMPLSAAMFQSERKNPAPQCPPRLEMQMLMPV
RyR2            PSTKLFPAVFAQATSPNVFQFELGRIKNVMPLSAGLFKSEHKNPVPQCPPRLHVQFLSHV
                *.********. .*  **:*****: **:*****.:*:**:***.*******.:*:*  *

RyR1            SWSRMPNHFLQVETRRAGERLGWAVQCQEPLTMMALHIPEENRCMDILELSERLDLQRFH
RyR2            LWSRMPNQFLKVDVSRISERQGWLVQCLDPLQFMSLHIPEENRSVDILELTEQEELLKFH
                 ******:**:*:. * .** ** *** :** :*:********.:*****:*: :* :**

RyR1            SHTLRLYRAVCALGNNRVAHALCSHVDQAQLLHALEDAHLPGPLRAGYYDLLISIHLESA
RyR2            YHTLRLYSAVCALGNHRVAHALCSHVDEPQLLYAIENKYMPGLLRAGYYDLLIDIHLSSY
                 ****** *******:***********:.***:*:*: ::** **********.***.*

RyR1            CRSRRSMLSEYIVPLTPETRAITLFPPGRSTENGHPRHGLPGVGVTTSLRPPHHFSPPCF
RyR2            ATARLMMNNEYIVPMTEETKSITLFP------DENKKHGLPGIGLSTSLRPRMQFSSPSF
                . :*  * .*****:* **::*****      : : :*****:*::*****  :**.*.*

RyR1            VAALPAAGAAEAPARLSPAIPLEALRDKALRMLGEAVRDGGQHARDPVGGSVEFQFVPVL
RyR2            VSIS------NECYQYSPEFPLDILKSKTIQMLTEAVKEGSLHARDPVGGTTEFLFVPLI
                *:        :   : ** :**: *:.*:::** ***::*. ********:.** ***::
```

```
RyR1            KLVSTLLVMGIFGDEDVKQILKMIEPEVFTEEEEEDEEEEGEEEDEEEKEEDEEETAQE
RyR2            KLFYTLLIMGIFHNEDLKHILQLIEPSVFKEAATPEEESDTLEKELSVDDAKLQGAGEEE
                **. ***:**** :**:*:**::***.**.*    *:*.:  *:* . :. : :    :*

RyR1            KEDEEKEEEEAAEGEKEEGLEEGLLQMKLPESVKLQMCHLLEYFCDQELQHRVESLAAFA
RyR2            AKGGKRPKE-------------GLLQMKLPEPVKLQMCLLLQYLCDCQVRHRIEAIVAFS
                 :. :: :*             *********.****** **:*:** :::**:*::.**:

RyR1            ERYVDKLQANQRSRYGLLIKAFSMTAAETARRTREFRSPPQEQINMLLQFKDGTDEEDCP
RyR2            DDFVAKLQDNQRFRYNEVMQALNMSAALTARKTKEFRSPPQEQINMLLNFKD--DKSECP
                : :* *** *** **. :::*:.*:** ***:*:***************:***  *:.:**

RyR1            LPEEIRQDLLDFHQDLLAHCGIQLDGE-EEEPEEETTLGSRLMSLLEKVRLVKKKEEKPE
RyR2            CPEEIRDQLLDFHEDLMTHCGIELDEDGSLDGNSDLTIRGRLLSLVEKVTYLKKKQ--AE
                 *****::*****:**::****:** : . : :.: *: .**:**:***  :***:  .*

RyR1            EERSAEESKPRSLQELVSHMVVRWAQEDFVQSPELVRAMFSLLHRQYDGLGELLRALPRA
RyR2            KPVESDSKKSSTLQQLISETMVRWAQESVIEDPELVRAMFVLLHRQYDGIGGLVRALPKT
                :  .::..*. :**:*:*. :******..::.******** ********:* *:****::

RyR1            YTISPSSVEDTMSLLECLGQIRSLLIVQMGPQEENLMIQSIGNIMNNKVFYQHPNLMRAL
RyR2            YTINGVSVEDTINLLASLGQIRSLLSVRMGKEEEKLMIRGLGDIMNNKVFYQHPNLMRAL
                ***.  *****:.** .******** *:** :**:***:.:*:***************

RyR1            GMHETVMEVMVNVLGGGESKEIRFPKMVTSCCRFLCYFCRISRQNQRSMFDHLSYLLENS
RyR2            GMHETVMEVMVNVLGGGESKEITFPKMVANCCRFLCYFCRISRQNQKAMFDHLSYLLENS
                ********************** *****:.****************::************

RyR1            GIGLG---MQGSTPLDVAAASVIDNNELALALQEQDLEKVVSYLAGCGLQSCPMLVAKGY
RyR2            SVGLASPAMRGSTPLDVAAASVMDNNELALALREPDLEKVVRYLAGCGLQSCQMLVSKGY
                .:**.   *:************:*********:* ****** ********** ***:***

RyR1            PDIGWNPCGGERYLDFLRFAVFVNGESVEENANVVVRLLIRKPECFGPALRGEGGSGLLA
RyR2            PDIGWNPVEGERYLDFLRFAVFCNGESVEENANVVVRLLIRRPECFGPALRGEGGNGLLA
                *******  ************* ******************:*************.****

RyR1            AIEEAIRISEDPARDGPGIRRDRRREHFGEEPPEENRVHLGHAIMSFYAALIDLLGRCAP
RyR2            AMEEAIKIAEDPSRDGPSPNSGSSKTLDTEEE-EDDTIHMGNAIMTFYSALIDLLGRCAP
                *:****:*:***:****. . .  :    **  *:: :*:*:***:**:***********

RyR1            EMHLIQAGKGEALRIRAILRSLVPLEDLVGIISLPLQIPTLGKDGALVQPKMSASFVPDH
RyR2            EMHLIHAGKGEAIRIRSILRSLIPLGDLVGVISIAFQMPTIAKDGNVVEPDMSAGFCPDH
                *****:******:***:*****:** ****:**:.:*:**:.*** :*:*.***.* ***
```

```
RyR1            KASMVLFLDRVYGIENQDFLLHVLDVGFLPDMRAAASLDTATFSTTEMALALNRYLCLAV
RyR2            KAAMVLFLDRVYGIEVQDFLLHLLEVGFLPDLRAAASLDIAALSATDMALALNRYLCTAV
                **:************ ******:*:******:*********::*:*:********** **

RyR1            LPLITKCAPLFAGTEHRAIMVDSMLHTVYRLSRGRSLTKAQRDVIEDCLMSLCRYIRPSM
RyR2            LPLLTRCAPLFAGTEHHASLIDSLLHTVYRLSKGCSLTKAQRDSIEVCLLSICGQLRPSM
                ***:*:**********:* ::**:********:* ******** ** **:*:*  :****

RyR1            LQHLLRRLVFDVPILNEFAKMPLKLLTNHYERCWKYYCLPTGWANFGVTSEEELHLTRKL
RyR2            MQHLLRRLVFDVPLLNEHAKMPLKLLTNHYERCWKYYCLPGGWGNFGAASEEELHLSRKL
                :************:***.********************** **.***.:*******:***

RyR1            FWGIFDSLAHKKYDPELYRMAMPCLCAIAGALPPDYVDASYSSKAEKKATVDAEGNFDPR
RyR2            FWGIFDALSQKKYEQELFKLALPCLSAVAGALPPDYMESNYVSMMEKQSSMDSEGNFNPQ
                ******:*::***: **::::*:**.*:*********:::.* *  **::::*:****:*:

RyR1            PVETLNVIIPEKLDSFINKFAEYTHEKWAFDKIQNNWSYGENIDEELKTHPMLRPYKTFS
RyR2            PVDTSNITIPEKLEYFINKYAEHSHDKWSMDKLANGWIYGEIYSDSSKVQPLMKPYKLLS
                **:* *: *****: ****:**::*:**::**: *.* ***  .:. *.:*:::*** :*

RyR1            EKDKEIYRWPIKESLKAMIAWEWTIEKAREGEEEKTEKKKTRKISQSAQTYDPREGYNPQ
RyR2            EKEKEIYRWPIKESLKTMLAWGWRIERTREGDSMALYNRTRRISQTSQVSVDAAHGYSPR
                **:**************:*:** * **::***:.    ::. *  . *  : *. .**.*:

RyR1            PPDLSAVTLSRELQAMAEQLAENYHNTWGRKKKQELEAKGGGTHPLLVPYDTLTAKEKAR
RyR2            AIDMSNVTLSRDLHAMAEMMAENYHNIWAKKKKMELESKGGGNHPLLVPYDTLTAKEKAK
                . *:* *****:*:**** :****** *.:*** ***:****.****************:

RyR1            DREKAQELLKFLQMNGYAVTRGLKDMELDSSSIEKRFAFGFLQQLLRWMDISQEFIAHLE
RyR2            DREKAQDILKFLQINGYAVSRGFKDLELDTPSIEKRFAYSFLQQLIRYVDEAHQYILEFD
                ******::*****:*****:**:**:***:.*******:.*****:*::* ::::* .::

RyR1            AVVSSGRVEKSPHEQEIKFFAKILLPLINQYFTNHCLYFLSTPAKVLGSGGHASNKEKEM
RyR2            GGSR-GKGEHFPYEQEIKFFAKVVLPLIDQYFKNHRLYFLSAASRPLCSGGHASNKEKEM
                .    *: *: *:**********::****:***.** *****:.:: * ************

RyR1            ITSLFCKLAALVRHRVSLFGTDAPAVVNCLHILARSLDARTVMKSGPEIVKAGLRSFFES
RyR2            VTSLFCKLGVLVRHRISLFGNDATSIVNCLHILGQTLDARTVMKTGLESVKSALRAFLDN
                :*******..*****:****.**.::*******.::*********:* * **:.**:*::.

RyR1            ASEDIEKMVENLRLGKVSQARTQVKGVGQNLTYTTVALLPVLTTLFQHIAQHQFGDDVIL
RyR2            AAEDLEKTMENLKQGQFTHTRNQPKGVTQIINYTTVALLPMLSSLFEHIGQHQFGEDLIL
                *:**:** :****: *:.:::*.* *** * :.********:*::**:**.*****:*:**
```

```
RyR1            DDVQVSCYRTLCSIYSLGTTKNTYVEKLRPALGECLARLAAAMPVAFLEPQLNEYNACSV
RyR2            EDVQVSCYRILTSLYALGTSKSIYVERQRSALGECLAAFAGAFPVAFLETHLDKHNIYSI
                :******** * *:*:***:*. ***: *.******* :*.*:******.:*::::*  *:

RyR1            YTTKSPRERAILGLPNSVEEMCPDIPVLERLMADIGGLAESGARYTEMPHVIEITLPMLC
RyR2            YNTKSSRERAALSLPTNVEDVCPNIPSLEKLMEEIVELAESGIRYTQMPHVMEVILPMLC
                *.***.**** *.**..**::**:** **:** :*  ***** ***:****:*: *****

RyR1            SYLPRWWERGPEAPPSALPAGAPPPCTAVTSDHLNSLLGNILRIIVNNLGIDEASWMKRL
RyR2            SYMSRWWEHGPENN----PERAEMCCTALNSEHMNTLLGNILKIIYNNLGIDEGAWMKRL
                **:.****:***      *  *   ***:.*:*:*:******:** *******.:*****

RyR1            AVFAQPIVSRARPELLQSHFIPTIGRLRKRAGKVVSEEEQLRLEAKAEAQEGELLVRDEF
RyR2            AVFSQPIINKVKPQLLKTHFLPLMEKLKKKAATVVSEEDHLKAEARGDMSEAELLILDEF
                ***:***:.:.:*:**::**:* : :*:*:*..*****::*: **:.: .*.***: ***

RyR1            SVLCRDLYALYPLLIRYVDNNRAQWLTEPNPSAEELFRMVGEIFIYWSKSHNFKREEQNF
RyR2            TTLARDLYAFYPLLIRFVDYNRAKWLKEPNPEAEELFRMVAEVFIYWSKSHNFKREEQNF
                :.*.*****:******:** ***:**.****.********.*:*****************

RyR1            VVQNEINNMSFLTADNKSKMAKAGDIQSGGSDQERTKKKRRGDRYSVQTSLIVATLKKML
RyR2            VVQNEINNMSFLITDTKSKMSKAAVS-----DQERKKMKRKGDRYSMQTSLIVAALKRLL
                ************ :*.****:**.       ****.* **:*****:*******:**::*

RyR1            PIGLNMCAPTDQDLITLAKTRYALKDTDEEVREFLHNNLHLQGKVEGSPSLRWQMALYRG
RyR2            PIGLNICAPGDQELIALAKNRFSLKDTEDEVRDIIRSNIHLQGKLED-PAIRWQMALYKD
                *****:*** **:**:***.*::****::***::::.*:*****:*. *::********:.

RyR1            VPGREEDADDPEKIVRRVQEVSAVLYYLDQT------------EHPYKSKKAVWHKLLSK
RyR2            LPNRTDDTSDPEKTVERVLDIANVLFHLEQKSKRVGRRHYCLVEHPQRSKKAVWHKLLSK
                :*.* :*:.**** *.** ::: **::*:*.            *** :************

RyR1            QRRRAVVACFRMTPLYNLPTHRACNMFLESYKAAWILTEDHSFEDRMIDDLSKAGEQEEE
RyR2            QRKRAVVACFRMAPLYNLPRHRAVNLFLQGYEKSWIETEEHYFEDKLIEDLAKPGAEPPE
                **:*********:****** *** *:**:.*: :** **:* ***::*:**:*.* :  *

RyR1            EEEVEEKKPDPLHQLVLHFSRTALTEKSKLDEDYLYMAYADIMAKSCHLEEGGENGEAEE
RyR2            EDEG-TKRVDPLHQLILLFSRTALTEKCKLEEDFLYMAYADIMAKSCHDEEDDDG----E
                *:*   *: ******:* *********.**:**:************** **..:.    *

RyR1            EVEVSFEEKQMEKQRLLYQQARLHTRGAAEMVLQMISACKGETGAMVSSTLKLGISILNG
RyR2            EEVKSFEEKEMEKQKLLYQQARLHDRGAAEMVLQTISASKGETGPMVAATLKLGIAILNG
                *   *****:****:********* ********* ***.*****.**::******:****
```

```
RyR1            GNAEVQQKMLDYLKDKKEVGFFQSIQALMQTCSVLDLNAFERQNKAEGLGMVNEDGTVIN
RyR2            GNSTVQQKMLDYLKEKKDVGFFQSLAGLMQSCSVLDLNAFERQNKAEGLGMVTEEG----
                **: **********:**:******: .***:**********************.*:*

RyR1            RQNGEKVMADDEFTQDLFRFLQLLCEGHNNDFQNYLRTQTGNTTTINIIICTVDYLLRLQ
RyR2            --SGEKVLQDDEFTCDLFRFLQLLCEGHNSDFQNYLRTQTGNNTTVNIIISTVDYLLRVQ
                  .****: ***** **************.************.**:****.*******:*

RyR1            ESISDFYWYYSGKDVIEEQGKRNFSKAMSVAKQVFNSLTEYIQGPCTGNQQSLAHSRLWD
RyR2            ESISDFYWYYSGKDVIDEQGQRNFSKAIQVAKQVFNTLTEYIQGPCTGNQQSLAHSRLWD
                ****************:***:******:.*******:**********************

RyR1            AVVGFLHVFAHMMMKLAQDSSQIELLKELLDLQKDMVVMLLSLLEGNVVNGMIARQMVDM
RyR2            AVVGFLHVFAHMQMKLSQDSSQIELLKELMDLQKDMVVMLLSMLEGNVVNGTIGKQMVDM
                ************ ***:************:************:******** *.:*****

RyR1            LVESSSNVEMILKFFDMFLKLKDIVGSEAFQDYVTDPRGLISKKDFQKAMDSQKQFSGPE
RyR2            LVESSNNVEMILKFFDMFLKLKDLTSSDTFKEYDPDGKGVISKRDFHKAMESHKHYTQSE
                *****.*****************:..*:::*::* .* :*:***:**:***:*:*:::: .*

RyR1            IQFLLSCSEADENEMINCEEFANRFQEPARDIGFNVAVLLTNLSEHVPHDPRLHNFLELA
RyR2            TEFLLSCAETDENETLDYEEFVKRFHEPAKDIGFNVAVLLTNLSEHMPNDTRLQTFLELA
                 :*****:*:**** :: ***.:**:***:*****************:*:*.**:.*****

RyR1            ESILEYFRPYLGRIEIMGASRRIERIYFEISETNRAQWEMPQVKESKRQFIFDVVNEGGE
RyR2            ESVLNYFQPFLGRIEIMGSAKRIERVYFEISESSRTQWEKPQVKESKRQFIFDVVNEGGE
                **:*:**:*:********:::****:******:.*:*** ********************

RyR1            AEKMELFVSFCEDTIFEMQIAAQISEPEGEPETDEDEGAGAAEAGAEGAEEGAAGLEGTA
RyR2            KEKMELFVNFCEDTIFEMQLAAQISESDLNERSANKE-----ESEKERPEEQGPRMAFFS
                 *******.**********:******.: : .: :.*     *:  * .** .. :   :

RyR1            ATAAAGATARVVAAAGRALRGLSYRSLRRRVRRLRRLTAREAATAVAALLWAAVTRAGAA
RyR2            ILTVRSALFALRYNILTLMRMLSLKSLKKQMKKVKKMTVKDMVTAFFSSYWSIFMTLLHF
                  :. .*   :       :* ** :**:::::::::::*.:: .**. :  *: .

RyR1            GAGAAAGALGLLWGSLFGGGLVEGAKKVTVTELLAGMPDPTSDEVHGEQPAGPGGDADGE
RyR2            VASVFRGFFRIICSLLLGGSLVEGAKKIKVAELLANMPDPTQDEVRGDGEEGERKPLEAA
                 *..  * : :: . *:**.*******:.*:****.*****.***:*:   *     :.

RyR1            GASEGAGDAAEGAGDEEEAVHEAGPGGADGAVAVTDGGPFRPEGAGGLGDMGDTTPAEPP
RyR2            LPSEDLTDLKELTEESDLLSDIFG------LDLKREGGQYKLIPHNPNAGLSDLMSNPVP
                 .**.  *  * : :.:   .  *           :** ::    .  ..:.*  .   *
```

```
RyR1            TPEGSPILKRKLGVDGVEEELPPEPEPEPEPELEPEKADAENGEKEE-VPEPTPEPPKKQ
RyR2            MPEVQEKFQEQKAKE-------EEKEEKEETKSEPEKAEGEDGEKEEKAKEDKGKQKLRQ
                 ** .  ::.: . :        * * : *.: *****:.*:***** . * . :   :*

RyR1            APPSPPPKKEEAGGEFWGELEVQRVKFLNYLSRNFYTLRFLALFLAFAINFILLFYKVSD
RyR2            LHTHRYGEPEVPESAFWKKIIAYQQKLLNYFARNFYNMRMLALFVAFAINFILLFYKVST
                  .    : * . . ** :: . : *:***::****.:*:****:**************

RyR1            SPPGEDDMEGSAAGDVSGAGSGGSSGWGLGAGEEAEGDEDENMVYYFLEESTGYMEPALR
RyR2            SSVVEGKELPTRSSSENAKVTSLDS-----------SSHRIIAVHYVLEESSGYMEPTLR
                *.  *..   : :.. ..  :. .*           ...    *:*.****:*****:**

RyR1            CLSLLHTLVAFLCIIGYNCLKVPLVIFKREKELARKLEFDGLYITEQPEDDDVKGQWDRL
RyR2            ILAILHTVISFFCIIGYYCLKVPLVIFKREKEVARKLEFDGLYITEQPSEDDIKGQWDRL
                 *::***:::*:***** **************:***************.:**:*******

RyR1            VLNTPSFPSNYWDKFVKRKVLDKHGDIYGRERIAELLGMDLATLEITAHNERK-PNPPPG
RyR2            VINTQSFPNNYWDKFVKRKVMDKYGEFYGRDRISELLGMDKAALDFSDAREKKKPKKDSS
                *:** ***.***********:**:*::***:**:****** *:*:::  .*:* *:  ..

RyR1            LLTWLMSIDVKYQIWKFGVIFTDNSFLYLGWYMVMSLLGHYNNFFFAAHLLDIAMGVKTL
RyR2            LSAVLNSIDVKYQMWKLGVVFTDNSFLYLAWYMTMSVLGHYNNFFFAAHLLDIAMGFKTL
                * : * *******:**:**:*********.***.**:******************.***

RyR1            RTILSSVTHNGKQLVMTVGLLAVVVYLYTVVAFNFFRKFYNKSEDEDEPDMKCDDMMTCY
RyR2            RTILSSVTHNGKQLVLTVGLLAVVVYLYTVVAFNFFRKFYNKSEDGDTPDMKCDDMLTCY
                ***************:***************************** * ********:***

RyR1            LFHMYVGVRAGGGIGDEIEDPAGDEYELYRVVFDITFFFFVIVILLAIIQGLIIDAFGEL
RyR2            MFHMYVGVRAGGGIGDEIEDPAGDEYEIYRIIFDITFFFFVIVILLAIIQGLITDAFGEL
                :*************************:**::****************************

RyR1            RDQQEQVKEDMETKCFICGIGSDYFDTTPHGFETHTLEEHNLANYMFFLMYLINKDETEH
RyR2            RDQQEQVKEDMETKCFICGIGNDYFDTVPHGFETHTLQEHNLANYLFFLMYLINKDETEH
                ********************.*****.*********:*******:**************

RyR1            TGQESYVWKMYQERCWDFFPAGDCFRKQYEDQLS
RyR2            TGQESYVWKMYQERCWEFFPAGDCFRKQYEDQLN
                ****************:****************.
```

Appendix 1. sequence alignment of RyR1 and RyR2. Highlighted in red are pathogenic variants either MH for RyR1 or CPVT for RyR2. The human RyR1 amino acids refer to the accession number NM_000540.2 and the rabbit RyR2 refers to the accession number Q29621. The sequence alignment was performed using Clustal W (153).

Appendix 2. Recombinant expression of the RyR1 HD1

2.1 Sequence alignment of the HD1 amino acid sequence from human and rabbit.

```
Rabbit      qagkgealrirailrslvplddlvgiislplqiptlgkdgalvqpkmsasfvpdhkasmv
Human       QAGKGEALRIRAILRSLVPLEDLVGIISLPLQIPTLGKDGALVQPKMSASFVPDHKASMV
            ********************:****************************************

Rabbit      lfldrvygienqdfllhvldvgflpdmraaasldtatfsttemalalnrylclavlplit
Human       LFLDRVYGIENQDFLLHVLDVGFLPDMRAAASLDTATFSTTEMALALNRYLCLAVLPLIT
            ************************************************************

Rabbit      kcaplfagtehraimvdsmlhtvyrlsrgrsltkaqrdviedclmalcryirpsmlqhll
Human       KCAPLFAGTEHRAIMVDSMLHTVYRLSRGRSLTKAQRDVIEDCLMSLCRYIRPSMLQHLL
            ********************************************:***************

Rabbit      rrlvfdvpilnefakmplkllltnhyercwkyyclptgwanfgvtseeelhltrklfwgif
Human       RRLVFDVPILNEFAKMPLKLLTNHYERCWKYYCLPTGWANFGVTSEEELHLTRKLFWGIF
            ************************************************************

Rabbit      dslahkkydqelyrmampclcaiagalppdyvdasysskaekkatvdaegnf
Human       DSLAHKKYDPELYRMAMPCLCAIAGALPPDYVDASYSSKAEKKATVDAEGNF
            ********* ****************************************
```

Appendix 2.1. Sequence alignment of the HD1 from rabbit RyR1 and human RyR1. The rabbit RyR1 amino acid sequence refers to the accession number P11716.1 and the human RyR1 amino acid sequence refers to the accession number NM_000540.2 The sequence alignment was performed using Clustal W (153).

2.2 Primer sequences used to amplify the RyR1 HD1

Primer Name	Primer Sequence	Melting temperature ° C
2093 F	GGCTTTGGATCCCGGTCCCTGCAGGAGCTGGTG	78
2148 F	GGCTTTGGATCCGTGGAAGACACCATGAGCCTG	73
2152 F	GGCTTTGGATCCATGAGCCTGCTCGAGTGCCTC	75
2156 F	GGCTTTGGATCCGAGTGCCTCGGCCAGATC	74
2366 F	GGCTTTGGATCCCCCGCCCTGCGGGGTGAGG	81
PGEX6P3 2525 R	GCGGTGCGGCCGCTTAGAACCCCACGTCCAGCACGTG	83
PGEX6P3 2536 R	GCGGTGCGGCCGCTTAGTCCAGCGAGGCGGCTGCCCT	82
PGEX6P3 2564 R	GCGGTGCGGCCGCTTACTTGGTGATGAGCGGCAGCACG	83
PGEX6P3 2570 R	GCGGTGCGGCCGCTTAAAAGAGCGGCGCACACTTGGT	81
PGEX6P3 2592 R	GCGGTGCGGCCGCTTACCGAGACAGGCGGTACACGGT	83
PGEX6P3 2614 R	GCGGTGCGGCCGCTTAGTACCTGCAGAGCGACATGAG	79
PGEX6P3 2653 R	GCGGTGCGGCCGCTTATAGTACTTCCAACAGCGCTCA	77
PGEX6P3 2708 R	GCGGTGCGGCCGCTTACCCGGCAATGGCGCACAGACA	84
pPROEXHTB 2525 R	GGCCTTAAGCTTTTGAACCCCACGTCCAGCACGTG	75
pPROEXHTB 2536 R	GGCCTTAAGCTTTTGTCCAGCGAGGCGGCTGCCCT	79
pPROEXHTB 2564 R	GGCCTTAAGCTTTTCTTGGTGATGAGCGGCAGCACG	74
pPROEXHTB 2570 R	GGCCTTAAGCTTTTAAAGAGCGGCGCACACTTGGT	73
pPROEXHTB 2592 R	GGCCTTAAGCTTTTCCGAGACAGGCGGTACACGGT	75
pPROEXHTB 2614 R	GGCCTTAAGCTTTTGTACCTGCAGAGCGACATGAG	71
pPROEXHTB 2653 R	GGCCTTAAGCTTTTTAGTACTTCCAACAGCGCTCA	69
pPROEXHTB 2708 R	GGCCTTAAGCTTTTCCCGGCAATGGCGCACAGACA	76
pET32a 2525 R	ATTATAAGCTTAGAACCCCACGTCCAGCACGTG	69
pET32a 2536 R	ATTATAAGCTTAGTCCAGCGAGGCGGCTGCCCT	73
pET32a 2564 R	ATTATAAGCTTACTTGGTGATGAGCGGCAGCACG	69
pET32a 2570 R	ATTATAAGCTTAAAAGAGCGGCGCACACTTGGT	67
pET32a 2592 R	ATTATAAGCTTACCGAGACAGGCGGTACACGGT	69
pET32a 2614 R	ATTATAAGCTTAGTACCTGCAGAGCGACATGAG	65
pET32a 2653 R	ATTATAAGCTTATAGTACTTCCAACAGCGCTCA	63
pET32a 2708 R	ATTATAAGCTTACCCGGCAATGGCGCACAGACA	70

Appendix 2.2. Primer sequences used to amplify RyR1 cDNA for subsequent cloning into bacterial expression vectors. The primer sequences have been numbered referring to the either the first amino acid number in the case of the forward primers or the last amino acid included in the case of the reverse primers. The forward primers could be utilised in all four vector sequences while

the individual reverse primers had to be designed for each to include specific restriction endonuclease sites for cloning into each vector.

2.3 Vector maps used for the expression of the RyR1 HD1

Vector maps of the bacterial expression vectors used to express different RyR1 regions have been summarised below. The names of the vector along with its length in base pairs has presented in the middle of the figure and functionally significant components of the vectors have been represented. All figures were produced using the SnapGene viewer 3.1.2 software.

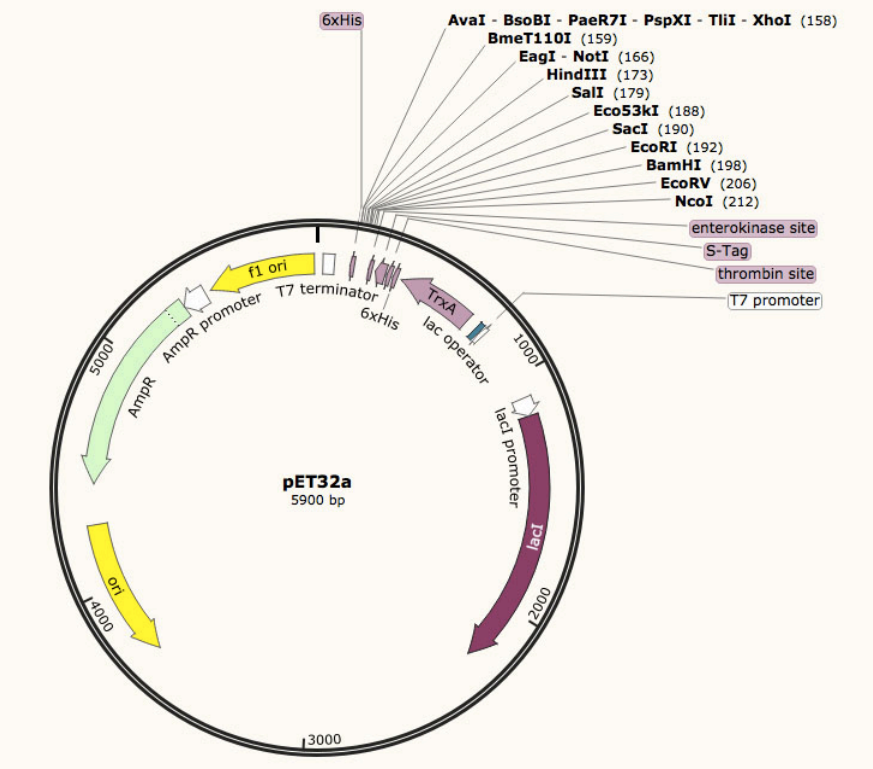

Appendix 2.3.1 Map of the pET32a vector. The vector map was created using the SnapGene viewer 3.1.2 software.

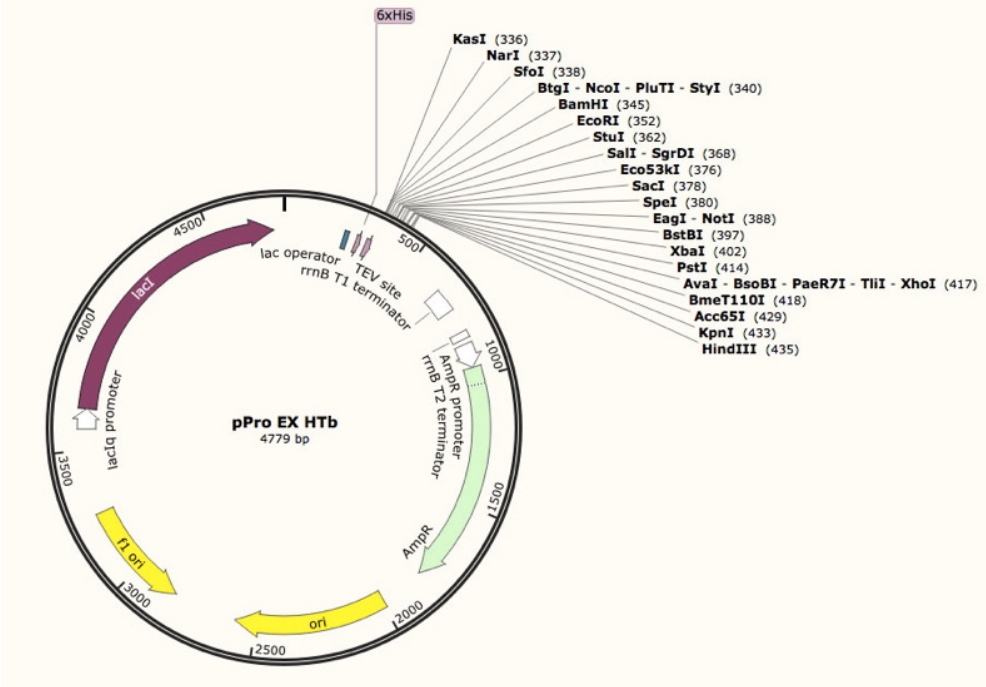

Appendix 2.3.2 Map of the pPro EX Htb vector. The vector map was created using the SnapGene viewer 3.1.2 software.

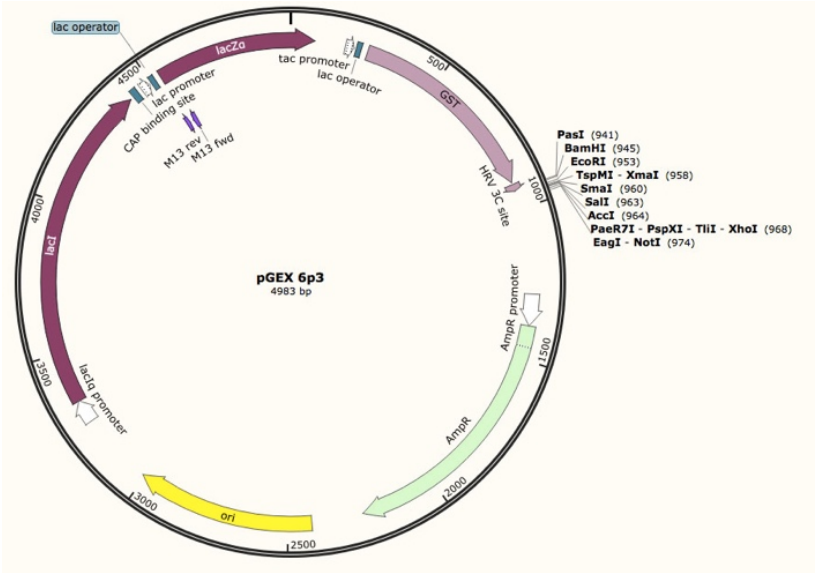

Appendix 2.3.3 Map of the pGEX 6p3 vector. The vector map was created using the SnapGene viewer 3.1.2 software.

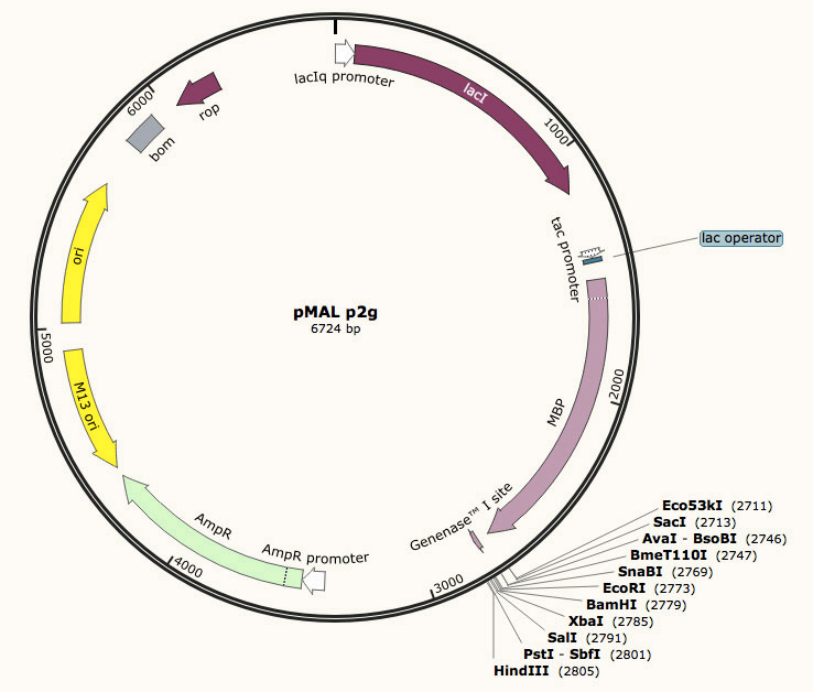

Appendix 2.3.4 Map of the pMAL p2g vector. The vector map was created using the SnapGene viewer 3.1.2 software.

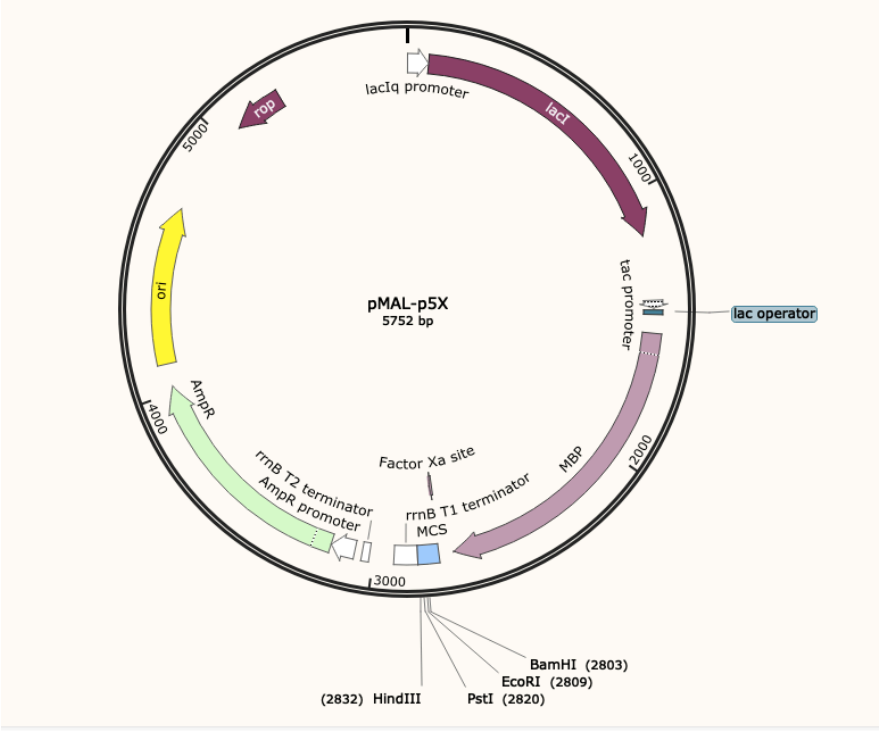

Appendix 2.3.5 Map of the pMAL-p5X vector. The vector map was created using the SnapGene viewer 3.1.2 software.

Appendix 2.4 An example of the cloning of *RYR1* into a bacterial expression vector.

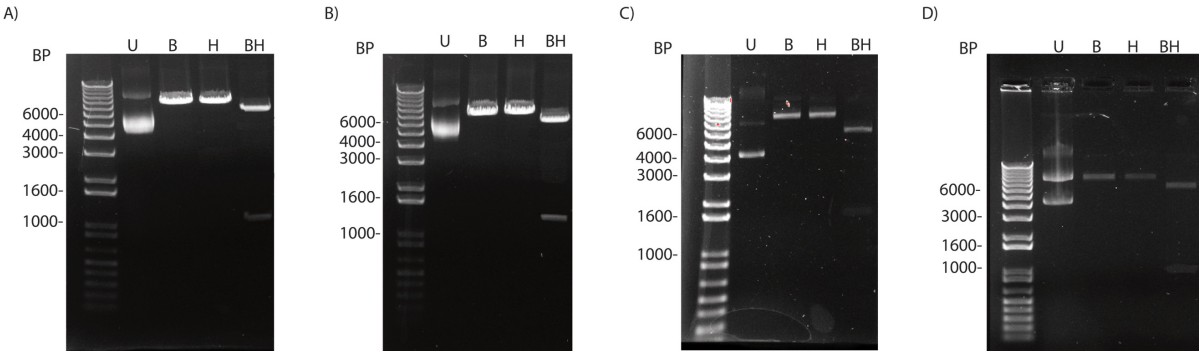

Restriction endonuclease digestion confirming the presence of the *RYR1* cDNA in the pMALp2g expression vector. U, uncut vector DNA. B, vector DNA digested with Bam HI. H, vector DNA digested with Hind III. BH, vector DNA digested with both Bam HI and Hind III. A) Digestion of the *RYR1* nucleotides 6,271-7468 within the pMALp2g vector. B) Digestion of the *RYR1* nucleotides 6,271-7575 within the pMALp2g vector. C) Digestion of the *RYR1* nucleotides 6,271-8065 within the pMALp2g vector. D) Digestion of the *RYR1* nucleotides 6430-7468 within the pMALp2g vector. The 1Kb+ Plus DNA ladder was used to estimate the sizes of DNA. DNA was separated on a 0.7 % agarose gel at 90 mv for one hour and was stained 0.5 µg/mL ethidium bromide and visualised using the image lab 5.1 software.

2.5 Partial purification of soluble RyR1 HD1 from different expression vectors.

2.5.1 Partial purification of RyR1 2091-2490 expressed from the pMALp2g vector.

The recombinant protein RyR1 2091-2490 was shown to be soluble following expression in E.coli BL21 (DE3) and could be partially purified following batch purification using amylose conjugated agarose (appendix 2.5.1.1).

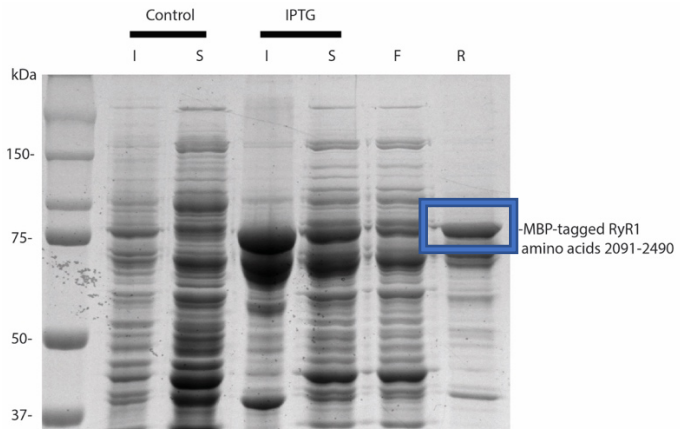

Appendix 2.5.1.1 Example of recombinant expression of RyR1 2091-2490 from the pMALp2g using dextrin amylose conjugated agarose. *E.coli* BL21(DE3) were transformed with the pMALp2g expression containing the cDNA corresponding to the RyR1 amino acids 2091-2490. Control represents a non-induced control, ITPG represents cells that have been exposed to 1 mM IPTG for three hours. I represents the insoluble fraction following cell lysis and S represents the soluble fraction following cell lysis. F represents the soluble fraction collected following batch purification following partial purification using amylose conjugated agarose. R represents proteins bound to the amylose conjugated resin following partial purification. The Precision plus size standard was used to estimate the mass of proteins. Proteins were separated by 10 % SDS PAGE for ninety minutes, proteins were visualised by Coomassie blue staining. The protein subjected to mass spectrometry is boxed in blue.

The identity of the protein thought to correspond to the tagged RyR1 region was confirmed using mass spectrometry (appendix 2.5.1.2)

RyR1 amino acids 2091-2490

```
1901 QEKEDEEKEE EEAAEGEKEE GLEEGLLQMK LPESVKLQMC HLLEYFCDQE
1951 LQHRVESLAA FAERYVDKLQ ANQRSRYGLL IKAFSMTAAE TARRTREFRS
2001 PPQEQINMLL QFKDGTDEED CPLPEEIRQD LLDFHQDLLA HCGIQLDGEE
2051 EEPEEETTLG SRLMSLLEKV RLVKKKEEKP EEERSAEESK PRSLQELVSH
2101 MVVRWAQEDF VQSPELVRAM FSLLHRQYDG LGELLRALPR AYTISPSSVE
2151 DTMSLLECLG QIRSLLIVQM GPQEENLMIQ SIGNIMNNKV FYQHPNLMRA
2201 LGMHETVMEV MVNVLGGGES KEIRFPKMVT SCCRFLCYFC RISRQNQRSM
2251 FDHLSYLLEN SGIGLGMQGS TPLDVAAASV IDNNELALAL QEQDLEKVVS
2301 YLAGCGLQSC PMLVAKGYPD IGWNPCGGER YLDFLRFAVF VNGESVEENA
2351 NVVVRLLIRK PECFGPALRG EGGSGLLAAI EEAIRISEDP ARDGPGIRRD
2401 RRREHFGEEP PEENRVHLGH AIMSFYAALI DLLGRCAPEM HLIQAGKGEA
2451 LRIRAILRSL VPLEDLVGII SLPLQIPTLG KDGALVQPKM SASFVPDHKA
2501 SMVLFLDRVY GIENQDFLLH VLDVGFLPDM RAAASLDTAI FSTTEMALAL
2551 NRYLCLAVLP LITKCAPLFA GTEHRAIMVD SMLHTVYRLS RGRSLTKAQR
2601 DVIEDCLMSL CRYIRPSMLQ HLLRRLVFDV PILNEFAKMP LKLLTNHYER
```

MBP

```
  1 MKIKTGARIL ALSALTTMMF SASALAKIEE GKLVIWINGD KGYNGLAEVG
 51 KKFEKDTGIK VTVEHPDKLE EKFPQVAATG DGPDIIFWAH DRFGGYAQSG
101 LLAEITPDKA FQDKLYPFTW DAVRYNGKLI AYPIAVEALS LIYNKDLLPN
151 PPKTWEEIPA LDKELKAKGK SALMFNLQEP YFTWPLIAAD GGYAFKYENG
201 KYDIKDVGVD NAGAKAGLTF LVDLIKNKHM NADTDYSIAE AAFNKGETAM
251 TINGPWAWSN IDTSKVNYGV TVLPTFKGQP SKPFVGVLSA GINAASPNKE
301 LAKEFLENYL LTDEGLEAVN KDKPLGAVAL KSYEEELAKD PRIAATMENA
351 QKGEIMPNIP QMSAFWYAVR TAVINAASGR QTVDEALKDA QTRITK
```

Appendix 2.5.1.2 Mass spectrometry analysis of the MBP-tagged RyR1 amino acids 2091-2490 expressed from the pMALp2g vector. The amino acids highlighted in red were detected during the mass spectrometry analysis while those in black were not detected. The RyR1 region is represented on the left with the MBP being represented on the right.

The recombinant protein was digested with TEV in doing so separating the MBP tag from the partially purified protein (appendix 2.5.1.3 A)). Initially this was performed with the recombinant protein bound to the amylose conjugated resin. In doing so the MBP tag should remain bound to the resin while the RyR1 region should be released into the supernatant. The identity of the proteins thought to correspond to the RyR1 region and the MBP tag were confirmed by mass spectrometry (figure 2.5.1.3 B). Only a partial digestion took place and interestingly both the $RyR1_{(2091\text{-}2490)}$ and the cleaved MBP tag were detected in both the supernatant and associated with the resin.

A)

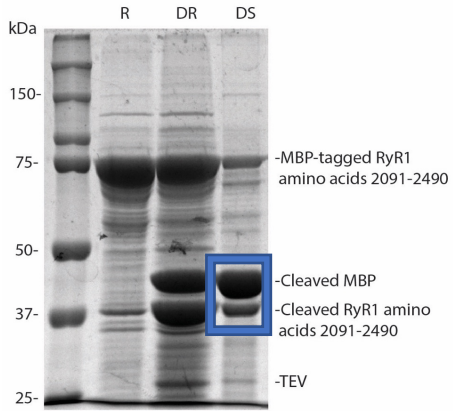

B)

40 kDa
RyR1 amino acids 2091-2490

```
1901 QEKEDEEKEE EEAAEGEKEE GLEEGLLQMK LPESVKLQMC HLLEYFCDQE
1951 LQHRVESLAA FAERYVDKLQ ANQRSRYGLL IKAFSMTAAE TARRTREFRS
2001 PPQEQINMLL QFKDGTDEED CPLPEEIRQD LLDFHQDLLA HCGIQLDGEE
2051 EEPEEETTLG SRLMSLLEKV RLVKKKEEKP EEERSAEESK PRSLQELVSH
2101 MVVRWAQEDF VQSPELVRAM FSLLHRQYDG LGELLRALPR AYTISPSSVE
2151 DTMSLLECLG QIRSLLIVQM GPQEENLMIQ SIGNIMNNKV FYQHPNLMRA
2201 LGMHETVMEV MVNVLGGGES KEIRFPKMVT SCCRFLCYFC RISRQNQRSM
2251 FDHLSYLLEN SGIGLGMQGS TPLDVAAASV IDNNELALAL QEQDLEKVVS
2301 YLAGCGLQSC PMLVARGYPD IGWNPCGGER YLDFLRFAVF VNGESVEENA
2351 NVVVRLLIRK PECFGPALRG EGGSGLLAAI EEAIRISEDP ARDGPGIRRD
2401 RRREHFGEEP PEENRVHLGH AIMSFYAALI DLLGRCAPEM HLIQAGKGEA
2451 LRIRAILRSL VPLEDLVGII SLPLQIPTLG KDGALVQPKM SASFVPDHKA
2501 SMVLFLDRVY GIENQDFLLH VLDVGFLPDM RAAASLDTAI FSITEMALAL
2551 NRYLCLAVLP LITKCAPLFA GIEHRAIMVD SMLHTVYRLS RGRSLIKAQR
2601 DVIEDCLMSL CRYIRPSMLQ HLLRRLVFDV PILNEFAKMP LKLLTNHYER
```

44 kDa
MBP

```
  1 MKIKTGARIL ALSALTTMMF SASALAKIEE GKLVIWINGD KGYNGLAEVG
 51 KKFEKDTGIK VTVEHPDKLE EKFPQVAATG DGPDIIFWAH DRFGGYAQSG
101 LLAEITPDKA FQDKLYPFTW DAVRYNGKLI AYPIAVEALS LIYNKDLLPN
151 PPKTWEEIPA LDKELKAKGK SALMFNLQEP YFTWPLIAAD GGYAFKYENG
201 KYDIKDVGVD NAGAKAGLTF LVDLIKNKHM NADTDYSIAE AAFNKGETAM
251 TINGPWAWSN IDTSKVNYGV TVLPTFKGQP SKPFVGVLSA GINAASPNKE
301 LAKEFLENYL LTDEGLEAVN KDKPLGAVAL KSYEEELAKD PRIAATMENA
351 QKGEIMPNIP QMSAFWYAVR TAVINAASGR QTVDEALKDA QTRITK
```

Appendix 2.5.1.3 TEV digestion of the RyR1 amino acids expressed from the pMALp2g vector with the fusion protein bound to the amylose conjugated resin. A) R, represents protein bound to the amylose resin following batch purification. DR represents the proteins still bound to the resin following digestion. DS represents the supernatant collected following TEV digestion. The Precision plus size standard was used to estimate the mass of proteins. Proteins were separated by 10 % acrylamide gel electrophoresis at 120 mV for ninety minutes and were visualised by Coomassie blue staining. The proteins subjected to mass spectrometry were boxed in blue. B) Mass spectrometry confirming the identity of proteins following TEV digestion. The size of the bands in each case have been identified by approximate size the left panel refers to the 40 kDa protein the right panel refers to the 44 KDa protein.

As the RyR1 region and the MBP tag could not be efficiently separated from each other by on gel TEV digestion the digestion was attempted following elution from the amylose conjugated resin (appendix 2.5.1.4 A)). Again, only a partial digestion could be achieved. Mass spectrometry was used to confirm the identity of each protein following digestion (appendix 2.5.1.4 B))

A)

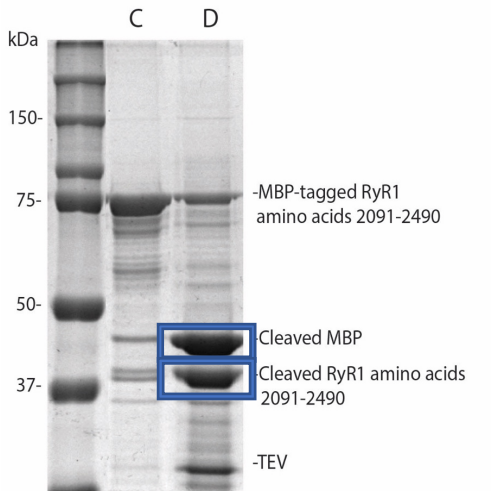

B)

40 kDa
RyR1 amino acids 2091-2490

```
1901 QEKEDEEKEE EEAAEGEKEE GLEEGLLQMK LPESVKLQMC HLLEYFCDQE
1951 LQHRVESLAA FAERYVDKLQ ANQRSRYGLL IKAFSMTAAE TARRTREFRS
2001 PPQEQINMLL QFKDGTDEED CPLPEEIRQD LLDFHQDLLA HCGIQLDGEE
2051 EEPEEETTLG SRLMSLLEKV RLVKKKEEKP EEERSAEESK PRSLQELVSH
2101 MVVRWAQEDF VQSPELVRAM FSLLHRQYDG LGELLRALPR AYTISPSSVE
2151 DTMSLLECLG QIRSLLIVQM GPQEENLMIQ SIGNIMNNKV FYQHPNLMRA
2201 LGMHETVMEV MVNVLGGGES KEIRFPKMVT SCCRFLCYFC RISRQNQRSM
2251 FDHLSYLLEN SGIGLGMQGS TPLDVAAASV IDNNELALAL QEQDLEKVVS
2301 YLAGCGLQSC PMLVAKGYPD IGWNPCGGER YLDFLRFAVF VNGESVEENA
2351 NVVVRLLIRK PECFGPALRG EGGSGLLAAI EEAIRISEDP ARDGPGIRRD
2401 RRREHFGEEP PEENRVHLGH AIMSFYAALI DLLGRCAPEM HLIQAGKGEA
2451 LRIRAILRSL VPLEDLVGII SLPLQIPTLG KDGALVQPKM SASFVPDHKA
2501 SMVLFLDRVY GIENQDFLLH VLDVGFLPDM RAAASLDTAT FSTTEMALAL
2551 NRYLCLAVLP LITKCAPLFA GTEHRAIMVD SMLHTVYRLS RGRSLITKAQR
2601 DVIEDCLMSL CRYIRPSMLQ HLLRRLVFDV PILNEFAKMP LKLLTNHYER
```

44 kDa
MBP

```
  1 MKIKTGARIL ALSALTTMMF SASALAKIEE GKLVIWINGD KGYNGLAEVG
 51 KKFEKDTGIK VTVEHPDKLE EKFPQVAATG DGPDIIFWAH DRFGGYAQSG
101 LLAEITPDKA FQDKLYPFTW DAVRYNGKLI AYPIAVEALS LIYNKDLLPN
151 PPKTWEEIPA LDKELKAKGK SALMFNLQEP YFTWPLIAAD GGYAFKYENG
201 KYDIKDVGVD NAGAKAGLTF LVDLIKNKHM NADTDYSIAE AAFNKGETAM
251 TINGPWAWSN IDTSKVNYGV TVLPTFKGQP SKPFVGVLSA GINAASPNKE
301 LAKEFLENYL LTDEGLEAVN KDKPLGAVAL KSYEEELAKD PRIAATMENA
351 QKGEIMPNIP QMSAFWYAVR TAVINAASGR QTVDEALKDA QTRITK
```

appendix 2.5.1.4 TEV digestion of the MBP-tagged RyR1 region after elution from the amylose conjugated amylose resin. A) C represents the non-digested partially purified RyR1 region. D represents the partially purified RyR1 region following TEV digestion. The Precision plus size standard was used to estimate the mass of proteins. Proteins were separated by 10 % acrylamide gel electrophoresis at 120 mV for ninety minutes and were visualised by Coomassie blue staining. The proteins subjected to mass spectrometry were boxed in blue. B) Mass spectrometry analysis of the MBP tagged RyR1 fusion proteins expressed from the pMALp2g vector following TEV digestion. The amino acids detected during mass spectrometry analysis are represented in red. Mass spectrometry confirming the identity of proteins following TEV digestion. The size of the bands in each case have been identified by approximate size the left panel refers to the 40 kDa protein the right panel refers to the 44 KDa protein.

After TEV digestion, a Ni^{+} conjugated agarose resin was used to remove both the $His_{(6)}$ tagged MBP and $His_{(6)}$ tagged TEV from solution, further purifying the $RyR1_{(2091\text{-}2490)}$. Following the purification, the resin was pelleted and the supernatant was collected (appendix 2.5.1.5).

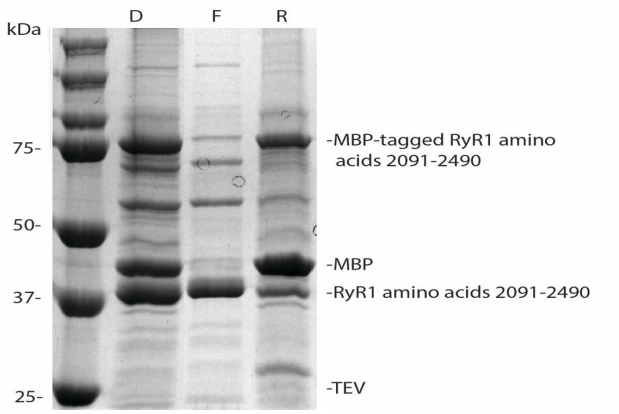

Appendix 2.5.1.5 partial purification of RyR1(2091-2490) using Ni^{+} conjugated agarose. D) The TEV digestion prior to purification. F) The flow through collected following purification. R) The resin following purification. The Precision plus size standard was used to estimate the mass of proteins. Proteins were separated by 10 % acrylamide gel electrophoresis at 120 mV for ninety minutes and were visualised by Coomassie blue staining.

Both the MBP and TEV proteins were able to form an interaction with the Ni agarose. $RyR1_{(2091\text{-}2490)}$ in both the non-digested and digested form was visible in the supernatant and bound to the resin. Indicating the Ni+ resin can be to an extent used in the purification of the protein.

2.5.2 Partial purification of RyR1 2091-2708 expressed from the pMALp2g vector

An amylose conjugated agarose resin was used to partially purify the MBP-tagged RyR1 2091-2708 the protein could be enriched from an *E.coli* BL21(DE3) cell lysate (appendix 2.5.2.1 A)). The identity of the protein thought to correspond to the MBP-tagged RyR1 region was confirmed using mass spectrometry (appendix 2.5.2.2 B)).

A)

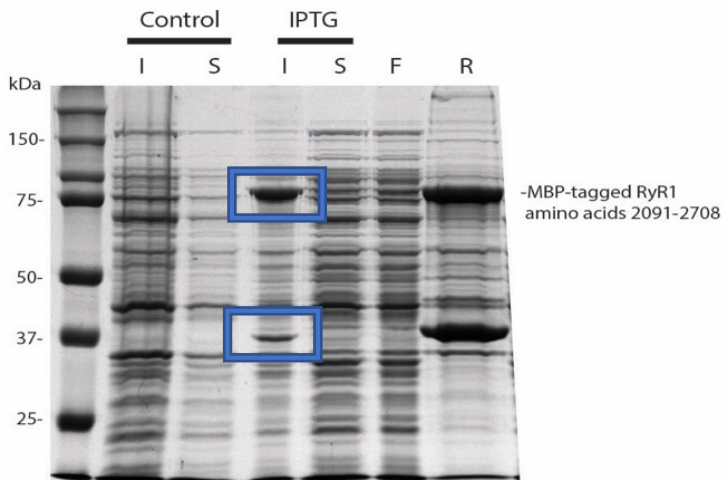

B)

RyR1 amino acids 2091-2708

```
1901 QEKEDEEKEE EEAAEGEKEE GLEEGLLQMK LPESVKLQMC HLLEYFCDQE
1951 LQHRVESLAA FAERYVDKLQ ANQRSRYGLL IKAFSMTAAE TARRTREFRS
2001 PPQEQINMLL QFKDGTDEED CPLPEEIRQD LLDFHQDLLA HCGIQLDGEE
2051 EEPEEETTLG SRLMSLLEKV RLVKKKEEKP EEERSAEESK PRSLQELVSH
2101 MVVRWAQEDF VQSPELVRAM FSLLHRQYDG LGELLRALPR AYTISPSSVE
2151 DTMSLLECLG QIRSLLIVQM GPQEENLMIQ SIGNIMNNKV FYQHPNLMRA
2201 LGMHETVMEV MVNVLGGGES KEIRFPKMVT SCCRFLCYFC RISRQNQRSM
2251 FDHLSYLLEN SGIGLGMQGS TPLDVAAASV IDNNELALAL QEQDLEKVVS
2301 YLAGCGLQSC PMLVAKGYPD IGWNPCGGER YLDFLRFAVF VNGESVEENA
2351 NVVVRLLIRK PECFGPALRG EGGSGLLAAI EEAIRISEDP ARDGPGIRRD
2401 RRREHFGEEP PEENRVHLGH AIMSFYAALI DLLGRCAPEM HLIQAGKGEA
2451 LRIRAILRSL VPLEDLVGII SLPLQIPTLG KDGALVQPKM SASFVPDHKA
2501 SMVLFLDRVY GIENQDFLLH VLDVGFLPDM RAAASLDTAI FSTTEMALAL
2551 NRYLCLAVLP LITKCAPLFA GTEHRAIMVD SMLHTVYRLS RGRSLTKAQR
2601 DVIEDCLMSL CRYIRPSMLQ HLLRRLVFDV PILNEFAKMP LKLLTNHYER
```

MBP

```
  1 MKIKTGARIL ALSALTTMMF SASALAKIEE GKLVIWINGD KGYNGLAEVG
 51 KKFEKDTGIK VTVEHPDKLE EKFPQVAATG DGPDIIFWAH DRFGGYAQSG
101 LLAEITPDKA FQDKLYPFTW DAVRYNGKLI AYPIAVEALS LIYNKDLLPN
151 PPKTWEEIPA LDKELKAKGK SALMFNLQEP YFTWPLIAAD GGYAFKYENG
201 KYDIKDVGVD NAGAKAGLTF LVDLIKNKHM NADTDYSIAE AAFNKGETAM
251 TINGPWAWSN IDTSKVNYGV TVLPTFKGQP SKPFVGVLSA GINAASPNKE
301 LAKEFLENYL LTDEGLEAVN KDKPLGAVAL KSYEEELAKD PRIAATMENA
351 QKGEIMPNIP QMSAFWYAVR TAVINAASGR QTVDEALKDA QTRITK
```

Appendix 2.5.2.1 Batch purification of the MBP-tagged RyR1 amino acids 2091-2708 expressed from the pMALp2g vector. A) Gel summarising the expression and partial purification of RyR1$_{(2091-2708)}$. Control represents cells that have not been exposed to IPTG. IPTG represents cells that have been exposed to IPTG. I represents the insoluble fraction following cell lysis. S, represents the soluble fraction following cell lysis. F, the flow through following batch purification. R, proteins bound the amylose conjugated agarose resin following batch purification. The Precision plus size standard was used to estimate the mass of proteins. Proteins that were expressed following exposure to IPTG were circled in blue. Proteins were separated by 10 % acrylamide gel electrophoresis at 120 mV for ninety minutes and were visualised by Coomassie blue staining B) Mass spectrometry analysis of the 90 kDa protein produced following the expression of MBP-tagged RyR1 amino acids 2091-2708. Amino acids detected were highlighted in red.

The partially purified RyR1 region was subjected to digestion by TEV while bound to the amylose conjugated resin. A partial digestion was detected, following digestion the RyR1 region and MBP have approximately the same molecular mass, mass spectrometry was used to determine the identity of the protein thought to correspond to RyR1 region (appendix

2.5.2.2). In this case both the RyR1 region and the MBP were detected indicating that both proteins were released from the resin following digestion.

A)

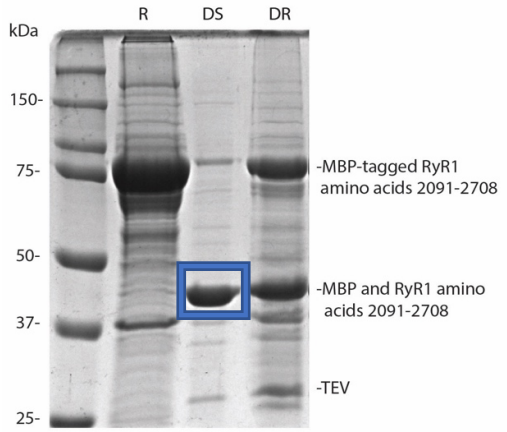

B)

RyR1 amino acids 2091-2708

```
1901 QEKEDEEKEE EEAAEGEKEE GLEEGLLQMK LPESVKLQMC HLLEYFCDQE
1951 LQHRVESLAA FAERYVDKLQ ANQRSRYGLL IKAFSMTAAE TARRTREFRS
2001 PPQEQINMLL QFKDGTDEED CPLPEEIRQD LLDFHQDLLA HCGIQLDGEE
2051 EEPEEETTLG SRLMSLLEKV RLVKKKEEKP EEERSAEESK PRSLQELVSH
2101 MVVRWAQEDF VQSPELVRAM FSLLHRQYDG LGELLRALPR AYTISPSSVE
2151 DTMSLLECLG QIRSLLIVQM GPQEENLMIQ SIGNIMNNKV FYQHPNLMRA
2201 LGMHETVMEV MVNVLGGGES KEIRFPKMVT SCCRFLCYFC RISRQNQRSM
2251 FDHLSYLLEN SGIGLGMQGS TPLDVAAASV IDNNELALAL QEQDLEKVVS
2301 YLAGCGLQSC PMLVARGYPD IGWNPCGGER YLDFLRFAVF VNGESVEENA
2351 NVVVRLLIRK PECFGPALRG EGGSGLLAAI EEAIRISEDP ARDGPGIRRD
2401 RRREHFGEEP PEENRVHLGH AIMSFYAALI DLLGRCAPEM HLIQAGRGEA
2451 LRIRAILRSL VPLEDLVGII SLPLQIPTLG KDGALVQPKM SASFVPDHKA
2501 SMVLFLDRVY GIENQDFLLH VLDVGFLPDM RAAASLDTAT FSTTEMALAL
2551 NRYLCLAVLP LITKCAPLFA GTEHRAIMVD SMLHTVYRLS RGRSLTKAQR
```

MBP

```
  1 MKIKTGARIL ALSALTTMMF SASALAKIEE GKLVIWINGD KGYNGLAEVG
 51 KKFEKDTGIK VTVEHPDKLE EKFPQVAATG DGPDIIFWAH DRFGGYAQSG
101 LLAEITPDKA FQDKLYPFTW DAVRYNGKLI AYPIAVEALS LIYNKDLLPN
151 PPKTWEEIPA LDKELKAKGK SALMFNLQEP YFTWPLIAAD GGYAFKYENG
201 KYDIKDVGVD NAGAKAGLTF LVDLIKNKHM NADTDYSIAE AAFNKGETAM
251 TINGPWAWSN IDTSKVNYGV TVLPTFKGQP SKPFVGVLSA GINAASPNKE
301 LAKEFLENYL LTDEGLEAVN KDKPLGAVAL KSYEEELAKD PRIAATMENA
351 QKGEIMPNIP QMSAFWYAVR TAVINAASGR QTVDEALKDA QTRITK
```

Appendix 2.5.2.2 TEV digestion of the RyR1 amino acids 2091-2708 expressed from the pMALp2g vector with the fusion protein bound to the amylose conjugated resin. A) Gel summarising the TEV digestion of $RyR1_{(2091-2708)}$. R represents the amylose conjugated agarose resin following batch purification. DS, represents the supernatant collected following TEV digestion. DR represents the proteins still bound to the resin following digestion. The Precision plus size standard was used to estimate the mass of proteins. Proteins that were expressed following exposure to IPTG were circled in blue. Proteins were separated by 10 % acrylamide gel electrophoresis at 120 mV for ninety minutes and were visualised by Coomassie blue staining. The proteins subjected to mass spectrometry were boxed in blue. B) Mass spectrometry analysis of the MBP tagged RyR1 fusion proteins expressed from the pMALp2g vector following TEV digestion with the fusion protein bound to the amylose resin. The amino acids detected during mass spectrometry analysis are represented in red. The amino acids corresponding to the RyR1 region are presented on the left and MBP on the right.

As the RyR1 region and the MBP tag could not be efficiently separated from each other following digestion so the digestion was repeated in this case the RyR1 region was eluted

from the resin and then subjected to digestion by TEV. Once again only a partial digestion could be performed, and the identity of the protein thought to correspond to RyR1 2091-2708 was confirmed by mass spectrometry (appendix 2.5.2.3).

A)

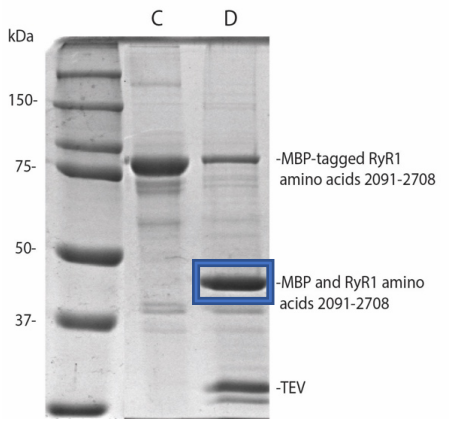

B)

RyR1 amino acids 2091-2708

```
1901 QEKEDEEKEE EEAAEGEKEE GLEEGLLQMK LPESVKLQMC HLLEYFCDQE
1951 LQHRVESLAA FAERYVDKLQ ANQRSRYGLL IKAFSMTAAE TARRTREFRS
2001 PPQEQINMLL QFKDGTDEED CPLPEEIRQD LLDFHQDLLA HCGIQLDGEE
2051 EEPEEETTLG SRLMSLLEKV RLVKKKEEKP EEERSAEESK PRSLQELVSH
2101 MVVRWAQEDF VQSPELVRAM FSLLHRQYDG LGELLRALPR AYTISPSSVE
2151 DTMSLLECLG QIRSLLIVQM GPQEENLMIQ SIGNIMNNKV FYQHPNLMRA
2201 LGMHETVMEV MVNVLGGGES KEIRFPKMVT SCCRFLCYFC RISRQNQRSM
2251 FDHLSYLLEN SGIGLGMQGS TPLDVAAASV IDNNELALAL QEQDLEKVVS
2301 YLAGCGLQSC PMLVARGYPD IGWNPCGGER YLDFLRFAVF VNGESVEENA
2351 NVVVRLLIRK PECFGPALRG EGGSGLLAAI EEAIRISEDP ARDGPGIRRD
2401 RRREHFGEEP PEENRVHLGH AIMSFYAALI DLLGRCAPEM HLIQAGKGEA
2451 LRIRAILRSL VPLEDLVGII SLPLQIPTLG KDGALVQPKM SASFVPDHKA
2501 SMVLFLDRVY GIENQDFLLH VLDVGFLPDM RAAASLDTAT FSTTEMALAL
2551 NRYLCLAVLP LITKCAPLFA GTEHRAIMVD SMLHTVYRLS RGRSLIKAQR
```

MBP

```
  1 MKIKTGARIL ALSALTTMMF SASALAKIEE GKLVIWINGD KGYNGLAEVG
 51 KKFEKDTGIK VTVEHPDKLE EKFPQVAATG DGPDIIFWAH DRFGGYAQSG
101 LLAEITPDKA FQDKLYPFTW DAVRYNGKLI AYPIAVEALS LIYNKDLLPN
151 PPKTWEEIPA LDKELKAKGK SALMFNLQEP YFTWPLIAAD GGYAFKYENG
201 KYDIKDVGVD NAGAKAGLTF LVDLIKNKHM NADTDYSIAE AAFNKGETAM
251 TINGPWAWSN IDTSKVNYGV TVLPTFKGQP SKPFVGVLSA GINAASPNKE
301 LAKEFLENYL LTDEGLEAVN KDKPLGAVAL KSYEEELAKD PRIAATMENA
351 QKGEIMPNIP QMSAFWYAVR TAVINAASGR QTVDEALKDA QTRITK
```

Figure 2.5.2.3 TEV digestion of the MBP-tagged RyR1$_{(2091\text{-}2708)}$ following elution from the amylose resin. A) Gel summarising the TEV digestion of RyR1$_{(2091\text{-}2708)}$. C represents the protein prior to digestion. D represents the protein fraction following digestion. The Precision plus size standard was used to estimate the mass of proteins. The proteins subjected to mass spectrometry were boxed in blue. Proteins were separated by 10 % acrylamide gel electrophoresis at 120 mV for ninety minutes and were visualised by Coomassie blue staining. B) Mass spectrometry confirming the identity of the protein produced following TEV digestion of the MBP-tagged RyR1 amino acids 2091-2708. The amino acids detected during mass spectrometry analysis are represented in red.

Appendix 2.5.3 Partial purification of RyR1 2091-2490 expressed from the pMALp5x vector.

RyR1 2091-2490 could also be partially purified from an *E. coli* BL21(DE3) cell lysate following expression of the pMALp5x vector. The identity of the protein was confirmed by mass spectrometry (appendix 2.5.3.1).

A)

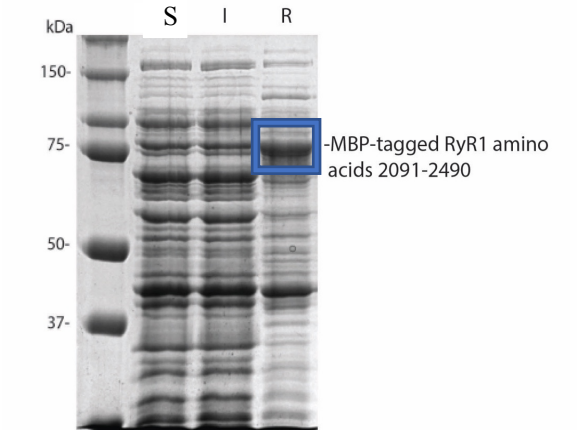

B)

RyR1 amino acids 2091-2490

```
1901 QEKEDEEKEE EEAAEGEKEE GLEEGLLQMK LPESVKLQMC HLLEYFCDQE
1951 LQHRVESLAA FAERYVDKLQ ANQRSRYGLL IKAFSMTAAE TARRTREFRS
2001 PPQEQINMLL QFKDGTDEED CPLPEEIRQD LLDFHQDLLA HCGIQLDGEE
2051 EEPEEETTLG SRLMSLLEKV RLVKKKEEKP EEERSAEESK PRSLQELVSH
2101 MVVRWAQEDF VQSPELVRAM FSLLHRQYDG LGELLRALPR AYTISPSSVE
2151 DTMSLLECLG QIRSLLIVQM GPQEENLMIQ SIGNIMNNKV FYQHPNLMRA
2201 LGMHETVMEV MVNVLGGGES KEIRFPFMVT SCCRFLCYFC RISRQNQRSM
2251 FDHLSYLLEN SGIGLGMQGS TPLDVAAASV IDNNELALAL QEQDLEKVVS
2301 YLAGCGLQSC PMLVARGYPD IGWNPCGGER YLDFLRFAVF VNGESVEENA
2351 NVVVRLLIRK PECFGPALRG EGGSGLLAAI EEAIRISEDP ARDGPGIRRD
2401 RRREHFGEEP PEENRVHLGH AIMSFYAALI DLLGRCAPEM HLIQAGKGEA
2451 LRIRAILRSL VPLEDLVGII SLPLQIPTLG KDGALVQPKM SASFVPDHKA
2501 SMVLFLDRVY GIENQDFLLH VLDVGFLPDM RAAASLDTAT FSTTEMALAL
2551 NRYLCLAVLP LITKCAPLFA GIEHRAIMVD SMLHTVYRLS RGRSLIKAQR
2601 DVIEDCLMSL CRYIRPSMLQ HLLRRLVFDV PILNEFAKMP LKLLTNHYER
```

MBP

```
  1 MKIKTGARIL ALSALTTMMF SASALAKIEE GKLVIWINGD KGYNGLAEVG
 51 KKFEKDTGIK VTVEHPDKLE EKFPQVAATG DGPDIIFWAH DRFGGYAQSG
101 LLAEITPDKA FQDKLYPFTW DAVRYNGKLI AYPIAVEALS LIYNKDLLPN
151 PPKTWEEIPA LDKELKAKGK SALMFNLQEP YFTWPLIAAD GGYAFKYENG
201 KYDIKDVGVD NAGAKAGLTF LVDLIKNKHM NADTDYSIAE AAFNKGETAM
251 TINGPWAWSN IDTSKVNYGV TVLPTFKGQP SKPFVGVLSA GINAASPNKE
301 LAKEFLENYL LTDEGLEAVN KDKPLGAVAL KSYEEELAKD PRIAATMENA
351 QKGEIMPNIP QMSAFWYAVR TAVINAASGR QTVDEALKDA QTRITK
```

Appendix 2.5.3.1 the expression of the RyR1 amino acids 2091-2490 from the pMALp5x vector. A) gel summarising the expression and partial purification of $RyR_{(2091-2490)}$ using amylose conjugated agarose. S represents soluble protein following the lysis of non-induced *E. coli*. I represents soluble protein following the lysis of induced *E. coli*. R represents the amylose conjugated agarose resin following the partial purification of the MBP-tagged RyR1 region. The Precision plus size standard was used to estimate the mass of proteins. Proteins that were expressed following exposure to IPTG were circled in blue. Proteins were separated by 10 % acrylamide gel electrophoresis at 120 mV for ninety minutes and were visualised by Coomassie blue staining B) Mass spectrometry analysis of the MBP tagged RyR1 fusion proteins expressed from the pMALp5x vector following TEV digestion. The amino acids detected during mass spectrometry analysis are represented in red. B) Mass spectrometry confirming the identity of the MBP-tagged RyR1(2091-2490). Matched amino acid sequences representing the RyR1 region have been presented on the left and amino acid sequences representing the MBP tag are presented on the right. The amino acids detected during mass spectrometry analysis are represented in red.

The tagged RyR1 region was then subjected to digestion by the protease factor Xa while bound to the amylose conjugated agarose resin. Where the MBP tag should remain bound to the resin and the RyR1 region should be released into the supernatant (appendix 2.5.3.2). Mass spectrometry was used to determine the identity of the protein thought to correspond to the MBP tag and RyR1 2091-2490. Only the MBP tag was detected, there were no sequence reads corresponding to the RyR1 region.

A)

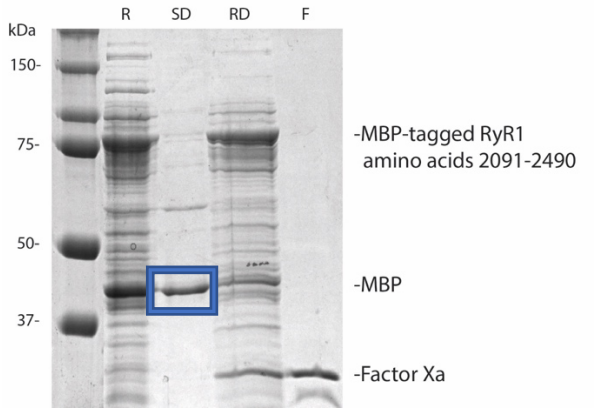

B)

```
  1 MKIKTGARIL ALSALTTMMF SASALAKIEE GKLVIWINGD KGYNGLAEVG
 51 KKFEKDTGIK VTVEHPDKLE EKFPQVAATG DGPDIIFWAH DRFGGYAQSG
101 LLAEITPDKA FQDKLYPFTW DAVRYNGKLI AYPIAVEALS LIYNKDLLPN
151 PPKTWEEIPA LDKELKAKGK SALMFNLQEP YFTWPLIAAD GGYAFKYENG
201 KYDIKDVGVD NAGAKAGLTF LVDLIKNKHM NADTDYSIAE AAFNKGETAM
251 TINGPWAWSN IDTSKVNYGV TVLPTFKGQP SKPFVGVLSA GINAASPNKE
301 LAKEFLENYL LTDEGLEAVN KDKPLGAVAL KSYEEELAKD PRIAATMENA
351 QKGEIMPNIP QMSAFWYAVR TAVINAASGR QTVDEALKDA QTRITK
```

Appendix 2.5.3.2 Factor Xa digestion of the MBP-tagged RyR1 amino acids 2091-2490 expressed from the pMALp5x vector bound to the amylose resin. A) gel summarising the Factor Xa digestion $RyR_{(2091-2490)}$ while bound to the amylose conjugated agarose resin. R represents the amylose resin prior to digestion. SD represents supernatnant following digestion. RD represents resin following digestion. F is a factor Xa control. The Precision plus size standard was used to estimate the mass of proteins. Proteins were separated by 10 % acrylamide gel electrophoresis at 120 mV for ninety minutes and were visualised by Coomassie blue staining. The proteins subjected to mass spectrometry were boxed in blue. B) Mass spectrometry analysis of the protein thought to correspond to the RyR1 amino acids 2091-2490 following on resin digestion by factor Xa. The amino acids detected during analysis are highlighted in red.

As the RyR1 region could not be detected following on gel digestion the protein was eluted from the column and was then subjected to digestion by factor Xa (appendix 2.5.3.3 A). The identity of the protein thought to correspond to the MBP tag and RyR1 2091-2490 was confirmed by mass spectrometry. In this case both proteins were detected.

A)

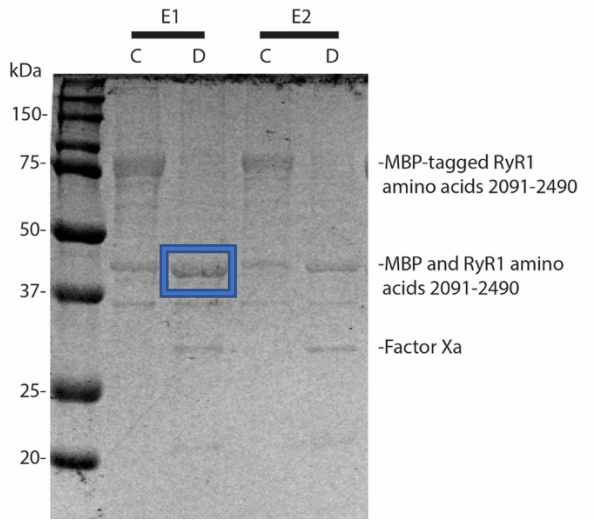

B)

RyR1 amino acids 2091-2490

```
1901 QEKEDEEKEE EEAAEGEKEE GLEEGLLQMK LPESVKLQMC HLLEYFCDQE
1951 LQHRVESLAA FAERYVDKLQ ANQRSRYGLL IKAFSMTAAE TARRTREFRS
2001 PPQEQINMLL QFKDGTDEED CPLPEEIRQD LLDFHQDLLA HCGIQLDGEE
2051 EEPEEETTLG SRLMSLLEKV RLVKKKEEKP EEERSAEESK PRSLQELVSH
2101 MVVRWAQEDF VQSPELVRAM FSLLHRQYDG LGELLRALPR AYTISPSSVE
2151 DTMSLLECLG QIRSLLIVQM GPQEENLMIQ SIGNIMNNKV FYQHPNLMRA
2201 LGMHETVMEV MVNVLGGGES KEIRFPKMVT SCCRFLCYFC RISRQNQRSM
2251 FDHLSYLLEN SGIGLGMQGS TPLDVAAASV IDNNELALAL QEQDLEKVVS
2301 YLAGCGLQSC PMLVARGYPD IGWNPCGGER YLDFLRFAVF VNGESVEENA
2351 NVVVRLLIRK PECFGPALRG EGGSGLLAAI EEAIRISEDP ARDGPGIRRD
2401 RRREHPGEEP PEENRVHLGH AIMSFYAALI DLLGRCAPEM HLIQAGRGEA
2451 LRIRAILRSL VPLEDLVGII SLPLQIPTLG KDGALVQPKM SASFVPDHKA
2501 SMVLFLDRVY GIENQDFLLH VLDVGFLPDM RAAASLDTAI FSTTEMALAL
2551 NRYLCLAVLP LITKCAPLFA GTEHRAIMVD SMLHTVYRLS RGRSLTKAQR
2601 DVIEDCLMSL CRYIRPSMLQ HLLRRLVFDV PILNEFAKMP LKLLTNHYER
2651 CWKYYCLPTG WANFGVTSEE ELHLTRKLFW GIFDSLAHKK YDPELYRMAM
2701 PCLCAIAGAL PPDYVDASYS SKAEKKATVD AEGNFDPRPV ETLNVIIPEK
```

MBP

```
  1 MKIKTGARIL ALSALTTMMF SASALAKIEE GKLVIWINGD KGYNGLAEVG
 51 KKFEKDTGIK VTVEHPDKLE EKFPQVAATG DGPDIIFWAH DRFGGYAQSG
101 LLAEITPDKA FQDKLYPFTW DAVRYNGKLI AYPIAVEALS LIYNKDLLPN
151 PPKTWEEIPA LDKELKAKGK SALMFNLQEP YFTWPLIAAD GGYAFKYENG
201 KYDIKDVGVD NAGAKAGLTF LVDLIKNKHM NADTDYSIAE AAFNKGETAM
251 TINGPWAWSN IDTSKVNYGV TVLPTFKGQP SKPFVGVLSA GINAASPNKE
301 LAKEFLENYL LTDEGLEAVN KDKPLGAVAL KSYEEELAKD PRIAATMENA
351 QKGEIMPNIP QMSAFWYAVR TAVINAASGR QTVDEALKDA QTRITK
```

Appendix 2.5.3.3 Factor Xa digestion of the RyR1$_{(2901-2490)}$ expressed from the pMALp5x vector following elution from the amylose conjugated agarose resin. A) Gel summarising the Factor Xa digestion of RyR1$_{(2901-2490)}$. E1 and E2 represent separate eluted fractions. C corresponds to the protein fraction prior to digestion. D represents the protein fraction following factor Xa digestion. The Precision plus size standard was used to estimate the mass of proteins. Proteins were separated by 10 % acrylamide gel electrophoresis at 120 mV for ninety minutes and were visualised by Coomassie blue staining. The proteins subjected to mass spectrometry were boxed in blue. B) Mass spectrometry analysis of the MBP-tagged RyR1 amino acids 2091-2490 following factor Xa digestion. The amino acids detected during mass spectrometry analysis are highlighted in red. The RyR1 amino acid sequence is represented on the left with MBP being represented on the right.

2.5.4 Partial purification of RyR1 2091-2490 expressed from pGEX6p3

RyR1 2091-2490 was only marginally soluble when expressed from the pGEX6p3 vector. Only a small amount could be enriched following purification utilising a glutathione conjugated sepharose (appendix 2.5.4.1 A). The identity of this protein was confirmed by mass spectrometry (appendix 2.5.4.1 B)). Only three unique sequence reads could be detected for the RyR1 region which likely a consequence of the small amount of the protein subjected to mass spectrometry.

A)

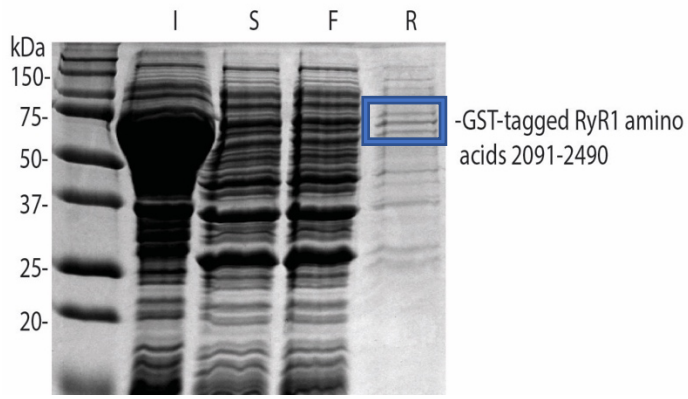

B)

RyR1 amino acids 2091-2490

2001	PPQUQINMLL	GFKDGTDEED	CPLPEEIRQD	LLDFHQDLLA	HCGIQLDGEE
2051	EEPEEETTLG	SRLMSLLEKV	RLVKKKEEKP	EEERSAEESK	PRSLQELVSH
2101	MVVRWAQEDF	VQSPELVRAM	FSLLHRQYDG	LGELLRALPR	AYTISPSSVE
2151	DTMSLLECLG	QIRSLLIVQM	GPQEENLMIQ	SIGNIMNNKV	FYQHPNLMRA
2201	LGMHETVMEV	MVNVLGGGES	KEIRFPKMVT	SCCRFLCYFC	RISRQNQRSM
2251	FDHLSYLLEN	SGIGLGMQGS	TPLDVAAASV	IDNNELALAL	QEQDLEKVVS
2301	YLAGCGLQSC	PMLVAKGYPD	IGWNPCGGER	YLDFLRFAVF	VNGESVEENA
2351	NVVVRLLIRK	PECFGPALRG	EGGSGLLAAI	EEAIRISEDP	ARDGPGIRRD
2401	RRREHFGEEP	PEENRVHLGH	AIMSFYAALI	DLLGRCAPEM	HLIQAGKGEA
2451	LRIRAILRSL	VPLEDLVGII	SLPLQIPTLG	KDGALVQPKM	SASFVPDHKA
2501	SMVLFLDRVY	GIENQDFLLH	VLDVGFLDPM	RAAASLDTAT	FSTTEMALAL
2551	NRYLCLAVLP	LITKCAPLFA	GTEHRAIMVD	SMLHTVYRLS	RGRSLTKAQR

Appendix 2.5.4.1 Batch purification of the GST-tagged RyR1 amino acids 2091-2490 using glutathione conjugated sepharose. A) Gel summarising the partial purification of the GST tagged $RyR1_{(2091-2490)}$. I represents the insoluble fraction following the lysis of induced cells. S represents the soluble fraction following lysis of induced cells. F represents the flow through following batch purification using a Glutathione Sepharose® resin. R represents the Glutathione Sepharose® resin following batch purification. The Precision plus size standard was used to estimate the mass of proteins. Proteins were separated by 10 % acrylamide gel electrophoresis at 120 mV for ninety minutes and were visualised by Coomassie blue staining. The proteins subjected to mass spectrometry were boxed in blue. B) Mass spectrometry analysis of the GST-tagged RyR1 amino acids 2091-2490 following partial purification. Amino acids detected during the analysis are highlighted in red.

2.5.5 Partial purification of RyR1 2091-2525 expressed from pGEX6p3

RyR1 2091-2525 was also soluble when expressed from the pGEX6p3 vector. Like RyR1 2091-2490 expressed from the same vector, pGEX6p3. RyR1 2091-2525 was only marginally soluble and could be enriched using glutathione conjugated Sepharose (appendix 2.5.5.1 A). The identity of the protein was confirmed to correspond to GST-tagged protein.

A)

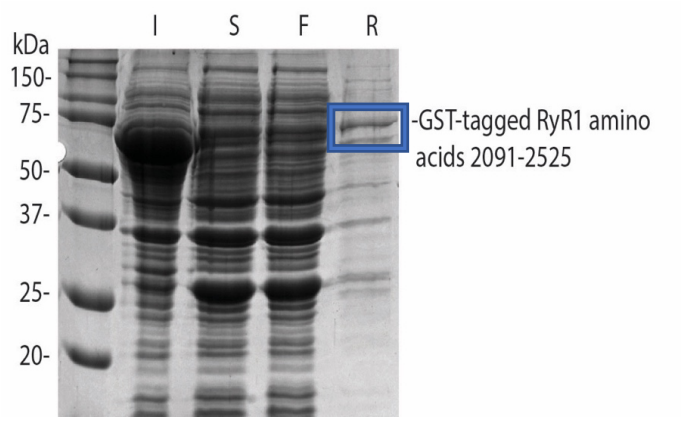

B)

RyR1 amino acids 2091-2525

2001	PPQUQINMLL	GFKDGTDEED	CPLPEEIRQD	LLDFHQDLLA	HCGIQLDGEE
2051	EEPEEETTLG	SRLMSLLEKV	RLVKKKEEKP	EEERSAEESK	PRSLQELVSH
2101	MVVRWAQEDF	VQSPELVRAM	FSLLHRQYDG	LGELLRALPR	AYTISPSSVE
2151	DTMSLLECLG	QIRSLLIVQM	GPQEENLMIQ	SIGNIMNNKV	FYQHPNLMRA
2201	LGMHETVMEV	MVNVLGGGES	KEIRFPKMVT	SCCRFLCYFC	RISRQNQRSM
2251	FDHLSYLLEN	SGIGLGMQGS	TPLDVAAASV	IDNNELALAL	QEQDLEKVVS
2301	YLAGCGLQSC	PMLVAKGYPD	IGWNPCGGER	YLDFLRFAVF	VNGESVEENA
2351	NVVVRLLIRK	PECFGPALRG	EGGSGLLAAI	EEAIRISEDP	ARDGPGIRRD
2401	RRREHFGEEP	PEENRVHLGH	AIMSFYAALI	DLLGRCAPEM	HLIQAGKGEA
2451	LRIRAILRSL	VPLEDLVGII	SLPLQIPTLG	KDGALVQPKM	SASFVPDHKA
2501	SMVLFLDRVY	GIENQDFLLH	VLDVGFLDPM	RAAASLDTAT	FSTTEMALAL
2551	NRYLCLAVLP	LITKCAPLFA	GTEHRAIMVD	SMLHTVYRLS	RGRSLTKAQR

Appendix 2.5.5.1 Batch purification of the RyR1 amino acids 2091-2525 expressed from the pGEX6p3 vector. A) gel summarising the partial purification of the GST-tagged RyR1$_{(2091-2525)}$. I represents insoluble protein following lysis of cells after induction with IPTG. S represents soluble protein following lysis of cells after induction with IPTG. F represent the flow through following batch purification. R represents proteins bound to the glutathione conjugated agarose resin following batch purification. The Precision plus size standard was used to estimate the mass of proteins. Proteins were separated by 10 % acrylamide gel electrophoresis at 120 mV for ninety minutes and were visualised by Coomassie blue staining. The proteins subjected to mass spectrometry were boxed in blue. B) mass spectrometry analysis of the GST-tagged RyR1 amino acids 2091-2525 following batch purification by Glutathione Sepharose®. Amino acids detected during the analysis are highlighted in red.

2.6 Mass spectrometry confirming the identity of proteins enriched following dextrin conjugated agarose purification of RyR1(2091-2708).

Proteins have been identified by Letter coding per figure 3.6

A)

RyR1

```
1901 QEKEDEEKEE EEAAEGEKEE GLEEGLLQMK LPESVKLQMC HLLEYFCDQE
1951 LQHRVESLAA FAERYVDKLQ ANQRSRYGLL IKAFSMTAAE TARRTREFRS
2001 PPQEQINMLL QFKDGTDEED CPLPEEIRQD LLDFHQDLLA HCGIQLDGEE
2051 EEPEEETTLG SRLMSLLEKV RLVKKKEEKP EEERSAEESK PRSLQELVSH
2101 MVVRWAQEDF VQSPELVRAM FSLLHRQYDG LGELLRALPR AYTISPSSVE
2151 DTMSLLECLG QIRSLLIVQM GPQEENLMIQ SIGNIMNNKV FYQHPNLMRA
2201 LGMHETVMEV MVNVLGGGES KEIRFPKMVT SCCRFLCYFC RISRQNQRSM
2251 FDHLSYLLEN SGIGLGMQGS TPLDVAAASV IDNNELALAL QEQDLEKVVS
2301 YLAGCGLQSC PMLVAKGYPD IGWNPCGGER YLDFLRFAVF VNGESVEENA
2351 NVVVRLLIRK PECFGPALRG EGGSGLLAAI EEAIRISEDP ARDGPGIRRD
```

Maltose binding protein

```
  1 MKIKTGARIL ALSALITMMF SASALAKIEE GKLVIWINGD KGYNGLAEVG
 51 KKFEKDTGIK VTVEHPDKLE EKFPQVAATG DGPDIIFWAH DRFGGYAQSG
101 LLAEITPDKA FQDKLYPFTW DAVRYNGKLI AYPIAVEALS LIYNKDLLPN
151 PPKTWEEIPA LDKELKAKGK SALMFNLQEP YFTWPLIAAD GGYAFKYENG
201 KYDIKDVGVD NAGAKAGLTF LVDLIKNKHM NADTDYSIAE AAFNKGETAM
251 TINGPWAWSN IDTSKVNYGV TVLPTFKGQP SKPFVGVLSA GINAASPNKE
301 LAKEFLENYL LTDEGLEAVN KDKPLGAVAL KSYEEELAKD PRIAATMENA
351 QKGEIMPNIP QMSAFWYAVR TAVINAASGR QTVDEALKDA QTRITK
```

C)

60 KDa chaperonin

```
  1 MAAKDVKFGN DARVKMLRGV NVLADAVKVT LGPKGRNVVL DKSFGAPTIT
 51 KDGVSVAREI ELEDKFENMG AQMVKEVASK ANDAAGDGTT TATVLAQAII
101 TEGLKAVAAG MNPMDLKRGI DKAVTAAVEE LKALSVPCSD SKAIAQVGTI
151 SANSDETVGK LIAEAMDKVG KEGVITVEDG TGLQDELDVV EGMQFDRGYL
201 SPYFINKPET GAVELESPFI LLADKKISNI REMLPVLEAV AKAGKPLLII
251 AEDVEGEALA TLVVNTMRGI VKVAAVKAPG FGDRRKAMLQ DIATLTGGTV
301 ISEEIGMELE KATLEDLGQA KRVVINKDTT TIIDGVGEEA AIQGRVAQIR
351 QQIEEATSDY DREKLQERVA KLAGGVAVIK VGAATEVEMK EKKARVEDAL
401 HATRAAVEEG VVAGGGVALI RVASKLADLR GQNEDQNVGI KVALRAMEAP
451 LRQIVLNCGE EPSVVANTVK GGDGNYGYNA ATEEYGNMID MGILDPTKVT
501 RSALQYAASV AGLMITTECM VTDLPKNDAA DLGAAGGMGG MGGMGGMM
```

D)

E. coli outer membrane protein F

```
  1 MMKRNILAVI VPALLVAGTA NAAEIYNKDG NKVDLYGKAV GLHYFSKGNG
 51 ENSYGGNGDM TYARLGFKGE TQINSDLTGY GQWEYNFQGN NSEGADAQTG
101 NKTRLAFAGL KYADVGSFDY GRNYGVVYDA LGYTDMLPEF GGDTAYSDDF
151 FVGRVGGVAT YRNSNFFGLV DGLNFAVQYL GKNERDTARR SNGDGVGGSI
201 SYEYEGFGIV GAYGAADRTN LQEAQPLGNG KKAEQWATGL KYDANNIYLA
251 ANYGETRNAT PITNKFTNTS GFANKTQDVL LVAQYQFDFG LRPSIAYTKS
301 KAKDVEGIGD VDLVNYFEVG ATYYFNKNMS TYVDYIINQI DSDNKLGVGS
351 DDTVAVGIVY QF
```

Appendix 2.6 Mass spectrometry of proteins enriched following purification using the MBPTrap™ HP column. Proteins have been identified by letter coding as indicated in figure 3.6. Amino acids highlighted red represent those identified during MS/MS analysis.

2.7 Partial purification of maltose binding protein expressed from the empty pMALp2g vector.

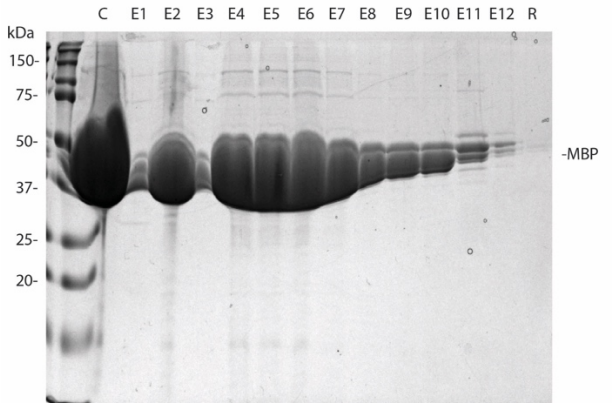

Appendix 2.7. Partial purification of maltose binding protein using an amylose conjugated agarose. Protein was eluted from the resin in 100 mM maltose. C, resin prior to purification. E1-12 represent individual elution fractions collected. The Precision plus size standard was used to estimate the mass of proteins. Proteins were separated by 10 % acrylamide gel electrophoresis at 120 mV for ninety minutes and were visualised by Coomassie blue staining.

Appendix 3. Immortalisation of primary myoblasts.

Appendix 3.1 Primer sequences

Primer name	Primer sequence	melting temperature ° C
hTERT F	GGGAGCACAGCTGCTGC	60
hTERT	GTACACTGTCCCATAGGC	52
Tel 1	GGTTTTTGAGGGTGAGGGTGAGGGTGA	68
Tel 2	TCCCGACTATCCCTATCCCTATCCCTA	64
Telomer Repeat (Double stranded DNA)	TTAGGGTTAGGGTTAGGGTT AGGGTTAGGGTTAGGGTTA GGGTTAGGGTTAGGGTTAG GGTTAGGGTTAGGGTTAGG GTTAGGG	
INFB1 F	GGTTACCTCCGAAACTGAAGA	55
INFB1 R	CCTTTCATATGCAGTACATTAGCC	56
36B4 F	CAGCAAGTGGGAAGGTGTAATCC	60
36B4 R	CCCATTCTATCATCAACGGGTACAA	59
Myosin heavy chain F1	CGCATCTCTACGCCAGGGTCCTTAA	65
Myosin heavy chain R1	AGCTCCAGCTTCGGTCTTAGCTGT	65
Myosin heavy chain F2	CGAAGCTGGAGCTACTGTAACAGTGA	63
Myosin heavy chain R2	GAACAAGCCTGAGTAGGTGTAGATCATCC	64
Myosin heavy chainF3	ATCTTGATCACCGGAGAATCTGGCGC	66
Myosin heavy chain R3	CTAGACTTCTCCAGAAGATATGTTTCAATAT	57
Myostatin F1	TGCCTACAGAGTCTGATTTTCTAATG	57
Myostatin R1	ACCAGTGCCTGGGTTCATGTCAAG	64
Myostatin F2	GGAGAAGATGGGCTGAATCCGTT	61
Myostatin R2	GCTTGGTGTACCAGATGAGTATGAGGA	63
Pax 7 F1	GGATTCCCTTTGGAAGTGTCCACC	62
Pax 7 R1	TCGCCACCTGTCTGGGCTTG	64
Pax 7 F2	GTGCCCTCAGGTTTAGTGAGTTCG	62
Pax 7 R2	CCGACTGCGTCGCTGCTTGCGC	71
Pax 7 F3	CGTGTGCAGGTCTGGTTCAGT	61
Pax 7 R3	GCTGAGGCCGGTGCACAGTG	66
Atrogen F1	GACCTCAGCAGTTACTGCAACAAGG	63
Atrogen R1	CCCAGGGTGCAATATCCATGGC	63
Atrogen F2	TGGTCCGGCTGTTGGAGCT	63
Atrogen R2	GAAGGCAGGCCTGGTGATCTG	62
Atrogen F3	CGAGCGGCAGATCCGCAAACGA	67

Atrogen R3	CGGATGGTCAGTGCCCTTCCAG	65
4833 HRM Forward	TCTCCTGGACATCGCC	53
4833 HRM Reverse	CACACCTGTTTCCCATTG	51

Appendix 3.2 Vector maps

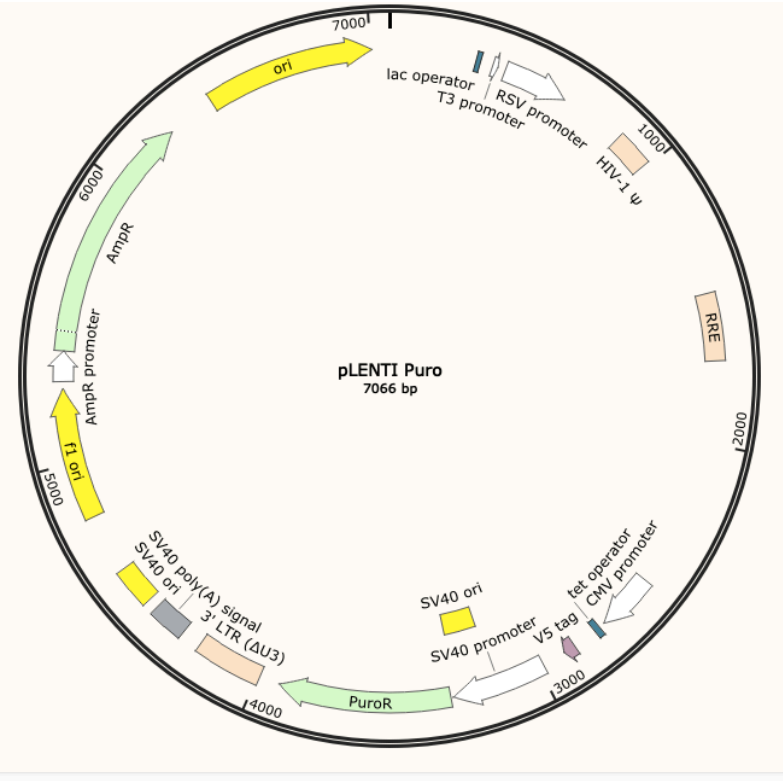

Appendix 3.2.1. Map of the pLENTI puro vector. The vector map was created using the SnapGene viewer 3.1.2 software.

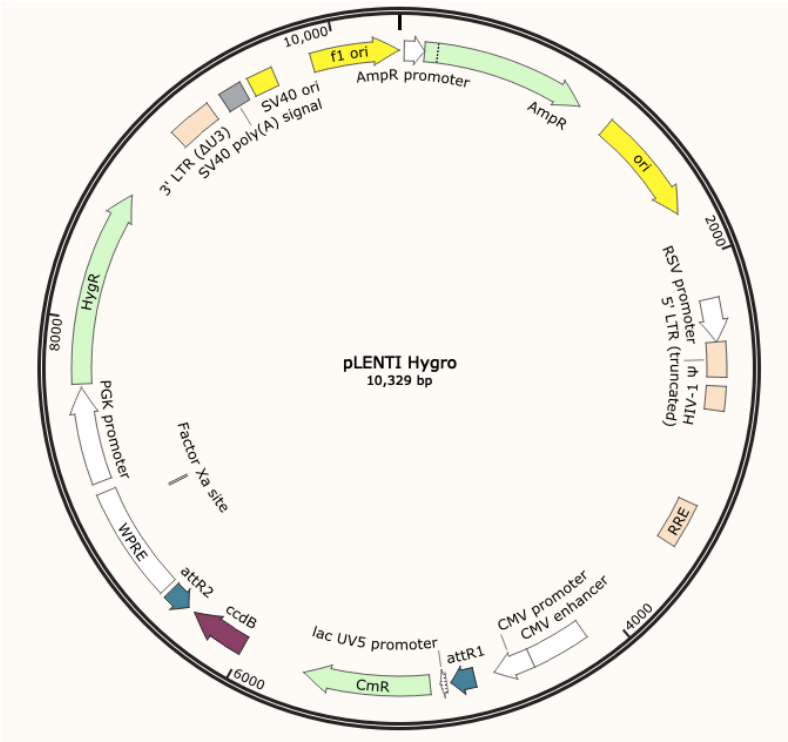

Appendix 3.2.2. Map of the pLENTI hygro vector. The vector map was created using the SnapGene viewer 3.1.2 software.

Appendix 3.3 Unedited western blot confirming the expression of myosin heavy chain in primary and immortal myobtubes

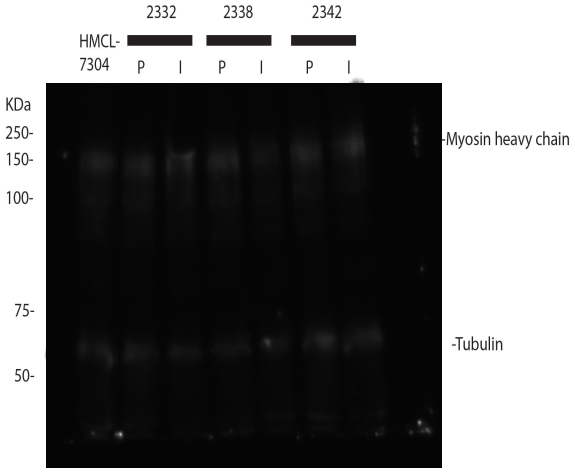

Appendix 3.3. Western blot analysis confirming the expression of myosin heavy chain in primary and immortal myotubes. Individual patient samples have been identified by number. P refers to protein extracted from primary cells and I refers to protein extracted from immortal cells. Proteins were separated by 7 % SDS polyacrylamide gel electrophoresis at 120 mV for ninety minutes and transferred to an immobilon membrane at 35 amps for 16 hours. Primary antibodies specific to tubulin and myosin heavy chain were used to detect the protein, a horse radish peroxidase conjugated secondary antibody was used to visualise the proteins.

3.4 Example of the raw data obtained during the Ca^{2+} release assays

3.4.1 Ca^{2+} release in immortal myotubes in response to 60 mM KCl.

A single myotube was selected and was exposed to 60 mM KCl. Following the data recording a base line was established for 20 seconds prior to the addition of 60 mM KCl. The recording was continued for forty seconds at which time it was noted no change in fluorescence was going to take place and 4-CmC was added to the well to a final concentration of 1000 µM at which time a change in fluorescence was noted (appendix 3.4.1).

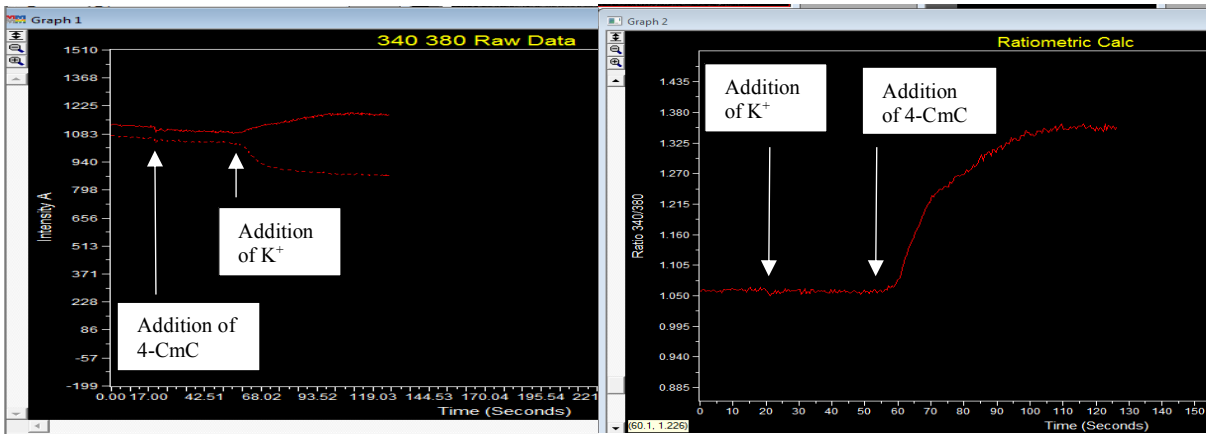

Appendix 3.4.1. Raw data obtained from the Metafluor software following exposure of immortal myotubes to 60 mM KCl and 1000 µM 4 CmC. The left panel is the flouresence emission obtained following exposure of cells to the wavelegths 340 nm and 380 nm. The right panel represents the 340 / 380 ratio data. The time points at which both 60 mM K^+ and 4-CmC were added have been indicated by arrows.

3.4.2 Response to 10 mM caffeine

In this case three immortal myotubes were selected. Following the data recording a base line was established for 30 seconds prior to the addition of 10 mM caffeine. The recording was continued for two minutes at which time it was noted no change in fluorescence was going to take place and 4-CmC was added to the well to a final concentration of 1000 µM at which time a change in fluorescence was noted (appendix 3.4.2). The addition of the RyR1 agonist confirms the cells were viable and the RyR1 was active within the cells.

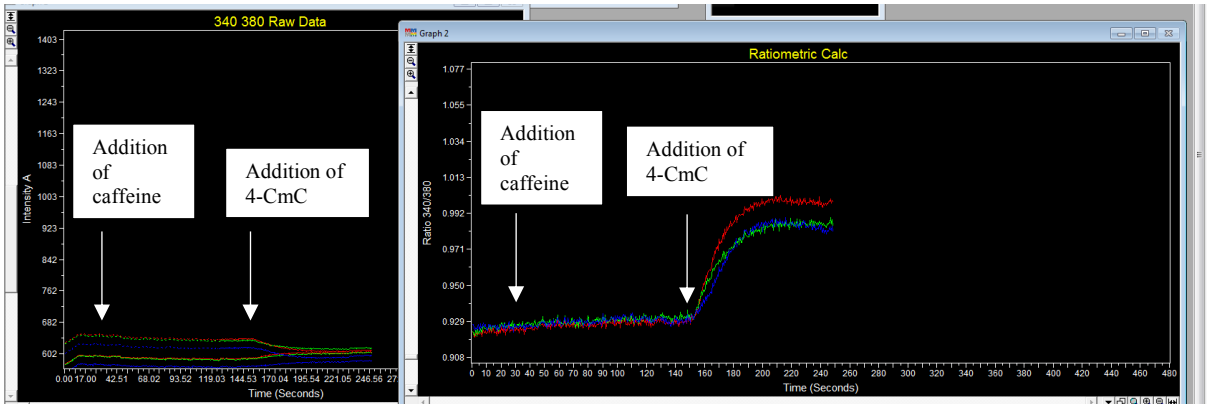

Appendix 3.4.2. Raw data obtained from the Metafluor software following exposure of immortal myotubes to 10 mM caffeine and 1000 µM 4-CmC. The left panel is the fluorescence emission obtained following exposure of cells to the wavelengths 340 nm and 380 nm. The right panel represents the 340 / 380 ratio data. Individual colours represent an individual myotube. The time points at which both 10 mM caffeine and 4-CmC were added have been indicated by arrows.

3.5 Optimising myoblast growth conditions.

Optimising the quantitative PCR for the genes myosin heavy chain, myostatin, atrogen and pax 7. RNA was extracted from myotubes and cDNA was produced by reverse transcriptase. Different primer pairs were trialled to efficiently amplify the desired genes. Primer pairs that could amplify a single product were further used to determine the relative gene expression of each gene following the treatment with dexamethasone.

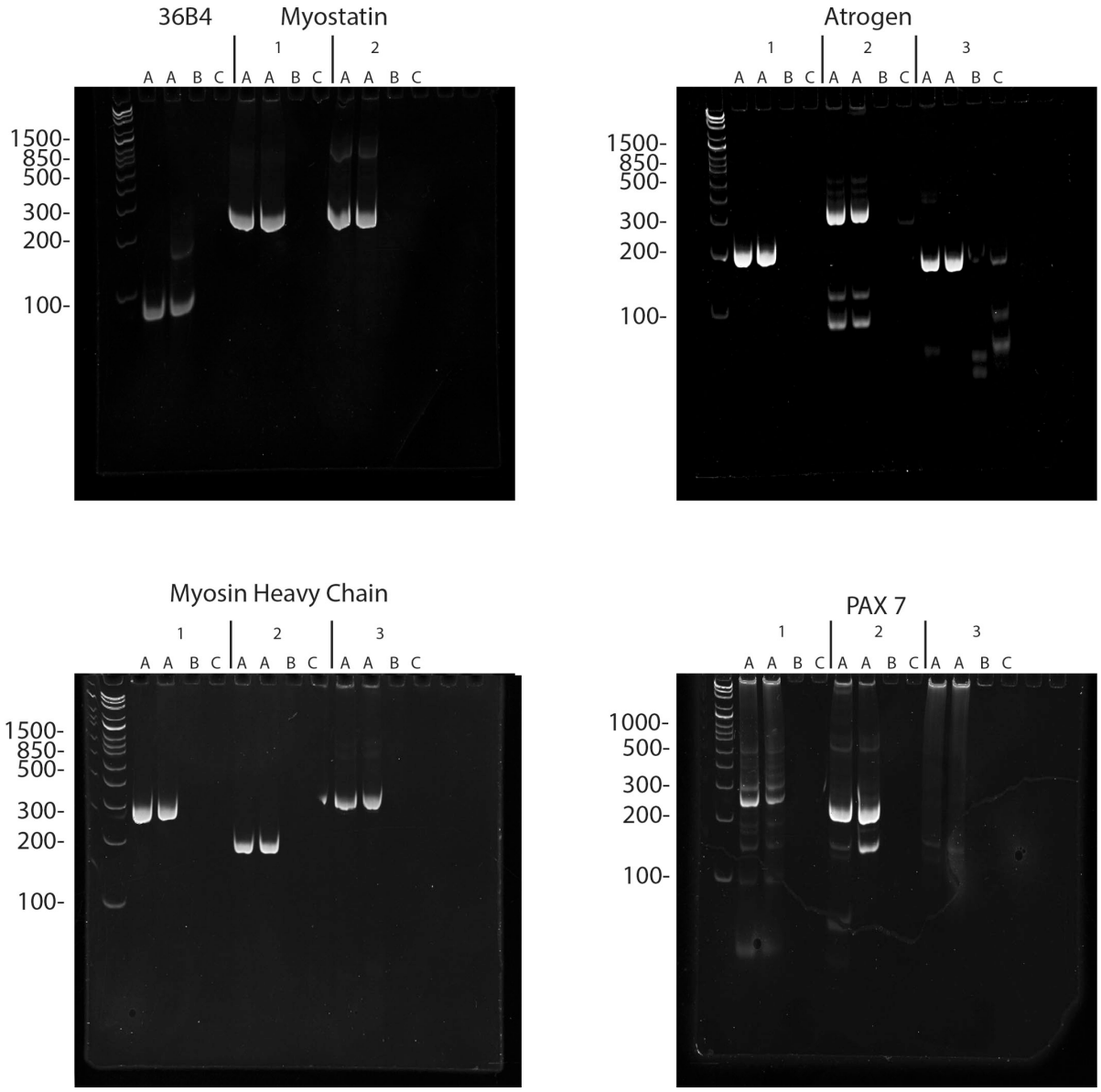

Appendix 3.5. Acrylamide gel electrophoresis following rtqPCR. Specific genes have been indicated by name and specific primer pairs have been labelled by number. A) amplification of cDNA. B) no template control. C) no reverse transcriptase control. DNA was separated by 10 % SDS polyacrylamide gel electrophoresis in TAE buffer for neinty minutes and stained with 0.5 mg/mL ethidium bromide and visualised under Uv light using the Uvitec Cambridge Uvidoc HD6.

Appendix 3.6. Characterisation of the *RYR1* variant c.14997C>T

Vector maps

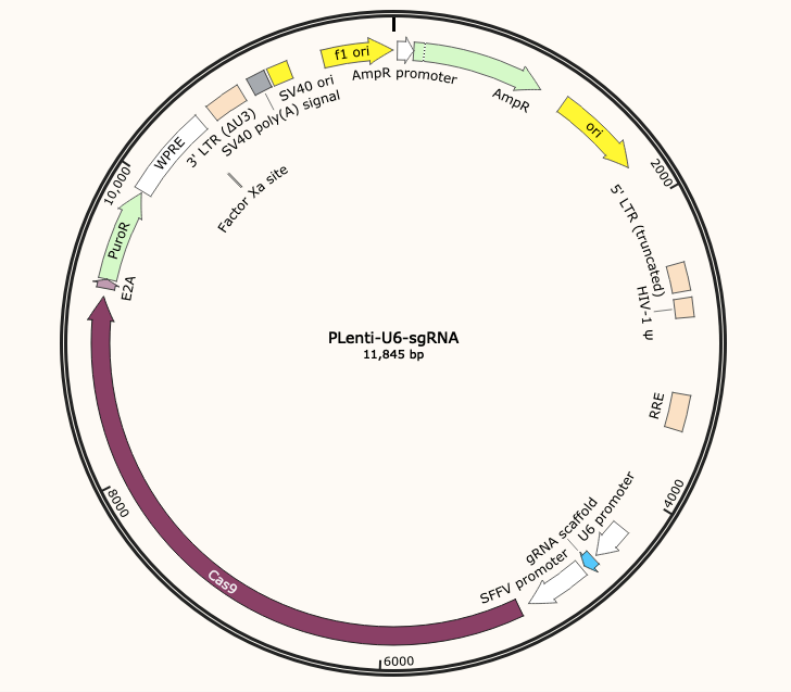

Appendix 3.6.1. Map of the pLenti-U6-sgRNA vector. The vector map was created using the SnapGene viewer 3.1.2 software.

Insert sequences corresponding to guide RNA within each vector

1. TGTCCTCTGTCACCCACAAT
2. CCCACAATGGGAAACAGGTG
3. TGTCACCCACAATGGGAAAC

3.6.2 Single stranded repair template

oligonucleotide name	Oligonucleotide sequence
His4833Tyr in Human RyR1. Single stranded DNA repair template	GGACACTACAACAACTTCTTCTTTGCTGCCCATCTCCTGGACATCGCC ATGGGGGTCAAGACGCTGCGCACCATCCTGTCCTCTGTCACCTACAA TGGGAAACAGGTGTGGGGAGGACCTGGCTGTGGGGCGTGGGCCAG CAGGGACCAGCGTGGCAGTGGGTGGTGAAGGGATAAGGGCCGG